Exoplanet Characterisation Observatory (EChO)

Assessment Study Design Report

Issue 4.0

ECHO-RP-0001-RAL

Prepared by: EChO Consortium Study Team
EChO Payload Study Consortium Team
Date: 30/11/13

R. Irshad
Compiled by:
Rain Irshad *(RAL Space)*
EChO Consortium Systems Engineer
Date: 30/11/13

Digitally signed by Paul Eccleston
Date: 2013.12.03 14:42:31 Z
Agreed by:
Paul Eccleston *(RAL Space)*
EChO Consortium Project Manager
Date:

Approved by:
Giovanna Tinetti (UCL)
EChO Consortium PI
Date: 3/12/13

DOCUMENT CHANGE RECORD

Issue	Date	Page	Description Of Change	Comment
0.1	27-May-12	All	New document created in preparation for Mid-Term Review	
0.2	11-June-12	All	Updates with population of introduction and starting to compile consortium input.	
0.3	13-June-12	All	Added input from consortium on ground segment, SWIR module	
0.32	13-June-12	All	Additional input from consortium added, saved as new filename due to network crash.	
0.33	13-June-12	All	Added LWIR, EWG, optics and Sci input. Circulated to consortium for critical review	
0.4	14-June-12	All	Updated with further inputs from consortium. Added introduction to science section. Circulated for final proof review.	
0.5	15-June-12	All	Completed missing sections, updated to address comments received from consortium.	
0.6	15-June-12	All	Added final missing sections, final proofing and corrections. Added executive summary.	
1.0	15-June-12	All	Released at Issue 1 for submission of MTR datapack	
1.1	16-June-12	19 145-147	Corrected formatting of Fig 4-5 to allow proper conversion to PDF. Corrected minor typo errors in list of consortium participants	
1.2	24-Aug-13	All	Document stripped out and structure used to set up for Assessment Phase Study Completion version of report – circulated for comment to consortium	
1.3	06-Sept-13	All	Added input sections from consortium on: VNIR module, MWIR module, FGS Detector & SW, LWIR module, FGS Optical module, Mechanical Systems, Thermal Systems	
1.4	11-Sept-13	All	Added updated sections on: Detector Systems, VNIR channel, FGS channel	
1.5	15-Sept-13	All	Updated with comments from consortium review of document. Added updated sections on: Detector Systems, FGS, Thermal Systems, Coolers, Mechanical Systems,	
1.6	16-Sept-13	All	Updated sections on: Systems architecture, Data rate and observational modes, SWIR Module, TRL levels, AIV, Reviewed d	
1.7	16-Sept-13	All	Included Section 11.2 and 12; Fixed Numbering of figures/tables. Added final input sections from PE & RI.	
1.8	16-Sept-13	All	Final updates to RD list. Updated list of participating scientists and key individuals.	
2.0	16-Sept-13	All	Released at Issue 2.0 for Preliminary PRR Datapack	
2.1	30-Sept-13	All	Corrections as a result of End of Phase A study review by ESA team and as result of EChO team additional reviews.	
3.0	30-Sept-13	All	Re-released at Iss 3.0 for PRR Datapack	
4.0	30-Nov-13	37	Updated Figures 4-3 and 4-4 to correct for plotting error and add description text to captions	

DISTRIBUTION LIST

Name	Organisation	Name	Organisation
EChO Payload Consortium Team (via Website)	Consortium	Martin Linder	ESA
Giovanna Tinetti	UCL	Ludovic Puig	ESA
Paul Eccleston	RAL Space	Kate Isaac	ESA

TABLES OF CONTENTS

LIST OF CONTENTS

LIST OF TABLES

LIST OF FIGURES

1 EXECUTIVE SUMMARY

This document presents the design overview of the instrument payload being developed for EChO (Exoplanet Characterisation Observatory), a candidate mission for the ESA M3 launch opportunity. This document provides an overall summary of the baseline design derived during the phase A study. It gives an overview of the evolution of the design to this point, although full details of the trade studies and alternative options that have been considered and studied are provided in many of the reference documents (also provided in the datapack).

The baseline design is for a 3 channel, highly integrated, common field of view, spectrometer that covers the full EChO required wavelength range of 0.4 µm to 11.0 µm. Also included in the Payload Instrument is the Fine Guidance System necessary to provide closed loop feedback to the high stability AOCS of the Spacecraft. The required spectral resolutions of 300 or 30 are achieved or exceeded throughout the band. The baseline design largely uses technologies with a high degree of technical maturity and almost entirely European technologies (with the exception of the detectors). A plan view of the baseline Focal Plane Unit (FPU) (integrated to the rear of a representative primary mirror) is shown below in Figure 1-1.

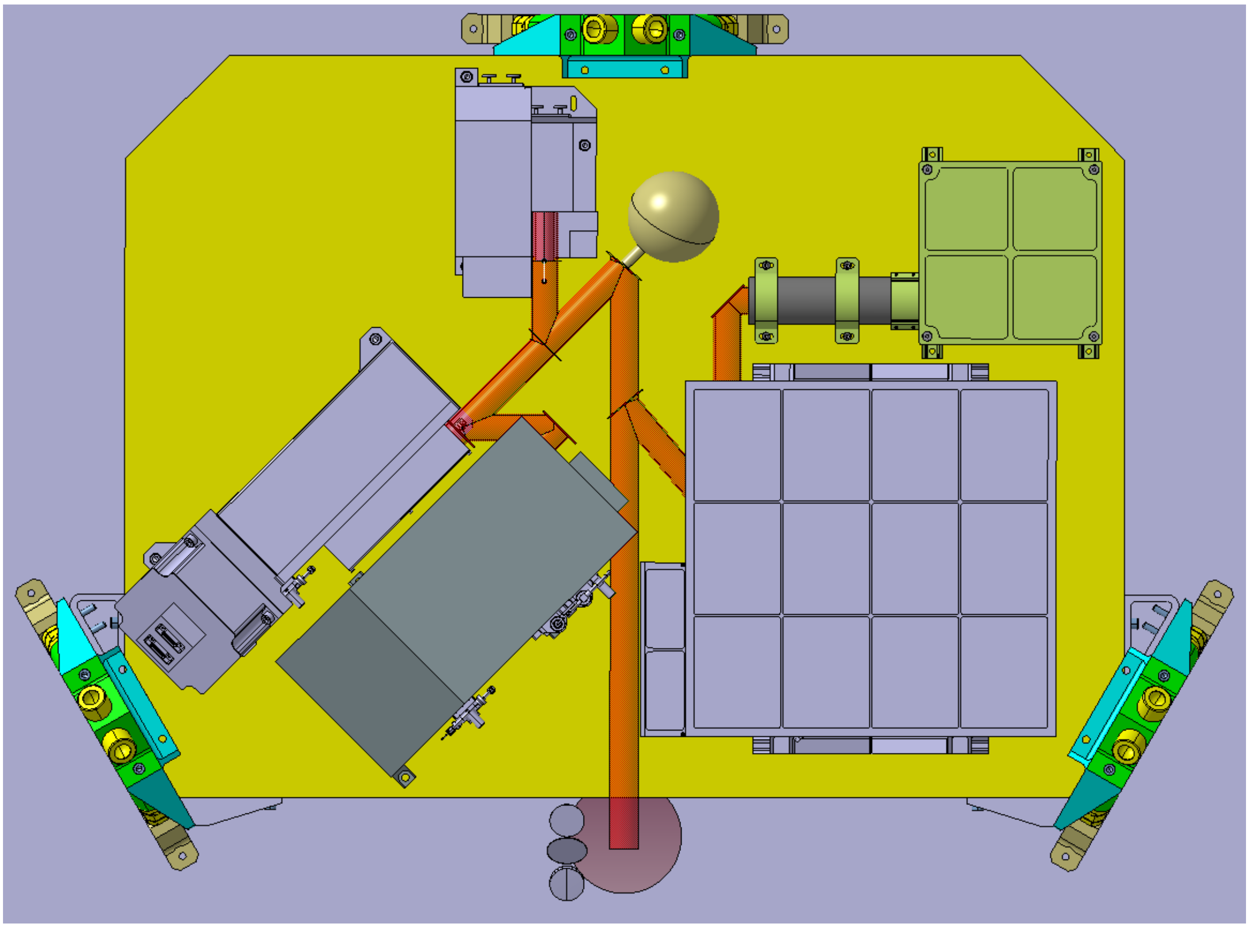

Figure 1-1: Baseline Opto-Mechanical Design

2 INTRODUCTION

This document presents the design overview of the instrument payload being developed in the frame of the assessment phase study for EChO (Exoplanet Characterisation Observatory), a candidate mission for the ESA M3 launch opportunity. For a background to the mission and the requirements on the spacecraft and payload see [AD1], [AD2] and [AD3].

2.1 PURPOSE

This document captures the design information relevant to the payload instrument being studied by a multi-national consortium of European institutes in frame of the assessment phase of the mission. This document contains design information and references to other detailed design documentation.

2.2 SCOPE

This document provides an overall summary of the baseline design derived during the study. It gives an overview of the evolution of the design to this point, although full details of the trade studies and alternative options that have been considered and studied are provided in many of the reference documents (also provided in the datapack).

This document concentrates on the technical design aspects of the study output. Although the identification of the driving science requirements and how these impact the design is considered here, the scientific justification for the missions and the derivation of the science requirements is beyond the scope of this document, this is covered elsewhere.

Detailed technical information and trade-off justifications are contained in a number of self-standing technical notes which are referenced from this report. Additionally, from Issue 1.2 of this document onwards, detailed information on the planning of instrument development program and AIV are contained in separate documents, the initial versions of the instrument DDVP and AIV plans.

2.3 APPLICABLE DOCUMENTS

AD #	APPLICABLE DOCUMENT TITLE	DOCUMENT ID	ISSUE
1	EChO Mission Requirements Document (MRD)	SRE-PA/2011.038	3
2	EChO Science Requirements Document (SciRD)	SRE-PA/2011.037	3
3	EChO Experiment Interface Definition – Part A (EID-A)	SRE-F/2012.097	0.2
4	EChO Response to AO	Tinetti / Eccleston / Consortium	1st Nov 2012
5	ESA EChO Radiometric Model Description	SRE-PA/2011.040	3 Rev 1

Table 2-1: Applicable Documents

2.4 REFERENCE DOCUMENTS

RD #	APPLICABLE DOCUMENT TITLE	DOCUMENT ID	ISSUE
1	EChO Payload Functional Block Diagram	ECHO-DW-0001-RAL	0.6
2	Payload Architecture Trade Study Write-up	ECHO-TN-0001-RAL	1
3	Deleted at Issue 1.2		
4	Deleted at Issue 1.2		
5	Deleted at Issue 1.2		
6	Deleted at Issue 1.2		
7	Deleted at Issue 1.2		
8	Deleted at Issue 1.2		
9	Deleted at Issue 1.2		
10	Deleted at Issue 1.2		
11	Deleted at Issue 1.2		
12	Deleted at Issue 1.2		
13	Deleted at Issue 1.2		
14	Deleted at Issue 1.2		
15	Deleted at Issue 1.2		
16	Borucki W.J., et al., Science, 325:709, 2009	N/A	2009
17	EChOSim Software Requirements Document	N/A	2.0
18	EChOSim User Requirements Document	N/A	3.0
19	Benchmarking the tools used to evaluate the radiometric performance of EChO	SRE-F/2012.071	June 5th 2012
20	Deleted at Issue 1.2		
22	EChO Instrument MICD	A1-5375-900	2
23	EChO Contamination Control Plan	ECHO-PL-0003-RAL	1.0
24	EChO Instrument Design, Development, Engineering and Verification Plan	ECHO-PL-0004-RAL	0.3
25	Barstow, J et al. 2013. On the potential of the EChO mission to characterize gas giant atmospheres	MNRAS 430 (2013)	2013
26	Evaluation of Science Impact of Reduced LWIR Resolution	ECHO-TN-0002-OXF	1.0
27	Hogue, H. et al. 2010. Update on Blocked Impurity Band detector technology from DRS.	Proc. of SPIE Vol. 7780 778004-7	2010
28	Liebe, "Accuracy performance of star trackers",	IEEE Trans. Aerosp. and El. Systems	2002
29	FGS Electronics	ECHO-TN-0001-UVIE	0.1
30	Pointing Jitter Impact on Photometric Stability	ECHO-TN-0003-UCL	1.2
31	Optical Analysis of the Fine Guidance System	ECHO-RP-0001-CBK	01
32	EChOSim Comparison to ESA Radiometric Model	ECHO-TN-0002-UCL	1.0
33	EChO IOB Material Trade-Off	ECHO-TN-MSSL-001	1.0
34	Noise Evaluation for EChO VNIR Detectors	IAPS/ECH/TN/01-013	1.0
35	EChO Detector Request for Information	ECHO-RS-0001-ATC	1.0
36	EChO Detector Selection Criteria	ECHO-TN-0002-ATC	1.0
37	EChO Consortium Cost and Financial Report	ECHO-RP-0002-RAL	0.3
38	EChO Focal Plane Unit GMM & TMM Document and Analysis Results	ECHO-TN-0001-IASFBO	1.0
39	Radiometric Background Modeling for the EChO Payload Instrument	ECHO-TN-0006-RAL	0.2
40	EChO Instrument Calibration and Data Processing Plan	ECHO-PL-0009-RAL	1.0
41	Consortium Project Management Plan	ECHO-PL-0005-RAL	0.6
42	Generation of a Target List of Observable Exoplanets with EChO	ECHO-TN-0001-UCL	1.0
43	The contribution of the major planet search surveys to EChO target selection	N/A	16/07/13
44	EChO Electronics	ECHO-TN-0001-OAA/UniFi	1.0
45	EChO Payload Instrument Noise Budget	ECHO-TN-0002-RAL	2.3
46	ECHO Science Ground Segment Implementation Plan	ECHO-PL-0008-RAL	0.3
47	NH3 Detectability: 11 μm vs 10.6 μm cutoff	ECHO-TN-0005-UCL	0.1

Table 2-2: Reference Documents

2.5 CONSORTIUM PARTICIPANTS AND STRUCTURE

The EChO consortium that has conducted and is conducting the work for this assessment phase study consists of the leading space science institutes from across Europe and combines both technical and scientific expertise in the areas of space instrumentation and exoplanet research. This mixture of technical and scientific expertise, often within the same institute, gives the EChO consortium a critical edge in the development and scientific evaluation of the payload and mission design.

Details of the structure of the consortium, the work-share and the participants can be found in the Consortium Project Management Plan, [RD41]. An overview of the national responsibilities is shown in Figure 2-1 below.

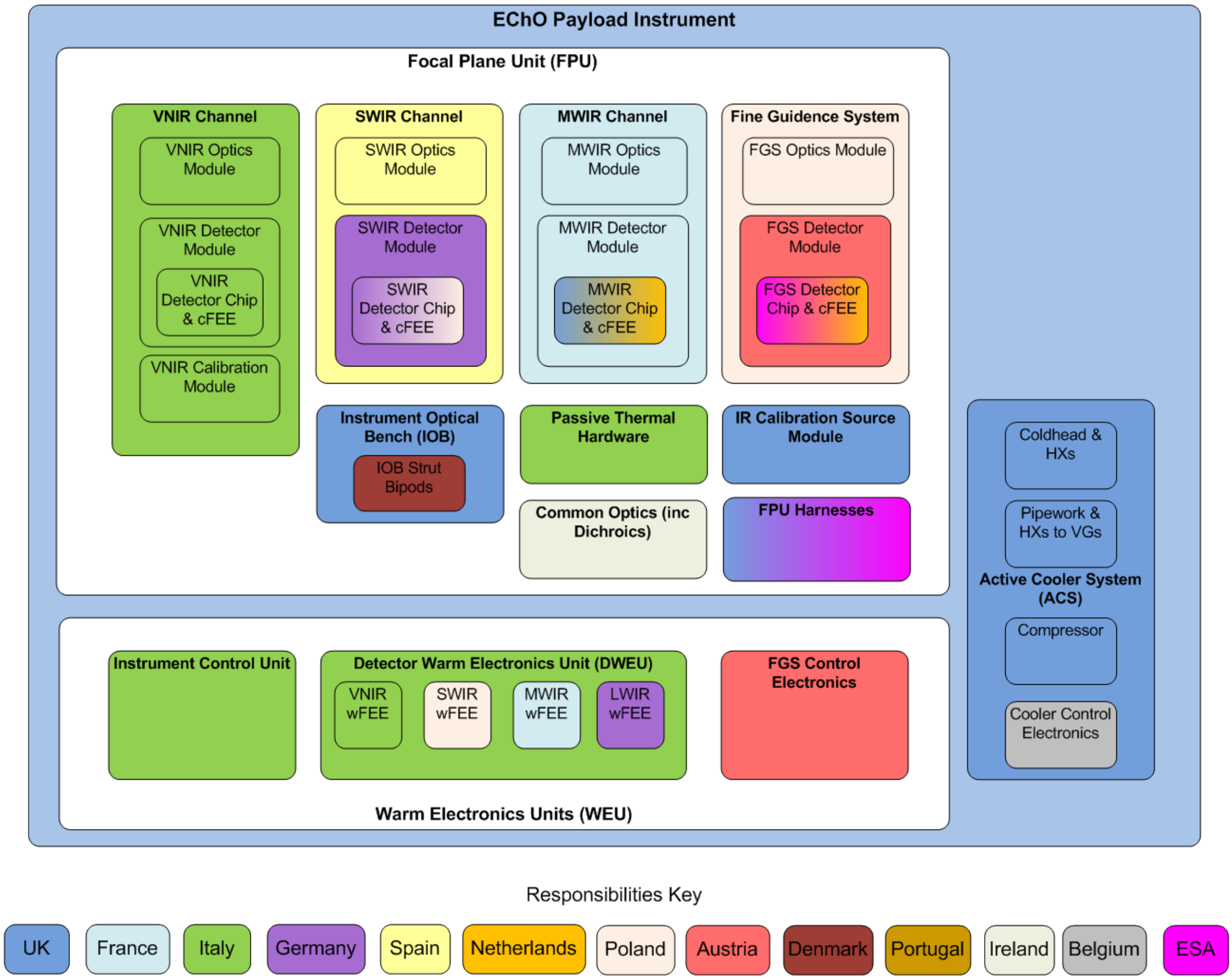

Figure 2-1: Overview of National Responsibilities

3 ECHO SCIENCE OVERVIEW

3.1 MISSION SCIENCE CASE

3.1.1 EChO Science Overview

The discovery and characterisation of extra-solar planets is one of the most rapidly changing and exciting areas of astrophysics. Since 1995, the number of planets known has increased by two orders of magnitude. NASA's Kepler mission is discovering many hundreds of new planets around some of the 100,000 stars it is surveying during its 3 to 4-year mission and the ESA-Gaia mission is expected to discover thousands more. The indirect detection techniques employed -- radial velocity, transits, astrometry and micro-lensing -- allow us to determine the basic parameters of the planets, i.e. their orbit, mass, size and basic nature (rocky or gaseous). However, to push our understanding of these worlds beyond these first steps, we must use spectroscopic techniques to probe for the presence of an atmosphere and, where one is present, to determine its physical nature and chemical constituents. Exoplanetary science stands on an exciting threshold, similar to our knowledge of the planets in our own Solar System before spectroscopic studies revealed their true nature and started to unravel the story of their formation and evolution. The observation of planetary atmospheres is at the cutting edge of exoplanet science, and in this context the Exoplanet Characterisation Observatory, EChO, has been proposed as an ESA "medium-class mission" for launch in the 2022-2024 timeframe.

The basic mission concept consists of a 1.2 m telescope passively cooled to below 50 K on a satellite in orbit around the second Lagrangian point (L2). The observation sequence consists of staring mode spectroscopic observations taken over the various phases of the target light curve as the planet transits in front and behind the host star (Figure 3-1). The spectrum of the planet is seen either in absorption against the stellar spectrum (primary transit) or in emission together with that of the star. The stellar spectrum is observed in the absence of the planet as the planet transits behind the star (secondary eclipse). The signal from the planet is isolated from the star by fitting a light curve to each observation.

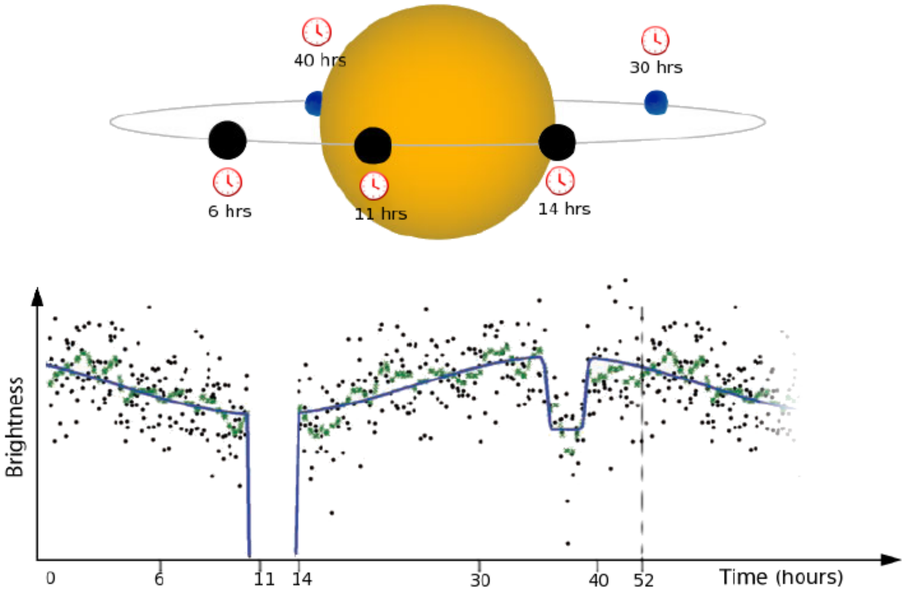

Figure 3-1: Optical phase curve of the planet HAT-P-7b observed by Kepler [RD16] showing primary and secondary transit measurements

The contrast between the star and the planet spectra depends on the stellar type and the size and temperature of the planet and varies strongly with wavelength. Typical values range from 10^{-3} for "hot Jupiters" in orbit around G stars to 10^{-5} for "temperate super-Earths" around M stars (Tessenyi et al 2012). To extract the spectrum of the planet therefore requires the co-addition of many transit observations in order to build up the total signal to noise ratio in the measurement. To achieve this to the level required demands a high level of stability in the detection system, requiring, in turn, a payload design with a high degree of integration between the various components and with the satellite systems. All aspects of the system and payload design need careful attention to detail especially with regard to factors that can affect the photometric stability of the system and/or provide spurious signals that might mimic the light curve signature from the target planetary systems. In this report we present such a design and show that, when integrated with the EChO satellite system, it will meet or exceed the requirements of the EChO mission.

3.1.2 EChO Science Objectives

EChO will address the following fundamental questions:

- *Why are exoplanets as they are?*
- *What are the causes for the observed diversity?*
- *Can their formation history be traced back from their current composition and evolution?*

EChO will provide spectroscopic information on the atmospheres of a large, select sample of exoplanets allowing the compositions, temperature (profile), size and variability to be determined at a level never previously attempted. This information will be used to address a whole range of key scientific questions:

- *Does the planet have an atmosphere?*
- *What are exoplanets made of?*
- *How were they formed?*
- *Did they migrate and if so how?*
- *How do (exo-)planets evolve?*
- *How are they affected by starlight, stellar winds and other time-dependent processes?*
- *Weather: how do conditions vary with time?*
- *What is the energy budget for the planet?*

And of course:

- *Do any of the planets observed have habitable conditions?*

These objectives, tailored for gaseous and terrestrial planets, are summarized in Figure 3-2 and detailed in Table 3-1.

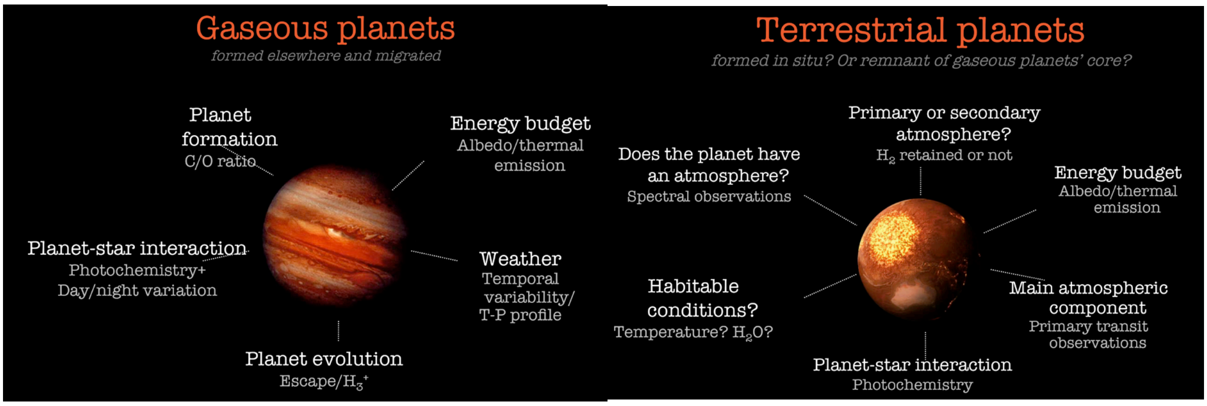

Figure 3-2: Key questions for gaseous and terrestrial planets that will be addressed by EChO

Planet type	Scientific question	Observable	Observational strategy	Observational mode
Gaseous planets	Energy budget	Incoming and outgoing radiation	Stellar flux + planetary albedo and thermal emission with VIS and IR eclipse band-photometry	Chemical Census
	Planetary interior	Density Hints from atmospheric composition?	Primary transit spectra Transit and eclipse spectra	Chemical census
	Chemical processes: Thermochemistry? Transport + quenching? Photochemistry?	Chemistry of planets around different stars & different T Day/night chemical variations Vertical mixing ratios (retrieved values > 10^{-7})	Transit and eclipse spectra of planets around different stars & different T Relative abundances of minor molecular species (HCN, NH_3, C_2H_2, etc.)	Chemical census + Origin mode
	Dynamics: Time scale of horizontal and vertical mixing	Vertical T-P profile Horizontal gradients Day/night variations Temporal variability	IR eclipse spectra IR Eclipse mapping IR orbital phase lightcurves Repeated observations & use of chemical species as tracers (e.g. CH_4, NH_3, CO_2, and HCN etc)	Origin & exo-meteo modes
	Formation: Core accretion or gravitation instability?	a. Density b. C/O ratio	Primary transit + mass from RV Relative abundances of carbon versus oxygen-bearing molecules	Origin mode
	Migration: Any evidence of the initial conditions?	Comparison star/planet metallicity (C/O, O/H, C/H..) Chemistry of planets around different stars.	Relative abundances of carbon-, oxygen-, bearing molecules…TBC Transit and eclipse spectra of planets around different stars & different T	Origin mode
	2D and 3D maps	Exoplanet image at multiple wavelength	Ingress and egress eclipse spectra, Orbital Lightcurves	Exo-Maps mode
	Evolution: Escape processes	H_3^+ detection and ionospheric temperature measurement (TBC)	Transit and eclipse spectra	Origin
Terrestrial planets	Energy budget Albedo & Temperature	Incoming and outgoing radiation	Stellar flux + planetary reflection and thermal emission with VIS and IR eclipse band-photometry	Chemical census
	Is there an atmosphere?	Flat spectrum or not	Transit spectra at multiple wl (IR in particular) to constrain the scale height	Chemical census
	Primary or secondary atmosphere?	Hydrogen rich atmosphere?	Transit spectra at multiple wl (IR in particular) to constrain the scale height	Chemical census
	Main atmospheric component	Scale height	Transit spectra at multiple wl (IR in particular) to constrain the scale height	Chemical census
	Planetary interior	Density Hints from atmospheric composition?	Primary transit + mass from RV Transit and eclipse spectra	Chemical census
	Formation:	Density	Primary transit + mass	

	Formed in situ? Migrated? Core of a giant planet? Frequency of Venus-like, Mercury-like, Ocean planetes..	Is there an atmosphere? Primary (H_2-rich) or secondary atmosphere? Atmospheric composition?	from RV c. d. Transit and eclipse spectra	Chemical Census
Temperate terrestrial planets	Habitability	Temperature Chemical composition (H_2O? CO_2? O_3?)	Eclipse measurements Transit or eclipse measurements at low R.	Challenging, need a late M star, bright in the IR

Table 3-1: Matrix Tracing Key Scientific Questions to Observables and Observation Modes

The details on how these science questions will be addressed by EChO are included in a series of Technical Notes coordinated by the Consortium Science WGs, in particular:

- Nelson, Turrini and Barbieri: *Planet formation*
- Leconte and Forget: *Composition of terrestrial planet atmospheres*
- Guillot and Stixrude: *Planetary interior*
- Barstow et al.: *Spectral retrieval*
- Tennyson et al.: *Spectroscopic data for EChO*
- Venot, Agundez and Selsis: *The chemistry of gaseous planets*
- Cho et al.: *Exo-weather and atmospheric dynamics* (in prep).
- Parmentier et al.: *Orbital lightcurves and maps* (in prep).

3.2 DRIVING SCIENCE REQUIREMENTS

The science requirements from [AD2] which play the strongest part in driving the instrument design are identified below. For critical items, Tech. Notes have been produced by the Consortium in addition to the work done by the SST, in particular:

- Waldmann et al.: *Photometric stability & EChO [RD30]*
- Varley et al.: *Generation of a target list of observable exoplanets with EChO [RD42]*
- Micela et al.: *New targets for EChO [RD43]*
- Tessenyi and Tinetti: *NH3 detectability: 11 μm vs 10.6 μm cutoff [RD47]*
- Barstow et al.: *Science case for 11–16 micron at R<30 [RD26]*
- Waldmann et al.: *Data reduction techniques for exoplanet atmospheres (in prep)*

3.2.1 Wavelength coverage

R-SCI-010: The instantaneous wavelength coverage of EChO shall span 0.55 to 11 micron.

G-SCI-020: The instantaneous wavelength coverage of EChO should span 0.4 to 16 micron.

3.2.2 Wavelength division

R-SCI-030: For wavelengths greater than 3 micron, division of the EChO waveband shall be made such that no cut falls between the following wavelength intervals (inclusive):

- 3.00 - 3.60 micron, 4.10 - 5.00 micron, 5.70 - 8.30 micron, 9.20 - 11.00 micron
- For wavelengths less than 3 micron, division of the EChO waveband shall respect each of the following constraints:
    - (1) No cuts are permitted between the following intervals (CO+CO_2 features):
        - 1.55 - 1.67 micron, 1.91 - 2.10 micron, 2.30- 2.39 micron, 2.65 - 2.82 micron
    - (2) Cuts may fall in not more than one of the four intervals listed for each of the two groupings below:
        - Group A (H_2O features): 1.10 – 1.20 micron, 1.31 - 1.50 micron, 1.75 - 2.02 micron, 2.38 - 3.00 micron
        - Group B (CH_4 features): 1.10 - 1.20 micron, 1.31 - 1.50 micron, 1.60 - 1.85 micron, 2.11 - 2.52 micron
    - (3) No cuts are permitted between the following intervals:
        - 0.55 – 0.61 micron (Sodium “D” lines doublet), 0.645 – 0.665 micron (H-alpha), 0.69 – 0.72 micron (CaH/TiO), 0.74 -- 0.80 micron (Potassium “D” lines doublet)

Restrictions on the wavelengths at which cuts can be made below 1 micron are TBC.

In-band (where in-band refers to a wavelength interval in which cuts cannot be made) performances should meet all other SciRD requirements. In the transition region between two adjacent bands, relaxation of in-band performance to 50% is allowed taking into account both adjacent channels i.e. at any wavelength in the transition band at least one of the two adjacent channels or the combination of signals from these channels has to have at least 50% performance. This is shown graphically in Fig. 3a: it is assumed that the point at which the performance falls to 50% for both channels is located at the centre wavelength of the transition band. The wavelengths of spectral features associated with key and goal species, as well as the corresponding intervals in which cuts should not be made, are tabulated in Table 4. These are also shown in Figure 3-4 and Figure 3-5, in which normalized, representative model spectra from these same species as seen in occultation are plotted over the 1 – 5 and 1 – 16 micron intervals respectively.

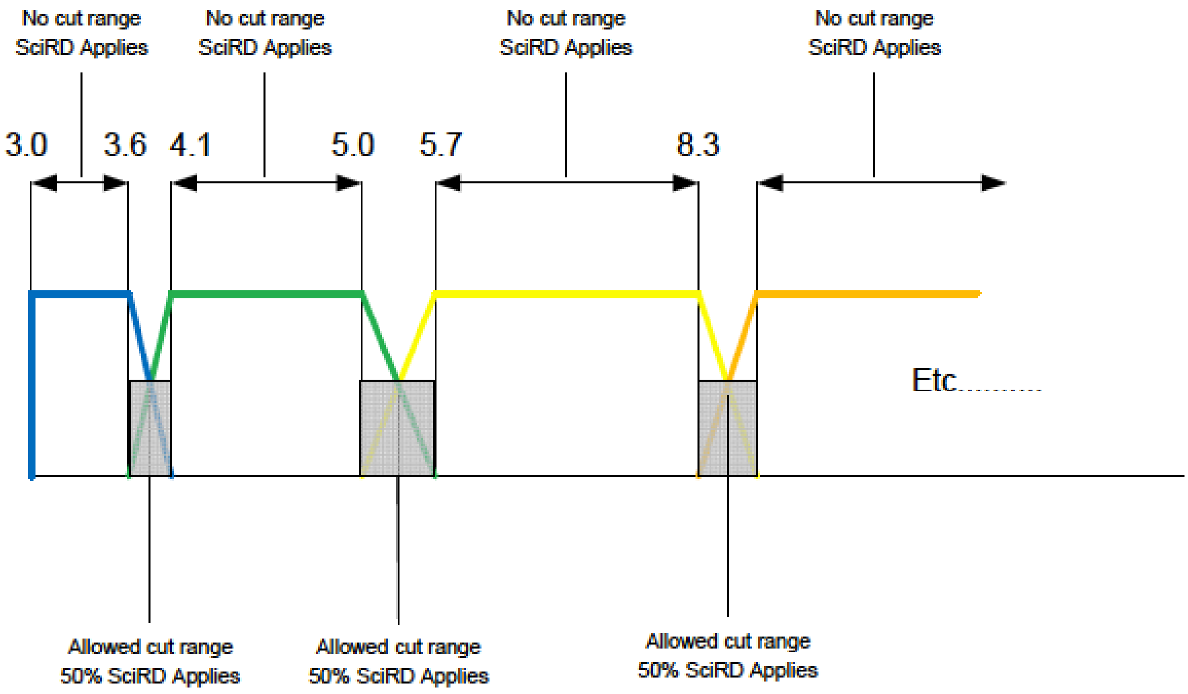

Figure 3-3: A pictorial illustration of how cuts in the EChO waveband should be made. Wavelengths are given in microns

G-SCI-031: Division of the EChO band should be made such that no cut falls in the following intervals (inclusive):

- 1.95 - 2.10 micron (H_3+); 2.50 - 2.70 micron (H_2S); 2.90 - 3.10 micron ($HCN+C_2H_6$);
- 3.30 - 3.50 micron (C_2H_6); 3.85 - 4.10 micron (H_3+); 4.10 - 4.40 micron (PH_3+H_2S)

G-SCI-031a: Division of the EChO waveband shall be made such that no cut falls in the wavelength interval 13.50 - 16.00 micron

The notes specifying the performance requirements in-band as well as in the transition band as detailed in R-SCI-30 hold for G-SCI-031 and G-SCI-031a also. It is recognized that there are large number of features associated with goal species and that it may not be possible to avoid placing a cut within the corresponding intervals for features that fall at wavelengths outside the interval given in G-SCI-031a. Wavelengths of these goal species features, along with their intervals, have been included for completeness.

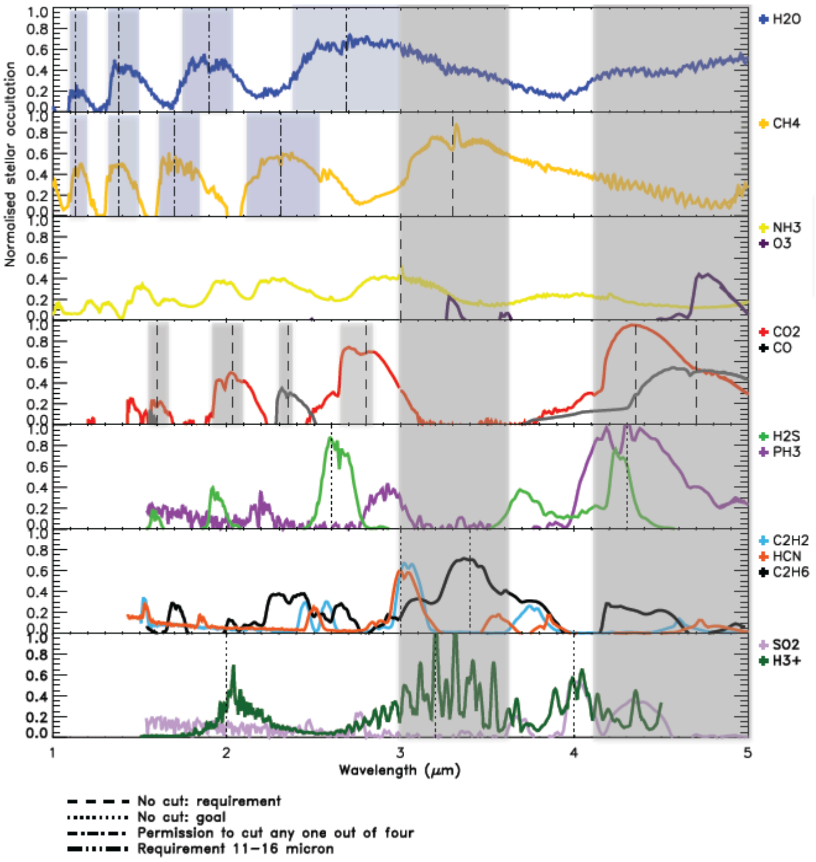

Figure 3-4: Plots of the normalised expected signal from a model exoplanet atmosphere observed during stellar occultation, as a function of wavelength for key and goal species

Note: Vertical lines indicate the centres of spectral features (see legend for further detail). Lightly shaded bands indicate the intervals around a spectra feature in which a cut must not fall, as specified in R-SCI-030. In the case of H_2O and CH_4 where necessary a cut can be made in any one of the four shaded (light blue) intervals indicated for each molecule.

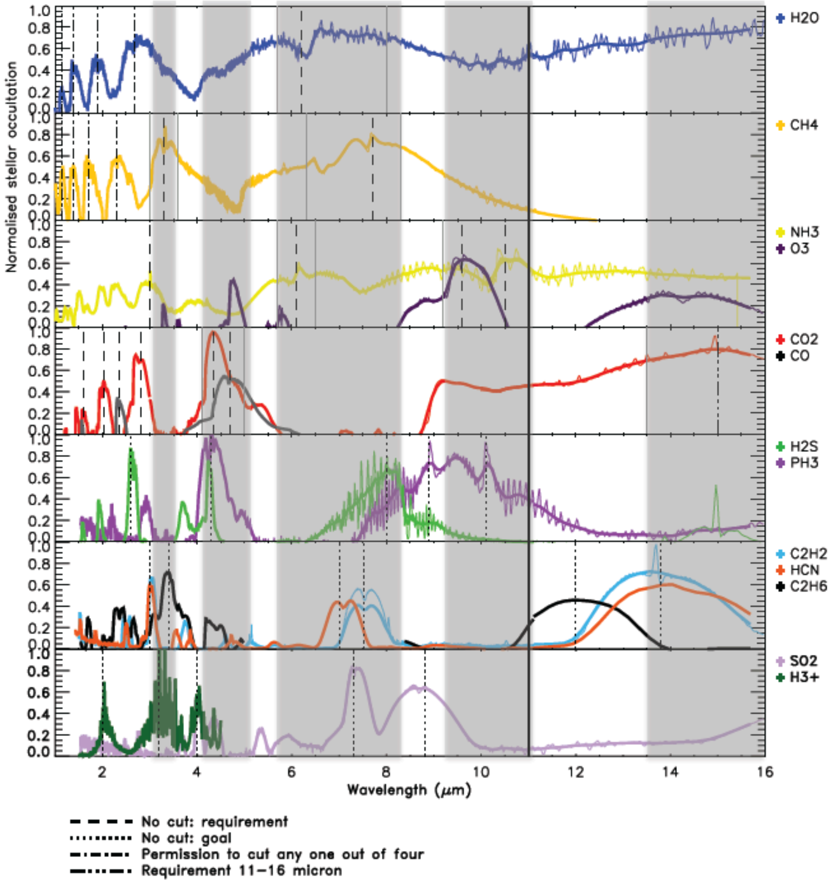

Figure 3-5: As Figure 3-2 above for wavelengths of 3 - 16 microns

R-SCI-032: The overlap between spectral channels shall be ≥ 5 resolution elements for λ <5 micron (assuming R≥300) and ≥ 1 resolution element for λ>5 micron (assuming R≥30).

R-SCI-033: A minimum of 80% of the in-channel average performance is required for each resolution element.

3.2.3 Resolving power

R-SCI-040: EChO shall have a resolving power of R ≥ 300 for λ <5 micron and R≥ 30 for λ >5 micron.

Note: $R=\lambda/\Delta\lambda$ where $\Delta\lambda \geqslant$FWHM of the monochromatic system PSF.

G-SCI-050: EChO should have a resolving power of R ≥ 300 over the wavelength range specified in G-SCI-020.

3.2.4 Photometric stability

R-SCI-080: Only photometric variations within the frequency band of $2.8\text{x}10^{-5}$ Hz to 3.7 mHz shall be included in the overall noise budget which is set by requirements R-SCI-055, R-SCI-056, R-SCI-057 and R-SCI-059

Note: R-SCI-080 shall apply post-processing, and needs to take into account intrinsic stellar variability in the corresponding frequency band

G-SCI-085: Only photometric variations within the frequency band of $3.8x10^{-6}$ Hz to 16mHz should be included in the overall noise budget which is set by requirements R-SCI-055, R-SCI-056, R-SCI-057 and R-SCI-059

Note: Achieving G-SCI-085 after post-processing needs to take into account intrinsic stellar variability in the corresponding frequency band.

3.2.5 EChO core sample and observational strategy

R-SCI-001: EChO shall observe a core sample of > 100 exoplanet targets, known as the EChO core survey.

G-SCI-002: EChO should observe a core sample of > 200 exoplanet targets, known as the EChO core survey.

R-SCI-003: The mission design shall allow observations to be carried out of a wide range of planetary sizes from gas giants to super-Earths. These will have a range of temperatures from hot (up to 3000K) to temperate (350 K) and are found orbiting a range of stellar types and magnitudes from cool M-dwarfs to hot F-stars. The mission design shall encompass both the faintest and brightest expected targets. Nominally these are exemplified by the systems GJ1214 (faint cold dwarf star) and 55Cnc (bright G star).

R-SCI-004: The survey will be divided into three survey modes: the names, characteristics and description of the each of the modes are given in Table 3-2.

The EChO Core Sample		
Name of survey mode	**Characteristics**	**Description**
Chemical Census	Survey	Exploring the chemical diversity of exoplanets. Average SNR~5: R=50 for λ<5 micron; R=30 for λ >5 micron.
Origins	Deep survey	Understanding the origin of exoplanet diversity. Average SNR~10: R=100 for λ <5 micron; R=30 for λ >5 micron.
Exo-meteo/mapping, Rosetta Stones	Ultra-deep survey	For a small sample of the very brightest targets: study of weather through repeated observations, 2D-3D mapping, phase curves + observations of a small number of high SNR benchmark transmission/emission spectra, up to the native resolution of the EChO instrument.

Table 3-2: A summary of the survey modes that make up the EChO core sample

R-SCI-005: More than 25 (TBC) of the planets observed in Chemical Census mode shall be observed in Origins mode.

G-SCI-006: More than 25% (TBC) of the planets observed in Chemical Census mode should be observed in Origins mode.

R-SCI-007: More than 10 (TBC) of the planets observed in Chemical Census mode shall be observed in Exo-Meteo/Maps/Rosetta Stone mode.

G-SCI-008: More than 10% (TBC) of the planets observed in Chemical Census mode should be observed in Exo-Meteo/Maps/Rosetta Stone mode.

Note: The EChO Project Scientist shall ensure that a list of targets is defined that meets the requirements expressed in this document and which can be observed within the mission lifetime. The list shall be based on the Design Reference Mission document [AD-11] that shall, in turn, be derived in consultation with the Community and Advisory Structure.

R-SCI-055: The average SNR achieved per spectral element for targets defined in the Chemical Census shall either be ≥5 at R=50 averaged over the 2 micron ≤ λ ≤ 5 micron wavelength interval, or shall be ≥5 at R=30 over the 5 micron < λ ≤ 11 micron wavelength: whichever is less demanding. The planet shall be observed in primary transit or occultation/eclipse, whichever is less demanding.

R-SCI-056: The average SNR achieved per spectral element for targets defined in the Origins Survey shall be either ≥10 at R=100 averaged over the 2 micron ≤ λ ≤ 5 micron wavelength interval, or ≥10 at R=30 over the 5 micron < λ ≤ 11 micron wavelength interval: whichever is less demanding. The planet shall be observed in primary transit and occultation/eclipse.

R-SCI-057: The average SNR achieved per spectral element for targets defined in the Rosetta Stone shall either be ≥20 at R=300 averaged over the 1 micron ≤ λ ≤ 5 micron wavelength interval, or shall be ≥20 at R=30 over the 5 micron <□λ ≤ 11 micron wavelength: whichever is less demanding. The planet shall be observed in primary transit or occultation/eclipse, which ever is less demanding.

G-SCI-058: The average SNR achieved per spectral element for targets defined in the Rosetta Stone shall either be ≥20 at R=300 averaged over the 1 micron ≤ λ ≤ 5 micron wavelength interval, or shall be ≥20 at R=30 over the 5 micron < λ ≤ 11 micron wavelength: whichever is less demanding. The planet shall be observed in primary transit and occultation/eclipse.

R-SCI-059: For all targets observed in primary transit the average SNR on the stellar signal per spectral resolution element at R=300 in the 0.55 – 1.0 micron waveband shall be ≥ 200 per transit event.

R-SCI-060: All targets in the target list shall be observed with at least 90% of the SNR defined in R-SCI-055 and R-SCI-056

G-SCI-065: All targets in the target list should be observed with at least 95% of the SNR defined in R-SCI-055 and R-SCI-056

R-SCI-070: Neighbouring sources that fall within the field of view of target stars shall make a negligible contribution to the noise budget. Observation of stars with neighbouring sources that make a larger contribution is TBD.

4 PAYLOAD SYSTEM DESIGN AND ARCHITECTURE

4.1 ARCHITECTURE TRADE STUDY AND OUTCOME

As an early part of this assessment study a detailed trade has been carried out to optimise the overall architecture. This has been run in conjunction with the other detailed trades conducted in the initial phase of the study on design aspects such as the channel division wavelengths and method, the mechanical architecture, the detector selection and others. This trade study is documented in detail in ECHO-TN-0001-RAL, [RD2], a summary of the trade methodology and outcome is given below.

The trade study considered the design options from a number of viewpoints relevant to optimising the systems engineering and project management of the overall payload instrument. These were:

- Scientific performance and Technical resource impacts, for example on mass, thermal budgets, power requirements;
    - The impact of the design option on the performance of the instrument against both scientific and technical requirements was assessed
- Interface definitions and complexity between payload modules and subsystems;
    - A detailed interface matrix was drawn up for each design option and the complexity of the interfaces between the items was assessed.
- Impact of architecture on module, instrument and spacecraft assembly, integration and verification (AIV) activities;
- Architecture impact on consortium organisation and management and estimated programmatic impacts.

In each case a quantitative assessment of the design was made whereby low marks indicate an advantageous set of properties. These items were then weighted and balanced and used to assess the relative strength of the possible alternative architectures.

The study considered 5 design alternative architectures for study, these were:

- Design baseline from the original proposal (November 2011).
- Option 1, the “Evolved Baseline” whereby the instrument architect has evolved in incremental steps from the initial baseline through the other detailed design trades covered elsewhere in this document.
- Option 2, the combination of the two MWIR and LWIR modules onto a single detector. This option would either require a very wide band spectrometer to cover this extended wavelength range, or a complex optical design to put multiple spectrometer paths onto a shared detector surface.
- Option 3, the use of the VNIR as FGS. In this option some unused light from the VNIR (for example the zeroth order from a diffraction grating) would be fed onto a detector as used as the feedback to close the loop on the FGS attitude control system.
- Option 4, the combination of the Instrument Optical Bench (IOB) and Telescope Optical Bench (TOB) into a single entity. This mass saving design would combine the support structures for the instrument hardware and the telescope onto a single entity.

The detailed assessment of each option is shown in detail in [RD2]. The summary results table is shown below.

Design	Individual Scores				Total (/ 100)
	Interface Complexity (/ 30)	Performance & Resources (/ 40)	AIV Activities (/ 10)	Programmatic (/ 10)	
Baseline	30.0	28.8	7.5	7.5	73.8
Option 1, Evolved Baseline	**28.0**	**22.9**	**4.5**	**6.0**	**61.4**
Option 2, MWIR + LWIR	25.4	24.1	10.5	10.5	70.5
Option 3, VNIR as FGS	26.5	26.5	10.5	6.0	69.5
Option 4, IOB / TOB Combo	29.3	24.1	12.0	12.0	77.4

Table 4-1: Overall Trade Study Weighted Scores

The conclusion of this study is that the evolved baseline design is the preferred choice of the possible architectures studied here. This was therefore selected prior to the Mid-Term Review and has remained a stable baseline for the last 12 months.

4.2 BASELINE ARCHITECTURE

The current baseline architecture is shown in detail in [RD1]. This is reproduced on the next page as a functional block diagram (Figure 4-2).

It incorporates six channels divided into four modules, mounted on a single Instrument Optical Bench (IOB), amongst which the field of view is divided by a series of dichroics.

There are two fibre-fed VNIR channels (one visible and one near-infrared) covering the 0.4-2.47μm wavelength range, one SWIR channel covering the 2.42-5.45μm range, two MWIR channels covering the 5.05-11.5μm range (5.05-8.65μm and 8.25-11.5μm) and a LWIR channel covering the 11–16μm range (which is a goal). The two MWIR channels are imaged on a single focal plane. The channel boundaries were chosen in such a way as to avoid potential weaknesses in the optical performances of the dichroic elements, and to ensure overlapping of spectral ranges between modules for full wavelength coverage and cross-calibration. The split between the channels is illustrated schematically in Figure 4-1.

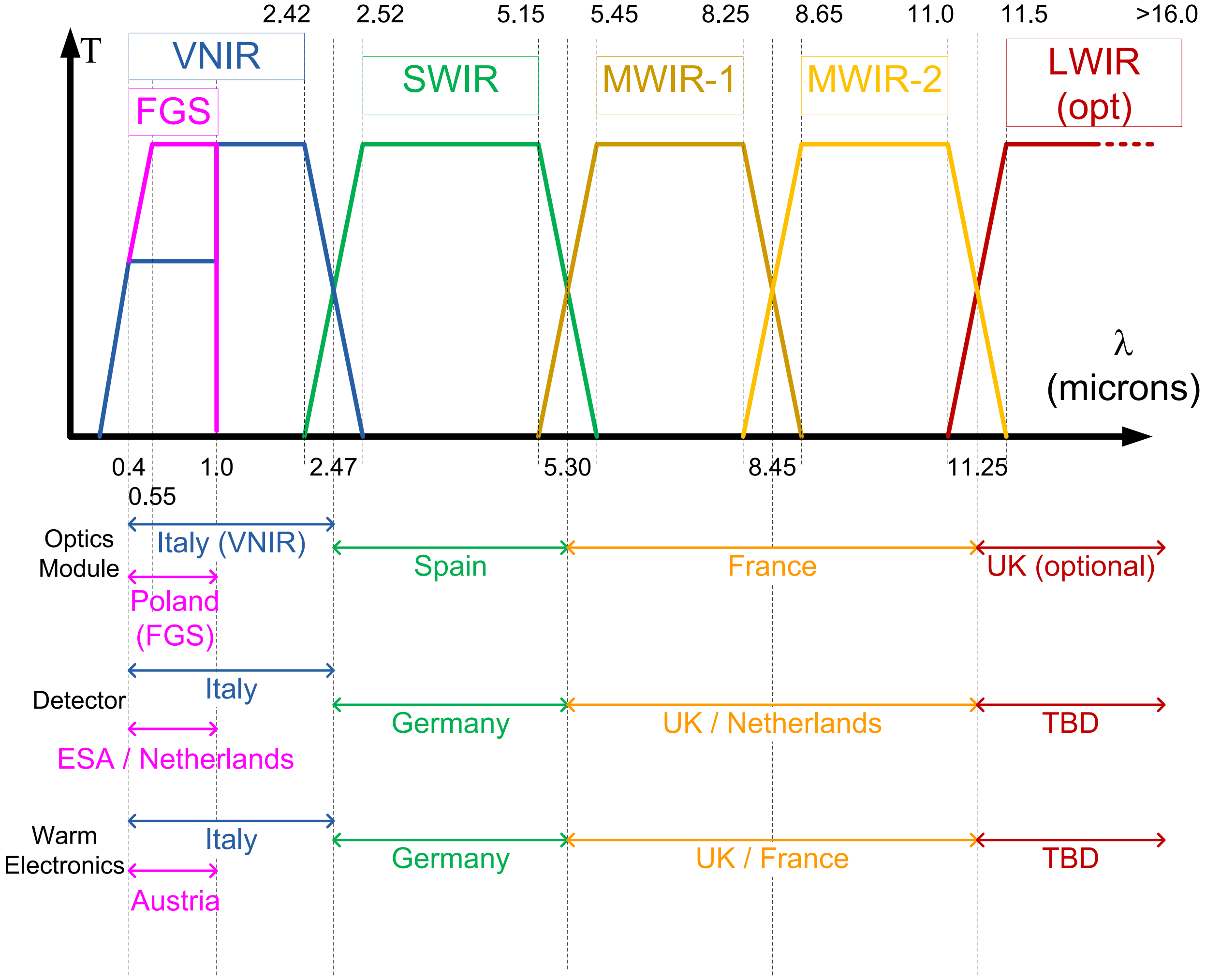

Figure 4-1: EChO Payload Instrument Channel Division

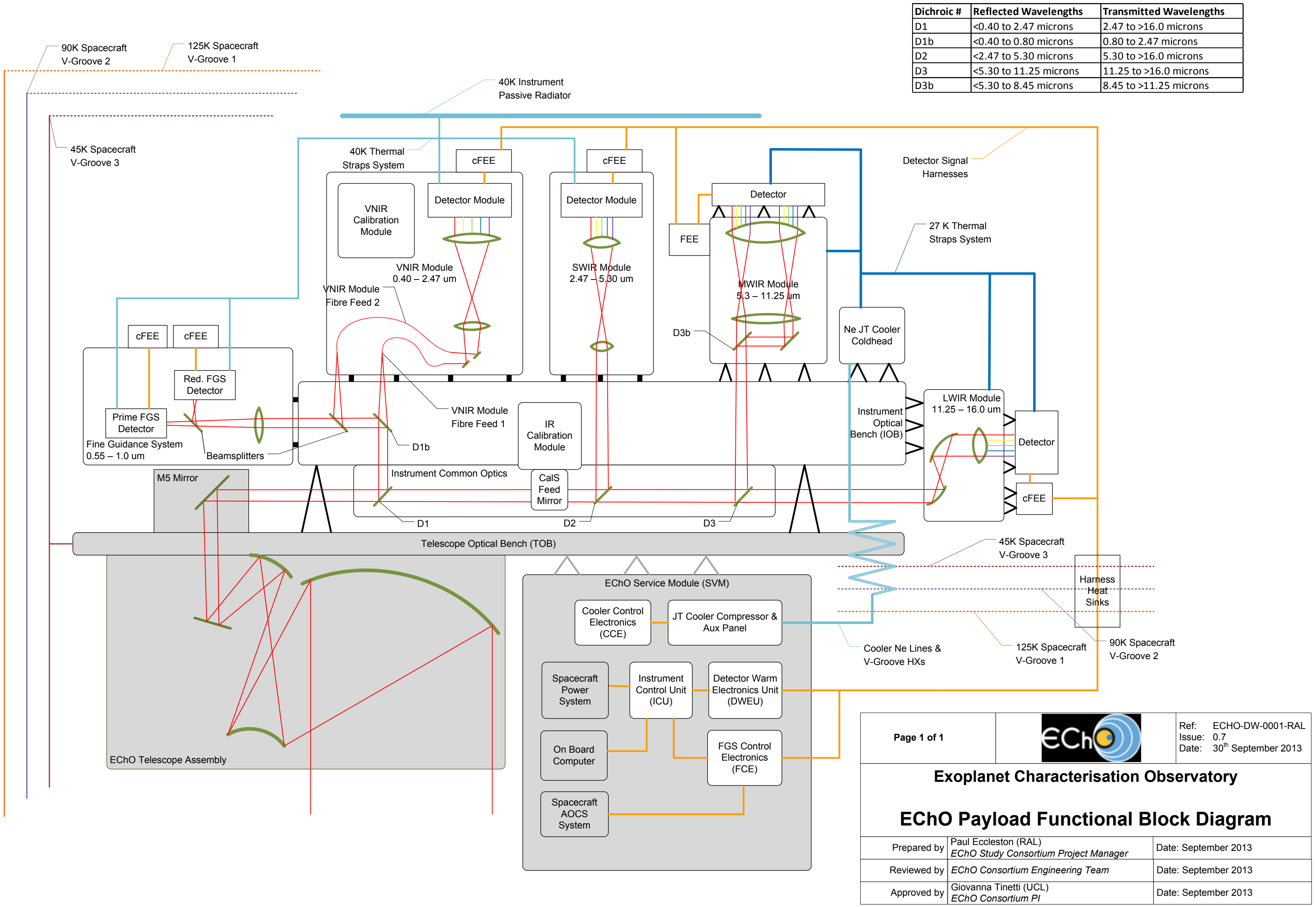

Dichroic #	Reflected Wavelengths	Transmitted Wavelengths
D1	<0.40 to 2.47 microns	2.47 to >16.0 microns
D1b	<0.40 to 0.80 microns	0.80 to 2.47 microns
D2	<2.47 to 5.30 microns	5.30 to >16.0 microns
D3	<5.30 to 11.25 microns	11.25 to >16.0 microns
D3b	<5.30 to 8.45 microns	8.45 to >11.25 microns

Page 1 of 1		Ref: ECHO-DW-0001-RAL Issue: 0.7 Date: 30th September 2013

Exoplanet Characterisation Observatory

EChO Payload Functional Block Diagram

Prepared by	Paul Eccleston (RAL) *EChO Study Consortium Project Manager*	Date: September 2013
Reviewed by	*EChO Consortium Engineering Team*	Date: September 2013
Approved by	Giovanna Tinetti (UCL) *EChO Consortium PI*	Date: September 2013

Figure 4-2: EChO Payload Functional Block Diagram

4.3 RESPONSIBILITIES AND DESIGN PHILOSOPHY

4.3.1 Modularity

The baseline design architecture has been selected to maintain a high degree of modularity in the design. This helps both technically and programmatically in allowing independent development of the channel module designs and in giving the maximum flexibility for future changes. To this end the optical design of the modules is decoupled from one another, and a common optical interface has been defined for all modules.

A common optical bench (separate from the structures of the individual modules) has been selected as the design baseline. Responsibility for this item is believed to best rest with the instrument team due to the interface management and the impact on AIV. The assumption of responsibility for the IOB by the instrument systems team allows the instrument to be built, assembled, aligned and tested as a unit and pre-calibrated prior to delivery to ESA. The internal co-alignment of the modules (critical to the success of the mission due to the shared field of view) can then be assured and checked at the earliest possible stage.

4.3.2 Material Selection

The design baseline is that all of the cryogenic components of the payload architecture are manufactured from a common material. This ensures that the design has a matched CTE, allowing warm alignment of the instrument to proceed, with a high degree of confidence that this will be maintained when cooled to operating temperatures. All reflective optical elements in the design are also assumed to be manufactured from Aluminium for the same reason. This builds on the significant design heritage within Europe of building all Aluminium space instruments for cryogenic operation such as Herschel SPIRE & PACS and JWST MIRI. Building in Aluminium also provides a robust design approach with minimum technical risk. Details of the trade-off conducted are contained in [RD33].

4.4 NOISE BUDGET

The detailed noise budget for the EChO Payload Instrument is contained in [RD45].

In the past, general-purpose, space-based instruments have suffered from a high level of systematic error. EChO will be an instrument that performs time series spectroscopy with unprecedented photometric stability from the visible to the mid-IR, simultaneously.

The total noise budget is divided into a number of different components, as shown in Table 4-2.

Noise Type	Noise Source
Detector Noise	Detector Dark Current Noise
	Detector Readout Noise
Thermal Noise	Emission from telescope and common optics Emission from Dichroic and beam splitter surfaces Emission from Module enclosure
Astronomical Noise	Photon noise arising from the target Photon noise arising from local zodi emission
Pointing Jtter	RPE and PRE effects on the position and shape of the detector sampled PSF

Table 4-2: Noise sources

The radiometric noise from these sources has been determined using EChOSim for a number of different conditions corresponding to the faintest and brightest target required to be observable with EChO, as expressed in R-PERF-090 and R-PERF-110, respectively, of the MRD.

The system noise (all noise sources in Table 4-2 with exception of the astronomical noise sources) can be compared to the total astrophysical photon noise (target source + zodi) to verify compliance with R-PERF-350. This is discussed in details in [RD45]. Here we show how the photon noise of the brightest (and faintest) source required to be observable with EChO (Figure 4-3 and Figure 4-4) compare with some of the system noise components, and we refer to [RD45] for a quantitative and more exhaustive breakdown and contribution to the total system noise level (R-PERF-350 in the MRD).

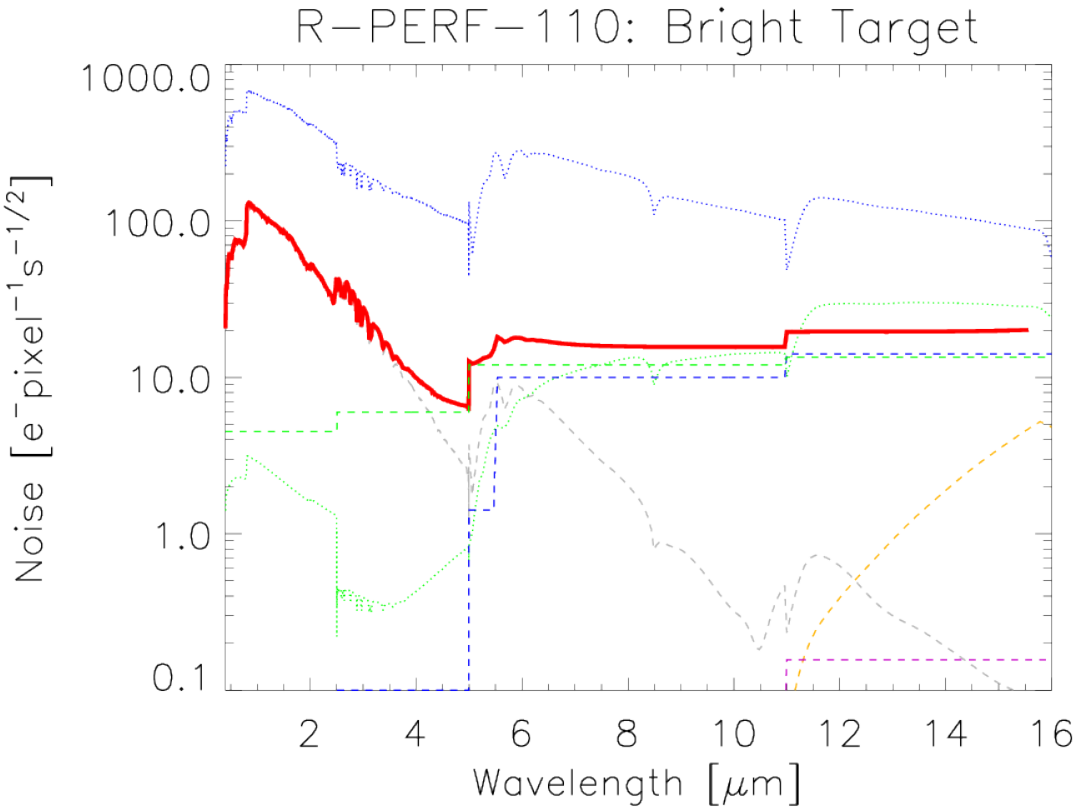

Figure 4-3: Noise analysis for the brightest target to be observed by EChO. Detectors are read following-up-the-ramp, with 12 non-destructive readings, corresponding to an integration time of 1.5s. The photon noise of the target and that of local zodi emission are shown by the dotted blue and green lines, respectively. The total system noise is shown by the red solid line and is obtained by summing in quadrature all noise components (but zodi and photon noise). The individual noise components contributing to the system noise are estimated using EChOSim simulations, and are shown in the plot: readout noise (dashed green); dark current noise (dashed blue); thermal emission from instrument enclosures (dashed violet); thermal emission from optical surfaces (dashed yellow); post-processing RPE+PRE photometric error (dashed grey). All EChO required channels (VNIR, SWIR, MWIR) are working at the limit of the photon noise arising from astrophysical sources (star +zodi). The EChO goal LWIR channel is also astrophysical photon-noise limited.

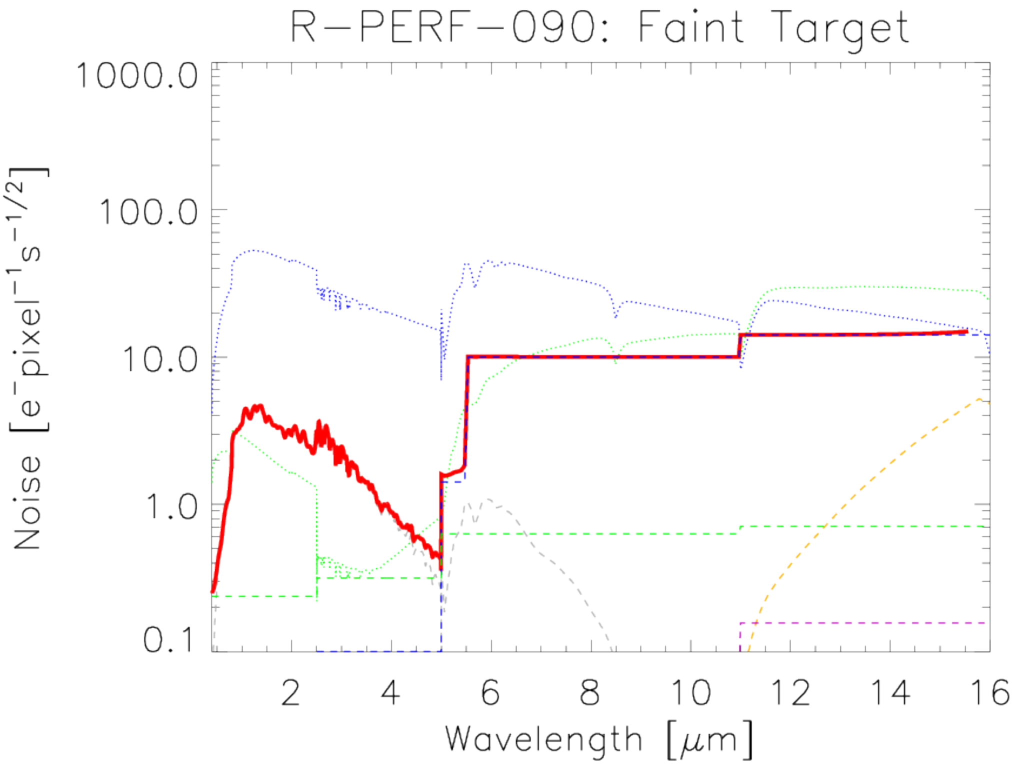

Figure 4-4: Noise analysis for the faintest target to be observed by EChO. Detectors are read following-up-the-ramp, with 30 non-destructive readings, corresponding to an integration time of 240s. The photon noise of the target and that of local zodi emission are shown by the dotted blue and green lines, respectively. The total system noise is shown by the red solid line line and is obtained by summing in quadrature all noise components (but zodi and photon noise).. The individual noise components contributing to the system noise are estimated using EChOSim simulations, and are shown in the plot: readout noise (dashed green); dark current noise (dashed blue); thermal emission from instrument enclosures (dashed violet); thermal emission from optical surfaces (dashed yellow); post-processing RPE+PRE photometric error (dashed grey). All EChO required channels (VNIR, SWIR, MWIR) are working at the limit of the photon noise arising from astrophysical sources (star +zodi). The EChO goal LWIR channel is also astrophysical photon-noise limited

4.5 PHOTOMETRIC STABILITY BUDGET

The photometric stability of the EChO system is critical to achieving our science goals. We discuss many of the aspects of the system performance and calibration that contribute to the photometric stability in sections 11 and 19. However we recognise that the pointing and thermal stability of the spacecraft and payload are particularly critical in establishing the required stability and have significant impact on the design and implementation of the spacecraft and telescope. In the framework of EChOSim (see section 13) we have therefore comprehensively modelled the performance of EChO. This allows the assessment of all aspects of the payload and satellite stability in order, among other things, to establish the optimum observing and calibration programme for the mission. This has been a complex task requiring the knowledge and resources of the scientific and technical members of the consortium and ESA.

The photometric stability of the instrument throughout consecutive observations lasting several to tens of hours is mainly governed by the following factors:

i. Pointing stability of the telescope quantified in terms of mean performance error (MPE), performance reproducibility error (PRE) and relative performance error (RPE) for the different AOCS solutions considered in the study. These pointing drifts manifest themselves in the observed data product via two mechanisms: 1) the drifting of the spectrum along the spectral axis of the detector, from here on referred to as ‘spectral jitter’; 2) the drift of the spectrum along the spatial direction (or ‘spatial jitter’). The effect of jitter on the observed time series is the introduction of correlated noise, characterized by the power-spectrum of the telescope pointing. The amplitude of the resultant photometric scatter depends on the amount of spectral/spatial displacement of the spectrum, the PSF of the instruments, the detector intra-pixel response and the amplitude of the inter-pixel variations.

ii. Thermal stability of the optical-bench and mirrors: Thermal emission of the instrument can be regarded as negligible for most wavelengths, but become observable at wavelengths beyond 12µm. Whilst thermal emission is a source of photon noise, temperature fluctuations constitute a source of correlated noise, which places constraints on the allowed temperature fluctuations over the duration of a transit/eclipse event.

iii. Stellar noise and other temporal noise sources: whilst beyond the control of the instrument design, noise is an important source of temporal instability in exoplanetary time series measurements. This is particularly true for M dwarf host stars as well as many non-main sequence stars. Correction mechanisms of said fluctuations must and will be an integral part of the data analysis of EChO - see section 11.4.

4.5.1 Calibration and coping mechanisms

4.5.1.1 Frequency bands of interest

The observing strategy of EChO is that of time resolved spectroscopy. By obtaining series of time consecutive spectra EChO will trace the transit/eclipse event of an exoplanet through time, yielding a lightcurve of the transit/eclipse for every single spectral resolution element of the instruments. Figure 4-5 (a) shows an example of a secondary eclipse of a typical hot-Jupiter planet. Figure 4-5 (b) shows the signal observed by EChO over the duration of 6 planetary orbits of a hot-Jupiter. From these figures it can easily be seen that time-correlated noise has the greatest impact on the retrieved science at temporal variations frequencies comparable to those of the transit/eclipse event, or a multiple thereof. Figure 4-5 (c) shows the frequency domain representation of Figure 4-5 (b) given a variety of orbital periods. It is clear that the desired signal is contained in discrete frequencies and their respective overtones. It is also apparent that frequency ranges beyond these shown in Figure 4-5 (c) are of no concern to the science objective and can safely be filtered out using pass-band filters without impairing the shape or amplitude of the lightcurve feature. This leads to the concept of 'crucial frequency bands' within the photometric stability must be kept at a level defined in the MRD R-PERF-290 to ensure the success of the mission.

Given the range of transit periods observed and the goal of accurate ingress and egress mapping, we find the 'crucial frequency band' to be from 1.9×10^{-4} to ~1.7×10^{-3} Hz (compatible with R-SCI-080), outside of which slow moving trends and high-frequency noise can effectively be filtered. The overall critical frequency band for EChO is determined by the longest observation expected and the need to Nyquist-sample the highest expected frequencies. It is specified in R-SCI-080 as between 2.8×10^{-5} Hz and 4×10^{-3} Hz.

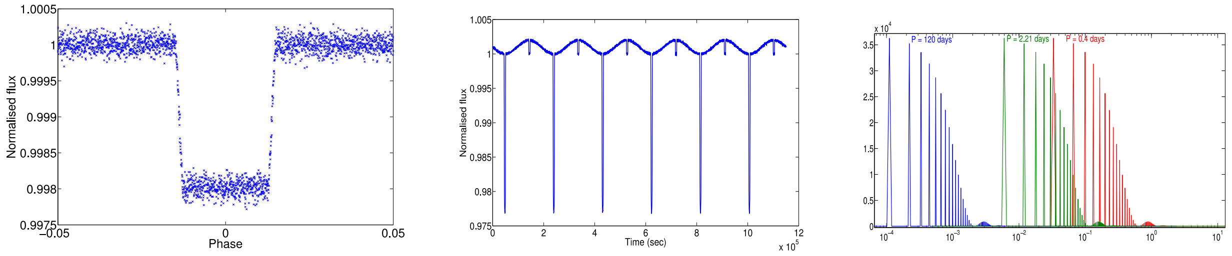

Figure 4-5: (a) Left: Secondary eclipse lightcurve of a hot-Jupiter type exoplanet with eclipse duration of 720min. Noise at 10^{-4} level was added. (b) Centre:Time series of 6 orbits of a hot-Jupiter (akin to HD189733b). The deep troughs are limb-darkened transits, smaller troughs are secondary eclipses and sinusoidal variations are due to the planetary phase curve as the planetary day-side rotates in and out of view. White noise of the level of 10-4 was added. (c) Right: Power spectra of time series shown in [a] for different orbital periods. Blue: Period = 120 days, Green = 2.21 days (akin to HD189733b), Red = 0.4 days. The sensitive frequency range extends from 1.9×10^{-4}- 1.7×10^{-3} Hz.

4.5.1.2 Spectral Jitter

If the effect of the satellite pointing drift is left uncorrected it can result in photometric instabilities of the order of 10^{-3} to 10^{-4}, severely impairing the quality of the final science result. This effect is particularly significant in areas of steep flux gradients whether due to stellar lines or black-body variations. An example of spectral jitter is provided in Figure 4-6 (a) for time consecutive spectroscopic observations covering the secondary eclipse of HD189733b (Waldmann et al. 2012). In this example the observed spectra are shifted with respect to each other (Figure 4-6) which constitutes the main source of systematic noise along the time (y) axis. In this example, the individual spectra were re-sampled onto a common wavelength grid by centroid-fitting thin stellar and/or telluric absorption lines of the observed spectrum.

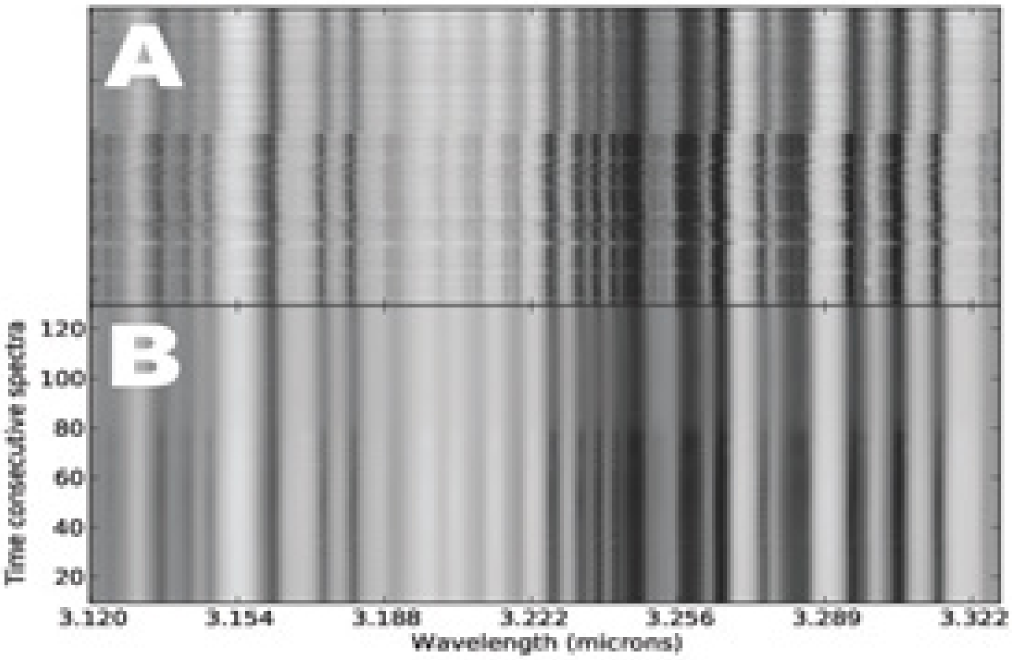

Figure 4-6: Example of time consecutive ground-based observations using a spectrograph (IRTF/SpeX). Each pixel row constitutes an individual spectrum. Dark lines are telluric and stellar absorption lines. Plot A: Observed spectra are shifted with respect to each other due to spectral jitter. Plot B: Spectra of plot A are resampled to a common grid. (Waldmann et al. 2012).

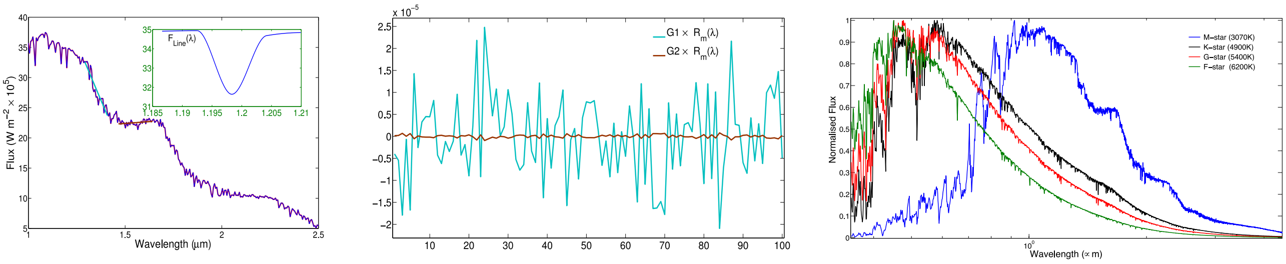

Figure 4-7: (a) Left: Spectrum of a solar analogue star between 1.0 and 2.5 µm. Red: spectrum at R = 300; Blue: interpolated spectrum; Inset: spectral line used to fit for the wavelength jitter; G1: flux gradient of stellar 'black-body' at 1.29 - 1.40 µm; G2: flux gradient at1.46 – 1.64 µm. (b) Centre: Fraction of residual fitting flux Ferr over the total flux of the star Fstar for both spectral flux gradients shown in [a]. G1 = -760 and G2 = 24 Wm^{-2}nm^{-1} . (c) Right:Phoenix stellar model spectra as used by EChOsim for M, K, G and F stars typically considered by EChO at resolution of R = 300. Note the plethora of suitable absorption lines in all these spectra, allowing for an accurate wavelength and spectral jitter calibration.

To estimate the feasibility of this approach for spectra observed by EChO, we computed Phoenix model spectra of a solar analogue at resolution of R ~ 300 and simulated consecutive observations with spectral jitter. The post correction noise is now given by the accuracy with which one can determine the centroids of thin absorption lines as well as the spectral gradient of the individual spectrum. An example spectrum is given in Figure 4-7 (a). The fitting residual is given by

$$R_m(\lambda) = \sqrt{\Delta_m^2(\lambda) - C_m^2(\lambda)}$$

where$\Delta_m^2(\lambda)$ is the spectral jitter for the mth spectrum and $C_m^2(\lambda)$ is the calculated centroid position.

$$F_{err}(\lambda) = G(R_m(\lambda) - \overline{R_m}(\lambda))$$

where$F_{err}(\lambda)$ are the counts due to imperfect jitter corrections and G is the local spectral gradient: $G = dF_{star}(\lambda)/d\lambda$.

The fitting residual can now be translated to a total flux error. Taking the ratio F_{err}/F_{star} we can derive the relative error due to residual jitter, Figure 4-7 (b). The flux error is dependent on the local stellar flux gradient. From Figure 4-7 (a), we derive two gradients: G1 = -760 $Wm^{-2}nm^{-1}$and G2 = 24 $Wm^{-2}nm^{-1}$.

For these two gradients, Figure 4-7 (b)shows that the relative flux error lies between 10^{-6}~ 2 × 10^{-5}.

Figure 4-7 (c) shows Phoenix stellar model spectra of M, K, G and F stars at a resolution of R ~300. All these spectra contain a significant number of suitable absorption lines, guaranteeing an adequate wavelength and spectral jitter calibration.

4.5.1.3 Spatial Jitter

To investigate the effect of spatial jitter on the time series observed by EChO, we performed extensive tests using the EChOsim simulator (see section 13).

Three proposed AOCS solutions with different predicted RPE and PRE performances have been studied. The telescope pointing jitter translates in photometric uncertainties arising from a change in shape and position of the instrument PSF over time, coupled to realistic intra and inter-pixel detector responses, as well as slit losses.

Simulations have been performed to investigate the implications of each solution on the photometric error budget after post-processing. This has required the implementation of an advanced data reduction pipeline which, coupled to the EChOSim output, is able to take full advantage of housekeeping information from, for instance, the FGS.

The assumptions, simulations and analysis are described in [RD30], where compliance of AOCS solution with mission requirements are discussed.

4.5.1.4 Thermal Stability

Using EChOSim, we have also investigated the impact of thermal emissions fluctuations of the optics on the photometric stability of the reconstructed spectrum. Whilst thermal emissions are not directly a problem to photometric stability (source of photon noise, and therefore white), they pose constraints on the temperature fluctuations (usually Brownian noise) allowed over the time span of an exoplanetary transit/eclipse in the reddest wavelengths. Using EChOSim simulations, we can derive the amplitude of the temperature fluctuation (for a given mean temperature) that would induce a signal comparable to an exoplanetary eclipse. For this study we used secondary eclipse spectrum of 55 cnc (R-PERF-090, brightest requirement), and GJ1214 (R-PERF-110, faint requirement). Figure 4-8 shows the result of the analysis which, we stress, does not impose a requirement on the physical stability of the temperature of the optics, but it does poses a constraint on the *precision* by which these temperature need to be monitored. As clearly shown in Figure 4-8, sub-K monitoring of relevant optical surfaces and instrument cavity are required only for the LWIR channel.

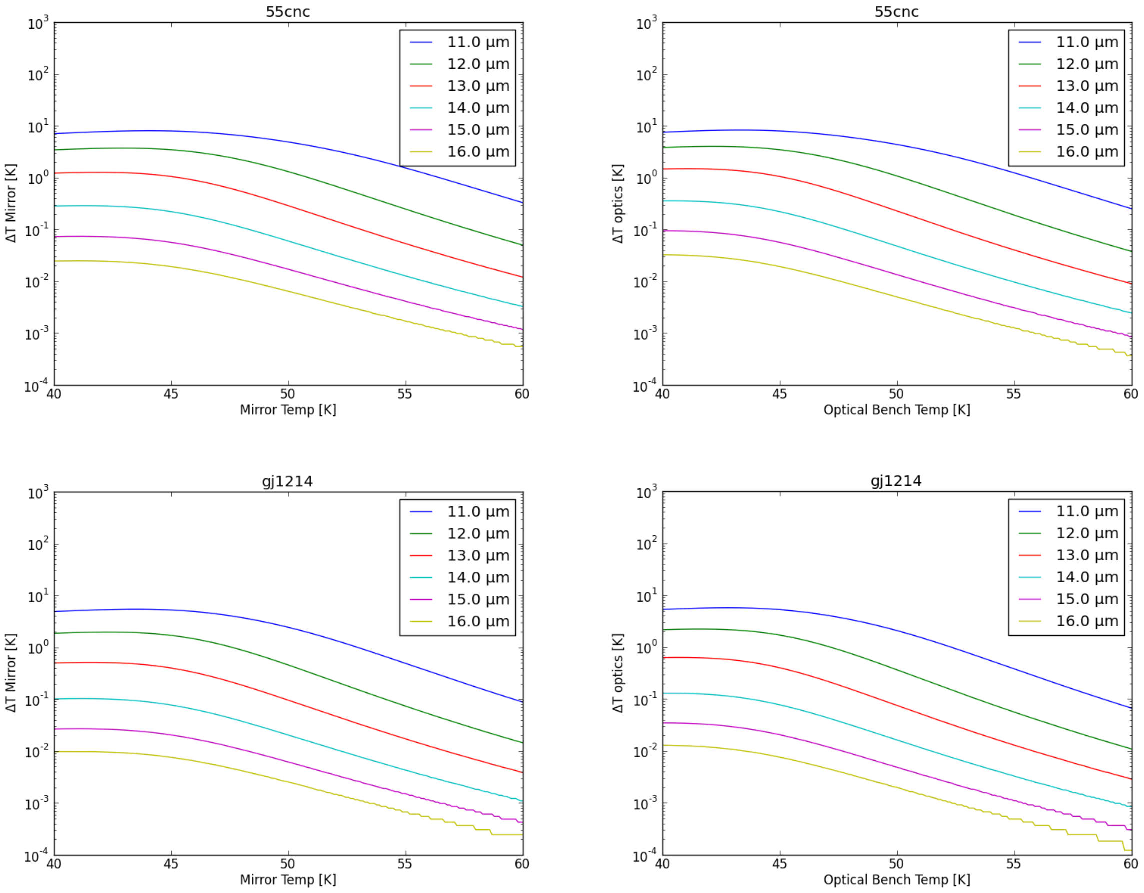

Figure 4-8: An assessment of the required temperature stability of the optics is conducted with EChOSim. On the y-axese of these plot is reported the temperature fluctuation giving rise to a signal equal to the depth in the light-curve of the observed target given in the panel titles. The temperature fluctuation of the telescope (ΔT_{Mirror}) or optical bench (ΔT_{optics}) are reported vs Mirror Temp or optical bench temperature, respectively. The analysis is carried for some relevant wavelength (from 11 to 16µm).

4.5.2 Required Pointing Stability Conclusions

The conclusion from the consortium study is that the specification for the pointing stability of the S/C platform should be consistent with the following requirements (which are captured in the EChO Payload Instrument EID-B):

- The RPE shall have a Power Spectral Density of ≤ 2.9 milli-arcsec/rt(Hz) (TBC) in the frequency range of 1 – 300 Hz and shall be ≤0.1 milli-arcsec/rt(Hz) above 300 Hz for the brightest targets (as defined by R-SCI-150)
    - Note: this is equivalent to an amplitude of ≤ 50 milli-arcsec RMS.
- The RPE shall have a Power Spectral Density of ≤ 7.5 milli-arcsec/rt(Hz) (TBC) in the frequency range of 1 – 300 Hz and shall be ≤0.1 milli-arcsec/rt(Hz) above 300 Hz for the faintest targets (as defined by R-SCI-120 & R-SCI-130)

  - Note: this is equivalent to an amplitude of ≤ 130 milli-arcsec RMS, or reaction wheels option 2 as defined to the consortium by ESA. Note that the rate of degradation of RPE for targets between the brightest and faintest will be defined in the next phase.
- The PRE shall have a Power Spectral Density of ≤ 317.0 milli-arcsec/rt(Hz) (TBC) in the frequency range of 0.028 – 4 mHz and shall be ≤ 1 milli-arcsec/rt(Hz) below 0.028 mHz
  - Note: this is equivalent to an amplitude of ≤ 20 milli-arcsec RMS. This requirement may be relaxed in subsequent stages as modelling of the de-correlation pipeline progresses

5 DETECTOR SYSTEMS

If the EChO mission had been started a few years ago, it is almost certain that the baseline detector selection would have been a CCD in the visible channel and US sourced detectors for all the IR channels – Mercury Cadmium Telluride (MCT) for 1 to ~5µm and Silicon Arsenide for the remainder. However there has been significant recent and on-going investment by ESA and some National Agencies/Institutes in European suppliers of Mercury Cadmium Telluride (MCT) based detectors. Although we do not repeat details here, the investments include ESA RFPs 6073 (large Format NIR), 7111 (Testing EChO Candidates) and 7201 (2D VLWIR for EChO) which are enhancing EChO specific capability in MCT Detectors. In addition there are related RFPs (6808 & 7328) for high background SWIR devices and the development of a European equivalent to the SIDECAR ASIC (RFP 6814) which add further to relevant European capability. Together these all form part of a larger ESA roadmap process which would long term give ESA more control/independence in mission design and reduced issues with ITAR. In the Assessment phase and the response to the Definition Phase AO in November 2012 we have reported both on these projects and on the complementary nationally funded activities.

In November 2012 the project elicited preliminary compliance data from the various potential suppliers against outline EChO detector requirements which confirmed the growing credibility of European suppliers. Those dialogues have continued in parallel with more detailed modelling and development of the requirements specification. One key outcome early on in the definition phase was the identification of an MCT detector with TRL 6 that worked up to 11 µm at an operating temperature of ~40K. This led to a change in instrument baseline with the expectation that we could have an all MCT solution with operating temperatures no lower than 25K. The big advantage of this is the simplification in the payload cooler by avoiding the risks associated with a 7K requirement.

5.1 NEW RFI TO INDUSTRY

During the early part of 2013, the EChO project established a Detector Systems Working Group to produce a co-ordinated approach to the specification of detector performance requirements for EChO. As well as Detector experts from several parties, the group also had representation from each of the channel design teams plus electronics, thermal and data/ground segment. The approach was initially on several fronts:

- first the group looked at the work done in the Mission Requirements Document (MRD) and in particular relating to noise performance and established a simple modelling tool that could allow us to vary detector parameters against the likely science targets and assess whether the goals and requirements set in the MRD could be met. This model was cross checked for consistentcy with the output of EChOSIM and eventually allowed EChOSIM to use more accurate detector data.
- the group established the options on physical parameters set by the instrument optical design – namely pixel size, number of pixels, focal plane size etc. The idea was that we should be flexible in accommodating existing manufacturer preferences for ROIC design
- we also reviewed options for control and data extraction in conjunction with the Electronics groups
- we established some ‘typical’ observing scenarios which would enable us to get a fair but realistic comparison between the potential suppliers
- we assessed other detector requirements on operability, radiation hardness, etc.
- we assessed thermal requirements and provided optional base temperatures
- we reviewed the existing data on known detectors and the latest ESA technology activities to ensure we were not asking for unreasonable performance
- we agreed a TRL requirement of 5 for the detector/ROIC/FEE which had to be demonstrated by the Instrument/System Requirements Review (currently early 2015)

Details of the crucial noise performance modelling are provided below. The full requirements were assembled into a formal RFI [RD35] that was released to Industry on 27 May 2013 and responses were gathered by early July. The following companies were issued with the RFI:

- in Europe: AIM, SELEX GALILEO (now SELEX-ES) and SOFRADIR (VIGO declined to participate)

- in the USA: Raytheon Vision Systems and Teledyne

Whilst the Suppliers were assessing their responses, the Detector Systems Working Group also agreed on criteria for making the Technical assessment of the responses. The Project Management Team made the final choice of baseline device based on additional factors such as price, availability of National Funding, Schedule etc.

The Technical Criteria, see ECHO-TN-0002-ATC [RD36] chosen to assess the Supplier inputs were divided into the following categories within which variable marks were awarded against a minimum requirement:-

- noise performance – measured against N_{min} (see later) for faint and bright targets
- compatibility of optical and thermal interfaces
- complexity of electrical interface to front end electronics
- operability – relating to read out modes and rates, handling cosmic ray events, cross talk, persistence, modulated transfer function, photo-responsivity non-uniformity.

In addition, the supplier response was also assessed against the TRL requirement and whether the proposed product already had the necessary requirement or the proposed TRL improvement plan was credible in the timeframe of the Instrument Requirements review.

5.2 ECHO DETECTOR NOISE PERFORMANCE REQUIREMENTS

The DSWG established a simple tool for comparing detector performance against the science requirements described in section 4 of the Mission Requirements Document and in particular the noise requirements of R-PERF-350 and G-PERF-351. These were arrived at via a process described in section 4 of the ESA EChO Radiometric Model Description [AD 5] which set a maximum noise (N_{min}) for detector noise plus a range of other payload related noises.

From the MRD the key noise requirement that the detectors must meet is defined in R-PERF-350:

$$Noise_{Total} \leq \sqrt{(N_0(\lambda, \Delta\lambda) + zodi) \times (1 + X) + N_{nim}}$$

Where N_0 is the input flux and *zodi* the zodiacal background as discussed later. In an ideal world the noise would be simply the square root of the sum of these two properties, i.e. the shot noise on the input flux. However, this is unrealistic and hence an X term was included as a scaling factor. Since this scaling factor is a proportionality constant, as the input flux drops to zero so would the allowed noise, which is unphysical - there will always be noise. Consequently the term N_{min} was introduced to accommodate this constant background noise. This has currently been set at a constant value of 200 el/s/spaxel.

The final IDL based tool essentially compares each suppliers' quoted performance against this performance requirement as described in section 5.5. The tool was also used however to help set the initial requirements in the RFI.

5.3 INPUT VALUES TO DETECTOR NOISE TOOL – THE MRD MODEL

The input flux used to calculate the detectors' performance is described in more detail in the MRD. The values used are shown in Figure 5-1 for the 'required' and the 'goal' objects for both faint and bright stars. Note that these are fluxes for *four* different star types, they are not simply requirements with associated goals. The light blue line indicates the Zodiacal background (Z). In the MRD it suggests that Z should be multiplied by a varying factor depending on the pointing direction relative to the plane of the solar system. An average value for the multiplying factor of 2.5 is used throughout (as recommended in the MRD).

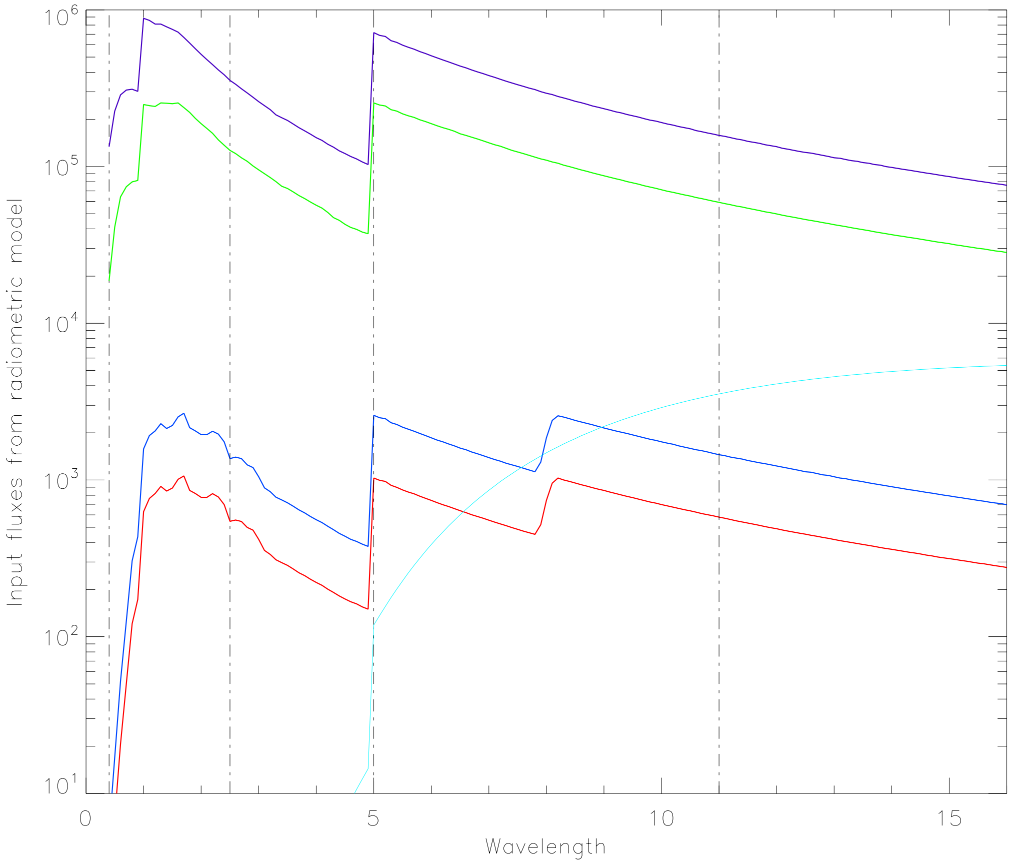

Figure 5-1: Flux for the four possible input objects defined in the MRD, given in electrons/sec. Blue and green are the "Required" faint and bright objects respectively, while red and purple are the equivalent "Goal" objects. The light blue line is the Zodiacal Background flux.

This flux is quoted in electrons per second as it includes an estimate of the quantum efficiency (QE) of the detectors for each channel. When calculating the performance of the proposed detectors, the QE is scaled accordingly.

A number of detector properties are similarly treated in the calculation of the typical input flux given in Figure 5-1. Each is then appropriately scaled in the real calculations. A list of the 'MRD model' values is given in Table 5-1.

Table 5-1: The 'MRD Model' values which were used for the calculation of the input fluxes

	Resolution	Throughput (%)	Pitch (microns)	Spatial Sampling (pixels)	Spectral sampling (pixels)	QE
VNIR	300	0.25	30	3	3	0.7
SWIR	300	0.25	15	3	2	0.7
MWIR	30	0.25	25	3	2	0.5
LWIR	30	0.25	25	4	2	0.5

The resolving power is treated quite differently in the real calculations to the MRD model values, as it naturally varies across the wavelength range of each channel due to the choice of dispersing element.

The values used are shown in Figure 5-2. Note that this treats the variation across the channel as being completely linear, which is a slight approximation.

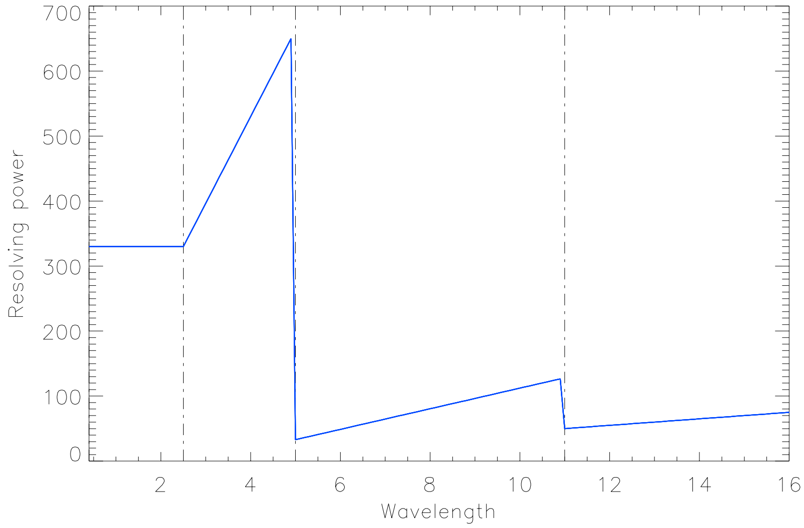

Figure 5-2: The varying spectral resolution across the bands

A typical example of the real input flux is shown in Figure 5-3, where the varying resolution and the QE have been included. This shows the input flux for only the required faint and bright object (not the goal objects). This also includes the Zodiacal contribution.

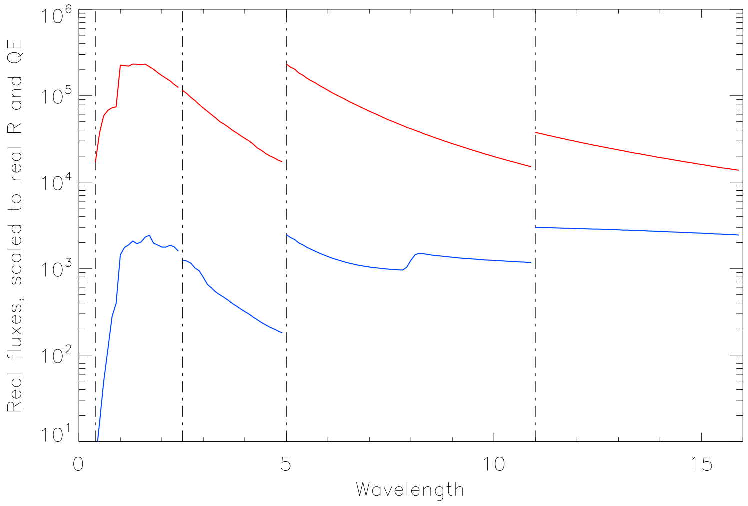

Figure 5-3: Actual signal generated in 1 second for the faint (blue) and bright (red) objects.

5.4 DERIVATION OF DETECTOR REQUIREMENTS

The following section details how each of the primary requirements related to detector noise were derived. These formed part of the full list of requirements in the Request For Information (RFI) that was sent out to industry.

For each wavelength channel, requirements were derived for a number of design 'options' to allow for different pixel sizes, as outlined in Table 5-2. Note that when an unspecified range of pixel sizes was given as an option (e.g. Option 3 for the MWIR) the number indicated in brackets was used for evaluation purposes.

Table 5-2: The optical design options presented in the RFI

Pixel Size (µm)	Option 1	Option 2	Option 3
VNIR	30	15	18
SWIR	18	15	
MWIR	25	18	TBD (30)
LWIR	25	TBD (40)	

The first stage was to calculate the typical signal expected in each pixel in one second for the optical design options and model parameters (Figure 5-3). Spectral and spatial samplings were also taken into account. These values are presented in Table 5-3. It can be seen that EChO must handle a very wide range of incident fluxes.

Below 1.0 micron the flux is expected to be considerably lower due to the reduction in throughput introduced as a portion of the incident flux is used by the Fine Guidance Sensors. Some of the tables that follow consequently include a value for 0.5 microns, this is shown separately for reference; in reality only one value was quoted in the requirements for each channel.

It should be noted that to calculate the flux per pixel, the total input flux (from Figure 5-3) was simply divided by the number of pixels required to sample the PSF of the telescope. No treatment was made for the actual properties of the PSF – i.e. for the fact that the central pixels would receive more flux than the pixels on the wings of the PSF. This will have generally led to an underestimation of the incident flux. As is discussed later, meeting the faint requirement is more challenging than the bright, and so underestimation of the flux effectively makes the requirements marginally tighter than they need to be – which is the correct way round.

Table 5-3: The expected input fluxes, for the brightest and faintest objects

	Option 1		Option 2		Option 3	
Signals (el/s/pixel)	**Max**	**Min**	**Max**	**Min**	**Max**	**Min**
VNIR 0.5	2250	1	562	0.3	810	0.4
VNIR	27236	173	6809	43	9805	62
SWIR	16821	28	11681	19		
MWIR	38078	455	19739	236	54832	655
LWIR	16347	1615	41848	4135		

To reflect the range of values in Table 5-3, it was decided to model two 'typical' exposures, one for bright and one for faint sources. Both assumed a non-destructive read as the basic operating mode. The initial selection for a 'bright' source was a 3s exposure, with 10 reads per second. The length of 'bright' exposure was effectively set by the typical well depth we could expect from knowledge of existing detector capabilities. The read rate was derived from a trade-off of the need for quick reads to handle cosmic ray contamination and get a reasonable read noise reduction against the higher thermal power dissipation and challenging data rates, especially in the larger VNIR channel, associated with faster read intervals. For the fainter sources a 600s exposure was selected with 150 reads up the ramp which would give good noise performance within the well depth available.

Note that these values were selected only for the purposes of deriving a first pass set of requirements for the detectors. Subsequent work (detailed in section 10.4 below) shows what the baseline set of ramp lengths and sample rates are. In the next phase the derived detector specifications will be iterated to harmonise to these values but the changes will be minor.

In practice the well depths specified in the RFI and listed in Table 5-4 were not quite consistent with the 3 sec 'bright' exposure but were deemed adequate at this stage as a reasonable *balance between what is desired, and what is currently technically feasible*. In the event that the well depth would be exceeded for the 3s and 600s exposure times, a limit was instead set in the Tool as the time to fill the well depth to 80%.

Table 5-4: Well depth requirements

Required well depth [el]	Option 1	Option 2	Option 3
VNIR	75,000	50,000	50,000
SWIR	75,000	75,000	
MWIR	100,000	100,000	100,000
LWIR	75,000	100,000	

The 'ideal' maximum dark current was calculated to be either 1/10th of the background, i.e. the zodiacal contribution, or 1/10th of the faint signal - whichever was lower. In Table 5-5 the calculated 'ideal' dark current is listed along with the actual value listed in the RFI which took account of more reasonable detector performance from known supplier data.

Table 5-5: The dark current requirements

	Option 1	Option 2	Option 3
'Ideal' dark current [el/pixel/s]			
VNIR 0.5	0.003	0.001	0.001
VNIR	0.07	0.02	0.16
SWIR	0.03	0.02	
MWIR	2.4	1.2	3.5
LWIR	109.2	279.6	
Required dark current [el/pixel/s]			
VNIR 0.5	0.01	0.01	0.01
VNIR	0.01	0.01	0.01
SWIR	0.1	0.1	
MWIR	75	75	75
LWIR	200	200	

The required read noise for correlated double sampling (CDS) of a signal *S* can be calculated by:

$$Read\,Noise = \sqrt{2S(\tfrac{1}{X^2} - 1)}$$

Here a scaling factor of *X*=0.8, is used to determine the relationship between the optimum performance (i.e. read noise = 0) and what can be realistically expected though once again the RFI requirement took account of what the best current detectors can hope to achieve.

Table 5-6: The read noise requirements

	Option 1	**Option 2**	**Option 3**
'Ideal' CDS read noise [sqrt(el/pixel)]			
VNIR 0.5	2	1	1
VNIR	19	14	17
SWIR	11	9	
MWIR	27	27	27
LWIR	24	24	
Required CDS read noise [sqrt(el/pixel)]			
VNIR 0.5			
VNIR	18	15	15
SWIR	18	18	
MWIR	25	25	25
LWIR	30	30	

The DSWG also felt that it would be useful to set a total noise budget for a typical exposure. Without this it is possible that a detector might meet the CDS read noise and dark current requirements, but due to the presence of additional noise contributions might not be fit for purpose. Also, a total noise budget is a useful property to test against and assumes a non-destructive read approach to sampling during the exposure.

$$Noise\,budget = X\sqrt{t.D_{current} + \frac{6R^2}{N}}$$

Here t is the exposure time (taken to be 600s), R the read noise and N the number of reads. Again X is a scaling factor, introduced to allow for the balance between a 'perfect' detector and reality. Note in this case the perfect system has noise only from read noise and dark currents, in reality other subtler signals (e.g. 1/*f* noise) may be present and should be accounted for. A value of *X*=1.1 was chosen. The values quoted in the RFI are shown in Table 5-7.

Table 5-7: The total noise on a 600s exposure requirement

Total dark noise [sqrt(el/pixel)]	**Option 1**	**Option 2**	**Option 3**
VNIR	5	5	5
SWIR	10	10	
MWIR	255	255	255
LWIR	294	294	

5.5 FINE GUIDANCE SENSOR

Late in the Definition Phase and after the RFI was issued, ESA and the Consortium agreed to transfer responsibility for the Fine Guidance Sensors (FGS) from the Spacecraft Industrial Contractors to the Consortium. This was to some extent based on the decision that the same sensor would be used for VNIR and FGS applications. Given the need for redundancy, two FGS focal planes are proposed using the same plate scale as the VNIR Focus. There was only time to advise suppliers of the additional model count that would be needed. The FGS devices operate as imagers to fulfil the guide function and therefore are expected to be in a continuous Read-reset mode. The read noise requirement is likely to be less however as the signal strength per pixel from the source will be concentrated in a small area rather than dispersed over the array as in the VNIR channel.

5.6 SUPPLIER RESPONSE TO THE RFI

Replies were received from four of the five suppliers by the deadline with SOFRADIR, who had staff resource availability issues due to competing bids, using a later teleconference to pass on their thoughts on the RFI. To respect the confidentiality of information provided by the suppliers this summary is limited in detail.

Two of the three European based suppliers (AIM and SOFRADIR) felt that while they could in principle get close to some of the specifications, they felt the timescales were very challenging. Both provided useful background information and suggestions but no pricing or useable data for technical analysis. They both thought the MWIR and LWIR dark current requirements were unlikely to be met by their technologies without significant development work. It should be noted that SOFRADIR made reference to development work at LETI that has been discussed in EChO reports in the past but to which they did not have direct access at present.

SELEX-ES provided a comprehensive response for the FGS, VNIR and SWIR channels but limited data for the MWIR and LWIR channels where they also felt the intrinsic dark currents from their production process were unlikely to get close to the performance required, especially in the timeframe available. Expected performance against the VNIR and SWIR channel requirements was slightly over the specification but well within the scientific target using N_{min} =200. They are currently working on three detector related technology development projects for ESA which give them initial steps on the TRL development plan needed for the VNIR and SWIR channels. Not surprisingly for a European supplier, the main developments they need to complete relate to a radiation hardened read out circuits which they plan to develop from the existing NIR contract with ESA, further work on thinning and broadband AR coating and agreeing a package design.

The responses from the USA based suppliers showed much higher TRL overall as one would expect. Raytheon Vision Systems proposed their VIRGO family of arrays for the FGS, VNIR and SWIR channels which would need to be space qualified or paired with a different ROIC. These have 20μm pixels. For the MWIR and LWIR Channels they proposed their SiAs product based on the devices delivered to the JWST MIRI Project. These had been the EChO Baseline choice earlier in the project but are currently not preferred because of the operating temperature around 8K.

Teledyne proposed their HAWAII2RG products for the FGS, VNIR and SWIR channels. These would be oversized at 2048 pixels square but doing so would enable reusing existing well proven space qualified designs without the need for repackaging etc. For MWIR, Teledyne provided details of an MCT device they are developing for a potential NASA mission – NEOCAM. Based on a HAWAII 1k * 1k ROIC, development models have been produced with test data available in the public domain. The operating temperature is about 25K and dark current and read noise are within specification. Teledyne did not offer any product for LWIR channel.

Assessing these responses against the Requirements using the selection criteria gave the following results in summary. For TRL we assigned a Compliant (C) mark if the proposed product was already at TRL 5 or above and a Conditional Compliant (CC) mark if we felt the constituent elements of ROIC and MCT layer were already above TRL 3 and there was a credible plan in place to get a detector to TRL 5 by the Instrument Requirements review. To meet the basic requirements, a device needed 500 for FGS/VNIR and 400 for the rest of the channels. Details of how the proposed devices perform against the crucial noise performance figures from the MRD are shown in the following section.

Table 5-8: Markings from Supplier assessment

	FGS & VNIR	SWIR	MWIR	LWIR
Raytheon	C 548	C 453	C 445	C 445
SELEX-ES	CC 552	CC 462	-	-
Teledyne	C 567	C 468	CC 488	-

5.7 SUPPLIER NOISE PERFORMANCE AGAINST R-PERF-350

Table 5-9 captures the responses from the detector suppliers that are relevant to the Noise Performance requirement. Note that not all suppliers provided data for all channels and a number of suppliers were unable to give full details for all parameters. Also there was no distinction made between values based on actual testing of real detectors and values predicted for future devices; although this was clearly taken into consideration through the TRL analysis in the selection process.

Note that the 'MRD model' properties are also included here for comparison.

Table 5-9: Input values received from industry used for calculating noise properties

Channel	Supplier	Pitch [microns]	QE	Read noise [sqrt(el/pixel)]	Dark current [el/pixel/s]	Well depth [el]	Temp [K]
VNIR	MODEL	30	0.7	15	0.01	75000	40
VNIR	SELEX	15	0.7	23	0.03	50000	40
VNIR	Raytheon	20	0.75	14.8	0.01	100000	40
VNIR	AIM	30	0.7	-	-	75000	40
VNIR	Teledyne	18	0.83	9.5	0.005	120000	40
SWIR	MODEL	15	0.7	18	0.1	75000	40
SWIR	SELEX	15	0.7	23	0.1	75000	40
SWIR	Raytheon	20	0.75	14.8	0.1	100000	40
SWIR	AIM	18	0.7	-	100	75000	40
SWIR	Teledyne	18	0.84	11.5	0.01	80000	40
MWIR	MODEL	25	0.5	25	75	100000	40
MWIR	Raytheon	25	0.6	26	75	250000	8.1
MWIR	AIM	25	0.5	-	200	100000	40
MWIR	Teledyne	25	0.5	22	75	70000	35
LWIR	MODEL	25	0.5	30	200	75000	40
LWIR	Raytheon	25	0.6	26	200	250000	8.1
LWIR	AIM	25	0.5	-	-	75000	40

Table 5-10**Error! Reference source not found.** provides an example of the output from the IDL assessment code. In this instance the performance of the different detectors has been assessed for typical faint and bright exposures, at a sample wavelength for each detector channel.

It is generally more difficult to achieve the required noise performance for the fainter sources and the addition of N_{min} therefore has a greater impact for these sources. To assess the need for N_{min} and what value it should be **Error! Reference source not found.** includes a calculation for the noise requirement on the faint sources with and without N_{min}. For the shorter wavelengths, where detector technology is generally more advanced, the anticipated performance is good, and it is not actually necessary to include an N_{min} term. This is reflected by the negative values in the “Required N_{min}” column. However, as can be seen for the MWIR, it is necessary to include N_{min}, although its value could be lower than the current 200 el/s/spaxel. For the longest wavelengths, where detector technology is currently less developed, the only proposed detector would require a much higher value for N_{min}. Note that the required value appears to be considerably higher than the difference between the predicted noise and requirement, this is because the N_{min} is effectively added in quadrature to the allowed noise level.

Table 5-10: Calculated noise performance for different detectors

Channel	**Supplier**	**Sample wavelength (µm)**	**Faint noise requirement without N_{min}**	**Faint noise requirement with N_{min}**	**Calculated faint noise**	**“Required” N_{min}**	**Bright noise requirement with N_{min}**	**Calculated bright noise**
VNIR	MODEL	1.5	765.9	802.8	671.8	-609.1	833.3	730.9
VNIR	SELEX	1.5	1250.8	1310.9	1097.6	-607.2	945.6	831.3
VNIR	Raytheon	1.5	1303.1	1361.7	1143	-652.6	978.8	858.6
VNIR	Teledyne	1.5	1370.9	1426.6	1202.4	-722.5	1029.7	903
SWIR	MODEL	3.5	417.6	499.4	366.6	-138.6	428.8	375.8
SWIR	SELEX	3.5	417.6	499.4	366.7	-138.5	428.8	376.1
SWIR	Raytheon	3.5	361.6	428.1	317.3	-149	378.5	331.6
SWIR	Teledyne	3.5	359.4	418.9	315.3	-167.2	376.1	329.5
MWIR	MODEL	8	562.4	605.8	575.5	76.3	335.1	296.6
MWIR	Raytheon	8	889.2	946.7	889.5	1.1	441.7	389.4
MWIR	Teledyne	8	470.5	506.8	481.5	76.4	280.3	249
LWIR	MODEL	13	764.5	791.3	840.3	759.6	304.6	277.5
LWIR	Raytheon	13	1395.8	1436.6	1486.8	589.8	333.4	301.3

Finally the same calculations as those shown in Table 5-10**Error! Reference source not found.** were performed across all wavelengths. To make results easier to interpret, Figure 5-4 shows the ratios between the predicted noise and the noise requirement, i.e. for a detector to meet the requirement, this ratio must always be below 1.0.

The graphs show the expected performance for both faint and bright sources. As can be seen for all wavelengths, the requirement on the bright sources can be met. This even applies for the LWIR, although it should be noted that the Raytheon detector being described operates at 8K, which would require additional cooling, which is not currently envisaged in EChO. Also of note, is that many of the brighter sources are approaching the shot noise limit, which leads to both relatively uniform performance across the wavelength region and also little variation between different manufacturers.

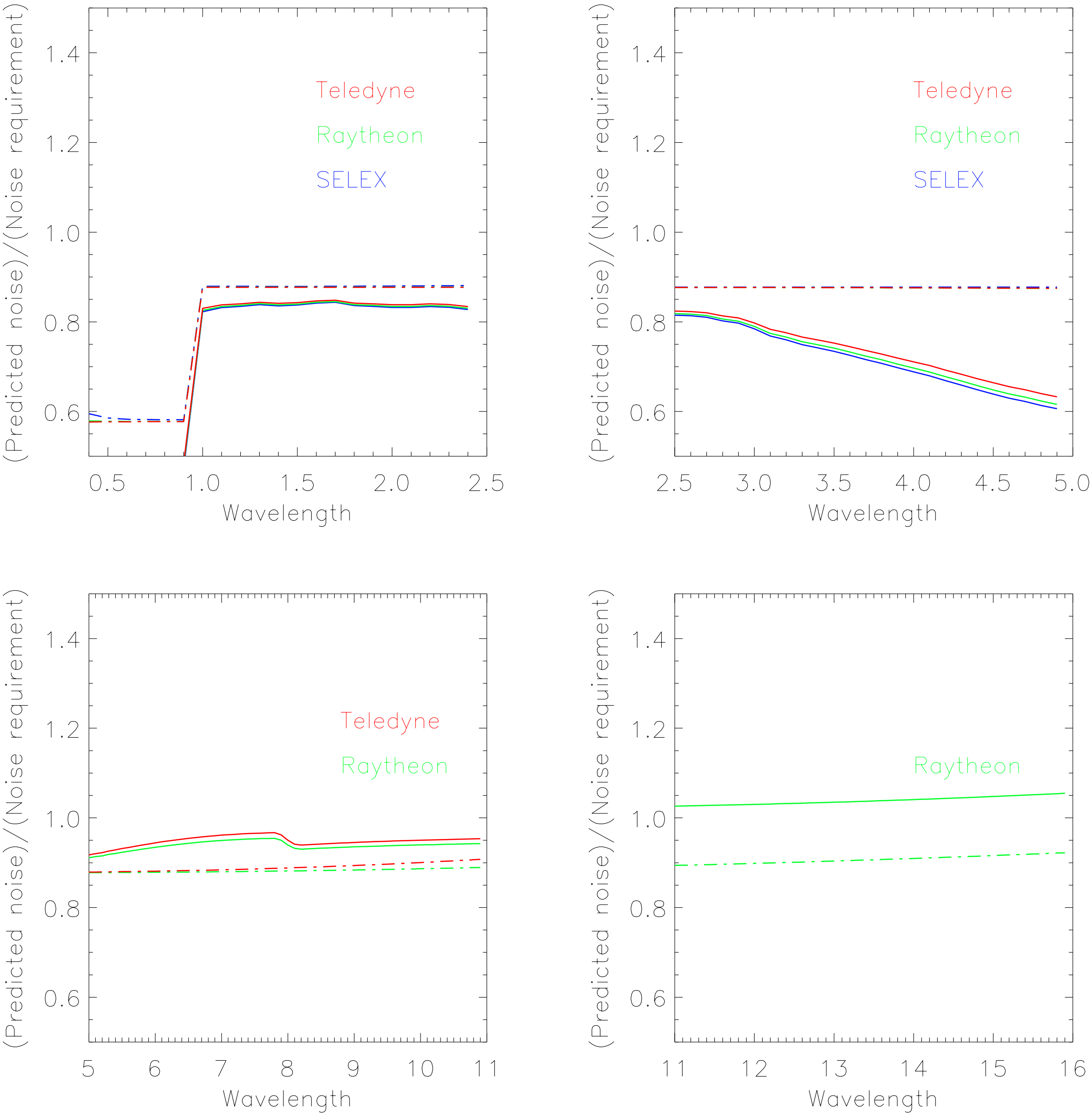

Figure 5-4: Comparing the theoretically predicted performance of different detectors against the noise requirement. Dashed and solid lines are for bright and faint objects respectively, while the colours indicate the manufacturer.

5.8 BASELINE DETECTOR CHOICE

The results of the technical assessment of the supplier RFI and the confidential pricing information were passed to the PI and PM. In discussion with the National Co-Is their decision was to baseline the Teledyne H2RG device for the FGS, VNIR and SWIR channels. It was noted that the European SELEX-ES devices were also potential candidates for these three channels, however the current TRL is relatively low when compared to Teledyne’s device. The preferred solution would have been to work with SELEX to fund development of their devices but after investigation it was decided that the predicted cost of this work would be prohibitive (see the Financial report, ECHO-RP-0002-RAL, [RD37]).

There currently appears to be no immediate European solution for the MWIR channel and so the Teledyne NEOCAM device has been selected as the baseline. The only readily available alternative is the SiAs device from Raytheon, but this requires cooling to 7K.

The DSWG have also been tasked with going back to the suppliers, especially in Europe to establish if they could meet a lower performance specification for the LWIR channel and that work is on-going. Investigations are also underway into an alternative SiGa based device but there have not at this stage been conclusions on this. For the LWIR the best option currently available is still the 7K Raytheon SiAs device.

6 SYSTEM OPTICAL DESIGN

6.1 INTERFACE TO TELESCOPE

The starlight gathering front optics is based on the present ESA Off-axis Korsch telescope baseline with a 1.131 m^2 elliptical entrance pupil. Following the convex off-axis hyperbolic secondary mirror M2, see Figure 6-1, a first image at the telescope intermediate focus is formed.

Using a LoS-defining central field position on-axis instead of off-axis, the combination of M1 and M2 appears as a fast large (~3m aperture) Cassegrain telescope used over a decentred offset but then clear of obstruction sub-pupil, leading to a nominal by-design good image quality at its focus, useful for front elements verification.

All modules have overlapping FoVs (shown below) at this plane which is a logical location for their co-registration verification. The sizing of the respective on-sky FoV is obtained from the condition of one Airy disc (from the point source nature of the targeted stars, unresolved angularly at all wavelengths) at the longest wavelength of each module, except the VNIR one, with added margin from the fine platform APE, taken here as 1” (larger than the specification in EIDA-R-0470).

The long dimension or spatial extent of the FoV is larger: taken as 20” for all IR modules to allow for local off-source background monitoring during acquisition. The VNIR FoV is limited by the size of the coupling device (optical fibre) but with 2” remains much larger (from ~x5 to x30) than λ/D for all VNIR in-band wavelengths. For out-of-field straylight rejection, a nominal oversized field stop of 25”x 15” translating into a ~2mm x 1.25mm aperture centred on the optical axis is expected here.

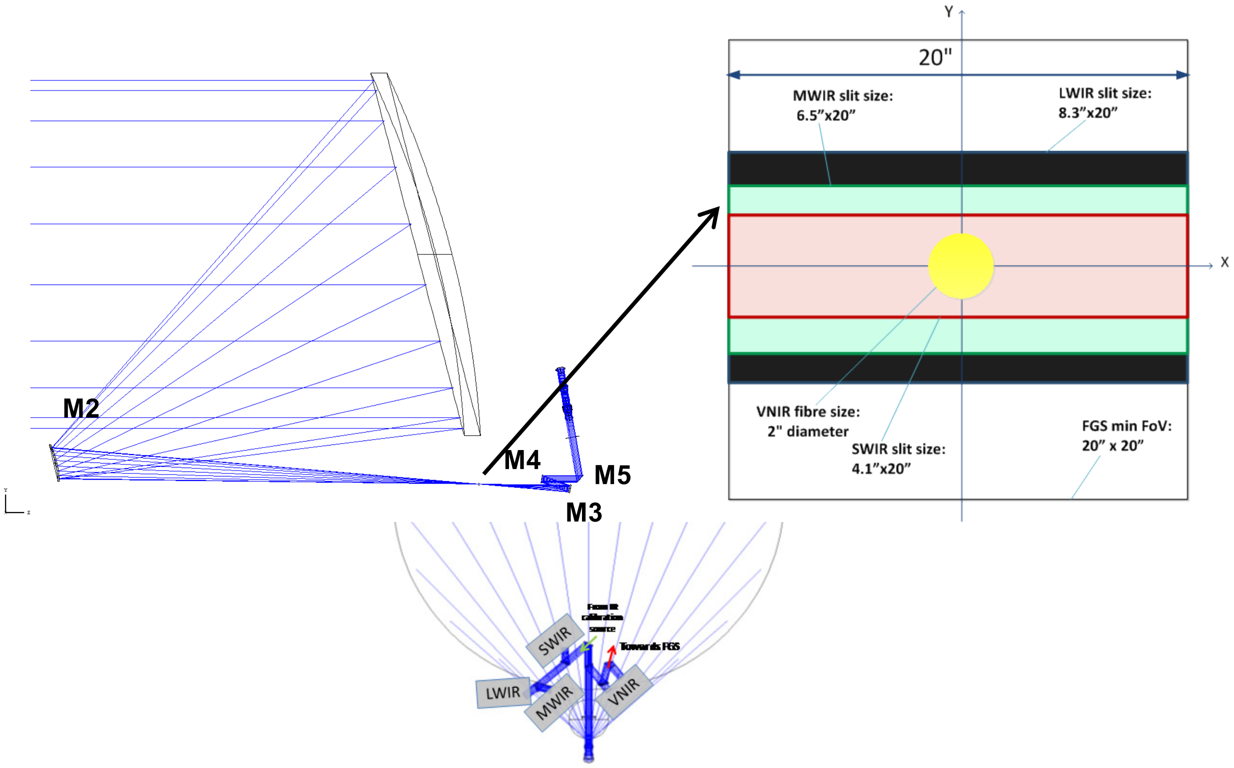

Figure 6-1: Optical layout of the EChO front and common optics concept. The relative size, nominal position and orientation of the different spectral modules’ fields-of-view at the telescope intermediate focus are indicated.

After the common telescope focus, re-collimation is performed by the off-axis mirror M3 leading to an afocal telescope output directed via the subsequent fold mirrors - M4 and M5 - towards the foreseen location of the instrument in the back of the primary M1.

Following the telescope Cassegrain focus, M3 can be then a simple off-axis parabola with characteristics tuned for transfer of the exit pupil closer to the instrument module, making it accessible for module external pupil alignment and provide a natural place for a pupil (cold) aperture stop, complementary in terms of straylight control to the first focus field stop in order to reject background from light reflected or emitted from the surrounding of the front telescope mirrors.

A nominal 25mm collimated beam major axis, associated with a ~x51.5 de-magnification, is chosen nominally as an intermediate trade-off between less controllable higher de-magnification and the maximum size limit associated with the components (dichroics) further down the optical train. The angular spread of the beam from the size-driven pupil de-magnification is ~+/-0.2deg.

The incidence angle on the dichroics is limited to 30deg max, and is typically adjusted to be between 20 and 30 deg for each of them in order to help the accommodation of the module.

6.2 CHANNEL DIVISION TRADE STUDY AND OUTCOME

Channel division was identified as one of the main trade-offs for study during the pre-MTR phase. The initial scheme for spectral separation of the different modules was based on a chain of dichroics, sequentially separating the different bands or more precisely sub-bands as due to concerns regarding how wide spectrally in shortwave reflection dichroics performances can be maintained. The high numbers of dichroics led also to concerns regarding their dominance on the overall spectral response and the impact on through in particular for the longwave IR channels which already receiving a reduced flux from the target.

The investigated options for spectral channel division were: dichroics (option 1), pupil division (option 2) and pre-dispersion (3). The results were the following:

Option 1 - Dichroics

Discussion with possible suppliers indicated that flatter and higher responses are better achieved in longwave transmit mode. There are some constraints in size, in particular for the IR dichroics (~50mm max diameter), presently limited and for best performances a not too high incidence is preferred.

Recent design, manufacturing and test of similar dichroics have indicated the possibility to cover wide spectral bands. In particular, the splitting of MWIR/LWIR is actually very close to the specification of a dichroic for an EarthCare instrument, with designed performances expected well above 90% average in R and T. The JWST/NIRCAM SW/LW beamsplitter indicated also similar R>90-95% average over 0.6-2.5μm – this provides good heritage for the splitting dichroics for the VNIR channel.

Option 2 - Pupil division

This is based on the principle of having different channels looking at different sub-zones of the collecting pupil via simple transmissive/reflective shaped aperture. Simpler than dichroics, it leads however to a reduction in the effective collecting area for the different channels compensated by quasi-perfect transmission with no spectral impact and which can be simply tuned at design stage by the size of the relative sub-apertures. Sub-apertures can also provide naturally a way to be more independent of signal variations across the pupil (e.g. from WFE variations) or near (e.g. from thermal environment fluctuations).

Option 3 - Pre-dispersion

Here a dispersing element is used in a pupil plane or focal plane to generate an associated coloured image or pupil respectively, sub-parts are collected by respective channels for further dispersion to match the required spectral resolution or projection on associated detector at a field or pupil plane. This option is much more integrated and overlap with the module designs, most being spectro-photometer based on disperser. In practice though, it was found that the disperser efficiency (grating) or the limited availability of transparent compliant material (prism) over the full spectral range brings severe limitations. More, it appears difficult to avoid some gaps between channels, which is against the main spectral coverage science requirements.

We conclude this trade-off by choosing option 1 i.e. spectral splitting via dichroics as baseline and pupil division as back-up option, and option 3 left for the internal module design but not for extension as spectral separation.

In parallel to this process, spectral regions, within the full EChO spectral range, of particular interest due to the presence of important spectral lines were defined by the Science Team in agreement with ESA. From these, regions avoiding the “no-cut” zones have been defined for inter-channel and intra-channel transitions. In agreement with the modules design iteration, the following “core” spectral range of each module has now become nominally:

- VNIR: from 0.4µm to 2.47µm
- SWIR: from 2.47µm to 5.3µm
- MWIR: from 5.3µm to 11.25µm
- LWIR: from 11.25µm to 16µm

The resulting updated baseline scheme, illustrated below, can be summarised as: 4 main spectral modules VNIR, SWIR, MWIR and LWIR separated by 3 main wide band dichroics and 2 internal-to-module dichroics and 1 beamsplitter (for FGS separation).

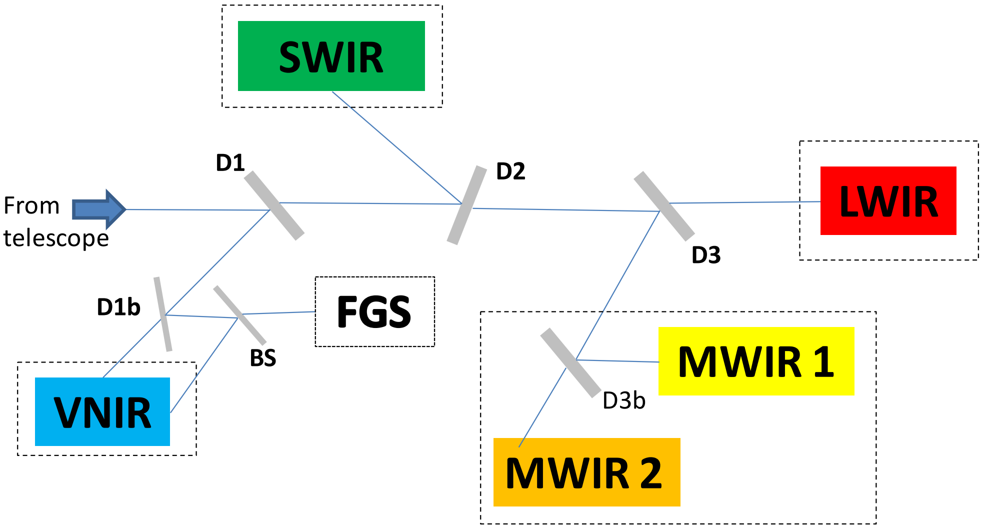

Figure 6-2: Baseline concept for the channel separation

The main concerns regarding the wideband operation of some dichroics have been reduced thanks to the existing heritage mentioned above for D1 and D3. Some modules (VNIR and MWIR), for optimal design, still have internal dichroics but these components have now relaxed R/T spectral coverage requirements.

Below are summarised the derived nominal spectral ranges of the baseline dichroics. These form the basis of the preliminary specifications for the dichroics submitted for detailed design and performances study to potential suppliers like the expert group at University of Reading. The beamsplitter is nominally taken here as 50/50 although this requires iteration with the FGS actual needs as determined by ESA and the industrial study teams.

Dichroic	Max R perf. range		Max T perf. range	
	R_{max} from	R_{max} to	T_{max} from	T_{max} to
D1	λ_{min}	λ_1	λ_1	λ_{max}
D2	λ_1	λ_2	λ_2	λ_{max}
D3	λ_2	λ_3	λ_3	λ_{max}
D1b	λ_1	λ_{1b}	λ_{1b}	λ_2
D2b	*No longer needed*			
D3b	λ_2	λ_{3b}	λ_{3b}	λ_3

Definition: transition wavelengths and associated local tolerance ranges

λ_{min}=0.55 +0.00/-0.15 µm
λ_{max}=16.0 +0.00/-0.50 µm
λ_1=2.47 +0.05/-0.05 µm
λ_2=5.30 +0.15/-0.15 µm
λ_3=11.25 +0.25/-0.25 µm
λ_{1b}=0.80 +0.10/-0.05 µm
λ_{3b}=8.45 +0.20/-0.20 µm

Table 6-1: Dichroics spectral ranges and associated transition wavelength, note that values for the variables in the table are given to the right

6.3 PAYLOAD OPTICAL LAYOUT

The instrument is split, via a dichroic-based spectral separating scheme detailed in the previous section, into 4 main optical modules. All modules collect and refocus the telescope collimated output achromatically via a simple reflective approach (off-axis parabola) onto their respective FoV-defining field aperture (slit or fibre core).

This is then generally followed by another off-axis parabola adjusted in focal length to match the spectral resolution driving the minimum internal pupil size on the disperser, the product internal pupil diameter with the angular dispersion baselined being necessary larger than the required spectral resolving power R.

Descriptions of the modules are found later in this document. The detailed beam layout is shown in the MICD [RD22].

The decoupling of the VNIR via optical fibre, as per heritage from any common fibre-fed MOS design on the ground, makes it effectively appear as fed by a single effective pixel of 2” diameter, noticeably reducing its sensitivity to any effect at lower scales. This multiple arcsec effective pixel size on-sky, while being achieved with fast but still paraxial module final optics without compromising on higher gathering of in-field Zodiacal background at longer wavelengths, can be expected to be ~1 minimum to 2 orders of magnitude larger than the pointing jitter. This leads to minimal impact on the photometry, although at the expense of limited monitoring from the science data, hence relying on the FGS. This aspect of the instrument system will be refined as the knowledge of the noise sources (e.g. RPE) and subsystems characteristics (e.g. chosen detector intra-pixel variations) become available.

The baseline payload instrument design takes account of straylight considerations in many ways as outlined in the text above[1] (provision of slits, cold stops, field stops etc, enclosed light-tight modules, out of band filtering at detector level etc). Out-of-band straylight will be controlled via detector spectral response-dependent spectral bandpass filters on a module per module basis.

6.3.1 Pupil Plane Spectrometer Study

A simple breadboard, shown below, was developed to assess the pros & cons of pupil plane spectrometers, in comparison to the more standard focal plane spectrometers baselined in each module (except the static FTS option for the LWIR channel).

---

[1] Ferlet, “Straylight considerations for NIR spectrographs”, Proc of SPIE, v 7014-36

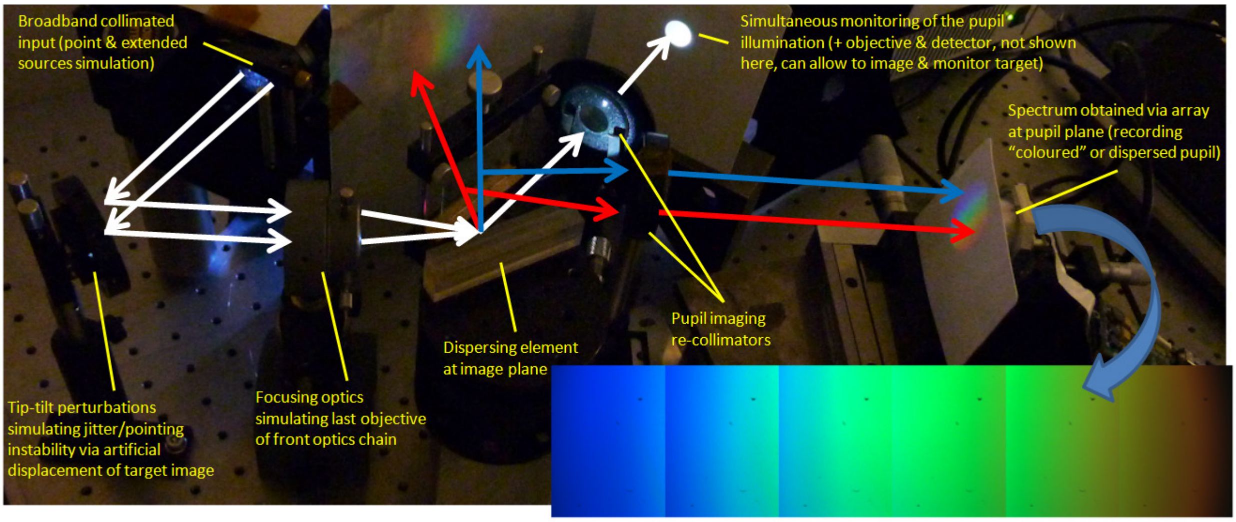

Figure 6-3: Visible domain breadboard to assess pros & cons of alternative (pupil plane) spectrometer

This is justified as pupil plane spectrometers can appear as potentially less sensitive to variations in focal plane illumination from imaged target under possible jitter/pointing instability. The preliminary results from this breadboard test indicated that:

- The reduced sensitivity to pointing instability is obtained at the cost of not monitoring off the target hence either relying on strong field limiting/spatial filtering at a focal plane ahead of the spectrometer (leading to more stringent alignment and risk associated with any internal stability issues) or the need for associated camera, which is implemented per channel would increase the overall complexity (e.g. number of detectors, etc.).
- Perturbation from an optical element not located at/near the pupil can induce pupil wandering and eventually vignetting if no longer telescope/instrument pupil matching hence flux reduction, which will affect the photometric signal; extra monitoring to identify this would be possible at the expense again of complexity and more/larger detectors.

Such a scheme is also not compatible with an on-axis telescope option as the entrance pupil obscuration would centrally vignette the resulting spectra.

6.4 CALIBRATION UNIT

An additional item in the common optics is the provision of an internal calibration source for the instrument. The proposed location is shown on the Mechanical Interface Control Drawing (MICD) [RD22]. Injection into most of the instrument modules (SWIR and longer wavelength) is via transmission through a small hole in the fold mirror FM1.

The nominal calibration source design would be an integrating sphere (a few cm diameter max) with thermal broadband sources. Existing space qualified sources such as those used for JWST-MIRI and/or NIRSPEC could be used or adapted for use over the EChO SWIR, MWIR and LWIR channels.

Such a scheme is not suited to the VNIR calibration in particular for wavelengths below 1μm (high brightness temperature required and very low transmission through D1). An approach closer to the scheme commonly used in the so-called "solar channels", i.e. visible and near-IR, of EO instruments could be used. This would involve a Sun-illuminated diffuser of well characterised surface properties (e.g. quasi Lambertian Spectralon-type), the re-emitted radiance of which is collected within a fixed geometry and therefore solid angle and re-directed via a TBD path to the VNIR module. Such a scheme is interesting as based only on passive hardware elements and rely on the extensive characterisation of the Sun although would require a path through some of the spacecraft systems to the Sun illuminated side.

This could potentially be a fibre fed system to limit the heat load impact of transmitting this solar illumination into the cryogenic payload module. The possibility of "chopping" this signal via a mechanism in the service module has been explored – this would potentially allow the superposition of the calibration signal on top of the science signal allowing continuous calibration in this channel.

6.4.1 Proposed Source: Tungsten Filament

The proposed source is a tungsten filament which borrows from the infrared calibration source heritage of the MIR Instrument on board JWST. The source itself is a wound tungsten coil, spot welded with copper-clad nickel-iron core alloy. The geometry and shape of the filament is shown in Figure 6-4 below and shows the presence of two filaments in the same cavity (one for redundancy).

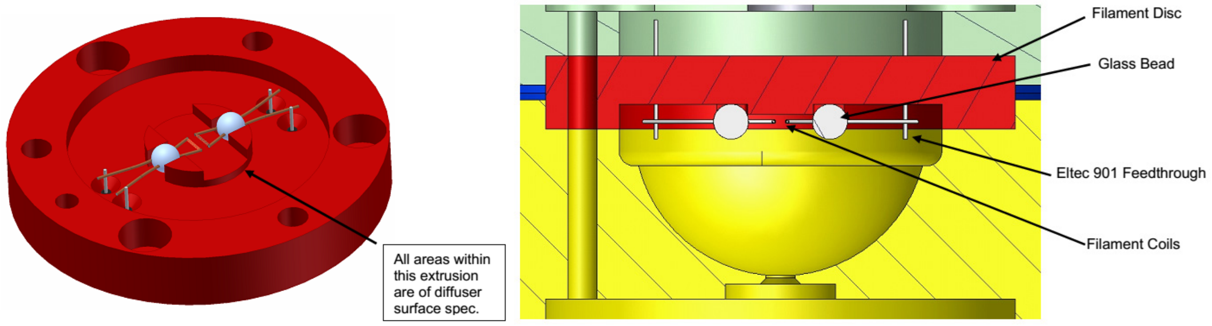

Figure 6-4: The two filaments are shown at the centre of the assembly in both pictures (top forward and Front view).The two glass beads which achieve mechanical bonding of the filaments are also visible. A forward semi-spherical cavity can be used as well as a PC (Parabolic Concentrator) which terminates in a waveguide feeding section (output) – see next section.

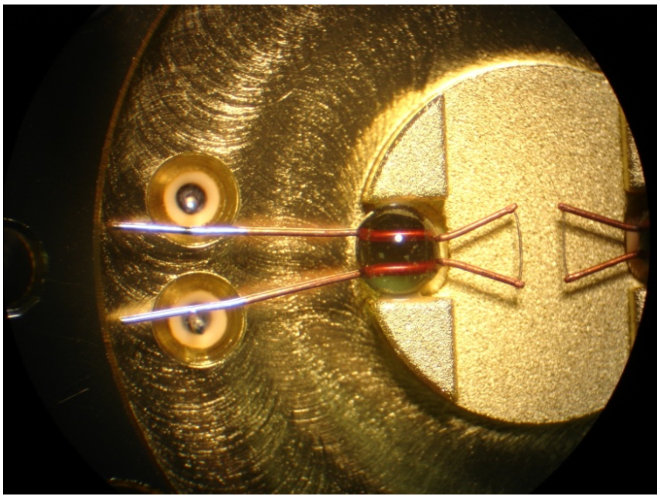

Figure 6-5: Microscope picture of the filaments (on the right) with the back-short in the background.

6.4.1.1 Electrical Interface

The current drive through the filament is used in a 4-wire configuration to allow current and voltage monitoring. The filament can be driven with currents in the range 0-15mA in order to produce a maximum temperature of approx 1300K (with a power dissipation of approx. 38mW).

Assuming the availability of a 24-bit DAC with which to drive the filament current, a current resolution of 1.192 nA is achievable which corresponds (at a max temperature of 1300K) to a temperature resolution of $\Delta T = 8x10^{-5}$ K which in turn suggests control of the output power to better than one part in 10^{6}. This exceeds the requirement for long term photometric stability so that for time scales comparable to the integration time, calibrator photometric stability can be obtained through a calibration source PID feedback loop.

6.4.1.2 Thermal constraints

In order to perform a conservative estimate of the power dissipation, the maximum temperature of 1300K (which is not necessarily required) can be considered for thermal budget estimations only. The electrical power dissipation can be split in first instance as ~ 3 mW dissipated directly to bath through conductive heating and ~ 35mW of radiated power (4 pi steradians) of the source.

Radiated power will then scatter in the integration sphere until either exiting from a small (~1 mm) hole in the fold mirror or being absorbed. The amount of power being output by the calibration source holder and fed into the optical beam will depend mainly on two parameters: The reflectivity of the internal surface of the calibration unit cavity, and the size (diameter) of the feed inside the cavity looking out into the optical bench.

While optimization of the calibrator cavity geometry will be performed in a second stage with a variety of possible solutions, for the purpose of the calculations in this section one can consider the simple case of a planar diffusing back-short in an integrating sphere with a 1mm diameter hole light-pipe looking out of a hole in the fold mirror.

It is expected that a significant fraction of the emitted power will be dumped on the calibration unit due to non-perfect reflections off the cavity walls. Hence the calibration sphere should be aluminium (internally coated in Infragold , <R> ~ 0.95) to minimize any differential contraction.

6.4.2 Optical Interface

The following is one possible implementation of the calibration source which services all modules but the VNIR which shares its input port with the FGS and has therefore a dedicated calibrator which is fibre-fed.

An alternative implementation that has been considered but is not reported below is that of module-specific calibrators inside each module. As a foreword, the obvious trade-off is the need for 3 separate sources (SWIR, MWIR, and possibly LWIR) which are placed inside their respective (cooled) modules and illuminate the arrays directly. This is balanced by the reduced amount of power which is required as the source proximity to the detector array would require reduced amounts of power (due to smaller losses).

6.4.2.1 Wavelength Coverage

A wavelength coverage from 2.4 to 11.5 microns (16 microns Goal) is required if one source is used across the modules. Due to the need to reach the 2.4 micron end of the spectrum it will be seen in Figure 6-10 that temperatures below 600K are not suitable for the filament as the Wien region of the emission will drop rapidly.

6.4.2.2 Optical Input Interface

The filament source can be placed in an integrating sphere with gold coating to minimize losses in reflection. This sphere will need to have an optical output in the main optical path of the instrument after the D1 dichroic. This can be achieved at the fold-mirror placed on the optical bench as in Figure 6-6 by placing the calibration unit behind the mirror and allowing the latter to have a small hole in its centre where the calibration unit output will “join” the input light from the telescope.

This solution creates a small obscuration in the pupil. As such this solution introduces a small decrease in optical efficiency $\Delta\varepsilon \cong 0.64\left(\frac{D[mm]}{2}\right)^2\%$ with *D* the diameter of the hole footprint on the surface.

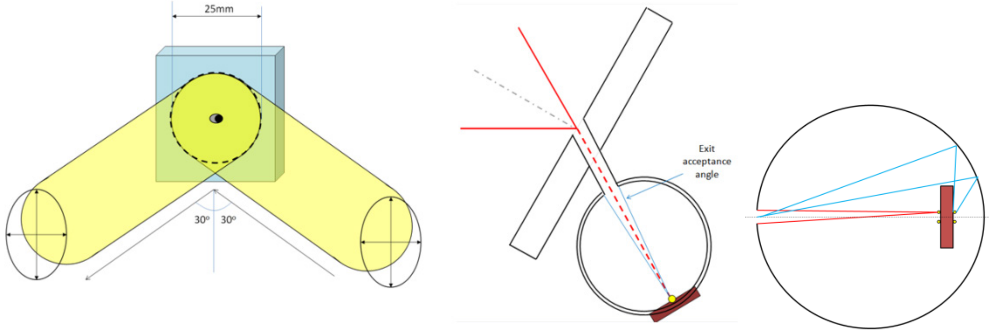

Figure 6-6: Left: Elliptical beam with almost circular footprint (25mm diameter) on the fold mirror with a small hole to allow the internal calibrator output. Center: A cross-section schematic parallel to the optical bench of a simple solution for a source at the back of a calibration sphere. The light exits through a cylindrical light-pipe connecting the sphere with a hole in the fold mirror. The direct acceptance angle is shown. Right: The same calibration unit with two calibration unit modules for bright and faint modes.

A back-to-back parabolic concentrator could be envisioned to deliver uniform angle distribution from the calibrator input to the collimated beam. This is simply designed by imposing a range of angles [$-\theta,\theta$] from the reflected optical axis.

For reasons which will be explained in Section 7, we consider the use of two identical calibrator sources (identified hereafter as S1 and S2), with S1 being allowed to shine directly through the hole and S2 – mounted on the opposite side of the source mount which acts as screen to the exit aperture allowing the filament to shine only via diffusion on the inside of the sphere.

6.4.3 Mechanical Interface

6.4.3.1 Mass

Estimation: The calibration unit only has an estimated mass ~10g. The additional mass of a small calibration sphere and potentially a solid cylindrical thermal link to the optical bench will still be kept under 100g.

6.4.3.2 Volume

Estimation: The overall cylindrical projection of the calibration source should be that of a sphere of 4 cm in diameter and height just above that of the fold mirror. Additionally, depending on the length of the parabolic concentrator used (if used), this could be either immediately behind the fold mirror or up to the entire length of the PC further back. Alternative geometries have been explored all of which require a smaller volume.

6.4.3.3 CTE Matching to IOB

Requirement: The calibration module should in principle have matching CTE to that of the OB - that of Aluminium 6061-T6. This can be implemented either by isostatic mounting or by matching the CTE of the module to that of the IOB. Additionally, the interface with the fold mirror could be contactless in the case of non-matching CTE.

6.4.4 Calibration source performance

Tests reported here were performed on the MIRI calibration sources in Cardiff University and are reported in D.J.Hayton et al. (Proc. SPIE vol.6265 -2006)

6.4.4.1 Time domain performance (Rise and fall at on and off stage)

The filament measured resistance and drive current (in mA) are graphed here as a function of time. This shows a ~1 sec time constant in rise and fall. This “waveform” represents the “cycle” which the filament has undergone during lifetime and repeatability tests.

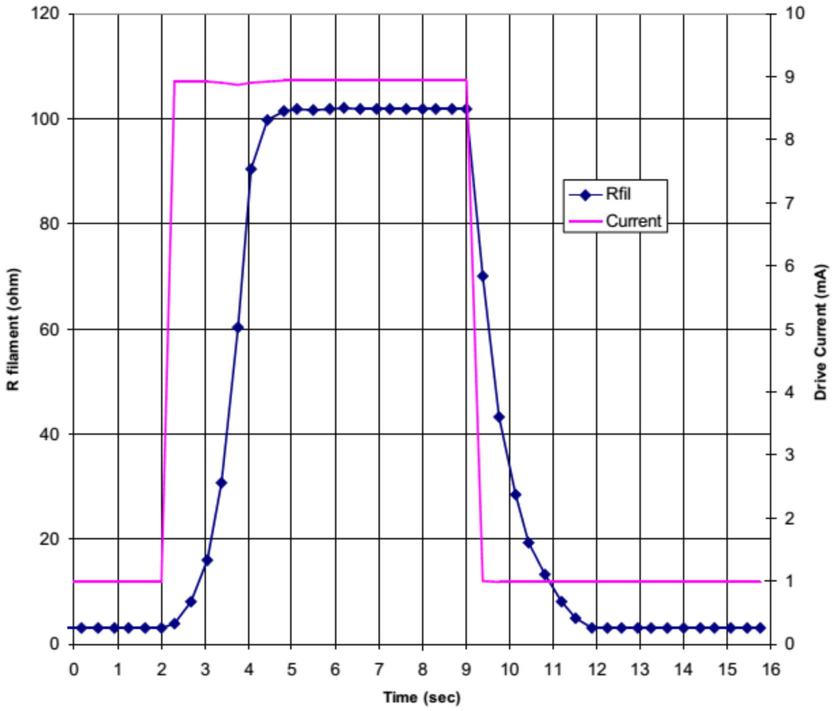

Figure 6-7: Pink: The square wave of applied drive current to the filament. Blue is the measured resistance of the filament. It can be seen that there is a delay of ~3 seconds from the drive current transition to the regime value of the filament resistance (and hence emitted power).

6.4.4.2 Life Expectancy and stability

The source life expectancy test has been performed in a relevant cryogenic environment under vacuum for the MIRI-JWST experiment. The filaments were tested one at a time. A total of 160000 cycles were performed over a period of 16 days via Labview software. Resistance measurements were performed and are shown in Figure 6-8 below.

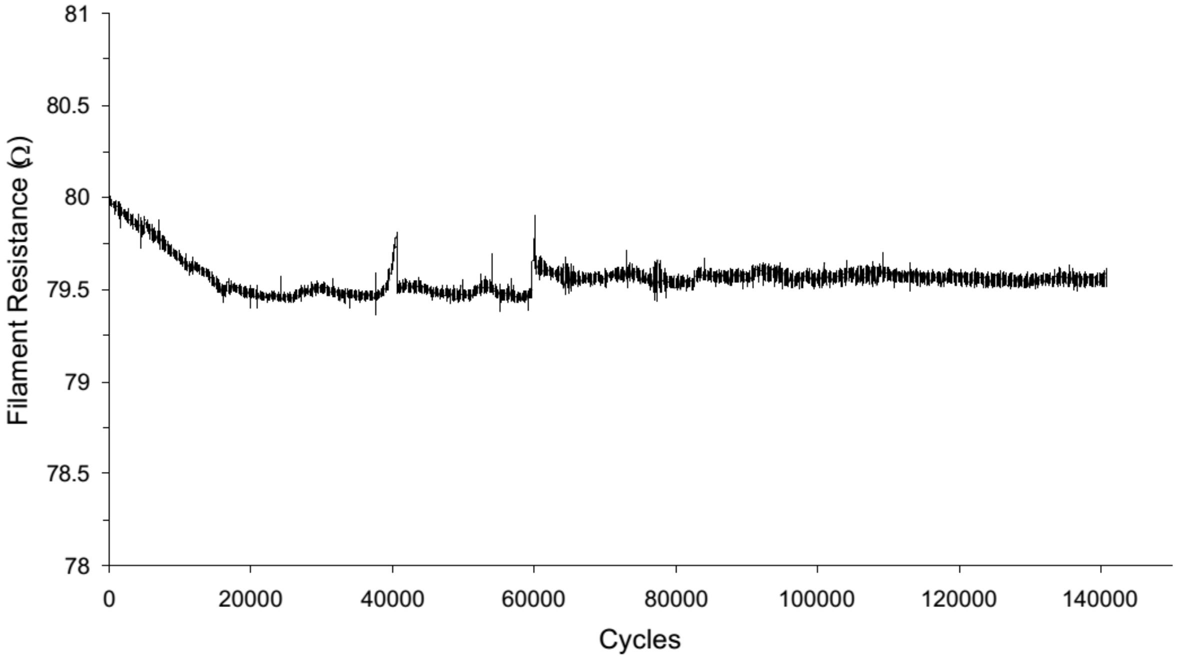

Figure 6-8: Life test results from one of the filaments heated at a nominal temperature of 800K. The initial 0.5 Ohm drift is likely due to the stabilization of the cryostats' liquid pressure vapour.

The rms variation (ignoring the few spikes) of the resistance value read, is roughly 0.05 Ohms. This is a repeatability of 1 part in 1600 (6e-4) based on a single cycle (as defined above).

Satisfaction of the above stability requirements can be achieved in two ways with the above single cycle performance (two improvements which can be both implemented):

1) Integration over a larger period of the "ON" phase (assuming white noise on the source) of ~300 seconds.
2) A PID feedback loop of the filament current drive assuming a time constant of ~1s will reduce the rms substantially.

6.4.5 Calibration source performance and compliance with requirements

The source has been modelled with the parameters in the following table in order to perform two important checks:

- The time interval or number of samples necessary for the calibration signal to reach a S/N of 104;
- The level of the signal compared to the observed source in order to avoid saturation of the well depth in the relevant observing mode

Parameter	Value	Dimensions
Temperature of source	800	[K]
Area of emission (of filament)	0.6	[mm^2]
Filament emissivity	0.2	
Efficiency due to self-shielding of coil geometry	0.6	
Calibration sphere hole diameter	1	[mm]
Calibration sphere diameter	80	[mm]
Fraction of light emitted by source S1 exiting cavity(*)	1.25e-4	
Fraction of light emitted by source S2 exiting cavity(**)	~1e-5	
Average etendue ratio: detector/calibrator output (ratio of solid angle entering slit/solid angle at slit plane from calibrator)	2.5e-3	
Number of spatial pixels/spectralbin from the FoV.	{11,13,25}	

Table 6-2: Coefficients used for simulation of the calibration flux

(*) this term is dominated by two quantities: cavity geometry and surface reflectivity. The number considered here is calculated with the aperture (1mm diameter) at the opposite side of a 40mm radius sphere. This number can be decreased arbitrarily as an alternative to a NDF.
(**) This number is a function of sphere hole diameter mainly but also of the exact position of the source unit inside the sphere.

Additionally, the same optical efficiencies and photon-electron conversion terms are applied as described in G-PERF-220 and 230 [AD2].

An expected flux plot is produced (such as a combined Fig.4 & 5 of [AD2]) where we add the contribution of the calibrator as such and the same with a 1% Neutral Density Filter. Figure 6-9 shows how reducing the source flux to 2% (either via NDF filtering or tuning of the aperture geometry and size) of the stated design, one can achieve a reasonable flux throughout all the bands even by maintaining the source temperature at T=800K (which is the operational value at which the source has undergone many tests for qualification on the MIRI module).

The ratio of yellow-to-green lines yields the percentage of well depth of the detectors which is required for the calibration source when in operation.

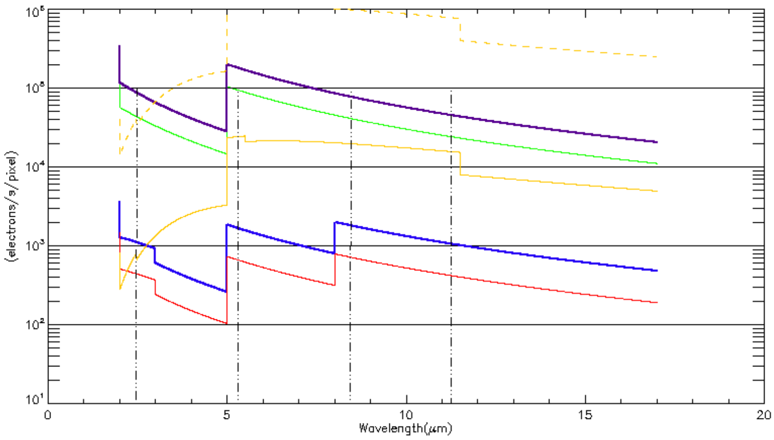

Figure 6-9: The specific flux after conversion to e⁻/s/pixel of brightest target (Goal: Purple, Req.:Green) and faintest targets (Goal:Red, Req.: Blue) compared to that of the calibrator (Yellow- dotted) and the same with a 2% NDF.

This leads to two different calibration strategies for the use of the internal calibrator depending on the mode of observation (bright/faint) illustrated briefly in Fig.6-11.

In bright mode, providing the integration time is adjusted to avoid well-depth saturation, calibration can be performed by turning on the cal source and registering samples with the planned reduced integration time (1.5s). This in turn implies throwing away the first 3 samples with cal.ON status while the source is reaching regime temperature. From this point onward, a number of samples that allows the required 10^4 dynamic range in S/N will be acquired and then switched OFF (again throwing away 3 subsequent samples).

In faint mode, calibration can either be performed before and after observations in the bright mode acquisition setting, or alternatively a lower power should be set considering that 5s of integration (in MWIR and LWIR) would be enough to saturate the well depth. With the integration time set at 240s for faint mode, this would not allow unsaturated samples during calibration operation. (the option of quick switch ON-OFF which does not allow the calibration source to reach regime risks to affect substantially the repeatability of the source)

The use of a second source which is shielded from the calibrator sphere aperture, will provide a weaker calibration signal by a factor of ~10.

In faint mode, this additional factor 10 implies that the calibrator alone would take approximately 30 to 100s to fill the detector wells (depending on the channel). This will allow the internal calibrator to be used in faint mode by performing single ON-OFF cycles of ~8 seconds for each 240s integration sample. The appropriate number of calibration samples can then be taken before and after the intended observation in order to achieve 10^4 S/N range.

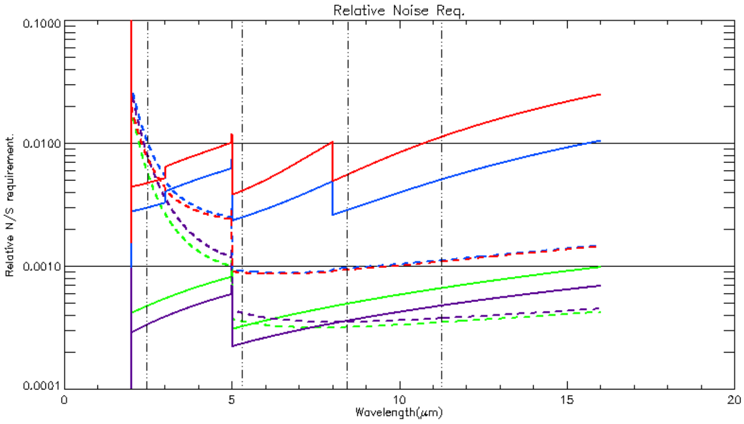

Figure 6-10: lot of Relative Noise requirement as in Fig.8 of [AD2] with hash traces to indicate where the "S" of N/S is the calibrator amplitude only (while the noise "N" includes all contributions).

A plot which represents the "Relative Noise Requirement" as in Fig.8 of [AD2] has the added hash traces for the N/S per second of the same sources when the relevant calibration mode is ON.

From this plot the necessary "integration time" and hence number of calibration samples can be inferred.

With the curve lying mostly beneath the 1e-3 line, an overall integration time of 100s which implies leaving the bright-calibrator ON for ~2 minutes to achieve the required S/N in the delta signal observed throughout the samples.

The same integration time in a faint observation on the other hand is "helped" by the intrinsic duration of integration (240s/sample). This reduces the above N/S by a factor 15. The lower wavelengths of the SWIR might require a few (<10) contiguous samples where the calibrator is cycled to obtain the required integration time. This scheme is showed in Figure 6-11.

Alternatively, it could also be possible (and will be object of further investigation) to raise the temperature of the source and decrease the throughput of the source to maintain the overall flux level while shifting the Wien region to lower wavelengths improving the S/N in the SWIR spectral region and decreasing the integration time required.

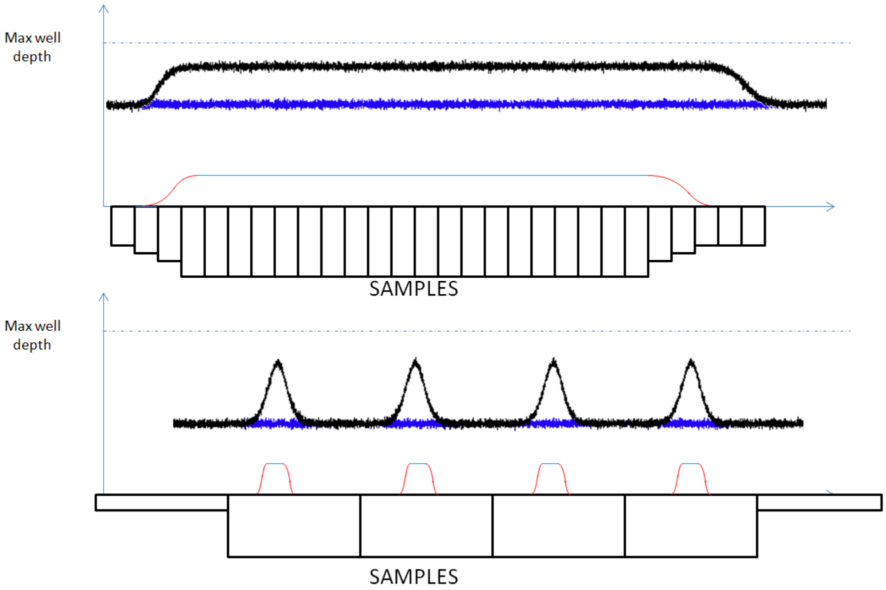

Figure 6-11: Scheme of operation of the two calibration sources for the two modes. Top: A long duration ON-phase superimposed over the bright source. Bottom: Pulsed cycles of short duration within each sample to provide the necessary integrated calibration accuracy.

6.5 OPTICAL BUDGETS AND PERFORMANCE

6.5.1 Throughput Budget

The throughput estimates include all optical elements along each science channel optical path up to respective detector. These estimates are based on the following assumptions:

- The common path front optics including the telescope mirrors (but excluding entrance pupil obscuration), the fold mirror and the reflective collimator are all assumed to be coated with typical UV-enhanced protected Silver coating, best available/with existing heritage for a wide spectral coverage down to 0.4μm and from existing spectral measurement data on qualified coated samples at different AoI, the front common optics spectral transmission is obtained;
- Average in-band R and out-of-band T of 90% for all the dichroics and 50/50 for the beamsplitter with the FGS. This assumption has been checked with relevant dichroic information and manufacturers and is thought to be a conservative estimate of the best achievable performance with current technologies;
- The science channel transmission including the optics and dispersing elements efficiency and fractional energy with a detector pixel achieved by the respective designs. Although such transmission is varying with wavelength inside each band, here as summary a single in-band average value is used, as reported by the different modules.

Overall modulation of the product of the above terms is done via 2 additional factors allowing for practical aspects (tolerances) of the entire optical system: one spectrally dependent related to the practical quality of the wavefront delivered to the science channels, the other one related to the throughput loss occurring from geometric pupil mismatch (pupil shear) due to static misalignment.

The optical throughput, as the efficiency the collected starlight is transmitted to the detector arrays in the different spectral channels (but excluding respective QE), is reproduced below in Figure 6-12. It includes realistic spectral reflectance values for all mirrors, specified reflection and transmission levels for all dichroics, fractional transmitted and coupled through slit and fibre, as well as optical modules internal transmission.

Alignment based modulating contributor such as from a 5% overall pupil shear budget are also included alongside generic contamination budget (<2% max) and short-wavelength-affecting surface micro-roughness, with nominal rms value of 5nm rms for common optics and 10nm rms for front telescope elements. This last value would lead to TIS~10% but most of the scattered light being distributed around the specular direction for polished surfaces, the actual throughput loss in the visible is limited not more so due to the integration and scrambling effect of the VNIR fibre. Typically 30-35% can be reasonably expected for wavelengths higher than the FGS 50/50 split cut-off, taken here as 800nm. The associated beamsplitter actual R/T specification will be re-evaluated as function of the future FGS performances.

These transmissions are implemented in the EChOSim simulation tool and allow good performance of the instrument.

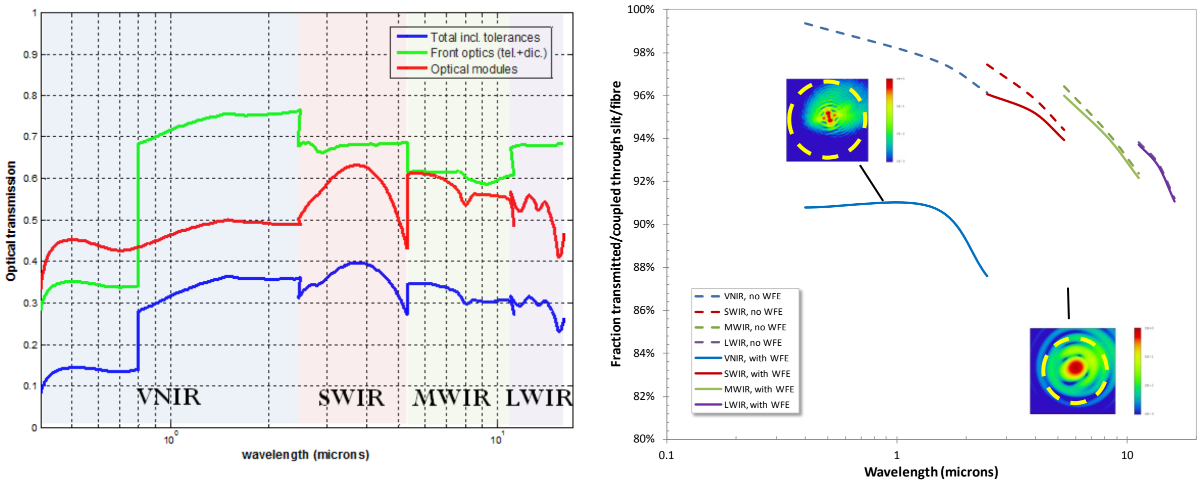

Figure 6-12: Estimates of the total optical transmission over the entire EChO spectral range (left) and details of the coupling/transmission at module slit/fibre planes (right) w/wo WFE in the input collimated beam from telescope. The WFE distribution, associated with diffraction-limited level at 5 microns, is based on equal spread over all primary aberrations (defocus, astigmatism, coma, spherical) and resulting log-scale PSFs for the edge of the VNIR channel spectral range are added as insert within the extent of the VNIR fibre core size, illustrating the high coupling.

6.5.2 Wavefront Error Budget

A preliminary wavefront error budget corresponding to a diffraction-limit at 5µm (i.e. 0.36 µm rms or 1.25 µm PTV) is included for the input beam from telescope to module. Assuming a large part of that budget is dedicated to the manufacturing of the primary mirror M1, such a budget could be decomposed as ~150nm rms and ~60nm rms surface figure error for M1 and M2 respectively, with a remaining 150nm rms of WFE allocated for assembly, alignment and environmental effect on the front optics.

The telescope back elements and common optics, all with less demanding shape and inch size apertures, are specified so that they marginally increase the $\lambda/14$ rms at $\lambda=5\mu m$ budget at all modules entrance. Such budget was used to estimate the coupling and transmission into the module input fibre and slit.

High coupling values are obtained in the VNIR range thanks to the large etendue accepted by a multimode fibre with standard off-the-shelf fused silica core diameter of 50µm and NA~0.22; although a strong dependence on the type of aberrations was found: defocus/power, and astigmatism have smaller coupling reducing impact than spherical aberration. The latter, if known to be present in the as-built telescope, could be compensated for (defocus-based spherical balancing) via refocusing. As for the other, coma can be better accepted and/or compensated for via angular re-alignment if constrained or known sufficiently early in the development of the payload. For wavelengths longer than 2.5µm, the impact of this input WFE level regarding the fraction transmitted through slit varies from low to negligible with increasing wavelengths.

The inter-module and telescope to modules alignment tolerancing criteria are based on maximum acceptable variations at the coupling/transmission through fibre and slit, and include the above input WFE budget (assumed flat Zernike spectrum of primary aberrations).

For the VNIR, less then ~5% coupling loss (worst-case at edge of band only) will be associated with 14.4" max in tip-tilt and unconstrained in roll about the optical axis by symmetry of the fibre core. For all IR channels, the spectral and spatial directions are treated separately. Less than equivalent on-sky to 1/10th of the narrowest (SWIR) slit gives <0.5% loss and converts into 20" maximum tilt in the plane orthogonal to the slit at telescope-instrument interface. The larger spatial direction is more constrained by consideration of co-registration between module and as such is spatial sampling dependent.

Referencing the modules co-alignment to the VNIR would lead to a criterion of <1" on-sky or via the telescope de-magnification <50" at interface to IR modules. The roll angle here is more constrained, to 0.5deg typically, due to the oriented nature of the slits. The transverse lateral positioning tolerances for all modules is set to a not demanding <200μm associated with <0.5% throughput loss via pupil mismatch. The stability (short and long term) dynamic levels are driven by maximum level lower than their on-sky equivalent compared to the platform RPE & PRE so that the instrument does not limit internally its own photometric stability. This translates into <5μm typical transverse positioning tolerance at fibre input face and <0.5" radial tip-tilt at telescope interface for the VNIR while <1" for the interface to all IR modules.

The impact of such budget would normally be mostly for the VNIR channel photometry while of limited consequence for the SWIR channel and negligible for all the longer IR channels. A fibre-fed VNIR spectrometer channel can provide some noticeable extra margin. Even if the some spatial filtering effect of a multi-mode fibre is limited, it will integrate over much a much larger area than the image of the unresolved target, reducing its sensitivity to image broadening by WFE, as well as general image jitter.

As such, a different approach is taken regarding the impact of WFE on the throughput estimates above. A WFE corresponding to a diffraction-limit at 3μm (regardless if achieved by front optics design or as budget from a near-perfect design as it is the case presently) is considered: via associated EE within the fibre core as first estimate of the input coupling for VNIR and via associated Strehl for all other channels. This is covered in more detail in section 15.2.6 and subsections.

6.5.3 Pupil Shear Budget

An overall value of ΔR/R=3.5% is preliminarily used here with a consequence of a 2.2% pupil shear induced throughput reduction for all channels. This is also further broken down into:

- ΔR/R=2% at instrument/telescope interface translating into 0.7mm max lateral offset and 1.7arcmin max tip of tilt (mostly of the overall IOB); and with a extra specific allocation for the nominal positioning of M3 (being actuated or not) of ΔR/R=0.5%;
- Instrument internal allocation of ΔR/R=2.5%, split into:
    - 0.5% for the respective transverse position of pupil image and possible associated stops (2, one in common optics and one per science channel typically, so 50μm typically each),
    - 1.5% for the mainly angular tolerances on common optics components i.e. typically 30" tilt max for each dichroic.

This would represent a preliminary static budget. Expected values for the dynamic part, i.e. the potential variations around the static values, would be much lower.

The opto-mechanical values used in this budget are consistent with alignment values that have been achieved on similar scale cryogenic instruments in the recent past (e.g. JWST MIRI). These have been proved to be possible by tight tolerancing of the mechanical components and by "dead-reckoning" on integration, active alignment and shimming are not thought to be necessary (although retained as an option if future analysis shows this to be required to meet the requirements).

7 SYSTEM MECHANICAL DESIGN

7.1 MECHANICAL BASELINE DESIGN

The 5 optical modules have been arranged to provide the best compromise between packing density and optical path. Minimising the overall size of the layout has helped significantly with achieving the design goal of >80Hz first resonant frequency for the Instrument Optical Bench (IOB).

The modules are arranged on the optical bench as shown in Figure 7-1.

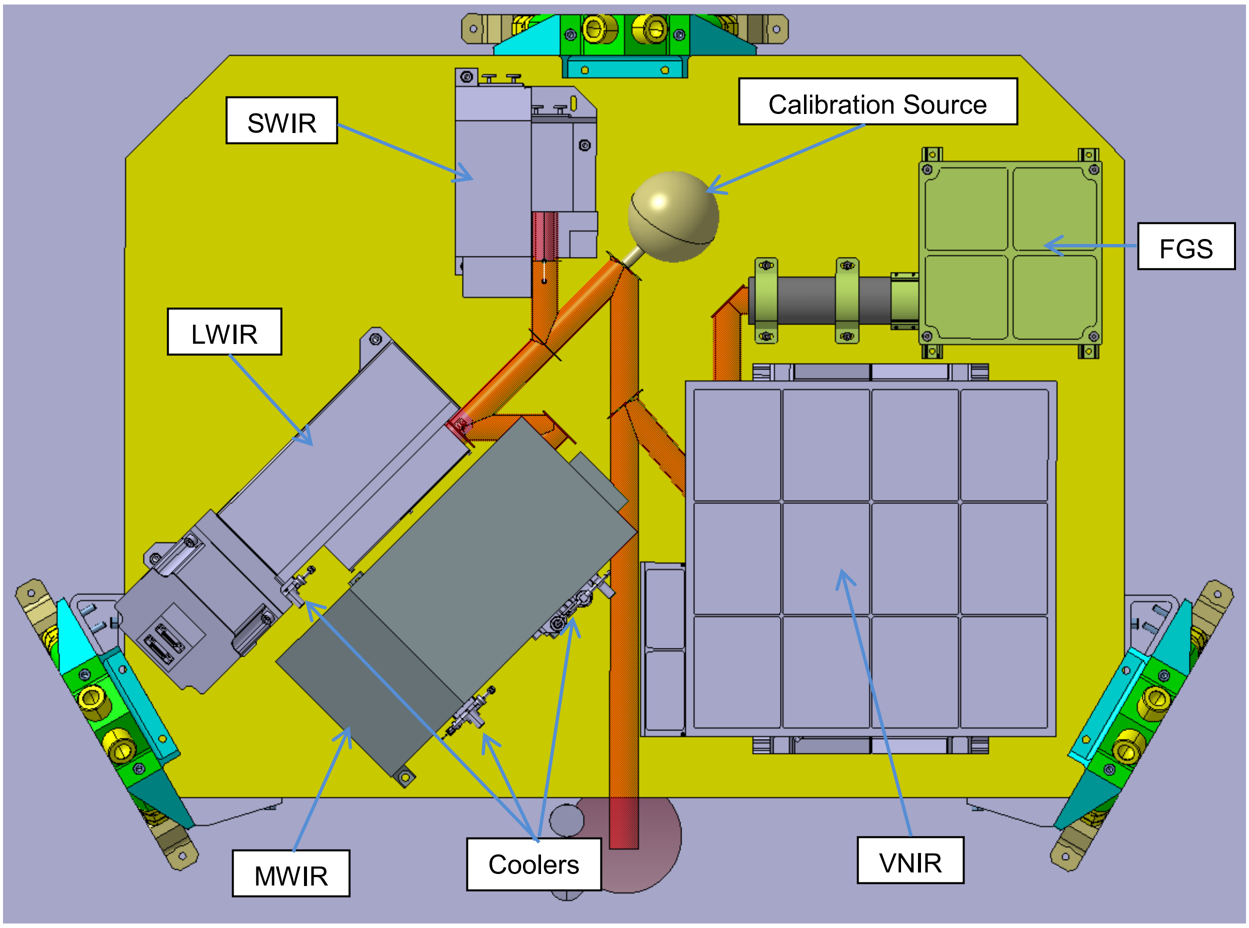

Figure 7-1: Chosen layout of the 5 optical modules

The EChO IOB has been designed as an all-aluminium structure to match sub-module interfaces and to allow room-temperature alignment of the optics. This alignment methodology was successfully implemented on the Hershel Spire Instrument. Aluminium is seen as a lower risk option for the IOB manufacture, as it is a very well-known material which responds well to both machining and post processing. The mounting between the IOB and the TOB is a kinematic interface and hence no additional stress will be introduced due to dissimilar materials.

As will be seen from the structural analysis an aluminium IOB can be designed to meet the stiffness requirements. From investigating the mechanical performance of a number of configurations it is believed that the use of SIC is unsuitable for this application.

A detailed material trade-off between candidate IOB materials is presented in [RD33]

7.2 MECHANICAL INTERFACES TO TELESCOPE (VOLUME ETC)

The TOB is to be manufactured from silicon carbide, therefore the interface between the IOB and TOB needs to be carefully designed to ensure excessive stresses are not generated during cool down. The IOB is to be kinematically mounted using 3 bi-pod structures which will allow for differential thermal contraction between the two benches whilst maintaining the instrument optical alignment. The bi-pods are arranged on a PCD which is centred along the input optical axis. One mount is at the 12 o'clock position on the input optical axis. This bi-pod could be made as a rigid mounting to secure the location of the IOB during cool down. The other bi-pod structures would then be made with flexures to allow for the differential contraction. However as the input beam for the instrument is collimated this is not really seen as necessary.

The three bi-pod mounts of the IOB will have Invar feet which interface to the TOB. The legs of the bi-pod mounts have been assumed to be Aluminium for provisional structural modelling, however depending on thermal requirements these may be changed to carbon fibre reinforced plastic. The mounting plane of the bi-pods has been purposefully offset in the vertical direction relative to the top surface of the IOB. This allows the instrument to meet the volume requirement, but also reduces the vertical offset between the overall centre of gravity and the mounting plane. Minimising this offset increases the structural stiffness of the entire system.

The instrument radiator is mounted from the IOB via 3 pairs of bi-pod legs. These bi-pods interface at the IOB mounting points so that the loads generated by the radiator should not influence the dynamic behaviour of the IOB.

The mass of the radiator is primarily driven by the thermal requirements. The structure will be optimised to support the large surface with minimal mass. The radiator needs to be angled relative to the IOB and TOB to ensure that it can be accommodated within the allocated volume.

The figure below shows an extract from the MICD which illustrates the angle of the radiator and shows the allocated volume for the system.

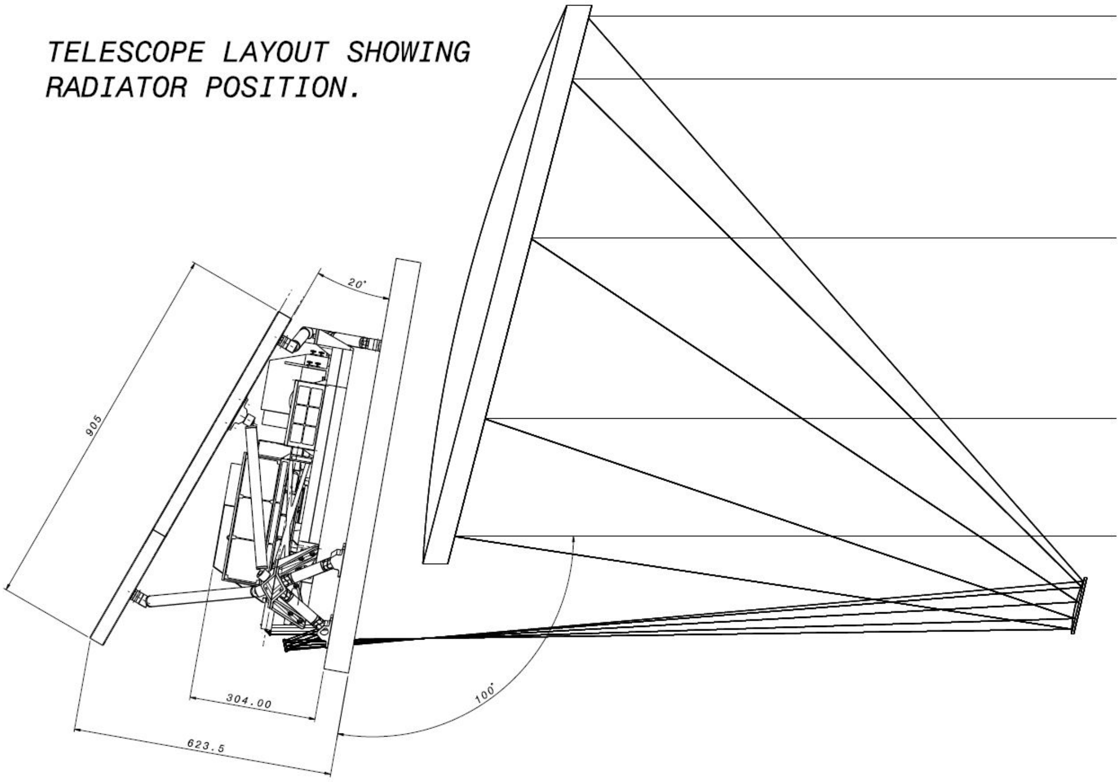

Figure 7-2: IOB Envelope illustration from MICD

7.2.1 Mass Budget

Instrument Modules	Basic Mass (kg)	Contingency factor	Nominal Mass [kg]
VNIR	5.52	0.20	6.62
SWIR	4.66	0.20	5.59
MWIR	4.83	0.20	5.79
LWIR	4.56	0.20	5.47
FGS	3.07	0.20	3.68
Coolers (MWIR and LWIR)	0.54	0.20	0.65
Sub Total	**23.18**		**27.81**

IOB and Additional Parts	Basic Mass (kg)	Contingency factor	Nominal Mass [kg]
Instrument Optical Bench (IOB)	20.00	0.30	26.00
IOB Supports	1.89	0.20	2.27
Common Optics	1.00	0.20	1.20
Harness	2.41	0.25	3.02
Calibration Source	0.50	0.20	0.60
Thermal Straps	0.87	0.20	1.04
Blankets	0.70	0.20	0.84
Radiator	13.00	0.20	15.60
Radiator Supports	2.00	0.20	2.40
Sub Total	**42.37**		**52.96**

Total Instrument Mass in EPLM (kg)			**80.78**
Compare to requirement			121.00

On SVM	Basic Mass (kg)	Contingency Factor	Nominal Mass [kg]
2 Stage J-T Cooler Compressor	6.00	0.20	7.20
J-T Cooler Aux Panel	1.50	0.20	1.80
J-T Cooler Harness	1.50	0.20	1.80
DWEU (Detector Warm Electronics Unit)	3.50	0.20	4.20
ICU (Instrument Control Unit)	7.50	0.20	9.00
CCE (Cooler Control Electronics)	6.50	0.20	7.80
FCU (FGS Control Unit)	6.50	0.20	7.80
Sub Total	**33.00**		**39.60**
Compare to requirement			137

Table 7-1: Mass Estimate Table

The IOB mass is based upon the current up to date structural mathematical model. The mass estimate includes margin for additional material that is needed for module interface mounting points, additional structural webs and local thickening for common optics, harness and thermal strap mounting points.

The radiator is also a significant mass and this estimate is supported by the current structural model. The radiator in the FEM is not a final design but an ideal mathematical representation of the minimal structure that is required. The mass estimate for radiator supports and local stiffening components have been generated from the CAD model. The radiator is fundamentally two aluminium sheets bonded to a honeycomb core. Additional material is required for protecting the edges of the panel and for mounting the bi-pod legs to radiator front face. Radiator support mass estimates are based upon worst case for bi-pod lengths.

The IOB additional items such as harnessing, common optics, thermal straps etc are based upon experience from previous projects. As harness and thermal strap routes are yet to be fully defined these estimates include some additional margin.

7.3 MECHANICAL DESIGN

7.3.1 Instrument Optical Bench

The IOB design is based upon a two piece fabricated monocoque structure. A light weight shell is manufactured by pocketing two 25mm thick pieces of aluminium and attaching the open shell faces together using the process of dip brazing. This means that the webs that are left in between the individual pockets are joined along their entire length and significant structural stiffness is obtained from the outer shell surfaces. The process is qualified for space applications and the brazed joint is positioned at the neutral axis of the optical bench (zero shear stress region when considering pure bending). The two halves are accurately located relative to each other using dowels.

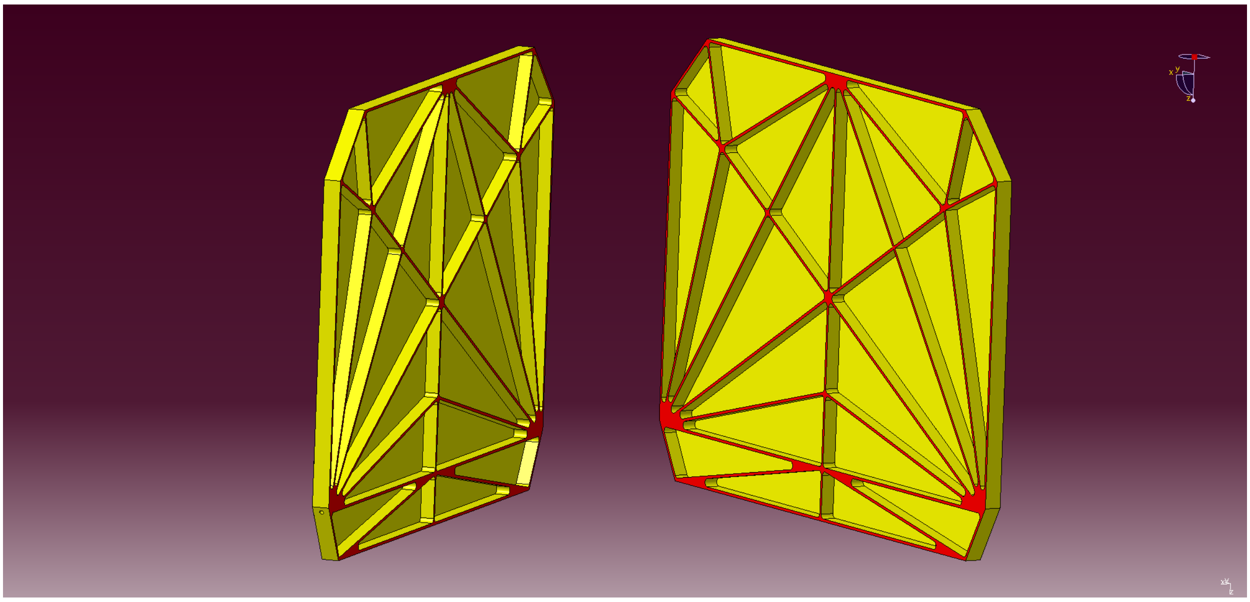

Figure 7-3: IOB shells showing stiffening webs, the parts are brazed together across the surface shaded red

Each pocket within the bench requires two holes which allow the hot salt solution to penetrate the assembly to heat the brazing region. The same holes also allow the salt solution to drain out after brazing. The internal joints can then be examined visually using an endoscope and the internal structure of the brazing can be x-ray inspected. The temper of the aluminium is not significantly affected by the heating during the process.

The webs inside the optical bench will be optimised to provide support to the mounting feet of each sub module and the top surface can be locally thickened to provide support for smaller items such as mirror/dichroic/beam splitter mounts. The current philosophy for the interface mountings is to use M6 interface bolts for all of the sub-modules thus simplifying the specification. Each interface mounting for each optical module will be made through a raised pads on the top surface of the IOB. After brazing of the IOB these pads will be machined to make sure that any possible distortion introduced by this processing is eliminated.

An alternative design approach using a more traditional pocketed Aluminium bench with a closeout panel which is bolted on is also possible. This would be marginally less stiff and would incur a small mass penalty (well within the mass margins held at this point). The manufacturing process for the bench will be subject to confirmation in the next phase.

The vertical offset of the bi-pod support plane is achieved using mounts which are bolted onto the IOB shell. The top of this mounting also provides the interface for the Radiator bi-pod mounting structure. This allows the radiator loads to be supported with minimal influence on the dynamic behaviour of the IOB.

7.3.2 Radiator Mechanical Design

The radiator has currently been maximised in surface area to provide margin of thermal performance above the predicted requirements of the instrument suite. The overall dimensions of the radiator have been set at 1.2m x 0.9m for the design study. This provides a worst case for both accommodation and the mechanical design of the large panel structure. This is larger than the radiator defined in the EID-A, but due to the consortium now taking on responsibility for this hardware, the design has been conducted accordingly. The design is compatible with the allowable envelope as defined to the consortium by the ESA project team based on the spacecraft thermal models and shadow allowed by the minimum V-Groove sizing.

The baseline design for the radiator is an aluminium composite approach. The top and bottom skins of the radiator will be bonded to a 30mm thick honeycomb core. The mounting points will provide local reinforcement and thermal connection between the support legs and the front (radiating) surface. The radiator will be coated according the mission requirements, and will depend greatly on the view of sun during transit to L2 orbit.

A FEM has been generated and included into the overall EChO structural model which shows that the a 30mm thick core with 2mm front skin, and 1mm rear skin, will be mechanically stiff enough for launch (~80Hz first mode).

The radiator will be supported by 3 sets of bi-pod legs which interface directly with the supports of the IOB. The detailed design of these legs has not been completed due to the need for a detailed mechanical and thermal design trade-off. Currently the material baseline for the radiator support struts is thin walled stainless steel tubes. As an alternative T300 carbon fibre reinforced plastic could be utilised to minimise the thermal parasitic load, and the design of these components would be based upon MIRI heritage.

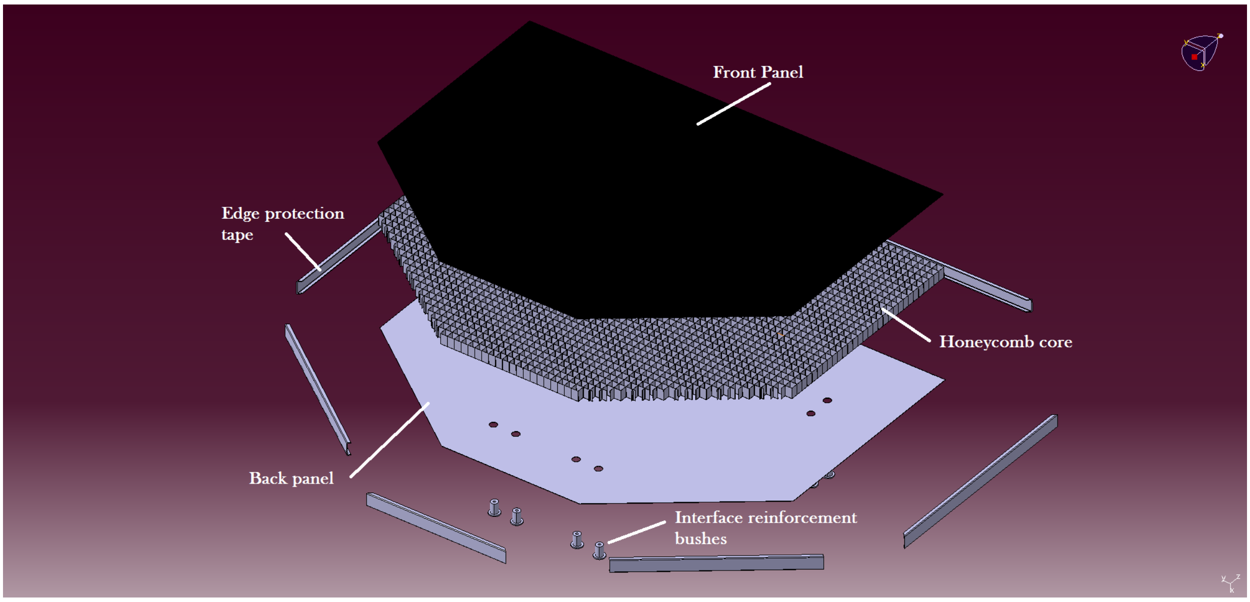

Figure 7-4: Exploded view of Radiator

The exploded view shown in Figure 7-4 illustrates the components that will make up the radiator assembly. The edges of the panel will have standard edging tapes to protect the honeycomb from mechanical damage and contamination.

Tests are underway to experiment with bonding the three main layers together using Stycast 2850FT adhesive, which is a carbon impregnated low CTE epoxy adhesive. MSSL has had a great deal of successful experience using this adhesive at temperatures down to 4K. The aluminium composite core of the test samples is perforated so that the system can be placed under vacuum to ensure an even compression of the three layers. Currently it is planned that both front and back panels will be Alocrom treated prior to bonding. The radiator coating is to be applied to the panel once it is assembled. Final coating material for the radiator is to be defined.

As a possible alternative solution to a composite aluminium design, is a radiator constructed along similar lines to the IOB. This would be an aluminium monocoque structure which is pocketed and dip brazed to form a complete shell. A mechanical model of this type of radiator was included in an early version of the FEM and showed that a structure of identical overall dimensions could be constructed to provide similar mechanical performance. This option however was slightly less mass efficient than the composite design. This design could be utilised if problems were encountered with the bonding of the honeycomb structure.

7.4 FPU MECHANICAL MODELLING RESULTS

A FEM was constructed based upon an aluminium IOB as described in section 7.3.1. The top and bottom faces were modelled in a separate group from the stiffening webs so that all of the key parameters could be tuned as required.

The 6 sub modules are modelled as lumped masses which are supported 150mm above the top surface of the IOB by rigid body elements. This means that the structure of the sub-module is assumed rigid but as all loads pass into the IOB in a small area at the assumed centre of gravity. Therefore the structural rigidity of the sub-modules do not contribute to the calculated stiffness of the bench. This is a conservative way of modelling the system until detailed interfaces of the sub-modules have been defined. All of the sub-module lumped masses were modelled as the per the current mass estimate values including margin. For the IOB and Radiator additional components such as harnessing and thermal straps were modelled using non-structural mass which is evenly distributed evenly across their surfaces.

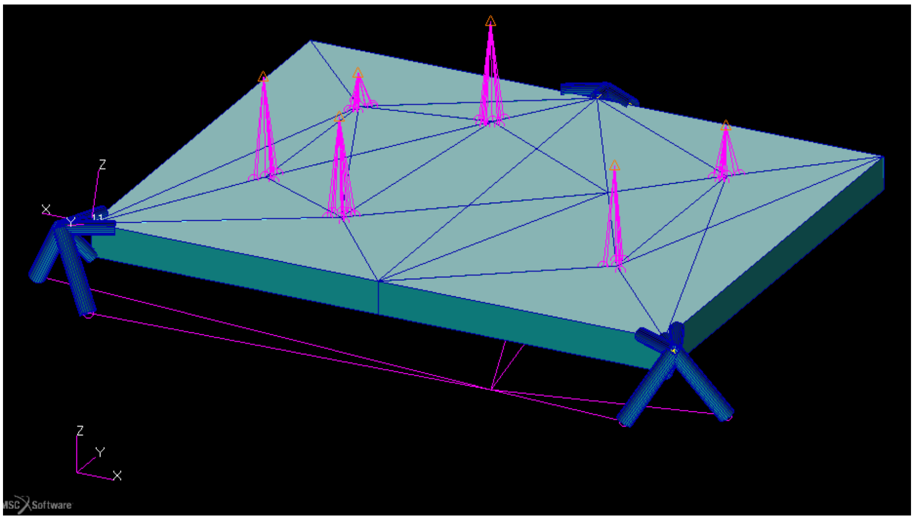

Figure 7-5: IOB on offset bi-pod supports with sub-modules modelled as lumped masses

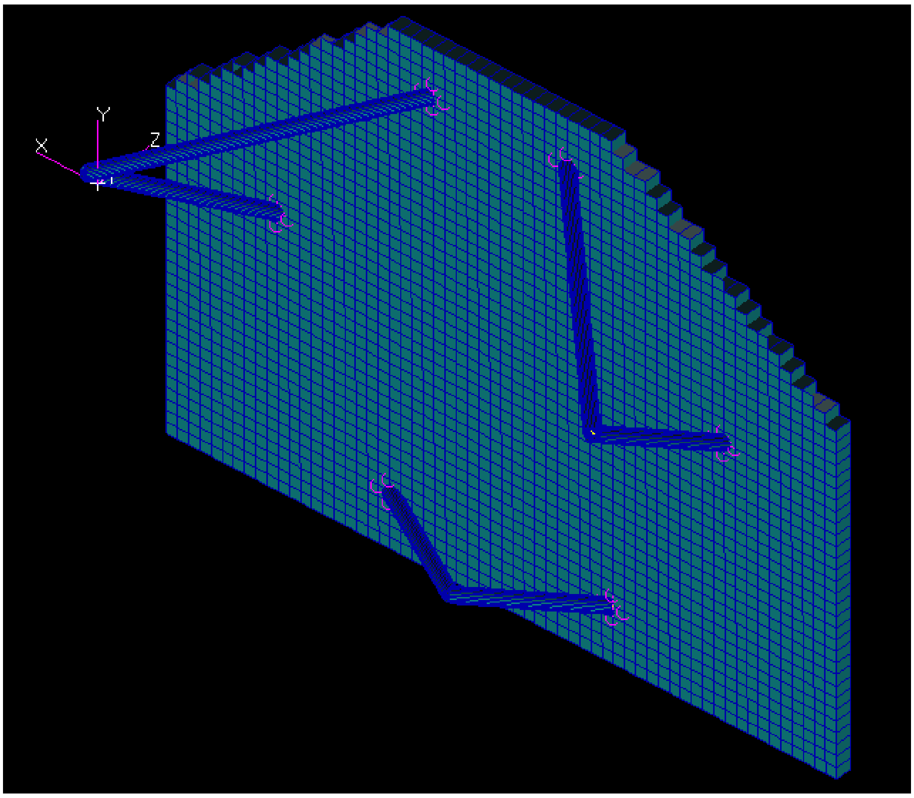

Figure 7-6: Underside view of the Radiator with bi-pod mounting supports

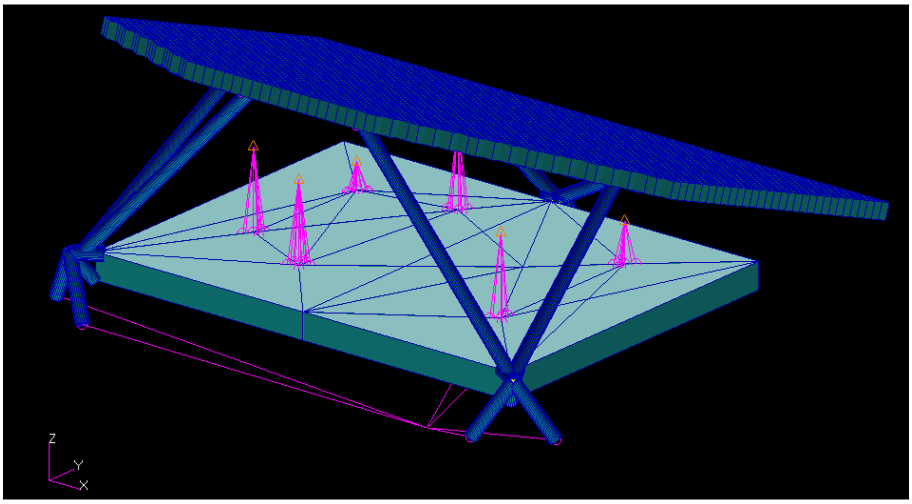

Figure 7-7: IOB FEM Model with Radiator in position

The IOB is mounted via simple beam supports which offset the bi-pods by 30mm from the IOB edge. The bi-pods are then constrained to a single point (using an RBE2). This is true to the CAD representation of the situation. The bi-pods are modelled as simple bar elements.

The radiator is constructed from three main components, the front sheet, the honeycomb and the rear sheet. For modelling simplicity the honeycomb was modelled as a square honeycomb structure which was assumed to be bonded to the two structural skins along all of the honeycomb edges. The radiator model does not have local details such as the mounting bosses. The interface between the bi-pod legs and the radiator panel are simply modelled using RBE2 features to locally spread the loads into the surfaces.

7.4.1 Normal Modes Analysis

A finite element model of the entire system was created and updated throughout the design study. The model is up to date with the current radiator configuration as shown in the CAD model of the system. The cooler is still modelled as a separate unit in this model however this has recently been combined with the optical units requiring specific cooling (MWIR and LWIR).

The optical bench has a requirement of 80Hz for the first mode, and in order to include some margin a minimum first frequency of 80 +20% = 96Hz must be achieved. The radiator is not mechanically coupled to the IOB and therefore this can have a lower first mode frequency.

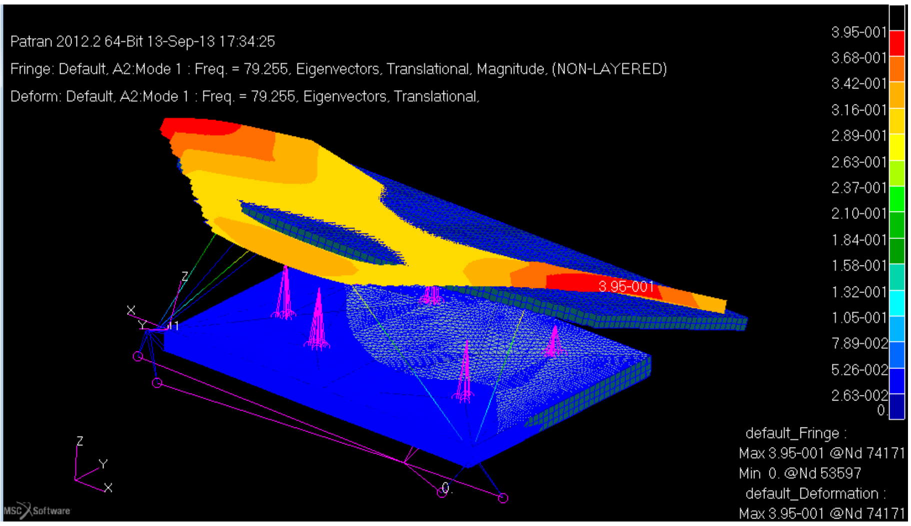

Figure 7-8: First mode: Dominated by the radiator which is in a flapping resonance – 79Hz

Figure 7-8 shows the radiator as having sufficient structural stiffness for launch. However this model uses the basic mass. The first mode frequency reduces significantly (~66Hz) when non-structural mass is applied to bring it up to nominal mass including the 20% margin. If the radiator was to increase significantly in mass the honeycomb core thickness may need to be increased. There is sufficient envelope inside the spacecraft for this and increasing the depth of the honeycomb core has minimal effect on the mass of the assembly. The plot shown in Figure 7-8 shows that the mode is dominated by the stiffness of the mounting bi-pods of the radiator. A full mechanical and thermal trade-off for these components needs to be carried out in the next stage of the project.

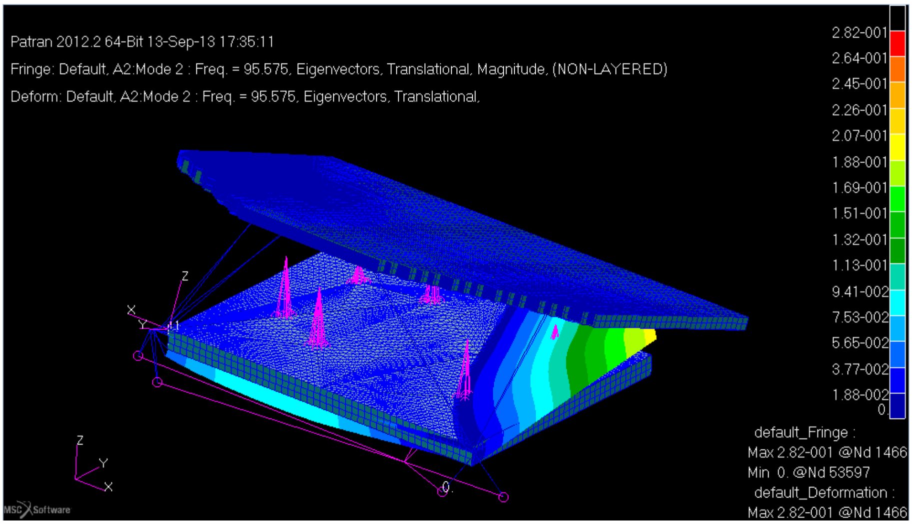

Figure 7-9: Second mode: IOB twisting mode-95Hz

The second mode frequency of 95Hz is dominated by a twisting mode of the IOB. This frequency is just below of target first table mode. However the IOB in the model is at maximum weight including all margins for all sundry IOB components such as the harness. The model is still considered to be very conservative as the optical modules are assumed to impart no structural rigidity to the assembly and the model contains the minimum number of webs and stiffeners.

The IOB bi-pods are not optimally positioned for structural stiffness. It was requested that one of the bi-pods was placed upon the input optical axis of the instrument, and therefore the IOB is supported by one bi-pod along the longest edge of the IOB. This results in the two predominant twisting modes shown in Figure 7-9 and Figure 7-10. From a trade-off study it was seen that the first mode frequencies of the IOB could be boosted by 5% by optimising bi-pod positions.

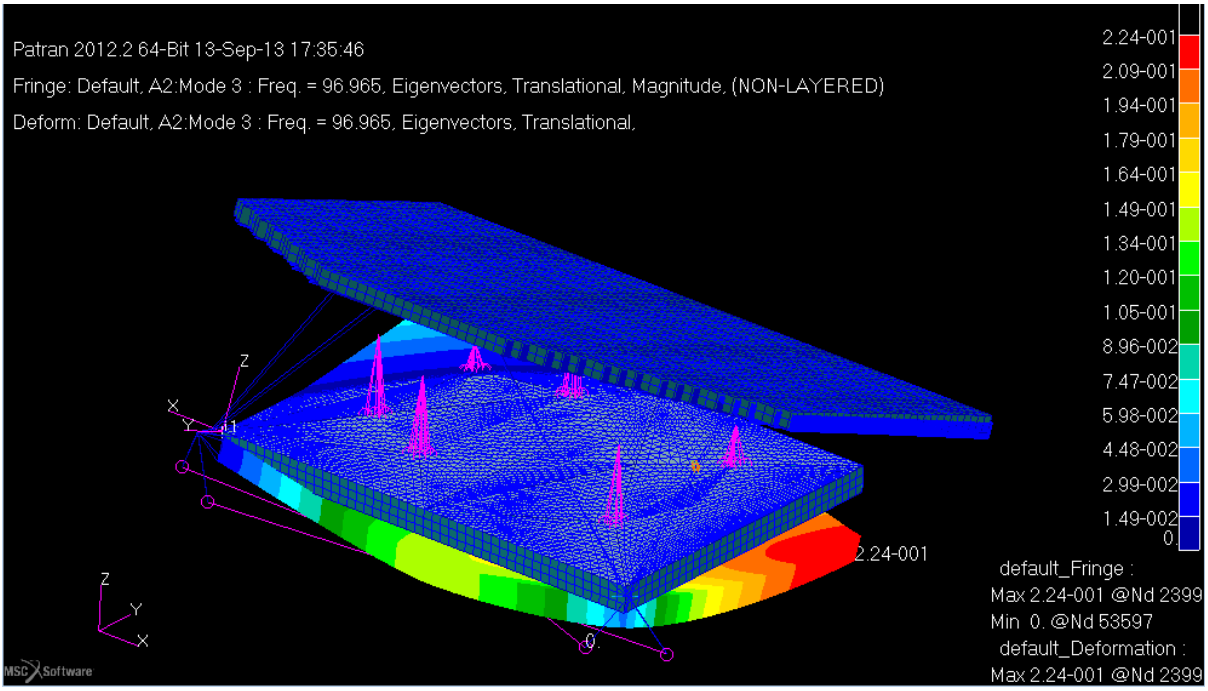

Figure 7-10: Third mode: IOB twisting mode – 97Hz

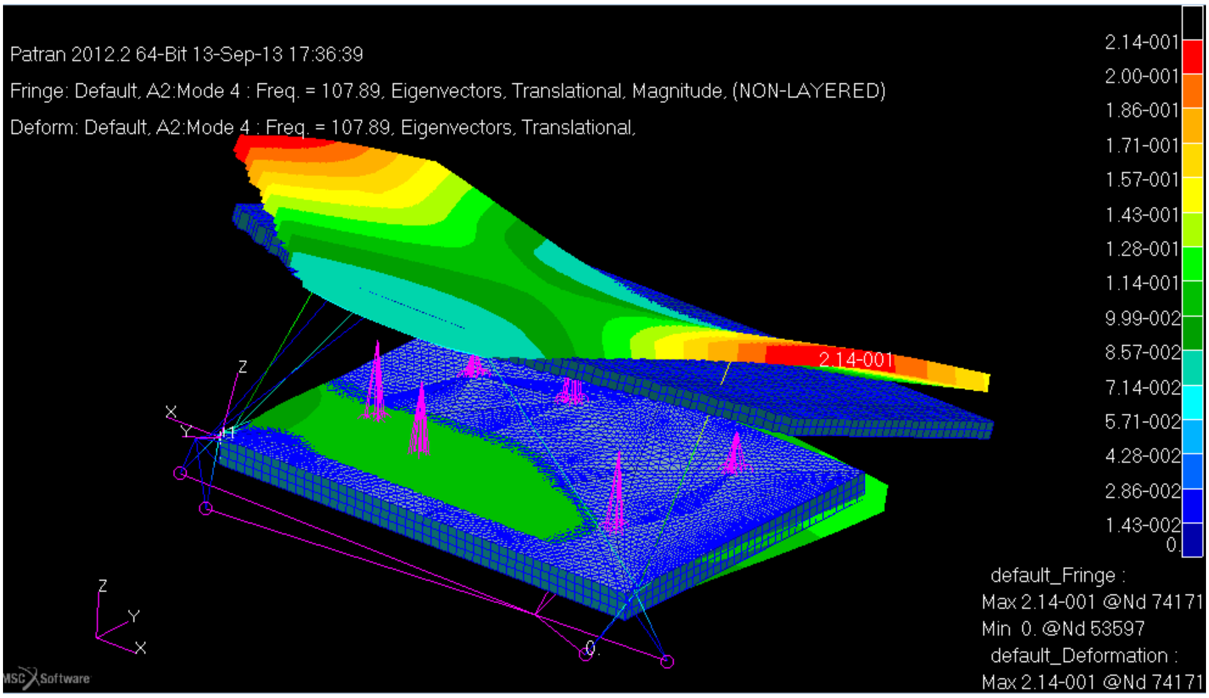

Figure 7-11: Fourth mode: Combined radiator and IOB mode: 107Hz

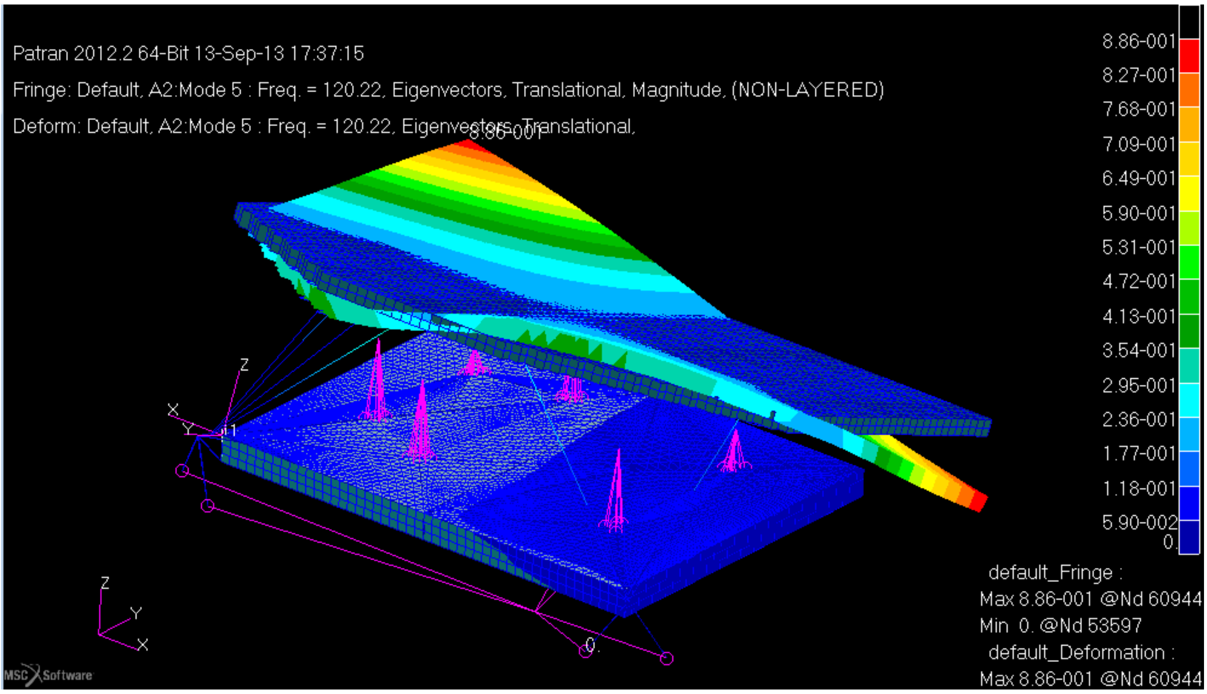

Figure 7-12: Fifth mode: Dominated by the radiator in flapping mode: 120Hz

The first five modes show that the IOB and radiator are sufficiently stiff to withstand a launch environment. All masses associated with the IOB were taken as the nominal masses which contain a minimum of 20% margin. A number of configurations were modelled during this design study, to investigate the effects of IOB mounting positions, Radiator sizes and mounting positions. The results from these models are not presented in this report for clarity, however it provides confidence that changes to the final design configuration can be accommodated in both the volume and mass allocations for the instrument.

The design optimisation is still to be carried out for both the Radiator and IOB. It may be found that slight increases in thickness of these components, further mass could be saved. These thicknesses have been kept relatively small at this stage in order to present a conservative model.

8 SYSTEM THERMAL DESIGN

8.1 BASELINE THERMAL ARCHITECTURE

The thermal architecture of the EChO payload is based on a combination of passive and active cooling systems (Figure 8-1). The first three cold temperature stages consist of V-Grooves passive radiators that, exploiting the favorable conditions of the L2 thermal environment, will provide stable temperature references for the modules, for parasitic heat leaks (harness, struts, piping, radiation) interception and for cryo-system pre-cooling. Three channel detectors will be cooled around 45K by means of a dedicated radiator that will benefit of the cold radiative environment set by the last V-Groove. Two channels need to work at a lower temperature, T < 30K (see Table 8-1): this is achieved by using a Neon JT cryocooler.

The EChO PLM main thermal requirements in terms of operating temperature are set by the baseline detectors/optical modules selection, derived from the basic scientific requirements, and can be summarized in the following table:

Channel	Optical Modules		Detectors		FEE	
	Op T (K)	ΔT [1] (K)	Op T (K)	ΔT [1] (K)	Op T (K)	ΔT [1] (K)
FGS	≤50	0.5	≤45	± 0.05	≤55 (TBC)	2
VNIR	≤50	0.5	≤45	± 0.05	≤55 (TBC)	2
SWIR	≤50	0.5	≤45	± 0.05	≤55 (TBC)	2
MWIR	≤32	0.5 (TBC)	≤28	± 0.005	≤55 (TBC)	2
LWIR	≤28	0.5 (TBC)	≤28	± 0.005	≤55 (TBC)	2

Notes: [1] Peak to peak value over a typical observation time

Table 8-1. Main thermal requirements for the EChO Instrument

In Table 8-2 are reported the best up-to-date assumptions (with 50% margin) for the dissipation of the active components of the Instrument in the cold PLM. The detectors and front-end electronics load is evaluated on the basis of the present design trade-off study of the channels detecting chain.

Channel	Detectors (mW)	T Control Stage (mW)	FEE (mW)
FGS	10	5	20
VNIR	10	5	20
SWIR	8	5	20
MWIR	5	5	20
LWIR	5	5	20

Table 8-2. Active dissipation of EChO cold units (with margin)

The Temperature Control Stage power is the predicted average load dissipated by the closed loop circuit when assumptions on the expected instabilities at the relevant thermal interfaces are made (see section 8.3).

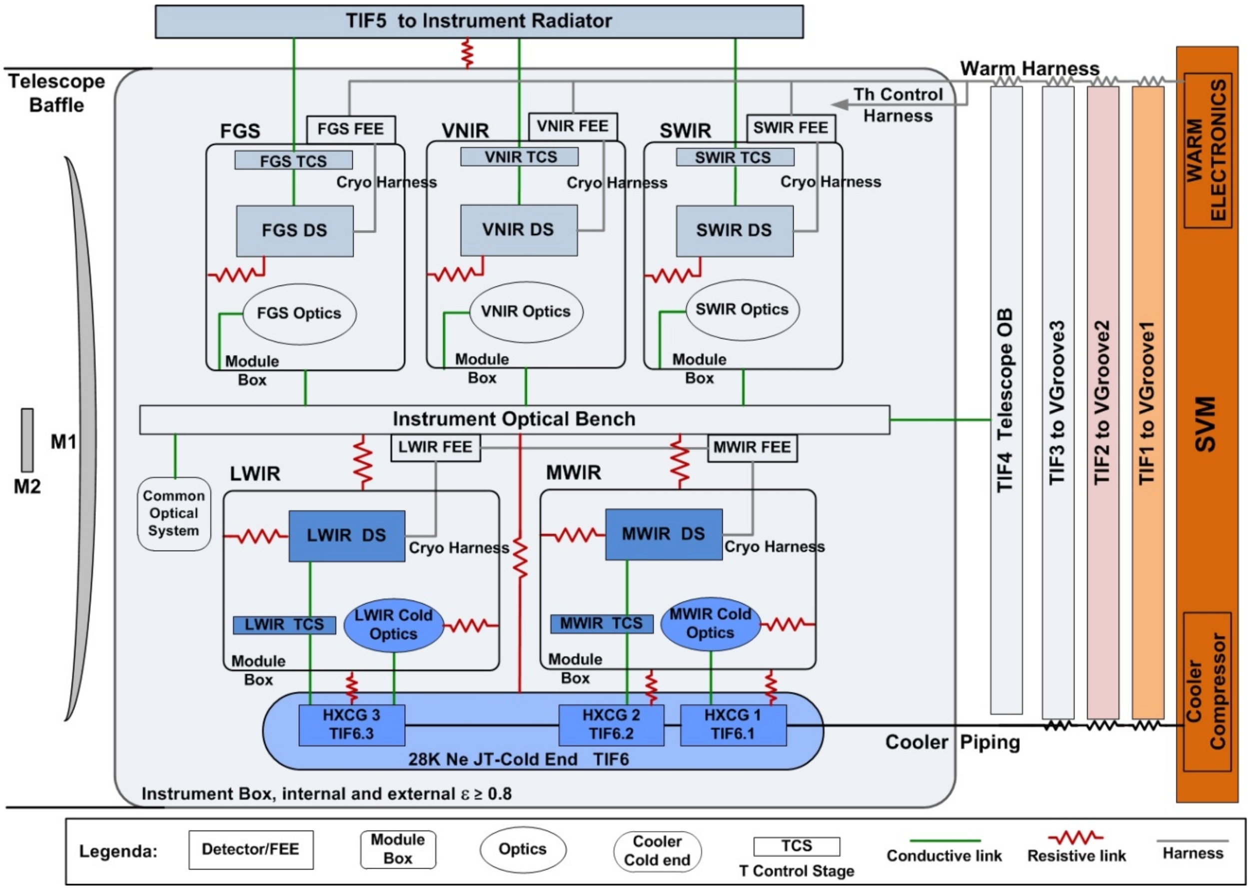

Figure 8-1: EChO thermal scheme with main thermal IF's to S/C

Each instrument channel module can be considered as thermally composed by a Box that includes an Optical Module (OM) and a Detector System (DS), composed by the Focal Plane Assembly (FPA) with its Temperature Control Stage (TCS). Due to electrical performance issues the cryo-harness connecting the FEE to their detectors cannot be longer than few tens of cm (around 20 cm max). From this follows that the FEE shall be mounted in proximity of the detectors. For the three warmer channels the cold driving electronics is installed on the module box nearby the detectors stage. For the L/MWIR modules, in order not to over load the cooler cold end, the FEE boxes is mounted on the Instrument Optical Bench (IOB). The FEE thermal coupling to the modules boxes, or to the IOB, shall allow a fast heat transfer to the Telescope Optical Bench (TOB) via the IOB itself. If the warm harness is thermally anchored to the TOB, a possibility may be offered by using the cables as conductive links to efficiently transfer heat from the cold electronics towards the TOB (TBC).

The general scheme of the EChO thermal architecture, with the six main thermal interfaces identified in the study, is shown in Figure 8-1. The FGS, VNIR and SWIR Modules share the same thermal design. The detectors operate at T ≤ 45K, cooled by a dedicated passive radiator stage (Instrument Radiator in Figure 8-1) located inside the cold environment set by the third VGroove and the Telescope Optical Bench (TOB). This radiator is mechanically supported on the Instrument Bench by means of insulating struts and is under Instrument responsibility. High conductive links connect the FGS, VNIR and SWIR detectors, through the thermal control stage, to the radiator. The Module Box of the FGS, VNIR and SWIR channels is mechanically supported on the IOB and thermally linked to the bench by using conductive mechanical supports. In this configuration, at steady state, the FGS/VNIR/SWIR optical units are expected to thermally equilibrate with the Instrument Optical Bench (IOB). The MWIR and LWIR detectors technology baseline requires lower operating temperatures, on the order of 30K, to achieve the required sensitivity. This temperature, with a load of tens of mW, can be reached only by using an active cryogenic system that exploits the V-Groove radiators as pre-coolers to improve efficiency and performance. The baseline The MWIR and LWIR module optics shall operate at low temperature, to minimize thermal background noise on the detectors. For this reason part of the internal optical units needs to be cooled by the refrigerator and thermally decoupled from the box, to limit heat lift requirements at the cooler heat exchangers. The L/MWIR Module boxes should be thermally decoupled from the IOB as much as possible to minimize heat leak to the cold end.

In order to provide the required cooling to detectors and optical units, the JT cooler cold end is split in three cold heat exchangers, each one supported on the two module boxes by insulating struts. The detectors and cold optics units are thermally linked to these references. The LWIR channel cold optics and detectors share the same temperature requirements. A single heat exchanger serves both units. Two separate heat exchangers are devoted to the MWIR optics and detectors, since they should work at different temperatures.

In general, each detector stage is thermally decoupled from the relative module box or optics, to ensure optimal performances of the FPA in terms of absolute temperature and stability. Coupling to the temperature reference stage (cooler cold end or radiator) is achieved through a Thermal Control Stage (TCS): this is a detector supporting flange that allocates an active closed loop thermal control system composed by a heater + thermistor couple driven by the ICU.

Instrument radiative thermal control is achieved by proper shielding and by the units IR emissivity. The radiative environment for the modules is set by the Instrument enclosure, defined by the IOB and a MLI/SLI shroud that surrounds the channel modules and the common optics to shield them from the external environment. This blanket shall have a very low emissivity on the external surface but may require high emissivity in the internal surface to limit straylight leaks (TBC). In this case, internally black coated MLI is required. The instrument cavity is passively maintained at a temperature ≤45 K by the radiative background set by the VGrooves and Telescope Optical Bench. The radiative coupling between subsystems inside the box is defined by the high IR emissivity requirement ($\varepsilon \geq 0.8$, TBC) needed to minimize straylight radiation contamination in the optical paths of the channels. The mechanical units (boxes and surfaces) inside the instrument cavity shall be externally coated with black paint or anodizing (TBC).

The warm electronics is located in the SVM. All harness from SVM to Instrument channels should be thermally linked to all the passive stages (VG1, VG2, VG3 and TOB) for maximum parasitic interception. In this way the heat leaks due to wiring on the Instrument cooling stages are minimized. The cryo harness heat leaks to detectors is controlled by thermally optimizing the harness design with respect to the required electrical performances (see 8.1.2).

8.1.1 Thermal Interfaces definition

In the EChO Instrument thermal configuration six main Thermal Interfaces (TIF’s) to the S/C and PLM have been identified (see Figure 8-1). The instrument thermal performance is ensured by flowing the basic instrument requirements (Table 8-1) down to the main thermal interfaces (Table 8-3). The absolute temperature values are set by detectors/optics operating point and the total conductance from these units to the TIF’s. The thermal stability requirements of the TIF's over a typical exposure time should ensure the required stability of the module units. The stability across longer periods, such as seasonal changes or the whole mission, will be defined in the next stage of the study once orbital operations can be derived from the S/C observations strategy. These requirements shall ensure best performances of the optical and detector systems over longer periods and full mission lifetime.

For a cryogenic instrument, internal and external thermal interfaces are the key to a successful design. The detectors must be thermally decoupled from the IOB, by resistive supports to improve their stability, while thermal contact with the cooling stage (JT cold end or cold radiator) must be maximized. This requires that the MWIR and LWIR modules and the cooler cold ends are located in a compact mechanical arrangement to minimize the thermal path (see Figure 8-2). The baseline JT cooler cold tip is split in three heat exchangers mounted at a convenient position on the modules by insulating supports. Detectors and cold optics couple to these cold references by thermal links under the responsibility of the modules team. The Instrument Radiator, is integrated on the Instrument Bench through bipods on three connection points (see Figure 9-2). The allocated volume is defined by the thermo-mechanical design of the PLM. High conductivity links are implemented to maintain the FGS, VNIR and SWIR module detectors at their operating temperature.

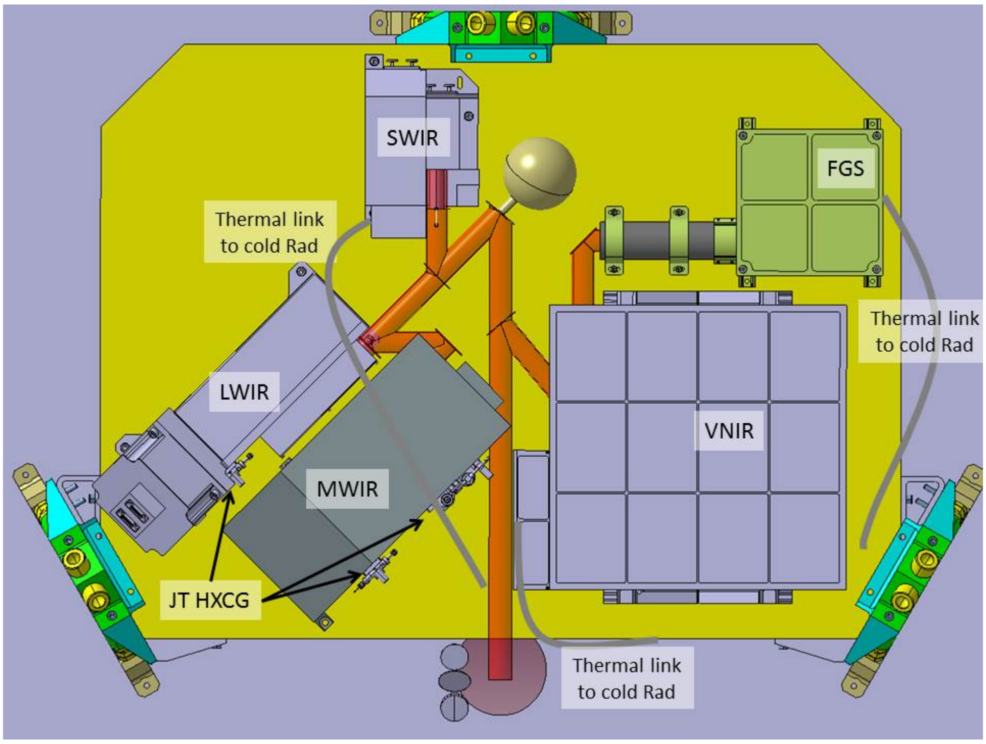

Figure 8-2. EChO PLM mechanical configuration on the IOB

The required conductance across each TIF is evaluated by analysis running thermal model simulations (see par. 8.2). A typical value of 500 W/m^2/K is assumed as the average surface thermal conductance of machined metallic interfaces when they comply to the specifications reported in the Thermal Passive Hardware Specification Document (ECHO-RS-0012-RAL). This value was achieved in several Planck couplings in the 20-45K range even with M4 bolts, using spring washers and, in some cases, a filler (gold sheet). The required conductance values and limits at the EChO TIF's have been bounded by running parametric analysis. A justification of the assumptions made on the main conductive links is reported in the TMM/GMM Technical Note ([RD38]). The required conductance of the Instrument units that couples to the TIF's are summarized in the following table:

I/F	Unit	I/F to	T (K)	ΔT[1] (K)	G across IF (W/K)	Contact Area (cm^2)
TIF1	VG1	Warm Harness, cooler piping	≤150	≤ 1	≥0.5	≥10
TIF2	VG2	Warm Harness, cooler piping	≤100	≤ 1	≥0.5	≥10
TIF3	VG3	Warm Harness, cooler piping	≤55	≤ 1	≥0.5	≥10
TIF4	TOB	Parasitics and channels FEE	≤55	≤ 1	≥0.5	≥10
TIF5	I Radiator	FGS, VNIR and SWIR detectors	≤45	≤ 0.1	≥0.2	≥4
TIF6	JT cold end	L/MWIR detectors and cold optics	≤28	≤0.05	≥0.1	≥2

Notes: [1] Peak to peak value over a typical observation time (several hours)

Table 8-3. TIFs main requirements

Each detector FPA is supported on a flange that works as the active Thermal Control Stage (TCS) by thermally sized stands to achieve a tuned thermal break. TIF5, for FGS, VNIR and SWIR, is located on the radiator. TIF6, for MWIR and LWIR, is split in three sub interfaces (6.1 to 6.3, see Figure 8-1): two are located directly on the MWIR module and one on the LWIR module, with a contact area of at least 2 cm^2. The required conductances can be achieved using common materials and solutions adopted already in previous experiments (e.g. MIRI and Planck, see [RD38]): G10 or CFRP (Kevlar is a backup possibility) for insulating struts and 5N Al for the high conductivity links. Standard Al alloys (such as 6061) are used for most of the instrument structures and boxes. Stainless steel bolts (A2-70) not smaller than M5 shall be used for the main mechanical couplings to Spacecraft and to the IOB. In general, to optimize the thermal contact, the maximum bolt dimension allowed by the mechanical allocations and design should be used. If needed, spring washers and a thermal filler (Gold or Indium for example) could be considered to improve conductance.

The main thermal links between the FGS, VNIR and SWIR detectors and the cold radiator is based on high purity 5N Al braids (wires or foils). Exploiting the high thermal conductivity of pure Al at low temperatures, it is possible to maintain dimensions, and mass, of the braids well within allocations. The total conductance between the radiator and the detectors, results from the combination in series of the contact conductance at the interfaces with the conductance of the thermal link. If the contact conductance at the IF's is 0.2 W/K, then a 0.1 W/K are required across the thermal braids. This value is tuned, by analysis, to minimize the stabilization control power at the TCS while allowing the required operating temperature at the detectors. The resulting total conductance is also compatible with annealing (TBC): should this process be required, it could be performed using the control stage heater. Being connected to the cold end by a G=0.05 W/K, a detectors ΔT of 10-15 K needs 500-750mW. A power that shall be within the capacity of the control heaters and low enough not to dramatically unbalance the radiator if applied only for few seconds.

In the 40-45K range the conductivity of high purity Al (5N) is around 2000 W/m-K. The total conductance of a metallic braids thermal link is commonly assumed to be

$$G_{braid} = \frac{kA}{L} \cdot \eta_p \eta_s \eta_e$$

where η indicate efficiency factors that take into account realistic inefficiencies in the density of wires (or foils) per unit area, in the effective length of the link (due to turn and bends) and in the welds of the braids to the end flanges. Assuming typical conservative values for these factors and imposing a safe estimation of the distance between the modules and the radiator, it is possible to evaluate dimensions and mass of the braids required to achieve a total conductance G ≥ 0.05 W/K across each link for the three EChO channels:

Channel	Effective L (cm)	Braid Section (cm^2)	End flanges dimensions LxWxT (cm)	Total Mass (g)
SWIR	70	0.4031	2 x 2 x 0.3	90.8
VNIR	100	0.5039	2 x 2 x 0.3	151.8
FGS	100	0.5039	2 x 2 x 0.3	151.8
			Total mass	394.4
			Mechanical Supporting struts	300.0
			Total mass w/ 50% margin	1041.6

Table 8-4: EChO thermal braids dimensions

The total mass of the thermal braids for the FGS, VNIR and SWIR channels, including supporting struts, gives a grand total of around 1 kg with 50% margin, that is well within allocated 1500 g.

8.1.2 Harness thermal analysis

Detectors wiring plus all the service harness (general HK, thermal control, heaters, thermistors etc.) consists of a high number of electrical connections. An appropriate selection of materials combined with an optimal combination of gauge wiring and harness length allows to keep the conducted load from the warm SVM to colder stages in the tens of mW range.

In order to minimize the parasitic load on the coldest stage, all the passive stages should be used for heat leak interception. In particular, for the EChO instrument thermal design optimization it should be evaluated the possibility of using the TOB as a warm harness thermalization stage to minimize the load of the FEE on the detectors. Working as a conductive link, the warm harness could efficiently remove cold electronics heat load towards the TOB.

A reliable definition and design of the harness will follow the finalization of the detectors and electronics architecture. The warm harness, in particular, will be under Spacecraft responsibility but, to evaluate a first order estimation of the possible heat loads due to instrument wiring for thermal analysis purposes, a simple trade-off study has been started on basic conservative assumptions. The cryo-harness (connecting the FEE to the detectors) design will be imposed by the electrical performance specifications and thermal optimization will likely be limited.

The main assumptions for the warm harness (from Warm Electronics to channels FEE) are:

- 100 AWG32 conductors per channel
- total of 500 (this conservative estimation includes shielding)
- 1 m length between each VGroove thermal stage (3 m total length)
- few common materials considered

Wire material	300K-150K (W)	150K-100K (W)	100K-45K (W)
Cu	0.96	0.328	0.528
CuBe	0.156	0.04	0.0176
PhBronze	0.1152	0.0272	0.022
Manganine	0.0528	0.0128	0.01144

Table 8-5: Warm harness materials analysis

Cryoharness, from FEE to detectors:

- 100 AWG36 conductors per channel, flexi-cable type (TBC)
- total of 300 wires going to the 45K detectors and 200 to 28K detectors (this conservative estimation includes shielding)
- 0.2 m length (this value can be critical for the harness electrical performances)
- few common materials considered

Wire material	55K-40K (W)	55K-28K (W)
Cu	0.28575	0.864
CuBe	0.00314	0.009504
PhBronze	0.00429	0.01296
Manganine	0.00200	0.006048

Table 8-6: Cryo harness materials analysis

The analysis, as expected, shows that Cu wires should be as much as possible avoided for the cryo-harness, preferring other materials (such as Phosphorous Bronze or Maganine), if the higher electrical resistivity is not an issue for the detecting chain performances. If Cu cannot be avoided, much smaller wire gauge should be used. According to previous thermal design with similar detector architectures, the flexi-cable that could be used for the cryo-harness has a thermal conductance of around 0.0015 W/K. This shall be confirmed by the detectors provider.

Thermal harness:

- around 25 Instrument thermistors, fully redundant (total is 50) in the cold PLM
- 5 cryocooler thermistors in the cold PLM
- All thermometers 4 wires readout, AWG32, twisted pairs (total of 240 wires, 300 is taken for a conservative estimation that includes shielding)

- Low k materials (e.g manganine and/or PhBronze) as baseline
- 10 heaters (nominal + redundant) for thermal control, 2 wires each need Cu wiring (AWG32) for a total of 20 wires
- 1 m length is assumed in between stages

Unit	300-150 (W)	150-100 (W)	100-45 (W)	55-40 (W)	55-28 (W)
Heaters	0.038	0.013	0.021	0.0058	0.0069
Thermistors	0.055	0.013	0.011	0.0013	0.0008

Table 8-7: Thermal harness loads across stages

That results in the following total loads (including 30% margin) due to thermal control harness on the stages:

Thermal stage	VG1 (TIF1)	VG2 (TIF2)	VG3 (TIF3)	Instrument Radiator (TIF5)	JT cold end (TIF6)
Total load (w/ 30% margin)	0.122	0.034	0.041	0.009	0.010

Table 8-8: Heat loads due to thermal harness

Once the instrument electronics architecture will be in the next advanced phase, a detailed analysis will allow to trade thermal performance with the electrical properties, reliability, mass and complexity for harness design optimization.

8.1.3 Thermal control hardware

The EChO Instrument active thermal control hardware consists of thermistors and heaters. The number and specifications of the thermometers have been defined on the basis of the minimum level of information needed to ensure a complete knowledge of the Instrument and TIF's during flight operations. Detailed temperature monitoring is achieved by the combination of direct measurements with units thermal prediction analysis, correlated with all ground test results at sub-system and system level.

Heaters are needed for thermal control of the channels detector. No decontamination heaters are, at this stage of the study, considered in the Instrument thermal hardware package. Anyway the control heaters can be sized to function as decontamination tools, for the detector stages, should this need arise.

All thermometers and resistors are assumed to be fully redundant, with the backup items connected to the redundant ICU.

A thermometer is installed in correspondence of each URP, main thermal interface or critical item. Temperature measurements shall be acquired at 1Hz (TBC): this value can be relaxed to a lower rate if the typical thermal fluctuations spectrum expected on the ECHO PLM will result dominated by lower frequency instabilities. All thermistor shall be read by 4-wires measurement and shall be connected by shielded (TBC) twisted pairs to the readout electronics to minimize EMI from external sources.

Unit	Position	Number	Type	Resolution	Accuracy
FGS	TCS	1 (+1 Red)	Cernox (TBC)	0.025K for T ≤ 60K 0.1K for T > 60K	0.050K for T ≤ 60K 0.25K for T > 60K
	Critical optical unit	1 (+1 Red)			
	Box	1 (+1 Red)			
VNIR	TCS	1 (+1 Red)	Cernox (TBC)	0.025K for T ≤ 60K 0.1K for T > 60K	0.050K for T ≤ 60K 0.25K for T > 60K
	Critical optical unit	1 (+1 Red)			
	Box	1 (+1 Red)			
SWIR	TCS	1 (+1 Red)	Cernox (TBC)	0.025K for T ≤ 60K 0.1K for T > 60K	0.050K for T ≤ 60K 0.25K for T > 60K
	Critical optical unit	1 (+1 Red)			
	Box	1 (+1 Red)			
MWIR	TCS	1 (+1 Red)	Cernox (TBC)	0.025K for T ≤ 60K 0.1K for T > 60K	0.050K for T ≤ 60K 0.25K for T > 60K
	Critical optical unit	1 (+1 Red)			
	Box (at coldend IF)	1 (+1 Red)			
LWIR	TCS	1 (+1 Red)	Cernox (TBC)	0.025K for T ≤ 60K with a goal of 0.005K 0.1K for T > 60K	0.050K for T ≤ 60K 0.25K for T > 60K
	Critical optical unit	1 (+1 Red)			
	Box (at coldend IF)	1 (+1 Red)			
Radiator	At straps IF (hot spot)	1 (+1 Red)	Cernox (TBC)	0.025K for T ≤ 60K 0.1K for T > 60K	0.050K for T ≤ 60K 0.25K for T > 60K
	At 1 bipod IF	1 (+1 Red)			
	Max gradient position	1 (+1 Red)			
IOB	At 1 bipod IF to Cold Rad	1 (+1 Red)	Cernox (TBC)	0.025K for T ≤ 60K 0.1K for T > 60K	0.050K for T ≤ 60K 0.25K for T > 60K
	At 1 bipod IF to TOB	1 (+1 Red)			
	Max gradient position	2 (+2 Red)			
	At critical optical units	2 (+2 Red)			
Total number on PLM		24 (+24 Red)			
SVM	ICU	2 (+2 Red)	PRT/DT (TBC)	0.1K	0.25K
	Warm Electronics	4 (+4 Red)	PRT/DT (TBC)	0.1K	0.25K
Total on Echo Instrument		30 (+30 Red)			

Table 8-9: Preliminary list of EChO Instrument thermistors

No JT cooler thermometer has been included in the above list as they are not controlled by the ICU. A total of few units (5 or less, TBC) are expected on the PLM part of the refrigerator hardware.

A total of 5 nominal + 5 redundant heaters are integrated for detectors thermal control, one per channel. The heaters are controlled by the ICU with feed-back closed loop logic. Heaters power supply shall be on the 28V line (TBC) and they should be sized so that the main performance specification are satisfied even at the minimum expected voltage value from the S/C on this line during operations. All heaters shall be connected to the control electronics by shielded twisted pairs to minimize EMI.

Unit	Position	Number	Type	Resistance (ohms)	Range (W)	Resolution (W)
FGS	TCS	1 (+1 Red)	Cartridge/Film	TBD	0-2(TBC)	0.001 (TBC) in the 0-0.020 W range
		1 (+1 Red)				
		1 (+1 Red)				
VNIR	TCS	1 (+1 Red)	Cartridge/Film	TBD	0-2(TBC)	0.001 (TBC) in the 0-0.020 W range
		1 (+1 Red)				
		1 (+1 Red)				
SWIR	TCS	1 (+1 Red)	Cartridge/Film	TBD	0-2(TBC)	0.001 (TBC) in the 0-0.020 W range
		1 (+1 Red)				
		1 (+1 Red)				
MWIR	TCS	1 (+1 Red)	Cartridge/Film	TBD	0-2(TBC)	0.001 (TBC) in the 0-0.020 W range
		1 (+1 Red)				
		1 (+1 Red)				
LWIR	TCS	1 (+1 Red)	Cartridge/Film	TBD	0-2(TBC)	0.001 (TBC) in the 0-0.020 W range
		1 (+1 Red)				
		1 (+1 Red)				
Total on PLM units		5 (+5 Red)				

Table 8-10: Preliminary list of EChO control heaters

8.2 STEADY-STATE THERMAL MODELLING AND PREDICTIONS

8.2.1 Reduced TMM Description

A reduced thermal model (TMM) of the EChO PLM has been built to study the thermal behaviour of the The EChO reduced TMM is composed by a relatively low number of nodes and conductors and has been implemented in ThermXL but a standard ESATAN type input file is also delivered as an appendix to this document. The model scheme is shown in Figure 8-3.

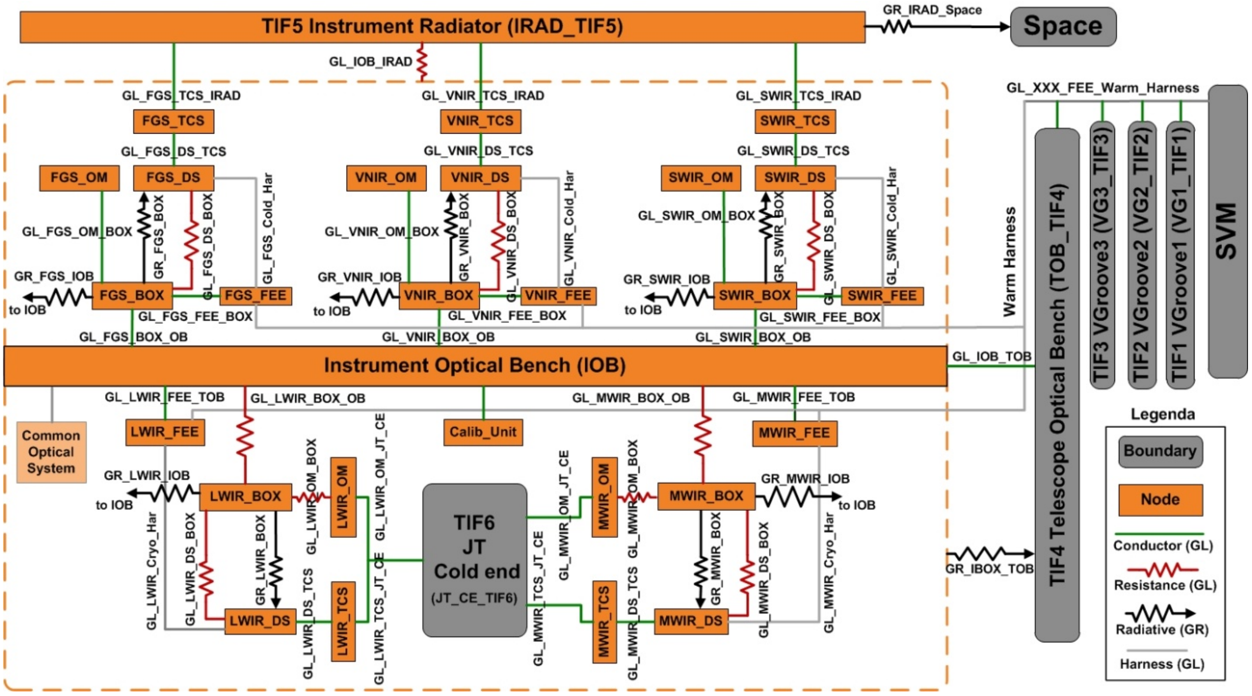

Figure 8-3. EChO reduced TMM scheme

This simplified model has been built to study the thermal behaviour of the system and its compliancy to the main requirements in terms of temperature, stability and heat fluxes allocated at the internal and external thermal interfaces.

The latest version of the reduced TMM is based on the best up-to-date assumptions for detectors and electronics dissipations. The model is Steady State version only, simplified, with few nodes per PLM unit. Each channel module is composed by 5 nodes: the box, the optical system, the detectors, the thermal control stage and the proximity electronics. The instrument cold radiator is a single node coupled to space with properties that replicate the performances of a more detailed TMM describing the radiator behavior. In this reduced steady state model the harness has been simulated as conductive links between stages and units on the basis of the harness analysis reported in [RD2]. The reduced TMM reproduces the thermal architecture scheme shown in Figure 8-1, including the Calibration Unit on the Instrument Optical Bench. The main thermal interfaces are all defined as boundary nodes, with the exception of the Instrument Optical Bench that, due to its strong conductive and radiative coupling, is a mechanical interface more than a thermal one. For this reason it is simulated as a diffusion node and provides an indication of how the whole instrument can follow the boundary environment.

The model has been run in what have been considered Hot and Cold Cases (VG3, IOB, IC at 45K) to bound the range of conductive and radiative environmental conditions.

A more detailed description of the reduced TMM with the justification of the assumptions made for the nodes and conductors is reported in the EChO TMM/GMM Description and Results Tech Note [RD38].

8.2.2 Reduced TMM results

The TMM results in terms of nodes temperature and heat fluxes for the Cold and Hot Casesbare reported in the following Table:

Node Name	Type	Q input (W)	T (K) ± 1K	
			Cold Case	Hot Case
LWIR_BOX	D		34.4021	48.8993
LWIR_OM	D		28.0634	28.2071
LWIR_DS	D	0.005	29.8116	32.1111
LWIR_TCS	D	0.005	28.2101	28.4192
LWIR_FEE	D	0.008	36.8528	52.2813
MWIR_BOX	D		35.0692	50.2254
MWIR_OM	D		28.0701	28.2202
MWIR_DS	D	0.005	29.8179	32.1235
MWIR_TCS	D	0.005	28.2107	28.4203
MWIR_FEE	D	0.008	36.8529	52.2814
SWIR_BOX	D		36.7970	52.3932
SWIR_OM	D		36.7970	52.3932
SWIR_DS	D	0.008	36.1162	44.8342
SWIR_TCS	D	0.005	35.1655	42.6480
SWIR_FEE	D	0.016	36.9817	52.4815
VNIR_BOX	D		36.7976	52.3937
VNIR_OM	D		36.7976	52.3937
VNIR_DS	D	0.01	36.3140	45.0319
VNIR_TCS	D	0.005	35.1984	42.6810
VNIR_FEE	D	0.064	36.9851	52.4849
FGS_BOX	D		36.7976	52.3937
FGS_OM	D		36.7976	52.3937
FGS_DS	D	0.01	36.3140	45.0319
FGS_TCS	D	0.005	35.1984	42.6810
FGS_FEE	D	0.064	36.9851	52.4849
IOB_BOX	D		36.7607	52.3806
Calib_Unit	D	0.0018	36.7787	52.3986

IRAD_TIF5	D		**34.8753**	**42.1108**
SVM	**B**		**253.0000**	**323.0000**
VG1_TIF1	**B**		**140.0000**	**150.0000**
VG2_TIF2	**B**		**90.0000**	**110.0000**
VG3_TIF3	**B**		**35.0000**	**55.0000**
TOB_TIF4	**B**		**35.0000**	**55.0000**
JT_TIF6	**B**		**28.0000**	**28.0000**
Space	**B**		**4.0000**	**4.0000**

Table 8-11. EChO reduced TMM nodes results

The results in terms of temperature distribution are very encouraging: they show very small gradients between the units and the respective interfaces. This provides some extra margin on the thermal coupling and interfaces optimization for the next thermal design phase.

The net heat load across the main thermal interfaces is reported in the next table:

Instrument Thermal Interface	Thermal Path	Cold Case heat flux (W)	Hot Case heat flux (W)
IOB to TOB	Conductive heat leaks from IOB to TOB	0.018	-0.026
Cold Radiator	Conductive heat leaks from spacecraft	0.005	0.026
	Conductive load from detectors	0.047	0.084
	Net heat flux rejected to Space	0.052	0.110
JT Cold-end	Conductive links from L/MWIR modules	0.055	0.127

Table 8-12. Reduced TMM heat fluxes at the Instrument main thermal interfaces

It is important to notice that even in the worst case of boundary conditions and parasitic leaks the total load on the JT cold end is well below the estimated heat lift capacity of the cooler (200mW). If this numbers will be confirmed in the next design phases, it will be possible to relax the heat load requirement to the cold end heat exchangers and optimize the cryo-system performance in a narrower range.

To all model results should be applied the uncertainty relative to this stage of the study, as specified in the present issue of the EID-A.

8.2.3 PLM TMM/GMM results

The PLM TMM/GMM (Figure 8-4) is based on the coupling of a “standard” M-size SVM with a possible configuration for the cold passive PLM. In the model are simulated the main radiative surfaces and representative supporting structures between the different stages. Detailed definitions of the instrument modules and a preliminary configuration of the cold radiator have been also integrated in the GMM for Instrument analysis purposes (Figure 8-5).

A more detailed description of the PLM TMM/GMM and results is reported in the EChO TMM/GMM Description and Results Tech Note [RD38].

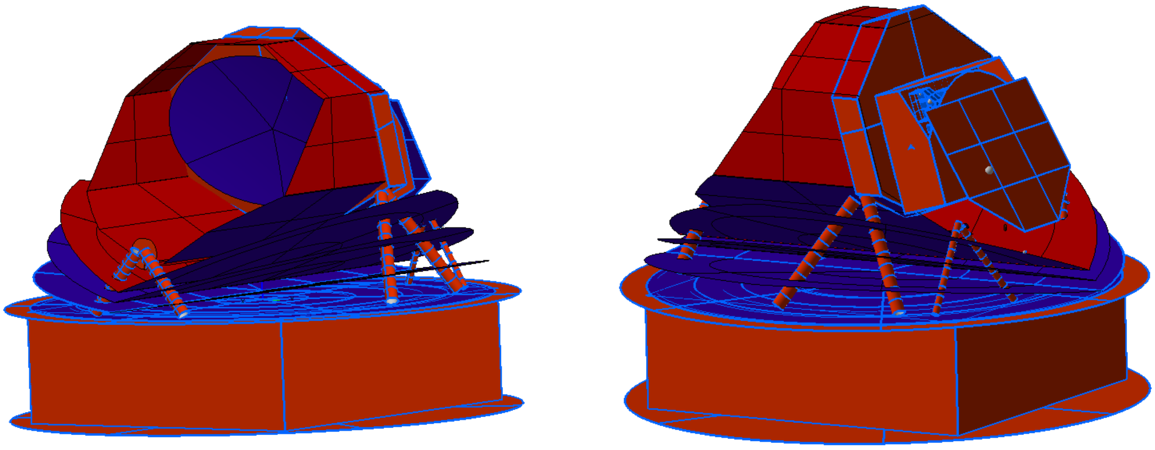

Figure 8-4. EChO geometric model view from two sides. On the right panel the radiator is visible on top of the instrument cover.

The PLM TMM has been based on the same nodes and conductors definition of the reduced TMM, with the exception of few items, due to the different level of detail of the two models. At the moment, the detectors thermal control stages are not taken into consideration in the Geometrical model and the detectors are directly coupled to their temperature references. FEE nodes have been added to simulate their loads on the PLM and Instrument units.

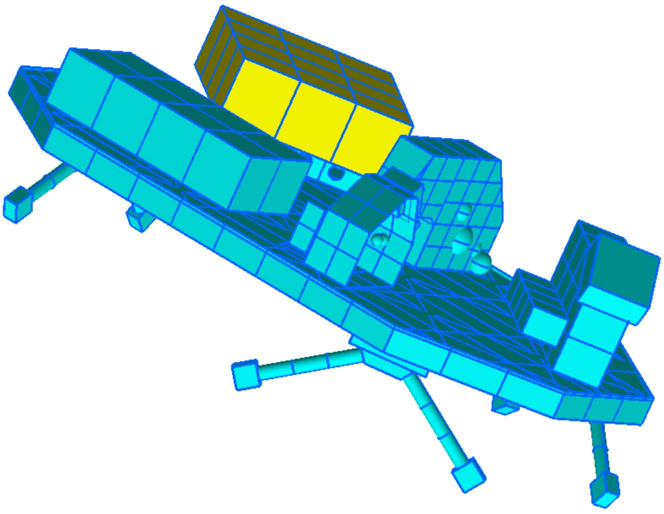

Figure 8-5. A view of the Instrument optical bench geometric model with the main units

8.2.4 PLM model results

In the following table are reported the temperatures at steady state conditions. The current version of the model is composed by 920 nodes and only the average values are reported in the table.

System	Sub-system	Unit	T (K)
SVM	Solar Array		312.95
	SVM average		249.30
VG1			148.81
VG2			93.05

VG3			48.30
Telescope	M1		33.34
	M2		33.42
	M3		33.34
	M4		33.34
	OB		33.34
	Baffle		32.89
Instrument	Optical Bench		37.49
	FGS	Box	37.57
		Detectors	35.02
		FEE	37.72
	VNIR	Box	37.52
		Optics	37.52
		Detectors	35.01
		FEE	37.68
	SWIR	Box	37.57
		Optics	37.56
		Detectors	34.98
		FEE	37.74
	MWIR	Box	36.98
		Optics	28.01
		Detectors	28.19
		FEE	37.55
	LWIR	Box	35.98
		Optics	28.20
		Detectors	28.20
		FEE	37.55
	Radiator		34.72

Table 8-13. TMM/GMM Units average temperature

The unit temperatures are graphically shown in the next figures.

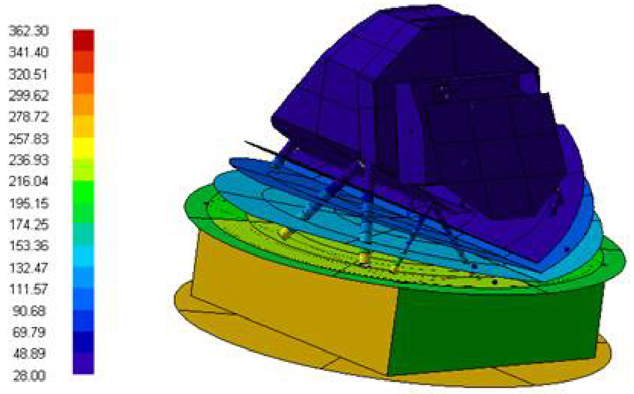

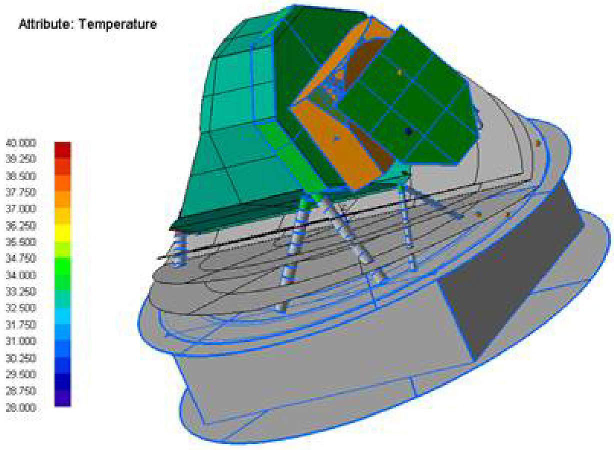

Figure 8-6. Spacecraft average temperatures (left). Cold PLM main units temperature (right)

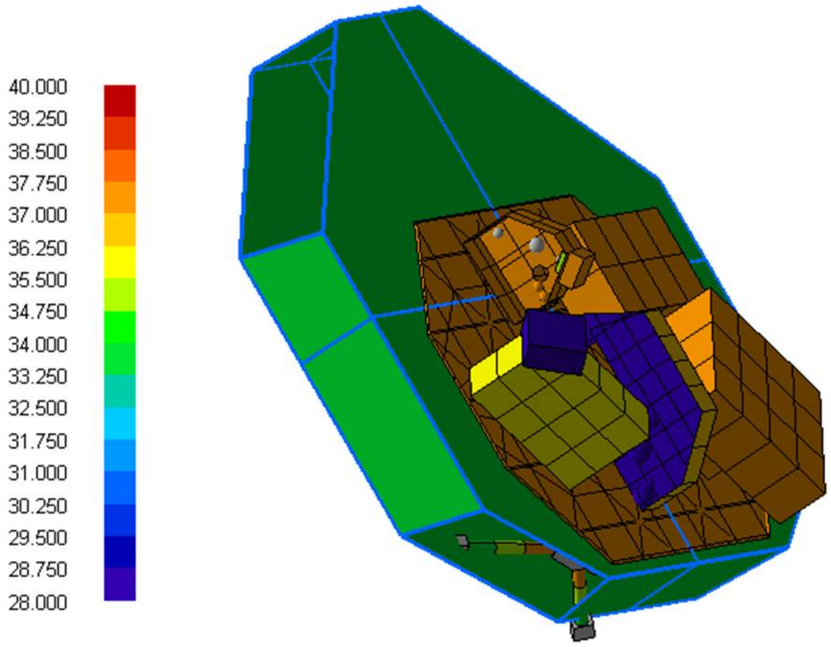

Figure 8-7. Instrument Optical Bench and Module boxes

The loads to the Instrument interfaces are evaluated by balancing the input/output heat fluxes to/from each node through all conductors. For the Instrument internal thermal analysis the main interfaces are the Cold Radiator and the JT cooler cold-end. The resulting heat flux values are reported in the following table:

Instrument Thermal Interface	Thermal Path	Heat flux (W)
Cold Radiator	Conductive heat leaks from spacecraft	0.0057
	Conductive load from detectors	0.0425
	Radiative load from warmer stages (VG3 and SVM)	0.0140
	Net heat flux rejected to Space	0.0627
JT Cold-end	Conductive leaks from L/MWIR modules	0.040

Table 8-14. TMM/GMM heat fluxes at Instrument main internal thermal interfaces

The cold radiator rejects more than 60 mW to space while, for the colder channels, almost 40 mW are loaded to the cooler cold heat exchanger.

The Geometrical Model most important results is to show how the whole spacecraft design is really efficient in rejecting heat radiatively, taking full advantage of the L2 favourable thermal conditions. The Telescope Optical Bench, the Telescope Baffle and the Instrument Cold Radiator work together as a single large surface, representing the coldest radiative stages in the spacecraft, at a temperature lower than 40K, 10-15K colder than the last VGroove. These results indicate, as expected, that the PLM thermal behaviour seems to approach tends to approach the Cold Case predictions.

To all model results should be applied the uncertainty relative to this stage of the study, as specified in the present issue of the EID-A [AD 3].

8.3 THERMAL STABILITY ANALYSIS

Operating in a stable thermal environment is a fundamental requirement for space instrumentation (detectors, optics) that needs to reach the level of sensitivity required by the EChO mission. For this reason, thermal stability is one of the key drivers of the mission thermal design. There are two possible thermal instability generators in the EChO PLM: the radiators (VGrooves and cold Radiator) and the cooler cold end. The main source of fluctuations on a radiator facing the cold sky are due to cooler mass flow dissipation (high frequency noise), to orbital changes of the solar aspect angle related to flight dynamics following the mission scanning strategy (on timescale of 10 hours or so) or seasonal variations (typically on longer periods like weeks, months, years). In general those are low frequency osciillations.

In a JT cooler, instabilities at the reference heat exchanger temperature are due to compressor modulation, with its typical high frequency spectrum (30-40Hz range), to cold-end internal mass flow 1- or 2-phase dynamics (on the order of tens of seconds) and to precooling stage variations (low frequency).

Thermal stability at the Optical Modules thermally connected to the IOB (FGS, VNIR and SWIR) is not expected to be a major concern given the typical instabilities of passive radiators in L2 either on the timescales of EChO detectors average exposure or on the seasonal. Even in the case of few hundreds of mK peak to peak fluctuations every several hours (10000s time scales), the thermal mass and resistances of the instrument channel boxes can easily filter out well below the required 0.5K peak to peak.

For the warm channels detectors and the L/MWIR modules the level of transmitted fluctuations could be at the limit of the required values. For this reason, the behavior of the units connected to the cooler cold end and to the cold radiator, has been analyzed assuming periodical oscillations with size estimated on the basis of what observed in other missions. Previous experience, based on missions like Planck, indicates that typical instabilities on radiators in L2 can be as high as 10mK over about 1000s (because of possible cooler mass flow changes) that can increase to the 100 mK range during change of SAA due to major pointing maneuvers

Detectors stability is a key issue for instrumental performance and requires a careful design of a proper thermal control system. Due to the harder requirements on temperature stability, FPA thermal control must be achieved by a combination of passive and active systems. The passive component again uses the thermal inertia of the detector system components (struts and frames) to damp T oscillations during their propagation from the instability source (the 45K radiator or the 28K cold end) to the detectors.

The finer active control is accomplished by a PID type controller on a stage thermally decoupled between the detectors and the source of temperature oscillations: the detectors supporting frame. Each detector is mounted on this supporting frame that is designed to integrate the thermal link to the temperature reference and to accommodate the control system: a thermometer plus heater couple. Since active control on detectors stage is critical for instrument performance, a fully redundant system is with two identical heater and sensor pairs.

A scheme of the proposed Thermal Control Stage (TCS) for all detector channels is shown in Figure 8-8. The TCS is the FPA supporting frame: maximizing TCS thermal inertia can help with fluctuation passive damping and reduces control power, that has an impact on the thermal budget of the mission.

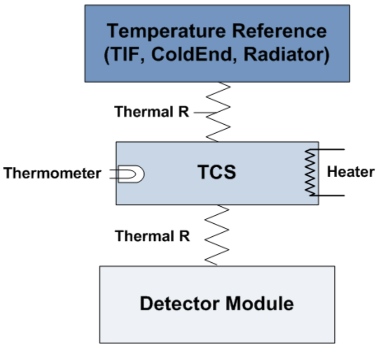

Figure 8-8. Modules Thermal Control Stage scheme

To verify the functionality of the active control stages design on the EChO modules, an analytical study correlated with a set of transient simulations have been carried out. If periodical thermal instabilities can be approximated with a sinusoidal function, then the temperature fluctuations transmitted passively at a certain stage (the TCS for example) connected to the thermal noise source are given by:

$$\Delta T_{TCS} \cong \frac{\Delta T_0}{\sqrt{1+\omega^2 R_{TCS}{}^2 C^2{}_{TCS}}} \cos(\omega t + \varphi)$$

where C_{TCS} is the thermal capacitance of the stage, $R_{TCS}=1/G_{TCS}$ is the resistance between the TCS and the cold radiator or the cooler coldend and ω is the pulsation of the oscillations. It follows from this result that the damping factor RC depends on the thermal mass of the stage and on the thermal break with the noise source. The thermal inertia of the Temperature Control Stages designed for the EChO detectors is very small. At the moment the TCS is an Al6061 flange of 2 cm x 2 cm x 0.3 cm indicative dimensions working as a supporting plate for the detectors. In this case the thermal resistance is the key parameter for oscillations passive damping. The conductance value between the detector TCS and its temperature reference is selected on the basis of a trade-off between the detectors operating temperature and the minimum power needed to achieve thermal control at the TCS.

In the next table are reported some conservative predictions of the possible fluctuations expected on the cold radiator stage and at the cooler cold end heat exchangers level based on what observed for radiators orbiting L2 in previous missions like Planck. Planck scanning strategy allowed the spacecraft to constantly maintain a low optimal solar aspect angle. The case for the EChO flight dynamics will likely push the mission to higher SAA values. This would reflect in possible oscillations at the radiator stages at each re-pointing step, inducing also oscillations in the cooler cold end: a conservative estimation of the pre-cooling stage induced fluctuations on the cooler is 0.01K/K. As this first analysis that has the objective of providing a safe figure for the thermal oscillations at various stage, it has been decided to assume conservative numbers in terms of expected oscillation frequency spectrum. These assumptions are shown in the first three columns of the following tables.

Time (s)	Frequency (Hz)	p-p ΔT (K) at radiator	ΔT at 45K TCS (K)	ΔT at 45K DS (K)	Q_tcs max (W)	Q_tcs ave (W)
10	0.1	0.002	3.181E-05	1.129E-06	1.909E-06	1.273E-06
100	0.01	0.005	0.0008	0.0003	4.550E-05	3.033E-05
1000	0.001	0.01	0.0048	0.0046	0.0003	0.0002
10000	0.0001	0.1	0.0500	0.0500	0.0030	0.0020

Table 8-15: Preliminary analysis of worst case temperature fluctuation spectrum at 45K stages

Time (s)	Frequency (Hz)	p-p ΔT at cold end (K)	ΔT at 28K TCS (K)	ΔT at 28K DS (K)	ΔT at Cold Optics	Q_tcs max (W)	Q_tcs ave (W)
10	0.1	0.00002	0.00001	7.933E-07	1.768E-08	1.768E-08	9.519E-08
100	0.01	0.00005	0.000025	1.557E-05	4.420E-07	4.420E-07	1.868E-06
1000	0.001	0.0001	0.00005	4.961E-05	8.707E-06	8.707E-06	5.953E-06
10000	0.0001	0.001	0.0005	0.0005	0.0004	0.0004	0.0001

Table 8-16: Preliminary analysis of worst case temperature fluctuation spectrum at 28K stages

In these tables the timescales and frequencies of the expected peak to peak fluctuations at the noise source (radiator or cold end) are then compared to the oscillations transmitted to the relative TCS and DS stage of the EChO channels (columns 4 and 5). It is clear from this very simple analysis how the thermal design of the units allows for an efficient passive filtering of most of the higher frequency noise. From this follows that all possible oscillations generated in the cooler are damped to negligible levels by the thermal inertia and resistance of the systems. Typical compressor frequencies are in the tens of Hz ranges while noise generated in the cold end due to mass flow instabilities typically happens over tens of second time scales with few mK variations. All these oscillations are expected to be filtered out, at the level of the cold optics due to the higher thermal inertia of their mass. Only the slower oscillations, mainly due to changes related to flight dynamic issues (such as re-pointing, orbital and seasonal modulations etc.) will pass through and need to be actively controlled. The last two columns report the maximum and average proportional control power needed to control the transmitted fluctuations weel below the required level. To verify the results of this analysis on the and to check the robustness of the EChO channels thermal design, a set of simple transient simulations have been run. Figure 8-9 and Figure 8-10 report the results of the ESATAN PID control routine run on both the 45K and 28K detector thermal control stages. Using low PID parameter settings (P=1, I=0.2, D=0) the simulations show that the TCS are very effective in controlling the residual oscillations well below the requirements. The average power for thermal control on 45K stages is 2.51 mW (3.95 rms), while the 28K stages need 2.54 mW (3.22 mW rms).

This first set of simulations shall be refined in parallel with the thermo-mechanical configuration evolution of the EChO detector systems in the next phases of the study. The aim of the future thermal model runs will be a more realistic representation of the DS thermal configuration in order to obtain the best estimation of PID parameters and trade-off analysis to minimize control power. In the end, the thermal control stages design is a trade-off between the detectors operating temperature, peak-to-peak fluctuation level and the PID power. If low thermal instabilities in the whole spectrum of possible frequencies will be demonstrated by detailed future PLM transient analysis, it can be decided to remove the control stages from some (or all) detectors stages.

Typical cooling rate of passive radiators after launch during LEOP of a mission in orbit injection to L2 is on the order of few K per hour. This rate should be sufficient to ensure safe cool-down of the optical elements and detectors avoiding mechanical stresses. Heaters can be mounted on critical elements for cooling regulation and contamination control if necessary. The thermal control system can be sized to be used during cool-down to avoid condensation of contaminants on the detectors surface. For what concerns the optical units and other instrument units, in the next phase of the study the need of proportional control with heaters dedicated to keep units in the 180-160K range during cooldown shall be evaluated.

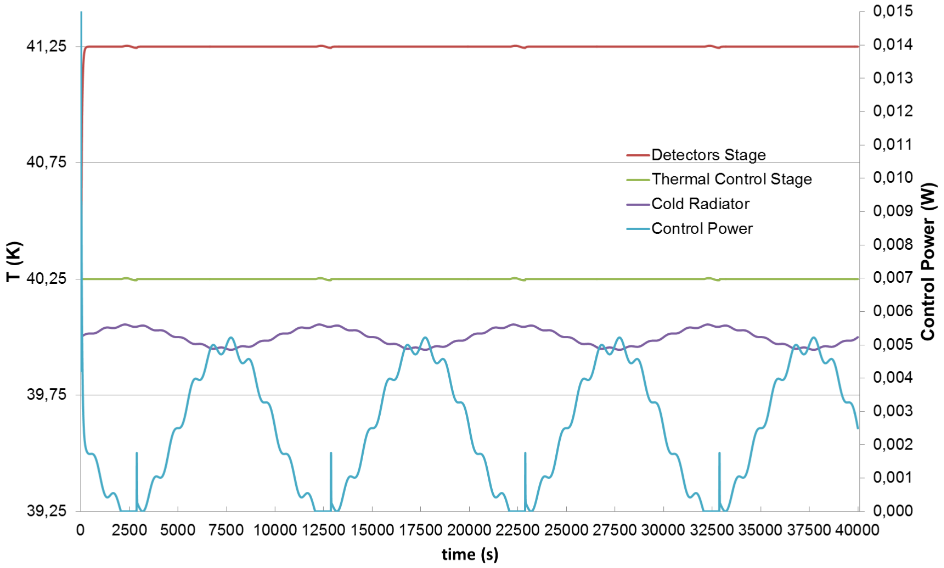

Figure 8-9. 45K stage thermal control simulation

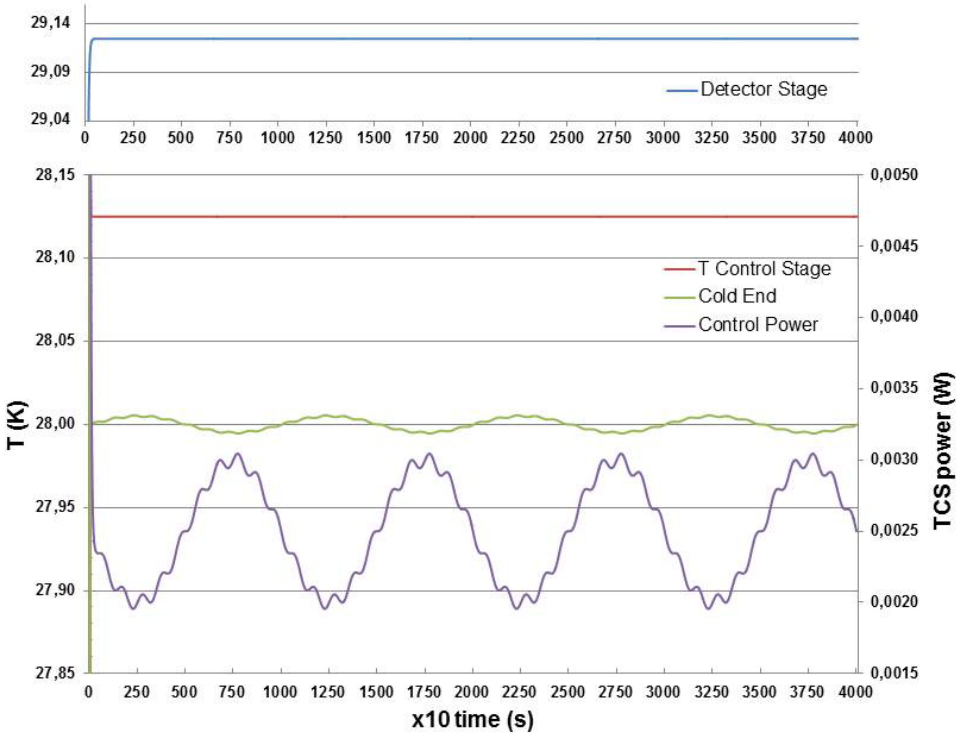

Figure 8-10. 28K stage thermal control simulation

8.4 THERMAL BUDGETS

The EChO PLM loads have been estimated on the basis of heritage from previous experience (MIRI, Planck etc.) for what concerns detectors dissipation, mechanical supports and harness leaks. These conservative estimations have been then checked and confirmed by thermal analysis and simulations with a reduced TMM and a PLM TMM/GMM (Chapter 8.2).

The budget resulting at the main Thermal Interfaces from all this analysis activity is reported in Table 8-17. The values correspond to the thermal boundaries Hot case, assumed as a sort of worst case to provide a conservative evaluation.

Thermal Interface	Location	IF to	T (K)	Load (mW) (w/50% margin)	Comments
TIF1	VGroove 1	Heat leaks from SVM (harness, struts, piping, radiation)	≤ 150	100	*From EID-A allocations, TBC*
TIF2	VGroove 2	Heat leaks from warmer stages (harness, struts, piping, radiation)	≤ 110	100	*From EID-A allocations, TBC*
TIF3	VGroove 3	Heat leaks from warmer stages (harness, struts, piping, radiation) + JT precooling	≤ 55	150	*From EID-A allocations, TBC* *Mainly conducted and radiated parasitics*
TIF4	Telescope OB	IOB, all channels FEE, parasitics	≤ 55	300	*Assumed most of FEE dissipation, loads from VNIR, FGS and SWIR modules + parasitic leaks (TMM analysis results)*
TIF5	Instrument Radiator	FGS, VNIR, SWIR detectors + T control stage loads	≤ 45	110	*Radiator dedicated to VNIR, SWIR and FGS detectors cooling*
TIF6	Ne JT cold end	MWIR and LWIR detectors & cold optics + T control stage loads + parasitics (struts+harness+rad)	≤ 28	127	*Best guess on detectors dissipation and TMM analysis*

Table 8-17: EChO TIF's requirements and budget

The resulting heat fluxes across the main Thermal Interfaces are all well within the allocated values.

"In particular, even if the reduced TMM results show low conductive loads from the Instrument to the TOB, the allocation on the TOB should be maintained at the 300 mW specified by the EID-A. In the present TMM configuration the TOB is assumed to be a boundary fixed at the EID-A temperatures. This is not fully representatives of the actual flight conditions as during operations the TOB and IOB temperatures will be similar. Moreover the harness from warm electronics to the FEE is assumed to be thermally insulating in the model. For this reason the FEE load is mostly dissipated on the detector stages. In the next phases of the study, solutions that maximize heat extraction from FEE to TOB shall be investigated: for example, a thermally conductive harness between the FEE and the TOB should be evaluated to increase the thermal coupling between the IOB and the TOB.

In summary, assuming the active (FPA and FEE, TCS) units dissipations and using conductance values for linkage between nodes on the basis of previous experience, the reduced TMM results demonstrate, within the resolution of the present level of detail, that the baseline thermal architecture is robust. The design is compliant to both the temperature requirements and the allocated heat loads on stages and thermal interfaces.

At this stage of the mission study a safe 50% margin has been applied to the loads budget for the thermal architecture and cryo-chain definition. Improving the knowledge of the systems and solutions, together with a better understanding of their interactions, in the next phase of the project will allow to justify and potentially relax (with ESA concurrence) the margin levels following the PDR.

9 CRYOGENIC SYSTEMS OPTIONS

9.1 COOLING FOR 40-50K STAGE (PASSIVE)

The VGroove-based design will provide a cold and stable environment for the PLM units: telescope, instrument and cryochain cold ends. The VNIR, SWIR and FGS channel requirements in terms of operating temperature, stability and dissipated loads need a dedicated cold radiator for their detectors cooling only. This extra passive stage, called Instrument Radiator or Cold Radiator, will be designed and developed under the responsibility of the Instrument. In the baseline thermal architecture configuration the assumptions in terms of temperature and load for the channel detectors linked to the radiator are:

Channel	Detectors			Thermal control
	Op T (K)	ΔT [1] (K)	Load (mW)	Load (mW)
FGS	≤45	± 0.05	10 (TBC)	5
VNIR	≤45	± 0.05	10 (TBC)	5
SWIR	≤45	± 0.05	8 (TBC)	5

Notes: [1] Peak to peak oscillation over one typical exposure time

Table 9-1. Assumed temperatures and active loads for FGS/VNIR/SWIR detector stages

VGroove3 allocation is 300 mW (TBC) with a temperature in the range 35K (cold case) – 55K (hot case). This heat load in the first place is used to intercept all parasitic leaks to the cold stage: harness, struts and radiation from warmer stages etc. In this way the 40K radiator is fully devoted to cool the channel detectors, with parasitic leaks due only to its own supporting struts and thermal control harness. The expected active load due to detector stages is around 43 mW. The radiator is mounted on the Instrument OB: if the total conductance of the radiator struts to the IC is lower than 0.002 W/K (achievable even with thick G10 fiberglass bipods) the expected conductive load on a 40K radiator is less than 25mW even in the hot case temperature (55K). Harness can contribute for less than 10 mW (see 8.1.2). In total, 80mW (including margin) is the expected load to the cold radiator, in the worst case.

At present, the allocated area (EID-A Issue 0.2) for the 40K radiator is 0.6 m^2 but, from all PLM studies, it looks clear that a larger radiator could fit in the allocated volume: 1 m^2 configuration options are being designed. At the moment a total area of 0.96 m^2 (shape and dimensions shown in Figure 9-1 and Figure 9-2) is being modeled in the radiative environment defined by the last VGroove and the Telescope Optical Bench. The orientation angle of the radiator inside the allocated volume is around 20° with respect to the vertical direction. Once the PLM thermo-mechanical architecture will be more defined, the shape and the orientation of the radiator will be optimized to maximize the exposed surface.

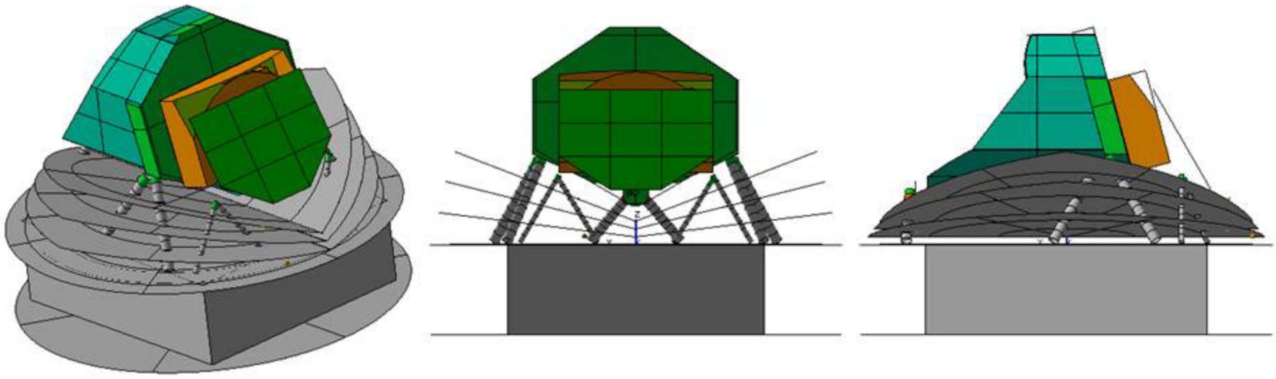

Figure 9-1. Latest configuration of EChO Instrument Radiator on PLM

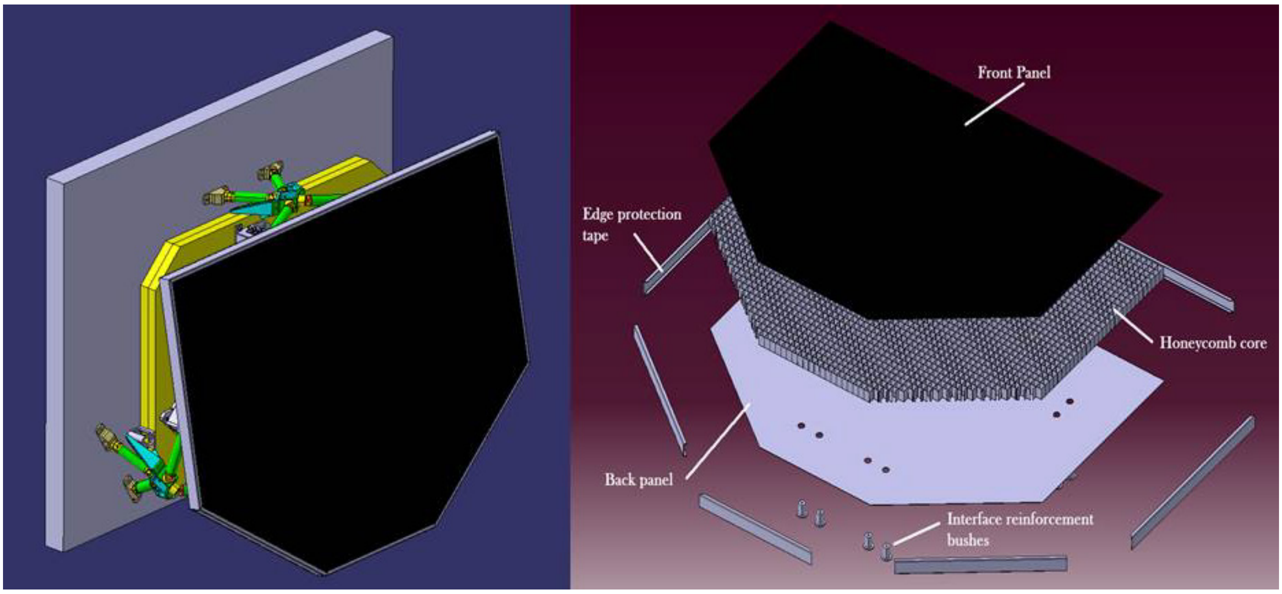

Figure 9-2. CAD view of: Cold Radiator on the IOB (left), sandwich structure (right)

A very conservative evaluation of the radiator heat rejection in L2 (to be confirmed by TMM) is based on the following assumptions:

- Radiator IR emissivity = 0.8
- Radiator efficiency = 0.8
- T sky = 4K
- View Factor = 1

The radiator emissivity and efficiency could be increased by using standard solutions (special coatings, honeycomb cell structure etc.). An IR emissivity of 0.8 is assumed given that the radiator may be coated with white paint to avoid overheating due to a possible Sun exposure during launch (TBC). Anyway, white coatings with emissivity over 0.9 are available. On the PLM internal surface, the radiator shall have a low emissivity coating (MLI or SLI, TBC) to limit radiation loads from the warmer parts of the spacecraft.

The radiator is composed by a simple sandwich of Al6061 (TBC) alloy layers. A honeycomb cells structure 3 cm thick, with 2 cm cell size and ribbon thickness of 1 mm, is packed between two 2 mm thick layers. This simple thermo-mechanical design allows for low mass and volume while ensuring at the same time a very good thermal conductance in all three directions. The system is mechanically supported on the IOB with 3 bipods made of insulating materials (TBD).

A first analysis based on simplified assumptions and design gives the following results (with 20% margin) for the radiator heat rejection capacity as a function of its equilibrium temperature for both surfaces (0.6 and 0.96 m^2):

Radiator T (K)		**40**	**45**	**50**	**55**	**60**
Q (mW)	0.6 m^2	63	100	153	224	317
	0.96 m^2	89	143	218	319	451

Table 9-2: 40K radiator heat rejection vs T and allocated area

The figures are given at different equilibrium temperature: as it is obvious, the more the detectors operating temperature can be relaxed, the more heat can be rejected to space. In the present configuration, the maximum gradient between the 45K units (FGS, VNIR and SWIR) detector and the radiator IF, is on the order of 2-3K.

A 35 nodes simple TMM model dedicated to radiator thermal performance has been developed. The three channel detectors with their active loads that include T control dissipation and thermal harness heat leaks, are connected to the central node to evaluate a worst case in terms of temperature distribution and gradients. An extra harness leak due to radiator thermal control harness is also simulated on an adjacent central node. Finally the parasitic loads due to struts are also simulated by evaluating the contribution of bipods made of G10 on four bipods (instead of the actual three).

The radiator is then coupled with cold space assuming an IR emissivity of 0.8 and an efficiency factor of 0.8. On the internal side, an emissivity of 0.05 is assumed. The boundaries (IOB and PLM cavity) are set at the worst, hot case, value of 55K.

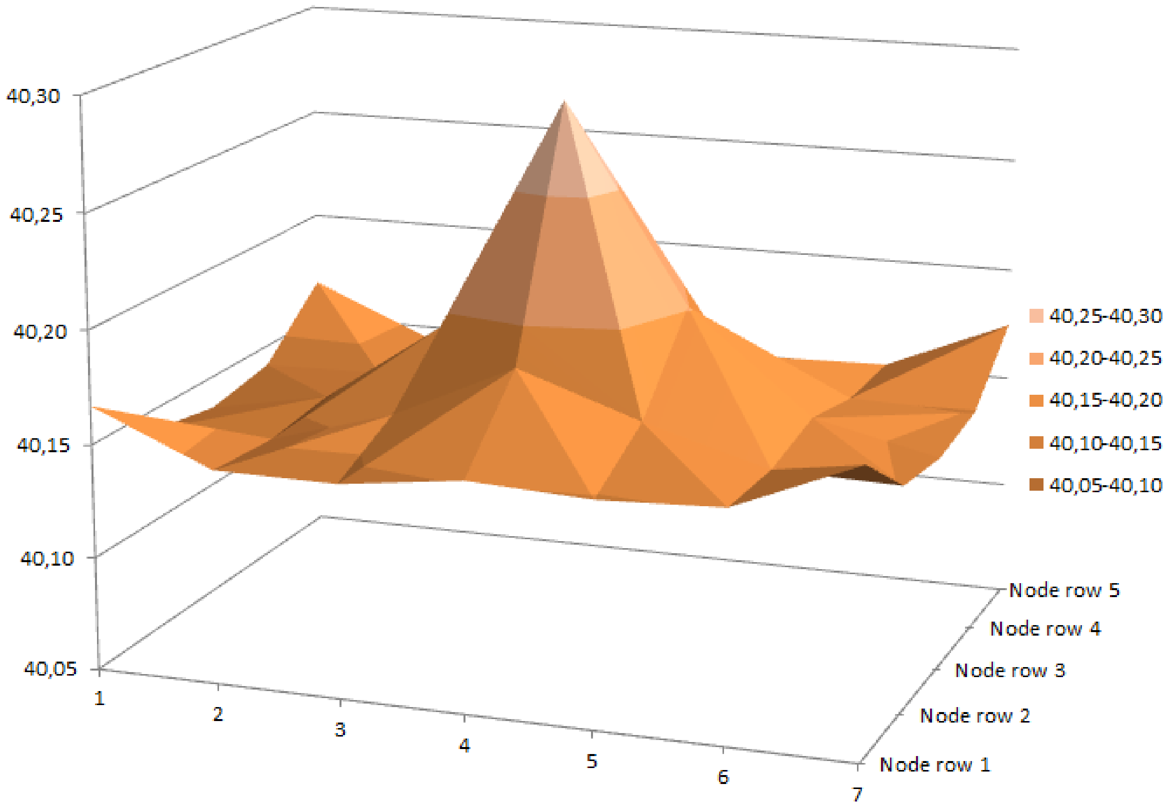

Figure 9-3: Radiator 3D temperature distribution

In Figure 9-3, the TMM temperature distribution is reported. The radiator equilibrates around 40K with a max temperature gradient of 250 mK, showing a very good uniformity even in a non-optimized configuration. In order to improve spatial gradient results, in the next phases of the study separated and evenly distributed interfacing spots for each channel will be evaluated.

9.2 COOLING BASELINE DESIGN FOR ~26K STAGE

The RAL Cryogenics and Magnetics group provided the 4K cooler for the Planck spacecraft and have designed and built many coolers for spacecraft. The designs of these coolers have been licensed to industry and have built up a reputation for being robust and having a long lifetime. There have been no failures in space. The basic design has been widely copied.

The baseline for the cooling system on EChO is a Neon Joule-Thomson (JT) system making use of the advanced compressor systems designed as part of the ESA 2K cooler development system. The heat exchanger system design will be designed in conjunction with the instrument design but for the purposes of this note, assumptions have been made concerning the available pipe lengths.

The system incorporates a compressor stage which boosts the gas pressure from around 1 bar to 10-11 bar. The gas then passes through an ancillary panel where the flow is measured and the gas is cleaned through a getter. The gas then passes through the connecting pipework and enters the heat exchanger system. There are filters on each of the stages. The gas is expanded on the focal plane assembly where it is heat exchanged with the elements to be cooled in a series of heat exchangers. The gas returns to the compressors down the low pressure side of the heat exchangers back to the compressors.

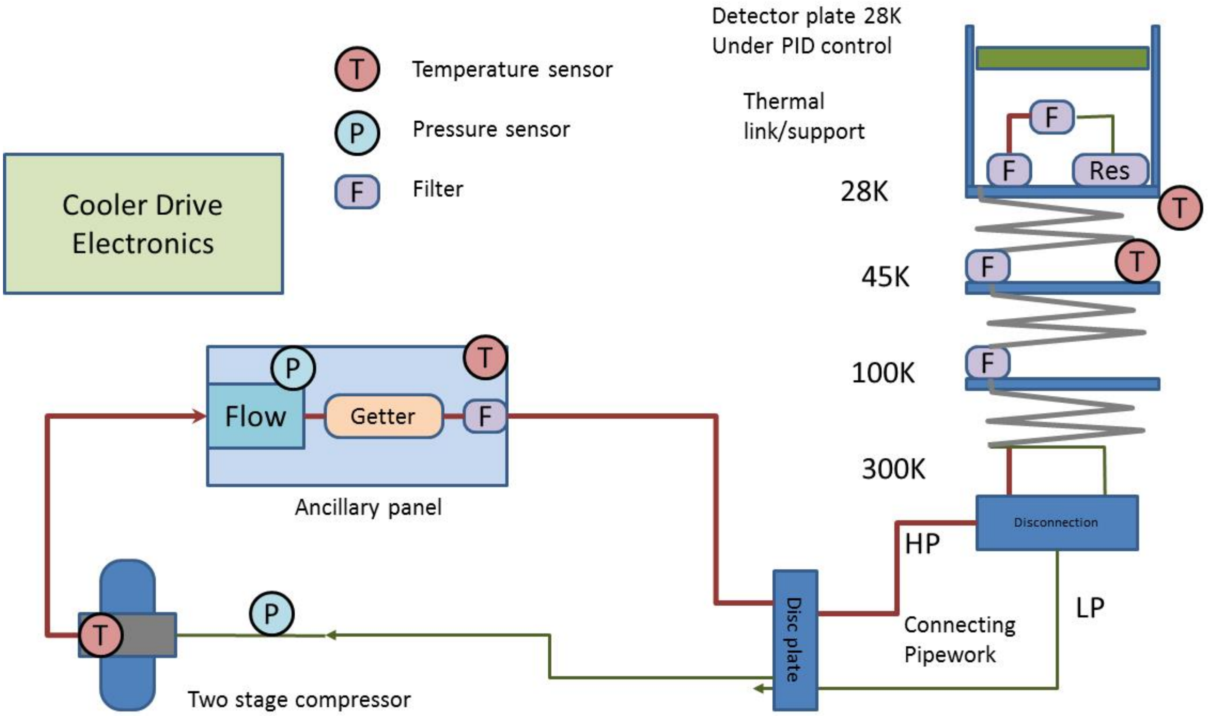

Figure 9-4: System configuration

9.2.1 Use of Neon

Neon is a noble gas with an atomic mass of 20. The main features for EChO is its boiling point of 27.05K at 1 atmosphere and its melting point of 24.55K. This is a very narrow operating range and restricts the temperature at which we are able to provide cooling. In practise we would prefer to operate the JT at slightly above 1 bar.

9.2.2 Heat exchangers:

The proposed system makes use of the cooling available at 100K and 45K. Between ambient and the stages heat exchangers are used to reduce the load on the stages. There is trade-off between the load on the stage and the pressure drop in the circulating gas. The heat exchanger construction is a tube in tube type. On each of the temperature stages there is a filter/heat exchanger which traps impurities and provides good heat exchange with the stage. The final heat exchanger is the JT heat exchanger and terminates in a filter before the high pressure gas passes through an expansion orifice where liquid is formed. This liquid is contained in a sintered element to prevent sloshing and flash evaporation effects disturbing the temperature stability. On EChO there are several cooling point and these will be served by multiple heat exchangers.

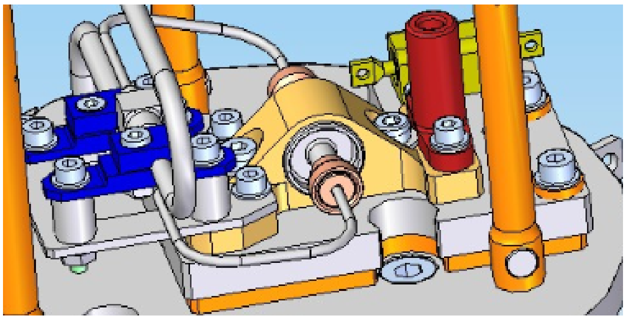

Figure 9-5: Stage filter and heat exchanger system

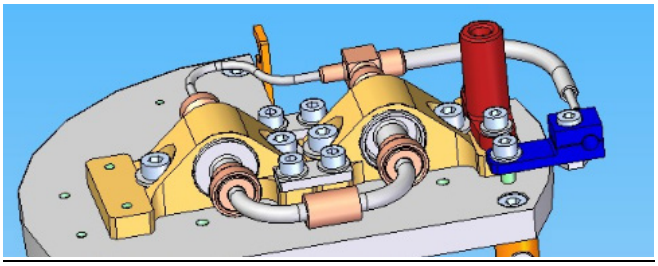

Figure 9-6: Final Stage Filter, Expansion stage and liquid reservoir

9.2.3 Compressors:

The RAL developed compressors can handle a pressure ratio of about 10 in two stages. The cooling power estimates (see below) assume a high pressure of 11 bar and a low pressure of 1.1bar. These estimates show that a mass flow of 35 mg/s is required to achieve the nominal cooling power of 200mW on the focal plane.

The mass flow rate of 35mg/s implies a volumetric flow of 38 x 10^{-6} m^3/s at 1.1 bar and 293K. This sort of flow rate is achievable with the RAL compressors. As a feasibility study, the Advanced 2K JT cooler compressor parameters have been used to model a two stage compression system with a 35mg/s mass flow rate. A design feature of the 2K compressor modular system is that the piston diameter can be easily adjusted over a wide range (10-45mm) to suit different operating requirements.

Initial modelling, without significant piston sizing optimisation and without frequency scanning, gives the following results;

Parameter	Value
frequency	40Hz
fill pressure	4.5bar
stroke	5.5mm (max=7mm)
total input power	95W
P high	12bar
P low	0.9bar
mass flow	35mg/s
piston sizes	1st stage 24mm, 2nd stage 14mm
spring rate	2-3N/mm

Table 9-3: Compressor modelling results

The requirements could be met by a two stage system, in essence this is the same JT cooler as that proposed for a 5K operation with, He but with minor modifications to the piston diameters. The spring rate requirement can be satisfied by removing some of the eight springs from the stack. If higher pressures were required then a four stage system would be implemented.

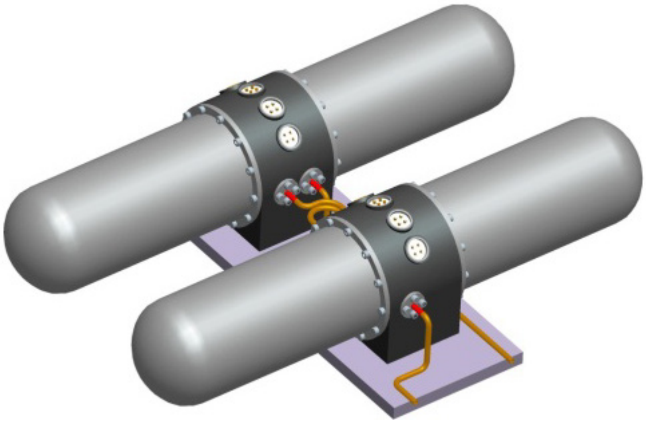

Figure 9-7: Four stage compressor designed for 2K system (EChO would use half of this)

The compressors are balanced in that they run in a head to head configuration. The exported vibration from balanced compressors on similar systems has been reduced to around 100mN with crude amplitude balancing. On Planck, with active vibration control, levels of a few mN were achieved. If required, we have algorithms that can be used to reduce the 100mN to acceptable levels.

9.2.4 Gas Cleanliness

Gas cleanliness is vital to long term operation of a JT cooler. On Planck we developed a pump, purge and fill protocol that ensured the gas cleanliness. In addition, the internal components of the system were monitored with a residual gas analyser to ensure that any outgassing was at an acceptable level. As part of the gas cleaning the gas was circulated through a hot reactive getter prior to launch and also during the cruise period to L2. Over the period since launch (2009-2013) there has been no sign of a blockage in the JT orifice which validates our procedure. We intend to re-use this protocol although advances in getter technology mean that a room temperature getter can be used.

In summary gas cleanliness is controlled by:

- Material selection for the internals of the compressors
- Monitoring of the internal outgassing rate using a residual gas analyser
- Pump, purge and fill protocol
- Cleaning of the gas by circulating prior to use
- Filter on each of the cold stages

9.2.5 Ancillary equipment:

For monitoring the health of the cooler we have a simple flow meter that is based around a differential pressure transducer, an orifice and a temperature sensor. Other pressure transducers are used to monitor the compressor performance and temperature sensors are also required. Each of the mechanisms has a position sensor for monitoring the amplitudes of the compressors and for closed loop control.

9.2.6 Thermal analysis:

Some basic calculations have been performed to demonstrate the possible heat exchanger configuration. We need to iterate with the instrument teams as the heat loads on each of the stages can be modified within bounds to alter the heat load. Reducing the heat load comes at a cost of increasing the pressure drop down the low pressure side and increasing the temperature.

In order to achieve ~200mW of cooling power a mass flow of around 35mg/s is required. This gives the following heat loads on the stages (unoptimised):

	Bottom HX	Middle HX	JT HX	JT effect	Cond	Total
293	-1018.9				-6.7	-1025.6
100	1078.1	-436.1			6.7	648.7
45		593.1	-48.7		0.8	545.1
28				-203.5	0.1	-203.4

Table 9-4: Thermal Analysis Heat loads (note that all powers are in mW, negative figure indicates cooling)

A health warning must be applied to these figures. The heat exchangers are not optimised and we need to look at the effect of increasing the high pressure with more compression stages. This will increase the pressure from which the Neon is expanded and the cooling power. These calculations are a first cut indication that the use of Neon is feasible

9.2.7 Cooler Control Electronics

The Cooler Control Electronics (CCE) drives the Joule-Thomson cryocooler compressors and also monitors performance and provides limit checking/protection as well as housekeeping data. The CCE could also be used to actively control residual exported microvibrations by continuous adjustment of the harmonic content of the compressor drive waveforms.

The CCE unit should be located as close as possible to the cooler mechanical compressors to limit the length of the high current drive harness which will be delivering of order 100W to the cooler motors.

9.2.7.1 Interfaces

The CCE unit nominal and redundant processor and drive buses are connected to the +28V spacecraft bus via latching current limiters (LCL). A pre-charge regulator should be inserted onto the drive bus after the LCL to smooth out the large fluctuations of the cooler compressor current waveform, which may typically be around 5Arms with peaks beyond 10A and a rich harmonic content. The unit is controlled by commands from the spacecraft Data Processing Unit (DPU), which would also provide the necessary synchronisation clocks.

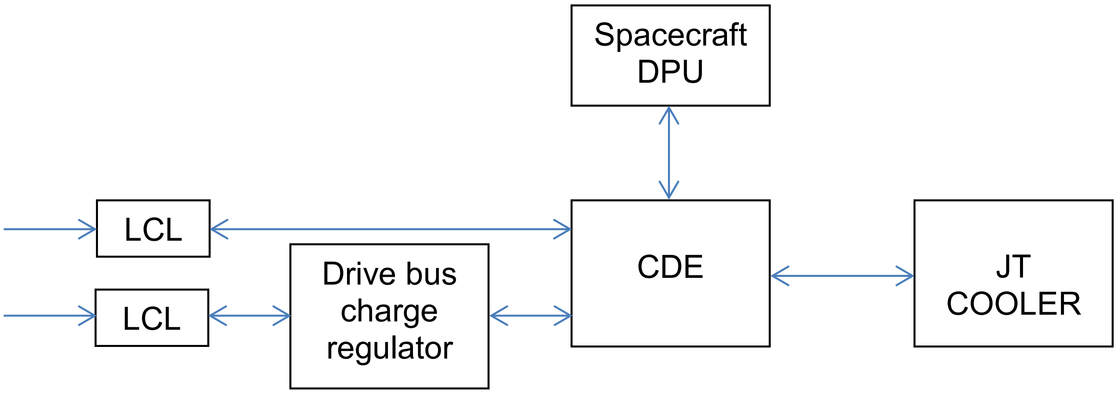

Figure 9-8: Cooler Control Electronics Interfaces

9.2.7.2 Elements

The main elements of a typical CCE are expected to be as follows.

- *Auxiliary Power Supplies*
    - For power supply from the drive and processor buses within the CDE
- *A Digital Signal Processor*

  - The DSP with associated memory, controls all cooler activities in response of DPU telecommands, it also continuously monitors the health of the cooler units and provides limit checking. If required then active vibration cancellation is controlled by this element.
- *DPU Interfaces*
  - Communication with the DPU is provided by telecommand, telemetry and clock interfaces.
- *Waveform generators (DAC)*
  - These are used to generate and output the compressor drive waveforms. In the event of a processor crash the generators continue their output to ensure that the cooler is still being driven.
- *Data acquisition sampling (ADC)*
  - For the purposes of performance monitoring and safety checking, as well as inputs for vibration cancellation algorithms and also to provide closed loop feedback control of the compressor mechanisms.
- *Closed Loop Servos and position decoders*
  - The mechanisms are operated in a closed loop mode based upon piston position feedback against a demanded waveform.
- *Power Amplifiers*
  - H-bridge amplifiers provide drive power to the compressor linear motor coils.
- *Auxiliary drives*
  - For miscellaneous drives to smaller power items, for example thermometers, orifice heaters, pressure transducers mass flow meter, etc…

9.2.7.3 Physical

The CCE for EChO is expected to be quite similar to that which was provided for Planck to drive the RAL 4K Joule-Thomson cooler, and would therefore expected to be a cuboid enclosure of edge around 200-250mm with mechanical and thermal interfaces to the base of the unit. The mass is expected to be around 10-12kg, including the pre-charge regulator, although for Planck this was provided as an additional enclosure. An additional 1kg should be allowed for harnesses.

For a nominal power output of 100W to the EChO cooler compressor mechanisms the CCE would be expected to consume 120-130W from the spacecraft bus, which includes allowances made for the CCE processor bus as well as pre-regulator, harness inefficiencies and standing powers.

9.3 BACK-UP DESIGN FOR SIAS DETECTORS – COOLING OPTIONS FOR ~8K STAGE

The baseline selection for the colder stage cooler of the EChO PLM is the evolution of the RAL "Planck-like" He JT cooler. The RAL group built the 4K cooler for the Planck spacecraft that has been shown to provide in orbit 20mW of lift at 4K with a 17K pre-cooler temperature (Figure 9-9-left). This was with 60W into the compressors, which equates to about 100W from the spacecraft bus including the electronics processor bus. The observed 4K cooler temperature variation over a one year period was found to be around 12mK. The on-ground measured exported vibrations from the Planck compressors was approximately at 40mN rms level; in flight this level is much lower due to the quieter electronic conditions.

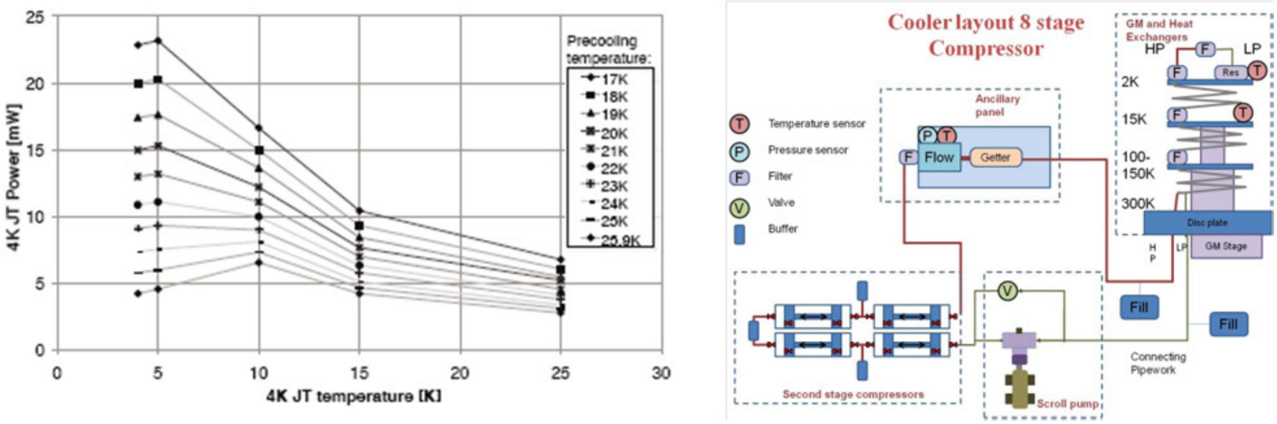

Figure 9-9: RAL 4K Planck cooler heat lift map (left); 2K JT Cooler Development Schematic(right)

RAL post Planck launch activities include the development of a 2K cooler based around the heritage of the 4K Planck cooler. The lessons learnt from these programmes are being applied to produce a next generation cooler with considerably simplified interfaces and mechanisms as part of an ESA TRP contract. The improved and lighter gas cleaning and monitoring panel, the improved motor design and configuration and improved mechanical alignment which will further reduce the exported vibration aspects of this design activity are all relevant to a potential 6K JT cooler for EChO. Additionally the EChO cooler compressor would be much lighter than those for Planck, since it will be based on a new design that enables massively improved heat rejection through the elimination of large mass copper thermal straps. The aim is to reach TRL level 5 by end of 2012.

The backup option is based on the verification of the scalability of the Darwin 4.5K He sorption cooler developed by the University of Twente cryocooler group. A physi-sorption carbon double-stage compressor working at 50K is able to maintain ~5mW of heat lift at the JT cold end. Power rejection at the 50K stage is around 2.5W and precooling load on the 18K cold end is on the order of 6 mW. A breadboard cooler has been implemented and tested, showing very interesting performances in terms of low power consumption (around 2W, excluded electronics) and a negligible level of exported vibrations. On the other side, the operations of a 4K sorption compressor on the 45K stage of the EChO PLM would basically double the loads allocated on Radiator 3, requiring a substantially larger surface area.

9.4 ALTERNATIVE COOLER CONFIGURATION FOR ~25K COOLING

Alternative cooler configurations are possible candidates for providing cooling for the MWIR (and LWIR) detectors at ~25K. These could be:

- Stirling cooler (based on RAL Cooler developments) – located in the SVM with the displacer on the top panel of the SVM. Thermal straps (or heat pipes) would be required to trandfer the thermal load from the detectors down to the coldhead. The parsistic loads on these straps would have to be carefully managed, and the straps would have to be sufficiently flexible to prevent transfer of micro-phonics from the displacers.
- Pulse-Tube cooler (based on CEA cooler developments) – similar to the Stirling cooler option above, would require transport of the cold end to the payload via straps.

9.5 SYSTEMS ARCHITECTURE AND INTEGRATION

The general scheme of the baseline thermal and cryogenic architecture is shown in Figure 9-10.

The system integration sequence is a fundamental issue that must be discussed and agreed with ESA and Industry. A preliminary evaluation of the thermal system integration from an Instrument perspective, has identified the following main steps:

1) Integration of inner section of V-Grooves, Telescope and Telescope Optical Bench on SVM
2) Cooler compressor (& driving electronics, TBC) mounting on SVM panel (cooler needs a connection between piping and compressor)
3) Instrument Optical Bench is integrated on Telescope Optical Bench
4) Instrument Modules, FEE's and common optics are mounted on the IOB, then the thermistors
5) SVM compressor panel closure
6) Cooler piping and pre-coolers are integrated on the V-Grooves
7) Cold-end piping and heat exchangers are integrated on the on the Module boxes (cooler needs another connection between the cold end and the piping)
8) Thermal straps are integrated on the FGS/VNIR/SWIR detector stage
9) Internal/external harness connection is finalized
10) Instrument radiative cover (MLI/SLI) is integrated
11) Cold radiator is integrated
12) Thermal link and harness are connected to radiator
13) External section of the V-Grooves is mounted

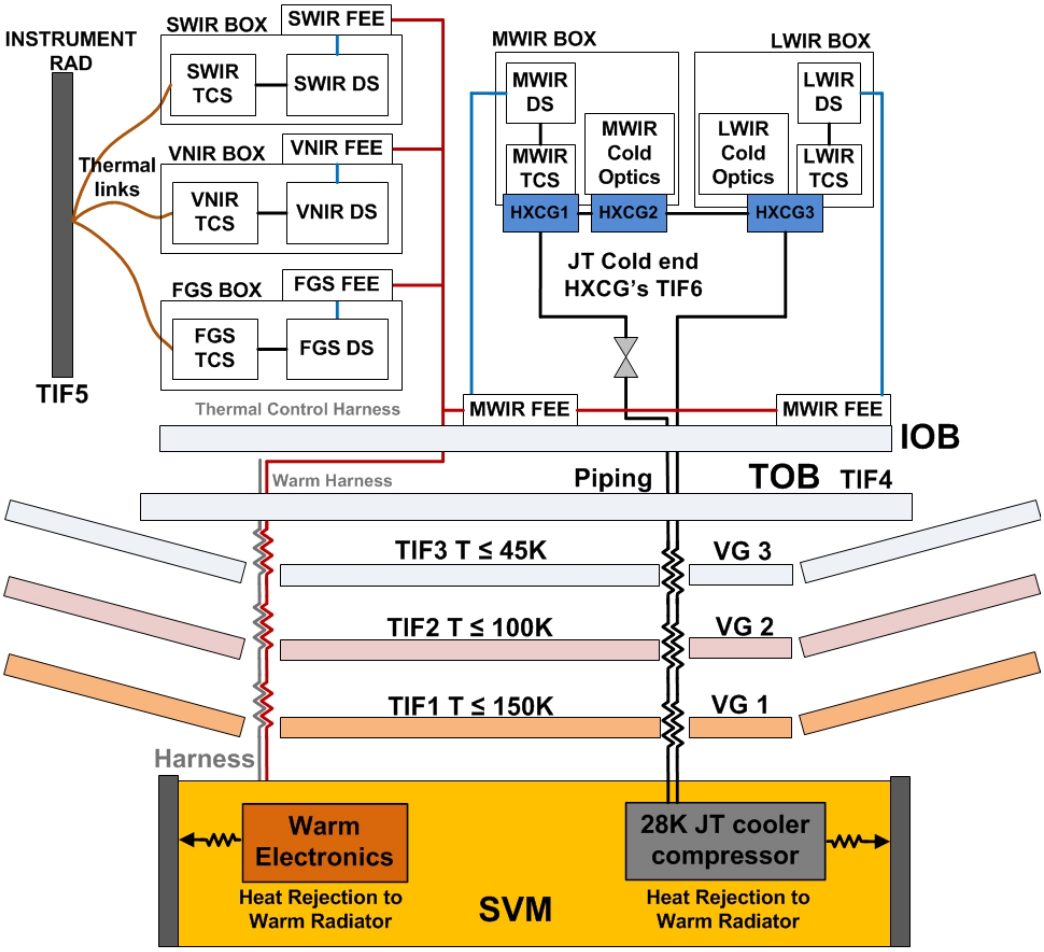

Figure 9-10. Basic scheme of thermal and cryogenic architecture

10 ELECTRICAL SYSTEMS DESIGN

10.1 BASELINE ELECTRICAL ARCHITECTURE

The EChO payload overall electrical architecture (Figure 10-1, Figure 10-2, Figure 10-3, see ECHO-TN-0001-OAA/UniFi [RD44] for details) can be basically subdivided in two sections: spectrometer's FPA detectors with their ROICs (Read Out Integrated Circuits) and cold front-end electronics (CFEEs) on one side and warm electronics on the other side. The cold detectors cavities are maintained @ ~45 K in order to meet the strict operative thermal requirements and are connected to the CFEEs and to the warm electronics by means of very low thermal conductance cryo-harnessing.

With reference to Figure 10-1, Figure 10-2, the FPAs analog readout signals are locally amplified by the ROICs and converted to digital values inside the A/D Cold front End Electronics (CFEEs) represented by ASICs (Application Specific Integrated Circuit) devices.

The Instrument Control Unit (ICU) interfaces the CFEE by means of the DWEU including the WFEEs, one per each scientific focal plane array.

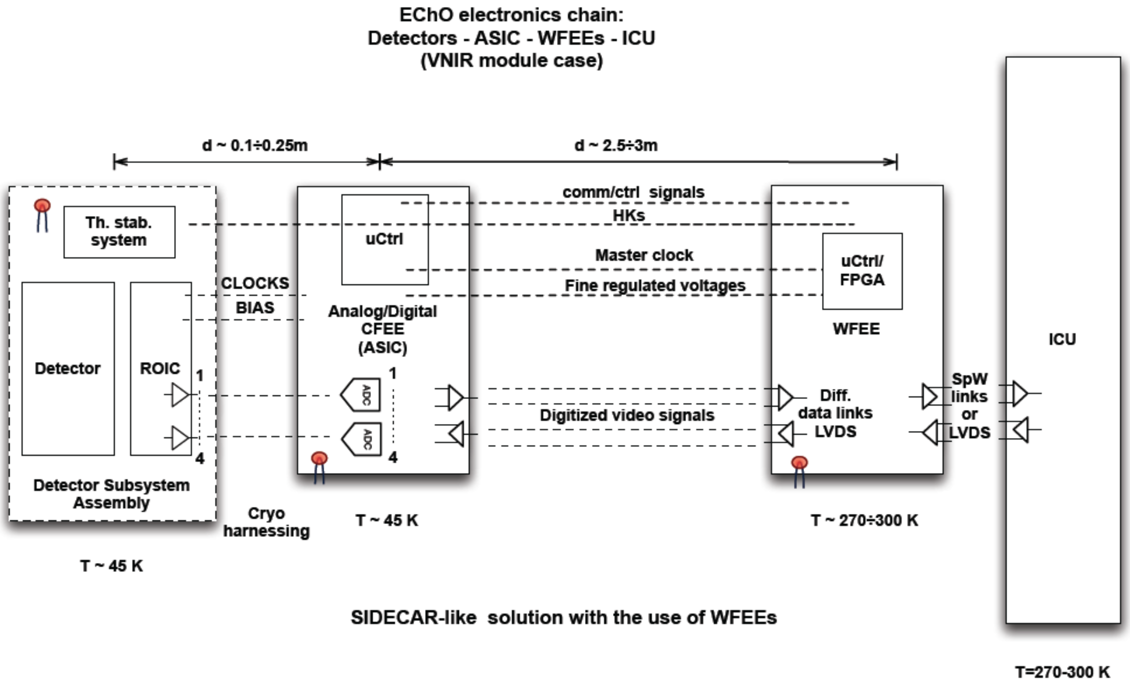

Figure 10-1: EChO payload overall electrical architecture (baseline solution with SIDECAR ASIC and DWEU).

ICU will implement the unique payload instruments interface to the S/C Data Management System (OBC+SSMM) hosting nominal and redundant connections for telemetry (TM), telecommand (TC), housekeeping and power supply lines.

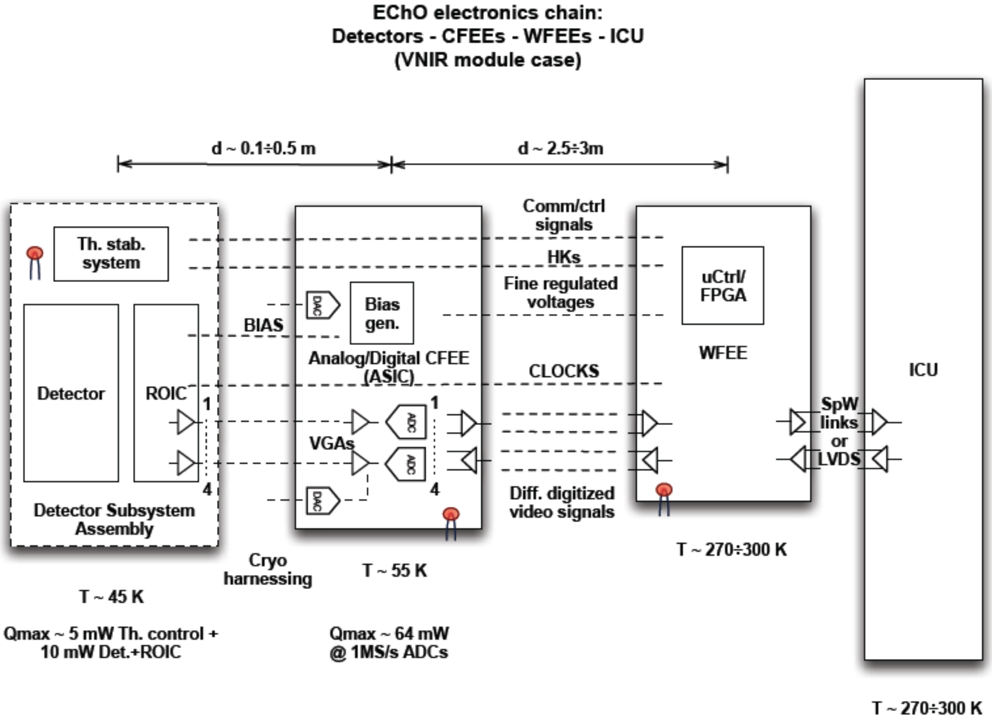

Figure 10-2: EChO payload overall electrical architecture (alternative solution with SRON ASIC and DWEU).

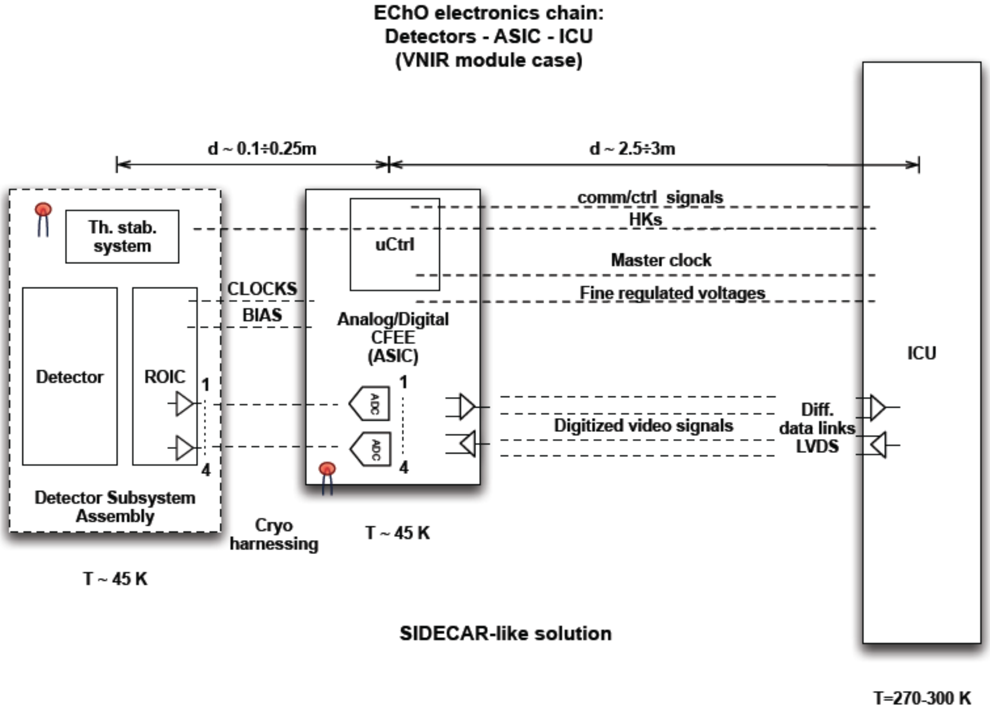

Figure 10-3: EChO payload overall electrical architecture (a possible solution without adopting DWEUs and interfacing directly the SIDECAR ASIC to the ICU).

ICU is structured in three main sub-units:

1. *Data Processing Unit (DPU)*: a digital sub-unit with processing capabilities. Its architecture is based on a rad-hard space qualified processor running the main Application SW (data processing SW) and some digital logics (two FPGA as baseline). The DPU will implement the scientific digital data on-board processing, the data storage and packetisation, the telemetry and telecommand packets handling and the clock/synchronization capability to temporally correlate the scientific data coming from the different spectrometer channels.
2. *Housekeeping and Calibration source Unit (HCU)*: a sub-unit designed to provide instrument/channel thermal control, calibration source and HKs management with the aim of a second rad-hard space qualified processor running the main Application SW (instrument control SW), as baseline, and an FPGA.
3. *Power Supply Unit (PSU)*: it will distribute the secondary voltages to the instrument subsystems and ICU boards by means of DC/DC converters.

A single common TM/TC interface is foreseen at ICU level to minimize and simplify the number of interfaces towards the spacecraft. The ICU electronics will rely on a cold-strapped redundant architecture with some trade-off solutions removing or reducing any electronics single-point failure.

10.2 THE DETECTOR WARM ELECTRONICS UNIT

The currently adopted ICU architecture interfaces the SIDECAR ASICs from Teledyne by means of WFEEs, which are included in the DWEU and shall be connected to the CFEEs and detectors modules by means of suitable cryo-harnessing.

The digital signals are then handled by the DWEU, which are located at a ~2.5÷3 m distance from FPA, and sent to ICU. The ICU will provide the main functionalities to manage all the instrument subsystems implementing detectors commanding, science and housekeepings (HKs) data acquisition and A/D conversion, calibration sources and mechanisms (if occurring) management and the overall on-board communication management.

In principle, it may be possible to interface the ICU directly to the SIDECAR ASICs, as reported in Figure 10-3, avoiding the need for the WFEEs. This architectural change will be studied in more detail in the next phase and finalised before the SRR.

ICU and WFEEs, being warm electronics units operating at ~273-300 K, will be located inside the SVM (Service Vehicle Module), which is thermally decupled by the telescope optical bench.

A possible accommodation for the DWEU boards (FGS excluded) is represented in Figure 10-4. The aluminium alloy box dimensions are 224x164x80 mm^3.

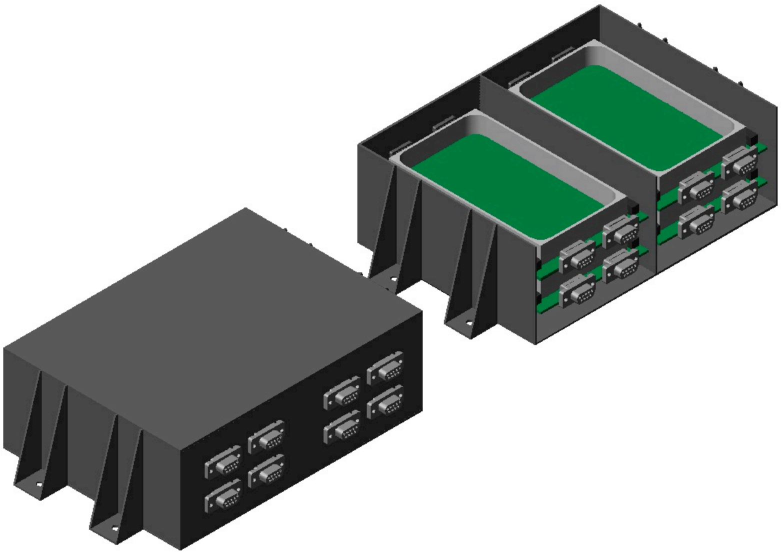

Figure 10-4: DWEUs mechanical design.

(connectors # and location are TBD/TBC and for illustration purpose only)

The DWEU box mass and volume budgets (for 4 WFEEs) are reported in Table 10-1 with an estimate of the power consumption (TBC). The provided overall dimensions are not taking into account the box mounting feet.

Description	Basic (EID-A R-1880)	Nominal (with 20% contingency) (EID-A R-1890)	Margin (EID-A R-1910) (EID-A R-0570)
Power	< 18 W	< 21.6 W	< 2.4 W
Mass	3.5 kg	4.2 kg	Tot. electr. < 25 kg
Volume	224 x 164 x 80 mm^3	-	26 x 76 x 100 mm^3

Table 10-1: DWEU budgets.

10.3 COLD FRONT END ELECTRONICS

The baseline detector selection (as detailed in section above) is to use US detectors coupled with a SideCAR ASIC as the Cold Front End Electronics (CFEE_. These are a well known and used technology with much information available online and in the literature about their use and performance.

The choice of the baseline detectors was however driven by cost considerations. In the case that a cost effect way can be found for a European detector supplier to be possible (for example through ESA technology development funding) then this would be the consortiums preferred choice. In this case an alternative CFEE would be required. This would be provided by the consortium and work has been undertaken in phase A in developing these devices. The European CFEE is being developed such that it could be tailored to be applicable to any of the potential European MCT detector suppliers.

10.3.1 Overview

The Cold Front-End Electronics (cFEE) will comprise of integrated circuits specifically designed for the detector arrays. They have a large dynamic range, very low noise properties and are very stable in time. The design will be based on an Application Specific Integrated Circuit (ASIC), which significantly reduces the budgets on mass, volume, and power, and allows for more flexibility in the board design and integration. To achieve low-noise high-stability detection, the readout ICs are placed as close to the detector as possible, in the cryogenic temperature range at 55K, cooled beyond the range of standard electronics built from discrete components.

The main driver for the use of an ASIC is that an integrated design allows for operation at a much lower temperature, resulting in a better performance because the analog signals from the detector have to travel only a short distance with no or just a small thermal gradient. The signal integrity and immunity to electromagnetic interference (EMI) are thus greatly improved. In the ASIC, the detector signals are amplified and digitized. Only the digital signals have to travel the longer distance from the cold detector environment to the warm ICU.

The most critical aspects of the detector control and readout are the amplification and digitization of the detector signals. Most is won by integrating the pre-amplifiers and the ADCs, which are critical for signal integrity. This ‘heart’ is formed by four independent signal processing chains (to match the four analog outputs of the detector). The requirements for the ADC are stringent. They combine low noise with a high stability and sampling rate, at a low power consumption.

Each analog signal chain consists of the following blocks:

1. Low-noise pre-amplifiers with gain and offset compensation
2. 16bit, 1 Megasample per second Analog-to-digital converters (ADCs)

Furthermore, the ASIC contains 4 voltage regulators for detector bias and reference voltages.

Each detector array is independently connected with one cFEE ASIC.

The ASIC design project is run and coordinated at SRON together with Dutch SME and a (potential) contribution from Belgian SME Caeleste and aims at delivering a chip with the following properties:

- operation at low temperature
- high stability
- space qualified.

The first prototype chip will be available for testing in February 2014.

10.3.2 Analog signal chains

The analog front-end is the heart of the ASIC and its quality is critical to the signal integrity. In Figure 10-5, the block diagram of the FAIR chip is shown.

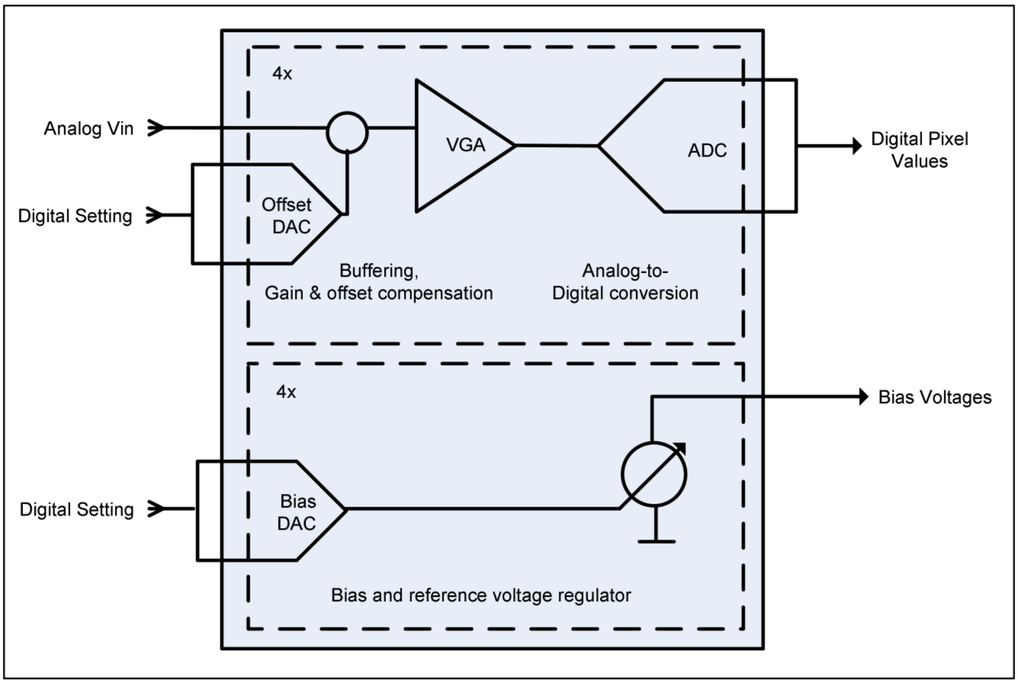

Figure 10-5: FAIR ASIC block diagram

10.3.3 FEE Detailed Specifications

10.3.3.1 General

Supply voltage	3.3V
Nominal operating temperature	55K

10.3.3.2 Analog front-end

Analog input voltage range	0.3 .. 2.5V
Gain settings	1x, 2x, 4x, 8x
Offset compensation range	1.0 .. 2.0V
Offset DAC resolution	24 bits
Analog input impedance	>100KOhm
Analog input capacitance	<20pF

10.3.3.3 Analog-to-digital converter

ADC sampling frequency fs	1.0 MSps
analog bandwidth	500kHz
number of bits (bus width)	16 bits
effective number of bits	14-15 ENOBs
INL	< 1.5 bits
DNL	< 1.5 bits
Input settling time	0.2μs

10.3.3.4 Bias and reference voltage generators

Output ref./bias voltage range	0.8 .. 2.5V
Ref./bias voltage output impedance	<1KOhm

- No. of reference/bias voltages 4
- Ref. voltage maximum current 1mA

10.4 DATA RATE BUDGET

The current observing scheme uses three observing modes, bright, normal and faint. The sampling scheme is currently under study with options such as sampling up the ramp, grouping samples and fowler sampling being considered. Initial results from this study are given in [RD34]. The three options are:

Bright Mode (Kmag < ~4)

- The ramp length can only be a few seconds to avoid saturation, therefore the maximum sample rate of 8 Hz is used.
- Ramp lengths of 3 seconds are possible with the baseline Teledyne detectors; other detector technologies with larger pixel sizes will imply a move to 1.5 second ramps.
- If all samples are transmitted to the ground this would be a rate about 250 Gbits/day.
- Therefore for this mode, only the evaluated ramp slopes and a goodness of fit will be transmitted to ground. This still gives a rate of 35 Gbits/day
- As a baseline the on-board processing will not need to deglitch ramps before evaluating ramp slopes, however there will be flexibility in the OBS to accommodate this if required.

Normal mode

- A 1 Hz rate is adopted (intermediate between 8Hz bright mode and 1/8th Hz faint mode),
- 32 second ramps are currently adopted
- This gives a primary rate of 32 Gbits/day if all samples are transmitted to ground
- If we group samples into groups of 8 we can achieve a rate of 4 Gbits/day with no goodness of fit transmitted although another option is to generate 8 groups of 4 samples giving a rate of about 8 Gbits/day, the first of these options is adopted as baseline at this time

For fainter targets

- The ramp lengths adopted are 240 seconds with 30 samples separated by 8 seconds.
- All samples will transmitted to the ground and the ramps and fitted in data processing on the ground
- This gives a primary rate of about 4 Gbits/day

The weekly allocated data rate (AD1) is 35 Gbits/week or 5 Gbits/day average.

Assuming a a H/K rate of 0.2 Gbits/day, a realistic duty cycle of 90% and a compression ratio of 2, then spending 10% of the mission in bright mode, 80% in normal mode and 10% in faint mode gives a data rate of 4.72 Gbits/day.

The current operational sampling scheme samples at 0.125 Hz for faint mode and all samples are transmitted to the ground. The ramp length of 240s is adopted to get 30 samples up the ramp (the best solution found for MIRI), to get reasonable well filling (about 30% in all channels except LWIR) but not to integrate too long to have all integrations affected by glitches. This is a current initial estimate and both the sample rate at integration time can be tuned further in the next phase. Since intermediate reads up the ramp (at 1/8 Hz) are all downloaded to ground, the cadence requirements of 90 seconds can be met, although with a non-optimal signal to noise ratio for the fainter targets.

	No. Spectral	No. Spatial	Tot Pix per frame	Masking % of frame	Tot pix after Digital Masking	Binning	Tot Spaxels after Binning	Max e/s/pix from ROE (worst case)	Primary Rate (Hz)	Ramp length (sec)	Realistic Well Depth	max at end of ramp	% Well	Samples /ramp	groups/ramp	spaxels/group	Actually used	Primary bits/sec	(16 bit/ramp) bits/sec	Primary Daily Rate	Binned Daily Rate
Bright Mode																					
NearVis	512	512	262144	70	183501	5*5	7340	9805	8	3	50000	29415	59	24	8	3	16	939524	117441	81	20
SWIR	1024	13	13312	100	13312	1x1	13312	16821	8	3	75000	50463	67	24	24	1	16	1703936	70997	147	12
MWIR-1	63	13	819	100	819	1x1	819	19739	8	3	100000	59217	59	24	24	1	16	104832	4368	9	1
MWIR-2	87	13	1131	100	1131	1x1	1131	19739	8	3	100000	59217	59	24	24	1	16	144768	6032	13	1
LWIR	50	6	300	100	300	1x1	300	16347	8	3	75000	49041	65	24	24	1	16	38400	1600	3	0
TOT.			262444		**199063**		**22902**		8											253	34.6
Normal Mode																					
NearVis	512	512	262144	70	183501	5*5	7340	1300	1	32	50000	41600	83	32	4	8	16	117441	29360	10	3
SWIR	1046	13	13598	100	13598	1x1	13598	2000	1	32	75000	64000	85	32	4	8	16	217568	54392	19	5
MWIR-1	63	13	819	100	819	1x1	819	2800	1	32	100000	89600	90	32	4	8	16	13104	3276	1	0
MWIR-2	87	13	1131	100	1131	1x1	1131	2800	1	32	100000	89600	90	32	4	8	16	18096	4524	2	0
LWIR	50	6	300	100	300	1x1	300	2000	1	32	75000	64000	85	32	4	8	16	4800	1200	0	0
TOT.					**199349**		**23188**													32.1	8.01
Faint Mode																					
NearVis	512	512	262144	70	183501	5*5	7340	62	0.125	240	50000	14880	30	30	6	5	16	14680	2447	1	0

SWIR	1046	13	13598	100	13598	1x1	13598	28	0.125	240	75000	6720	9	30	30	1	16	27196	907	2	0
MWIR-1	63	13	819	100	819	1x1	819	153	0.125	240	100000	36720	37	30	30	1	16	1638	55	0	0
MWIR-2	87	13	1131	100	1131	1x1	1131	153	0.125	240	100000	36720	37	30	30	1	16	2262	75	0	0
LWIR	10	13	130	100	130	1x1	130	907	0.125	80	75000	72560	97	10	10	1	16	260	26	0	0
TOT.					**199179**		**23018**													3.98	0.61

Table 10-2: Data Rate Calculation for Three Defined Modes

10.4.1 Example Calculation

VNIR with 512x515 array gives 262144 pixels/frame. Only 70% of the frame is used = 183501 pixels. If 5x5 binning is adopted this gives 7340 spaxels.

For bright mode 3 second ramps sampling at 8 Hz is adopted. Each readout is a 16 bit number.

Therefore the primary bits/second is 7340x8x16 = 939524. This translates into a daily rate of 81 Gbits/day.

Instead of sending all 24 samples to ground we could form groups of N samples. The rate is now 939524/N. Assuming a value of N of 8 (to be compliant with the sampling cadence requirement goal of 30 seconds) this gives a daily rate of 10 Gbits/day or 20 Gbits/day if a goodness of fit is also sent to the ground.

10.5 ICU ASSEMBLY

The EChO payload electrical block diagram, as reported in Figure 10-6, focuses mainly on data and command flows, clock/synchronization and power distribution, data processing and data formatting. The cold proximity electronics are interfaced to the detectors ROICs bonded to the MCT sensors arrays in the VNIR, SWIR, MWIR and LWIR modules (the latter hosts a Si:As detector as baseline). These proximities will provide the amplified analogue HKs (temperatures, voltages and currents) to the warm front-end electronics and ICU, where multiplexing and HKs analogue to digital conversion will take place.

The proposed payload architecture has been designed to minimize and simplify the number of interfaces. In particular, the ICU will be the unique payload interface with the spacecraft Power Conditioning and Distribution Unit (PCDU) and the On-Board Computer (OBC) and Solid State Mass Memory (SSMM) – (ref. EChO EID-A).

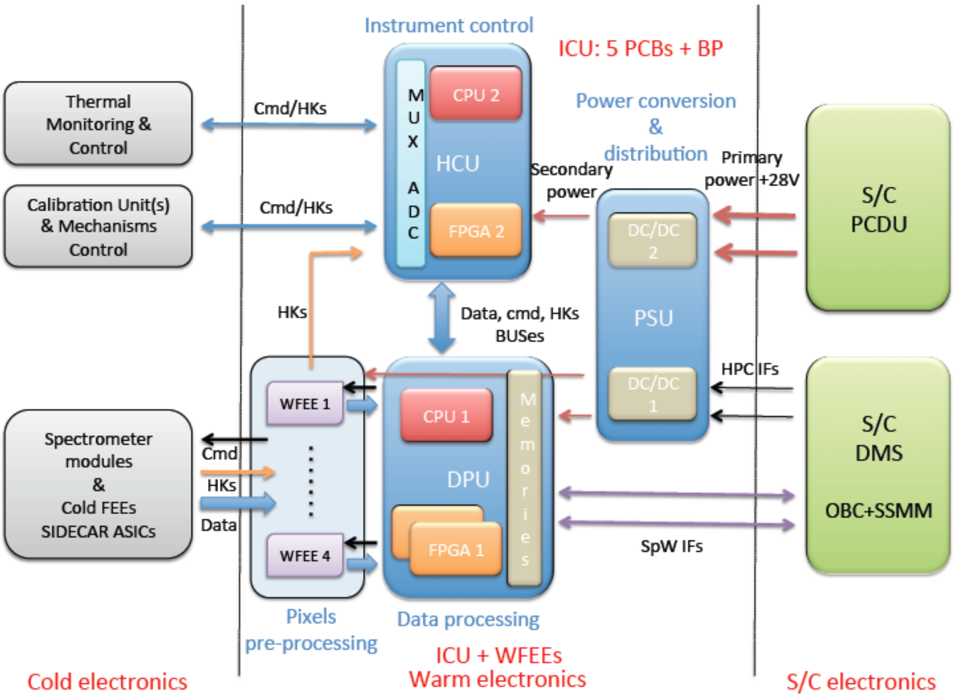

Figure 10-6: EChO payload electrical architecture block diagram (baseline solution).

ICU is mainly a digital unit with processing and data buffering capabilities interfacing both the spacecraft electronics and the digital section of the payload warm front-end electronics for commanding, data and housekeepings (HKs) acquisition, A/D conversion and dispatching, data packetisation and spectra pre-processing, as well as providing finely regulated voltage levels to all its subsystems and FEEs. Cold front-end electronics ASICs send digitised data and analog HKs (TBC) to WFEEs for packetisation in CCSDS format before sending them to the ICU by means of N+R Spacewire (SpW) links.

A Data Processing Unit (DPU), a HK and Calibration Source Electronics (HCU) and a Power Supply Unit (PSU) are the main blocks of the ICU, as schematically represented in Figure 10-6 and Figure 10-7 (the latter as alternative solution without using DWEUs).

The currently adopted ICU architecture interfaces 4 warm front-end electronics communicating with an on-board ICU digital subsystem with processing capabilities, the Data Processing Unit (DPU) and the Housekeeping and Calibration source Unit (HCU) both based (as baseline) on a rad-hard space qualified processor and devoted, respectively, to the *Data Processing Function* and to the *Instrument Control Function*. Both processors (CPUs) run the main Application SW suitably designed to perform separately the two functions, to manage the payload operating modes (instrument managing) and the overall data acquisition procedures and processing.

This architecture also presents the advantage to be compliant to a possible split of responsibilities and test and AIT/AIV procedures as well as EGSE provision between two different institutions respectively in charge of the data processing task and the instrument control task.

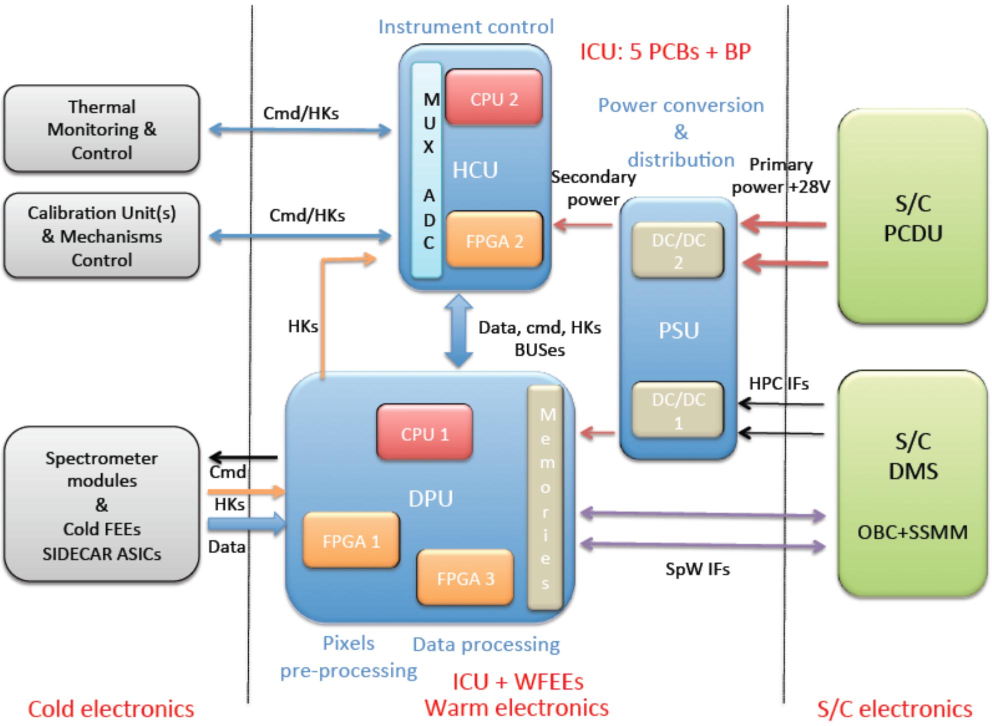

Figure 10-7: EChO payload electrical architecture block diagram (alternative solution).

The data processing function at pixel level will be supported by two rad-hard FPGAs working @ 80 MHz (assumed frequency for the processing resources evaluation) acting as co-processors to perform on-board (HW implemented functions) pixel-based data processing procedures.

The DPU will implement the digital data processing, the data storage and packetisation, the telemetry and telecommand packets handling and the clock/synchronization capability to temporally correlate the scientific data coming from the different spectrometer channels. A single common TM/TC interface is foreseen to minimize and simplify the number of interfaces towards the spacecraft.

As baseline, DPU is composed by a processing board hosting the scientific digital data processing CPU and the two ancillary FPGAs working as a co-processors and a memory board hosting all the memories needed to load and run the Application SW (PROMs, EEPROMs and SRAMs) and buffer the incoming scientific data (SDRAMs or FLASH – TBD) prior digital processing and data formatting. Memories addressing functions could be performed by one of the two FPGAs that will also acts as a memory controller for data buffering.

DPU and HCU will host and share an internal PCI interface to the PCI bus including data, address and control buses. Alternatively an AMBA bus could be used (TBD/TBC). The PCI bus is connected to the rad-hard processors (an ITAR-free LEON2 AT697F or a LEON3 from ATMEL running @ 60 MHz were considered, as baseline, to evaluate the processing and instrument control power needs) and to the main digital logics hosting a PCI I/F.

ICU manages both processors and logics to perform all the required tasks as digital processing (pixels sum, average, digital binning, windowing, spectra cropping and masking, pixels deglitching -if needed TBC/TBD-, data and HKs compression) and memory management.

A Power Supply Unit (PSU) will distribute the secondary voltages to the instrument subsystems by means of rad-hard DC/DC converters whereas the HCU will provide instrument/channel thermal control, calibration sources, mechanisms (TBC) and HKs management.

PSU will be feed by two (N+R) +28V power interfaces and will be equipped with two (N+R) BSMs (Bi-Levels Switch Monitors) to report to the S/C the unit status (switched ON/OFF) as defined by two Main (ON/OFF) plus two Red (ON/OFF) High Voltage - High Power Pulse Commands (HV-HPC) with interface characteristics as defined by ECSS standards.
DC/DC converters are hosted by two boards of the PSU in order to feed all the ICU subsystems and provide the basic voltage levels to the WFEEs, so the present ICU design foresees as baseline 5 Extended Double Eurocard (233.4 mm x 220 mm) electronics boards in a fully redundant architecture aboard the same PCBs in a cold strapped configuration exploiting the ICU back panel board interfacing all the electronics subsystems. The ICU redundancy policy is based on a trade-off solution removing or reducing to an allowed level the impact of any single-point failure thanks to its cross-strapped fully cold-redundant architecture.

Scientific channel:	VNIR	SWIR	MWIR-1	MWIR-2	LWIR
Detector Frame Format	512x512	1024x13	63x13	87x13	50x6
Pixel pitch (µm)	18	18	25	25	25
Binning	5x5	1x1	1x1	1x1	1x1
Digital masking	70%	100%	100%	100%	100%
# bit/pix	16	16	16	16	16
Primary rate (Hz) - Bright targets case	8	8	8	8	8
Ramp lenght (s) - Bright targets case	3	3	3	3	3
# Samples per ramp	24	24	24	24	24
Housekeepings TM (Gbit/day)	0.2				
Efficiency (R-PERF-060)	85%				
Contingency (EID-A R-2430)	50%				
Available ossless compression factor (CR)	2÷2.5				
# CPUs (LEON-like running @ 60 MHz)	2 (Processing & Instrument Control)				
# FPGAs (RTAX 2000-like running @ 80 MHz)	3 (Px pre-processing, memory manag. and aux fnc)				
SRAM needed (MBytes)	16 (8 x 2 banks)				

SDRAM needed (MBytes)	20
EEPROM/PROM (MBytes) - BOOT SW, BIOS SW, ASW	8 (4 x 2 banks)
Daily averaged data rate	< 60 kbit/s
Peak data rate (burst mode, if needed)	< 10 Mbit/s
Science TM (Gbit/day)	< 5
TOT. expected daily data volume – science + HKs (Gbit/day)	< 5

Table 10-3: ICU processing power, data rate, data volume, required amount of memories.

Note: Table 10-3 *values strongly depend on data processing required for on-board (ICU) deglitching procedures, compression task and pixels pre-processing. Presently pixels deglitching is foreseen to be operated on-board but could be avoided given the short integration times for bright targets and the very low likelihood of cosmic rays hits on pixels (ref. Technical Note IAPS/ECH/TN/01-013, Issue 0.1).*

Table 10-4 reports the ICU daily data volume, the data rates to the S/C, the CPUs expected processing power and memories usage. The followings assumptions have been taken into account: the averaged number of clock cycles/elementary operation is 3 (1 MIPS = 3 M clock cycles); the number of elementary operations/pixel take into account the OS background activity overhead; digital data are stored in memory (SRAM and SDRAM) by a FPGAs before CPU processing; masking is performed by a FPGA aboard WFEEs before making data available to the CPU; payload control refers to TC activity between ICU and the 4-channels instrument including calibration units management. Once pre-processed scientific data are temporarily buffered and sent immediately to the DMS Solid State Mass Memory.

Our basic assumption is that we sample up-the-ramp pixels in a non-destructive manner with a relative high rate sampling (presently up-to 8 Hz). There will be destructive readouts after some seconds (integration times for bright, normal and faint sources) with the length of the ramp determined either by the saturation limits of the detector for a particular target – determined during operations planning – or by experience of the maximum length of a ramp allowed before a cosmic ray hit. This will be determined by in flight tests and calibrations and on-ground simulations activities. The highly sampled ramps are then fitted and the pixels photocurrent extracted. These data will then on-board processed also for pixels deglitching by cosmic rays (as baseline), lossless compressed and transmitted to the S/C.

The ICU will carries out all communication and commanding tasks of the instrument. It will also serves as the central data-handling unit. Incoming science data will be processed, compressed and formatted in CCSDS format according to the operating mode.

All the ICU processing and buffering capabilities are presently evaluated taking into account a 50% of margin, as usually adopted at the ending of the Assessment Study (Phase A) and as reported by EID-A R-2430.

10.6 WARM FRONT-END ELECTRONICS

10.6.1 Baseline adopted solution

WFEEs (see Figure 9 and Figure 10-4) are equipped with digital LVDS transceivers to communicate with each CFEE (to send/receive digital commands and collect digitised data) and host a digital logic (mainly an FPGA and/or a microcontroller, TBC) to produce command and control signals and digital clocks to manage the detectors ROICs and CFEEs (mainly the Master Clock and Sync signals for the SIDECAR ASIC).

In the baseline design the A/D conversion will be performed on board the CFEEs ASIC as well as detector clocking, wave shaping and filtering while spectra pre-processing (e.g. digital masking and image cropping - TBC) on board the WFEEs by means of a suitable FPGA, as reported in Figure 10-8.

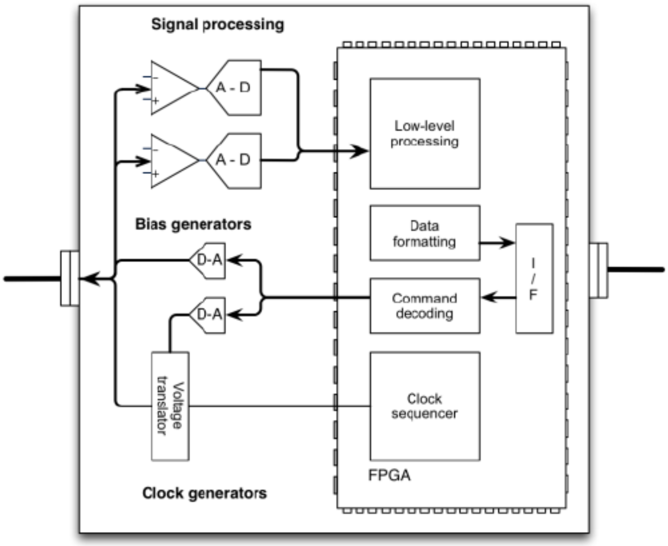

Figure 10-8: DWEUs electronics.

WFEEs also generate precise secondary voltage levels to feed the CFEEs electronics, which, in turn, produce fine-regulated biases for the detectors FPA assemblies.

WFEEs will be connected to the ICU by means of a nominal + a redundant SpW link or a LVDS I/F (TBD/TBC). These interfaces will be implemented by means of IP cores inside the hosted FPGA. Alternative option

As a possible alternative solution (see Figure 10-3) we could interface directly the SIDECAR ASIC to the ICU, so no DWEUs are foreseen in that case.

10.7 ELECTRICAL BUDGETS

The ICU power, mass and volume budgets are reported in Table 10-4.

Description	Basic (EID-A R-1880)	Nominal (with 20% contingency) (EID-A R-1890)	Margin (EID-A R-1910) (EID-A R-0570)
Power	20 W	24 W	0
Mass	7.5 kg	9 kg	Tot. electr. < 25 kg
Volume	250 x 240 x 150 mm^3	-	0 x 0 x 30 mm^3

Table 10-4: ICU budgets.

The ICU basic mechanical design is represented in Figure 10-9. The ICU box dimensions are 250x240x150 mm^3 mounting brackets and feet excluded. All the electronics boards are fixed by means of space qualified card lock retainers and are reinforced by an aluminium structure hosting the connectors as depicted in the figure.

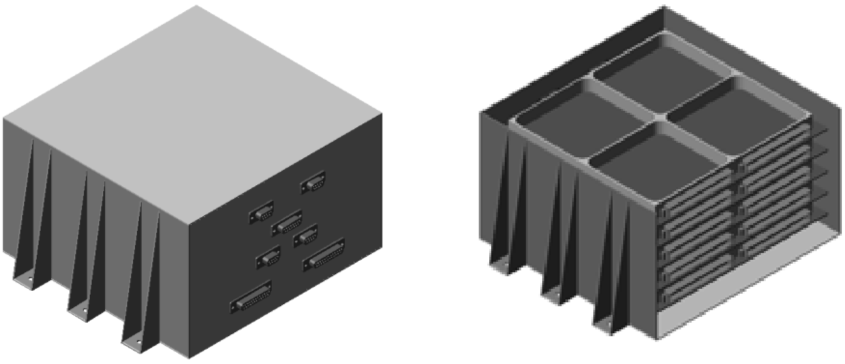

Figure 10-9: ICU mechanical design.

(connectors # and location are TBD/TBC and for illustration purpose only)

The ICU box, made by aluminium alloy, will be provided by an external bonding stud to connect analog and digital grounds to the unit chassis, as a possible configuration for testing and external noise shielding.

10.8 ELECTRICAL GROUND SUPPORT EQUIPMENT

The detailed architecture of the EGSE will be designed in phase B. For the phase A study it has been assumed that a SCOS-2000 system will be used at the MOC and hence this system will also be used for ILT. Figure 10-10 shows the basic SCOS configuration that could be used to support the instrument test.

The spacecraft simulator and associated interfaces are supplied by ESA. The test equipment and test equipment interface will be developed at RAL using an adapted setup from the MIRI instrument test campaign. The common router was initially developed for the Herschel test campaigns and has recently been reused for the Solar Orbiter SPICE instrument. The QLA system will be supplied by Portugal, and will be based on the same system as the Herschel SPIRE and Solar Orbiter SPICE instruments. The MIB development system (not shown) will be specified by the prime. The remaining architecture in particular the storage of TM/TC and definitions is TBD and will be developed in phase B in collaboration with ESA.

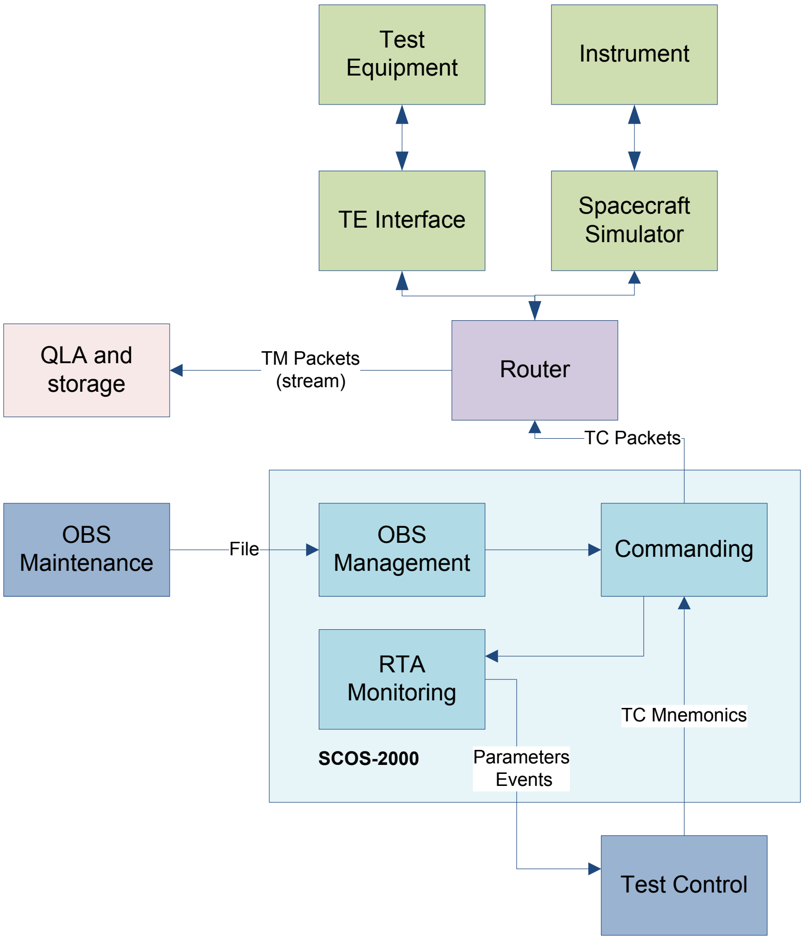

Figure 10-10: EGSE for Instrument Level Test

10.9 ICU SIMULATORS

The electronics simulator (ref. ECHO-IAA-SP-0001) is intended to provide an independent functional platform for testing and simulations. Its main purpose is to simulate the behaviour of the ICU operating on board the EChO payload, providing useful data and metrics to analyse and monitor sensors, FEEs electronics and ICU performance.

The present simulator (Figure 10-11) provides TM and HKs acquisition and is virtually controlling two emulated devices retrieving randomly generated data. This setup serves as an early testing environment and letting the team test debug and improve the simulator in lack of real devices.

The development of the simulator is based on a FPGA, which manages all housekeepings, telecommands and telemetry data. All the acquired information is sent to a computer via Ethernet connection for further analysis. The board containing the core of the simulator is GR-XC6S, manufactured by Pender Electronics (Figure 10-12). The FPGA model is a Xilinx Spartan-6 XC6SLX75.

ICU simulator consists of four modules: one for H/W interfaces (red box) and the three remaining ones make up the S/W architecture (violet boxes: simulation, control and monitoring and user interfacing). From this point of view, the system simulation is running the ICU components loaded and provided by the control module, which is also in charge of stand-alone monitoring of every parameter of the system and it's operated through the user interface, providing the user with the whole needed functionality for practical operation, configuration and inspection of the simulation system.

The FPGA integrates an IP core of LEON3 processor. The simulator application running on the development board is coded in C++ and controlled by RTEMS, a fully featured and open-source real-time operating system widely used in embedded platforms.

The software architecture is based on two main components, Device Manager and HK Manager, controlling Device data acquisition and HKs sensor sampling, respectively. Everything is coordinated by a Core component, in charge of TC reception and TM retrieving, and responsible for communication between managers and users.

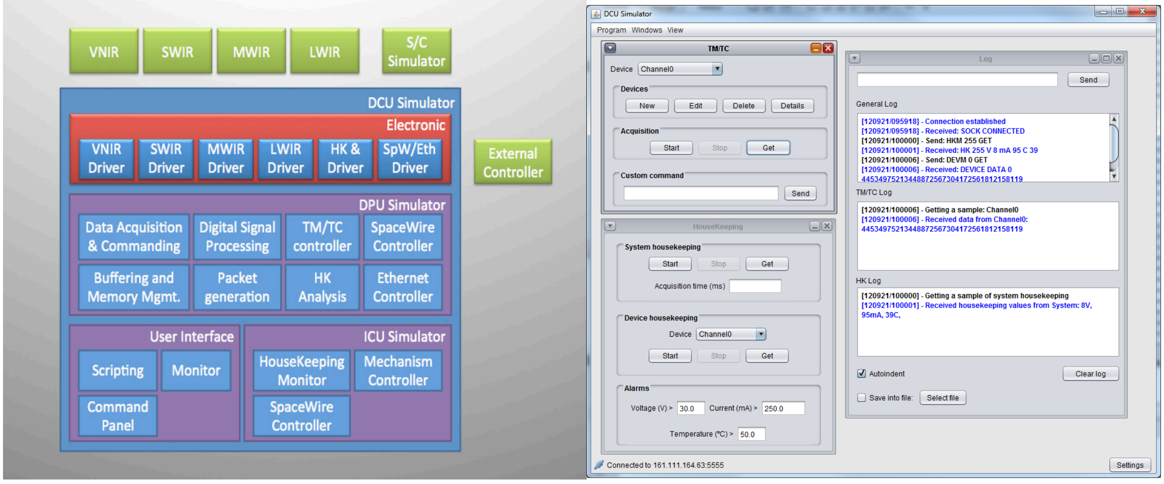

Device: Channel0

Acquisition time (ms):

Device: Channel0

Voltage (V) > 30.0 Current (mA) > 250.0

Temperature (°C) > 50.0

Connected to 161.111.164.63:5555

General Log

```
[120921/095918] - Connection established
[120921/095918] - Received: SOCK CONNECTED
[120921/100000] - Send: HKM 255 GET
[120921/100001] - Received: HK 255 V 8 mA 95 C 39
[120921/100006] - Send: DEVM 0 GET
[120921/100006] - Received: DEVICE DATA 0
44534975213448872567304172561812158119
```

TM/TC Log

```
[120921/100006] - Getting a sample: Channel0
[120921/100006] - Received data from Channel0:
44534975213448872567304172561812158119
```

HK Log

```
[120921/100000] - Getting a sample of system housekeeping
[120921/100001] - Received housekeeping values from System: 8V,
95mA, 39C,
```

☑ Autoindent

☐ Save into file:

Figure 10-11: ICU simulator (SW interface).

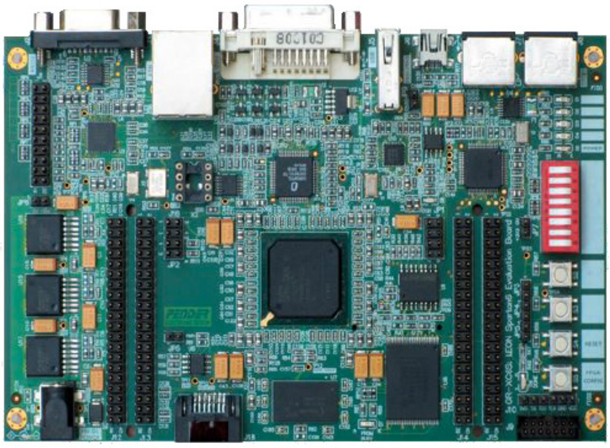

Figure 10-12: Electronics board containing the SW/FW core of the simulator.

10.10 ECHO ON-BOARD SOFTWARE FUNCTIONAL ANALYSIS

The EChO ICU is responsible for the following main activities:

1. Telemetry and Telecommand exchange with the S/C CDMU;
2. Instrument Commanding, based on the received and interpreted TCs;
3. Instrument monitoring and control, based on the Housekeeping data (HKs) acquired from the focal plane instrument units;
4. Synchronization of all the scientific payload activities;
5. Detectors readout data acquisition, pre-processing and formatting according to the selected Telemetry protocol;

6. Science Data download towards the S/C Mass Memory.

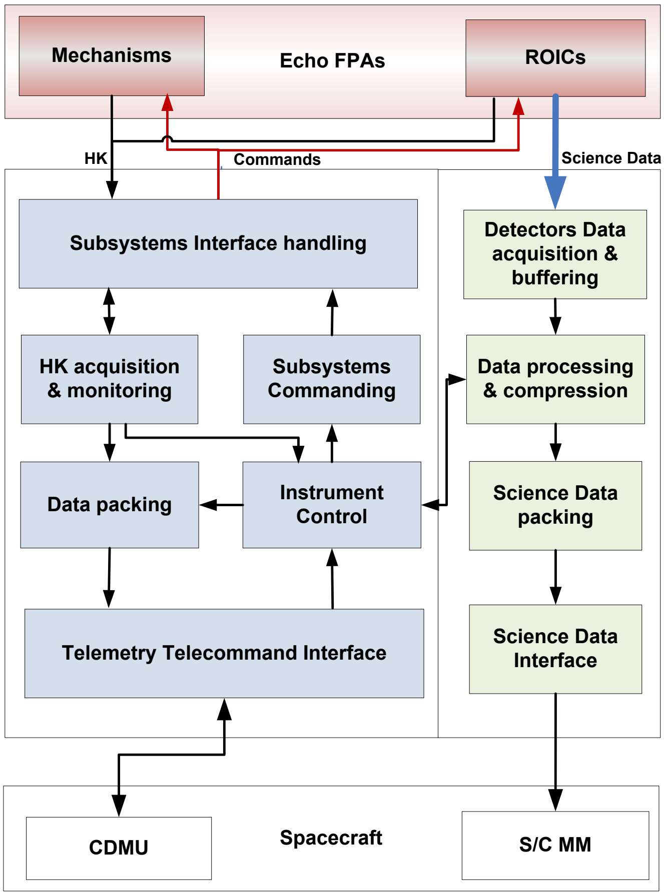

Figure 10-13: ICU OBS functional components block diagram.

These activities can be grouped into the *Instrument Control* and *Data Processing* software: these two SWs will constitute the On Board Software (OBS) of the EChO science payload (P-OBS). The On Board Software will be implemented as a real-time multitask application.

The Block Diagram reported in Figure 10-13 shows the main ICU functional components. The two different colors indicate the different groups of functionalities of the Instrument Control and the Data Processing software.

10.10.1 Software layers

The EChO Payload instruments On Board Software (P-OBS) layers structure is presented in Figure 10-14. The boot software component refers to the start up software described in the previous section: it is installed in the PROMs of the ICU boards and allows for the application software loading. It contains all the low level drivers for the CPU and its related interfaces.

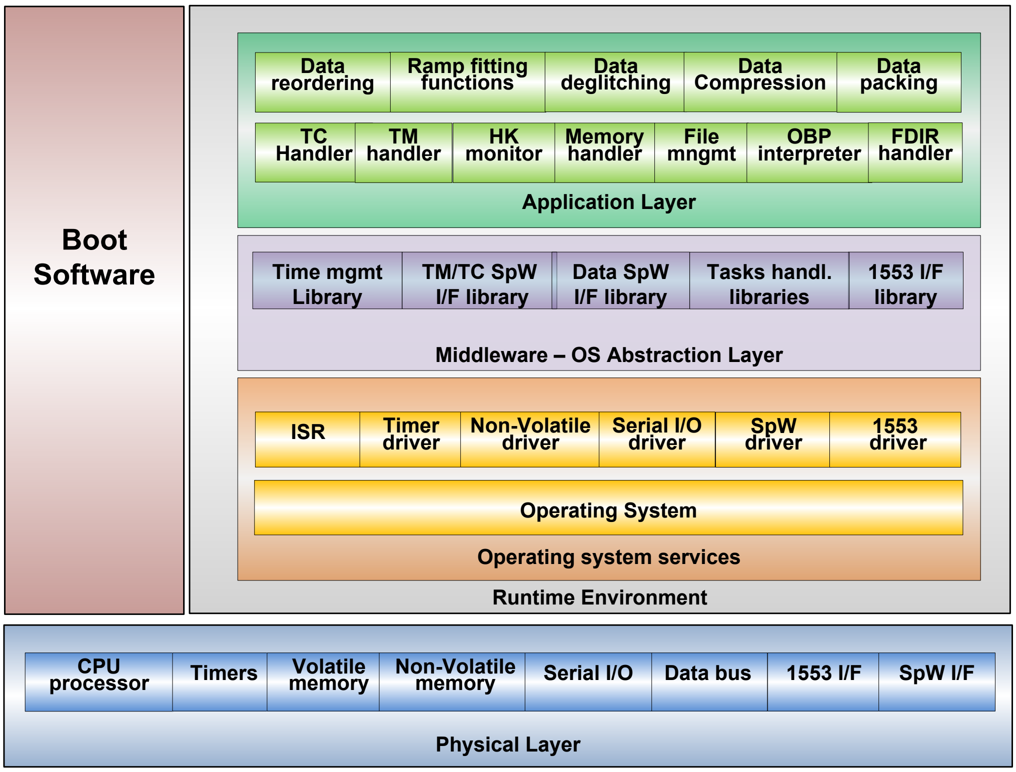

Figure 10-14: SW layers structure of the EChO Payload instruments On Board Software (P-OBS).

The physical layer includes all ICU HW components with a direct level of interaction with the on board software. In particular, the considered baseline CPU is a LEON processor. It is a 32-bit SPARC-compliant processor, which results from ESA's efforts in the development of processors for space applications. It will be used in several space missions (e.g. the Swedish PRISMA mission, the European Space Agency Proba-2, GAIA and Bepi-Colombo missions) and it is planned to use it also in a number of medium size missions competing in the frame of the ESA Cosmic Vision program.

The Runtime environment includes the Real Time Operating System (RTOS) layer, necessary to provide multi-tasking support. In case the baseline architecture based on the LEON processor will be confirmed, the RTEMS operating system is a good RTOS candidate, being already used for applications on board ESA satellites. The other indicated operating system services include the drivers for the onboard memories, the onboard HW timers and the local data bus. The other OS services mentioned in the structure of Figure 10-14 are those not directly provided with the OS kernel.

An OS abstraction layer has then been included, in which all middleware libraries have been considered. The middleware services are based on the use of RTOS function calls. They include all library functions dedicated to the low level handling of the ICU HW devices/interfaces. All the middleware libraries will be developed in house and will provide a mean for developing an Application Software virtually independent from the HW and OS below it. This layer is very important and will ease the testing activities.

The Application Layer includes both the ICU instrument control software and the data processing software. The ICU instrument control software will implement the functions listed in points from 1 to 4 of the list in section 10.10: i.e. the TM/TC S/C interface handling, the payload housekeeping data acquisition and monitoring, the instruments operating modes management and the autonomous function execution. The software will be written in C++, though some functions may need to be coded in assembly to optimize their performance.

In case stringent timing requirements have to be met for subsystem commanding, an interrupt-driven command sequencer (On Board procedures, OBP interpreter) can be included into the ICU on board software. Based on the experience of Herschel's HIFI and SPIRE instrument control software, this is a flexible and effective solution to implement time-critical commanding procedures. Some preliminary tests on the performances of a simplified implementation of such a sequencer on a LEON 3 based SOC implemented on an FPGA development board (GR-XC3S-1500) have been already carried out. A 1 MHz timer has been used to trigger the highest priority interrupt of the system. Under normal work load conditions (only two tasks running, CPU load < 50 %), an average time jitter of the order of 1 us (for an overall test duration of more than 1 hour) has been measured, as expected. The proposed sequencer offers high flexibility and re-programmability possibilities, thanks to the straightforward way in which scripts can be reloaded during in-flight operation; this feature can be exploited to modify instrument control or measurement procedures in response to changed mission requirements. The sequencer is described in "*Di Giorgio et al. 2008*" and *"Liu et al. 2012"*.

The Data Processing Software implements all the necessary onboard processing functionalities, included the on-board lossless compression (i.e. RICE). After the compression the SW prepares CCSDS packets for the transmission to the S/C Solid State Mass Memory.

11 IN-FLIGHT CALIBRATION AND DATA PROCESSING

11.1 IN-FLIGHT CALIBRATION REQUIRED

The measurements to made by EChO require that the stability of the system is either maintained, or monitored to allow removal of drifts in the system performance, to around 1 part in 10000. This will necessitate both a highly optimised design for the spacecraft and instruments, and a calibration scheme capable of monitoring the system performance to within the specified limits. A full discussion of the in flight calibration required for EChO, and the detailed plans for calibration and data processing are to be found in [RD40]. We present here a summary of the effects that the calibration scheme will need to deal with and a basic overview of the calibration approach that we will take

Several effects will be encountered in the EChO measurement process, and will need to be corrected for in the data processing/calibration. They can be gathered in 3 classes in order to distinguish between how they are monitored and controlled:

- The astrophysical effects: These are associated with the observing "scene" and require measurement and monitoring schemes as they are outside of the design parameters of the mission.
  - The stellar activity and the stellar signal in general – this is monitored directly during the observation
  - The contribution of the zodiacal cloud of our solar system : it is an extended source which is due to the solar light scattering in the visible, and the thermal emission of dust in the infrared. We will provide dedicated off –axis detectors to monitor the Zodiacal contribution.
  - The contribution of the zodiacal cloud of the target : it is an IR excess compared to the stellar SED, associated to other effects on the transit lightcurve, either in the visible or in the IR spectral range.
  - The contamination of the background stars in the target field
  - The effects of the L2 environment such as proton impacts, scattered light from the Earth

- Spacecraft effects: These are associated with changes in the pointing, temperatures and, possibly, mechanical stability of the spacecraft and, although the design minimises their impact, certain spacecraft housekeeping parameters will be required to be monitored.
  - Telescope and associated baffle temperatures – monitored through housekeeping
  - Absolute pointing performance – monitored through the AOCS and FGS system
  - Pointing stability – monitored through the FGS
  - Optical stability of the telescope – monitored through the FGS
  - Mechanical micro-vibrations from spacecraft systems (reaction wheels, coolers etc) – monitored partly through the FGS and partly through housekeeping parameters associated with the sub-systems
  - Variations in the straylight environment due to spacecraft orientation – monitored by off axis detectors

- The instrument effects: these are mainly linked to the detection process and the associated detection chain.
  - Radiation glitches in the detectors

- Detector gain variations (droop associated with readouts, drift due to radiation, drift due to thermal fluctuations etc)
- Detector ramp non linearity due to saturation
- Detector dark currents variations with radiation and (more likely) thermal drift
- Detector pixel spatial response non uniformity
- Detector afterglow following bright observations
- Instrument temporal optical transmission variations (aging and any possible association with thermo-mechanical variations)
- Instrument temporal optical distortion (possible thermo-mechanical variations)
- Ageing of the instrument performance (surface degradation, contamination etc)
- Variations in the instrumental thermal and straylight background (also see spacecraft)
- Offsets in the electronic chain
- Electronic cross talk / ghosts

This initial list is subject to review but captures the essential parameters that will need to be monitored and gives the outline for the measurements required under the calibration plan. During the mission there will be a combination of long term housekeeping monitoring (temperatures, voltages etc), dedicated long term measurements (use of off axis detectors, dark detectors etc), short term measurements using internal calibration sources and medium and long term measurements on stellar calibration sources for both stability and absolute flux measurements. The EChO Instrument Calibration and Data Processing Plan [RD40] contains more detail on the likely approach we will take to monitoring and calibration, however, a fully documented calibration and monitoring plan is beyond the scope of the current development phase at it requires detailed knowledge of, most especially, the detector operation and performance.

11.2 ON-BOARD DATA PROCESSING REQUIRED

The most demanding module from the point of view of digital processing are the SWIR and the VNIR one as the latter is based on a MCT panoramic detector composed by 512 x 512 - 18 µm pixels as baseline, or 512 x 512 – 15 µm pixels as an alternative choice (Selex device). In order to perform on board DPU data processing and pixel deglitching from cosmic rays hitting the VNIR FPA before digital pixels binning (on-chip binning is also possible, as baseline) to produce spaxels[2], the two FPA halves will be digitally masked and cropped rejecting all pixels hosting no VIS and NIR spectra information, reducing the overall pixels number to be processed by masking to about 70% of the entire array. Digital masking and image cropping will be performed aboard WFEEs FPGAs (TBD/TBC) in order to reduce the overall DPU processing load. The EChO payload digital processing is therefore a distributed digital processing.

11.2.1 On-board processing steps

All detectors will be read non-destructively and periodically reset after a certain number of samples have been acquired. The length of the reset interval will be adapted to the brightness of the source. The ramp-fitting implementation used in this study does assume uniform sampling and samples grouping if needed to save processing and reduce data volume (up-the-ramp multi-accumulation sampling).

Before operating individual pixel processing it will be performed (TBD, channel by channel) detector windowing and/or array digital masking and/or image cropping respectively at detector level and WFEEs

---

[2] Spaxels are defined as nxn binned pixels along the spatial and spectral dimensions.

level in order to limit the effective number of pixels owning to the produced spectra to be successively processed by WFEEs and ICU.

At the beginning of the procedure, basic corrections will be applied to individual pixels, while after the binning each spaxel (VNIR case) is processed individually.

The main processing steps as illustrated in Figure 11-1 (mostly for the VNIR channel one, but useful also for all the other channels) are:

- Bias correction: an internal bias is subtracted to bring all samples to the same "ground". This is necessary for later binning of the data down to spaxel resolution;
- Pixel reordering: pixels are extracted from the serial stream in output from the readout electronics and reordered, bringing them into a more suitable order in memory for subsequent data processing steps. History and average buffers with ancillary data can be formed at this level;
- Saturated pixels identification and rejection: by defining a cut-off value for the upper limit of the linear region of the detector's response curve;
- Responsivity correction: correction based on radiometric calibration, thanks to an array responsivity map, will be applied if necessary;
- Spatial and spectral pixel binning to build spaxels;
- Temporal samples co-addition: depending on the ramp fitting algorithm, "scans" and "groups" have to be formed (*m* scans per group) if needed;
- Rejection of the data that don't satisfy the noise requirement at beginning of the ramp, when necessary;
- Non-linearity correction: if necessary, the ramps will be linearized, even during the multi-accumulate processing);
- Progressive *linear least square fit* to calculate ramps slope (pixels/spaxels photocurrents);

  Note: The above four steps could be necessary to decrease readout noise to specifications. Frames in a group must be contiguous and in the number necessary to reach the required total noise performance limit after co-addition (assuming a multi-accumulation readout mode). These processing steps must run at the spaxels readout speed. Using a fixed very simple parameterization (to be optimized during calibration and algorithm tuning procedures on ground), it can be conveniently performed in hardware.

- Cosmic rays and other glitches identification (TBC/TBD): proper glitch detection and rejection strategies will be implemented, if necessary, with a proper algorithm still to be defined;
- Bad spaxels correction and linearization;
- Frame generation: processed science frames created here will be received on ground;
- Frame buffering;
- Lossless Compression (compression of the data to save data volume and bandwidth);
- Packetisation according to the required TM format: all data products will be packaged;
- Storage in mass-memory (SSMM) and scheduling for transmission.

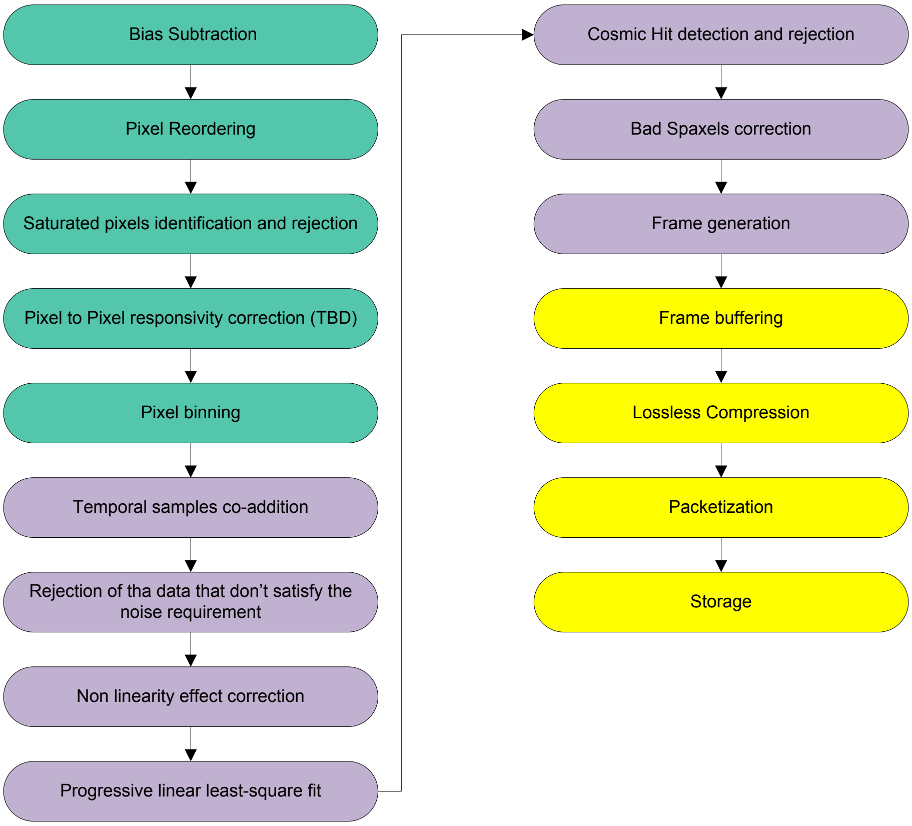

Figure 11-1: Scheme of the data processing steps: green blocks refer to pixel pre-processing activities; purple blocks refer to processing steps at spaxel level and yellow blocks identify frame level processing activities.

The listed steps refer to the processing of a single focal plane spectrometer. It is a standard on board processing chain, see for example Offenberg et al. 2001 and 2005, Bonoli et al. 2012, and a parallel processing of more than one instrument operating simultaneously at the focal plane should be taken into account.

The final overall processing of EChO data will be defined during Phase B and tailored for each one of the focal plane spectrometers. Dedicated simulated data flows will be used to verify the effectiveness of the data reduction steps. In particular the deglitching algorithm performances should be verified against the expected data redundancy, the data acquisition rate and the spaxels dimensions.

Finally, the need to implement lossless compression on-board is strictly related to the results of the on-board deglitching study. If confirmed, a dedicated trade off activity to evaluate the performances of different standard lossless compression algorithms on the on-board CPU processor should be planned.

11.2.2 Pixel deglitching

Deglitching detectors pixels arrays from cosmic rays hits is commonly an operation to be performed basically at pixel-level. Operating binning on-chip (e.g. on-board the VNIR detector ROIC) would lead to lose any pixel-based info on cosmic rays hits that would blur the spaxel integrated signal at the same time.

Taking into consideration the predicted cosmic rays flux for JWST-MIRI instrument and an integration time from 1.5 to 3 seconds for bright targets only less than 0.02% (ref [RD34]) of pixels would be interested by cosmic rays hits, so an option to be considered could be discarding any on-board deglitching operations based on pixels processing at least for bright targets.

The classical deglitching pixel-based procedure is a demanding processing task for the DPU CPU that would require the heavy use of the processor FPU (Floating Point Unit) for the second derivative calculus needed for the glitches recognition and correction. Probably it would be better to perform deglitching at "spaxel" level (i.e. 36 px/spaxel for the VNIR channel one) by detecting cosmic rays hits and discard them as outliers w.r.t. e.g. a median operation performed on sub-arrays. Pixels affected by cosmic rays hits should be flagged and not considered for the rest of the ramp production but properly replaced. In this manner we should avoid heavy processing tasks, like the derivative calculus and a heavy FPU use. A possibility to be explored could be to perform this kind of simplified deglitching procedure at FPGA level (HW-level).

The number of pixels owning to a spaxel and affected by a cosmic ray hit should be determined by the hit geometry and particles energy. They likely would affect mainly the detector array through the direction parallel to the optical axis and the angle defined by the optics F/# and buffles. So just few pixels should be interested by a single cosmic ray hits and it should be possible to operate deglitching only for the faint targets (if needed) which require longer exposition times with a bigger and not neglecting hit likelihood.

Deglitching from cosmic rays hits has surely a big impact on the overall ICU processing architecture and should be carefully evaluated in respect of the overall system budgets. Deglitching is presently foreseen at CPU level in the ICU processing needs evaluation procedure.

11.2.3 Data compression

Once performed pixels and spaxels on-board processing all the scientific data defining spectra (ramps slopes defining pixels/spaxels photocurrents) will be compressed, prior sending them to the OBC SSMM to be stored and suitably formatted in order to send them to ground. The present compression task takes into consideration Rice or Smallrice algorithms that are written in C, C++ and/or assembler for the most demanding sub-tasks. The foreseen lossless compression ratio (CR) is presently estimated to be between 2 and 2.5.

11.3 GROUND DATA PROCESSING

The infrastructure required for the ground data processing will be at the Science Operations Centre (SOC) and will be supplied by ESA. The data processing pipeline software and associated calibration will be supplied by the Instrument Operations and Data Processing Centre (IOSDC). The choice of software and scripting languages will be a joint decision between ESA and the IOSDC and given the rapid evolution of technology it should not be specified until needed.

The data processing pipelines will require spacecraft parameters in particular for de-trending hence access to these parameters is required for development. ESA will provide the processing of spacecraft pointing data to the extent that enough information is available for the instrument pointing to be reconstructed. Processing of the FGS data can remain internal to the IOSDC.

The software repository and configuration control system is an IOSDC responsibility and the IOSDC will provide a ticketing system for SPRs and SCRs (such as the Herschel JIRA system). It is TBD whether the SOC will use the same system to manage its internal software but this would be desirable. A modern software industry standard system involving continuous integration builds of a development system will be installed and maintained by the IOSDC. It will be regularly e.g. every six months branched into operational plus (next version) development builds with the operational branch undergoing a stabilisation period before being released. Further details are given in the ground segment implementation plan [RD46]

11.4 DATA ANALYSIS AND EXTRACTION

Data product levels 0, 1 and 2 are specified in the EID-A section 5. Data will be stored in the EChO archive and accessed by the Instrument teams and the Community. The following levels have been identified.

- Level 0: Unpackaged/decompressed raw data for all packet types for each individual observation. Data are stored in the EChO database.
- Level 1: Spectra for each observation are calibrated and kept under the form of cubes containing the spectra as a function of time per spectral sample of the EChO spectrometer.
- Level 1.5: Individual transit and/or occultation spectra for each exoplanet stacked to include all transits/occultation observed over the course of the mission.
- Level 2: Averaged exoplanet spectra in emission (secondary transit), transmission (primary transit) and phase curves.
- Level 3 (TBC): A catalogue of exoplanet spectra.

The following steps are required to process the data from level 0 to level 1

- Unpack and Decompression
- Time Correlation
- Masking
- Conversion to Physical Units
- Engineering Calibration of Science Data
- Re-construct ramps
- Level 0.5 Data
- Data Processing Level 0.5 to Level 1
- Determine and Subtract Dark Current
- Flag Bad Ramps
- De-Glitch Ramps
- Correct for Droop
- Linearisation and extract ramp signals
- Correct for Responsivity Time variation
- De-Trending
- Correct to Reference Responsivity
- Background Subtraction
- Flatfield
- Correct for Crosstalk/Ghosts
- Bad Pixel Masking II
- Correct For Optical Distortion
- Correct for Pointing Jitter
- Rebin Into Spectral Timelines
- Assign Wavelength
- Correct For RSRF and Convert to Astronomical Flux
- Correct for stellar variability and activity

For exoplanet observations the level 1.5 processing will stack transits into a single 4-D dataset. The production of Level 1.5 data will be an iterative process that will generate cubes containing spectral timelines that record the observed flux as a function of time (binned per cadence interval), per spectral channel. Other products will include stacked emission and transmission spectra. This approach is similar to the pipeline of the Hubble Space Telescope, data being re-reduced from scratch with the latest instrument model and pipeline version whenever one downloads from the archive.

For the core science programme and similar community programmes level 2 processing will extract the transiting body spectrum. The level 2 automated processing at the start of the mission will not produce optimum science results as the target's signal to noise will build up by the co-adding of several observations. There is likely to be other products required such as the stellar spectrum but these products are still TBD.

It is TBD whether a level 3 product is to be produced. If it is this may be a catalogue including line lists for the exoplanet spectra. Further details on these processing steps and the calibration plan can be found in [RD40].

12 SCIENCE GROUND SEGMENT

The EChO ground segment concept has been developed be the science ground segment working group chaired by the ESA ground segment study manager. The outcome of this study is detailed in the science operations assumptions document (SOAD) and a detailed implementation plan for the IOSDC has been formulated, [RD46].

12.1 GROUND SEGMENT ARCHITECTURE

Essentially the ground segment has three components:

- The Mission Operation Centre (MOC) situated at ESOC in Germany responsible for communications with the spacecraft and it's safe operation.
- The SOC situated at ESAC in Spain responsible for mission planning, running the data processing software and archiving and also for all interactions with the community
- The IOSDC which is distributed across consortium institutes and is responsible for all the instrument related software, the instrument calibration, the instrument health and safe operation and for the long term planning

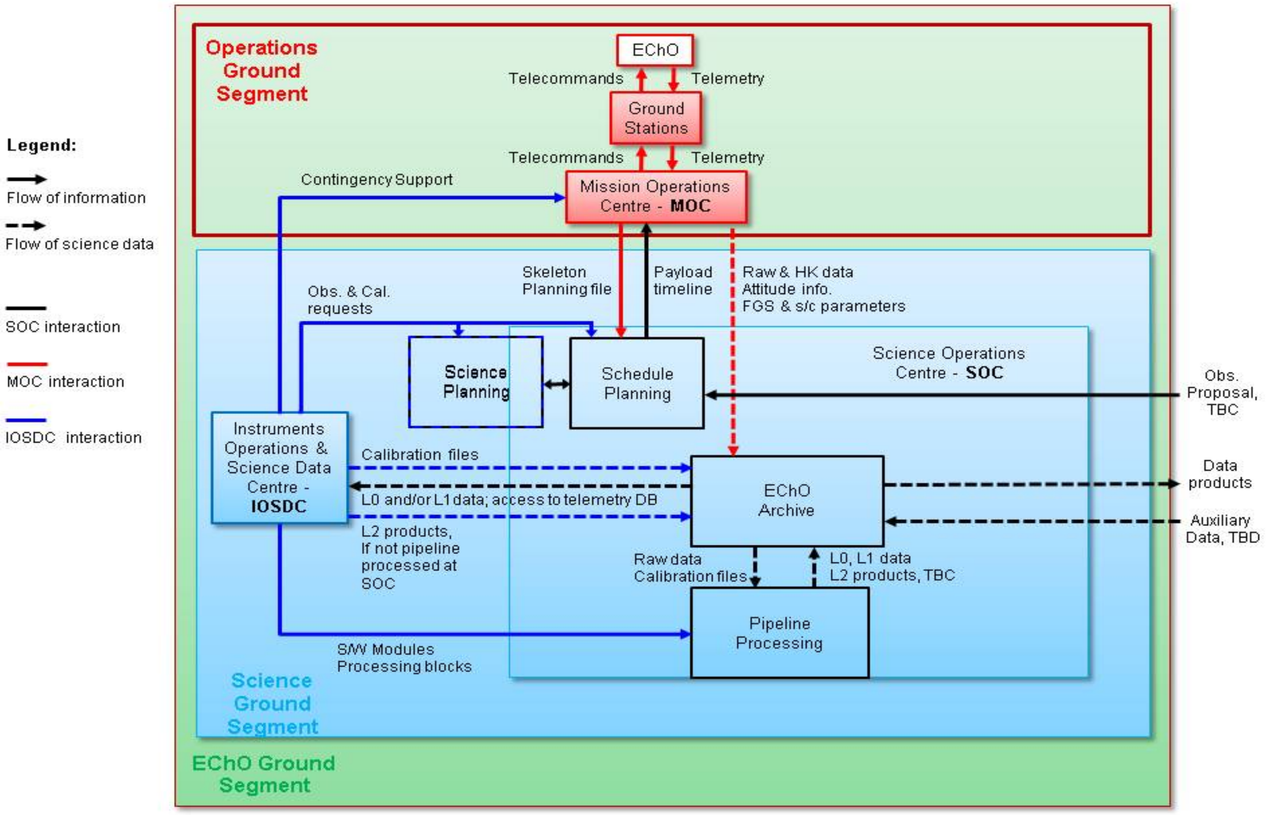

Figure 12-1: Overview of the EChO Ground Segment

Figure 12-1 shows the overall ground segment architecture and interfaces. While much of this is standard for ESA missions a particular feature of the EChO mission is the need to continuously schedule fixed time observations. This adds complexity to the scheduling and has been studied in detail by the IOSDC during phase A, and further details can be found in [RD46]. Following these studies, for the mission, the current baseline is that the IOSDC will generate the long term schedule.

The only other non-standard feature to note is that it is not yet clear whether level 2 products can be produced by an automated pipeline, therefore the automated pipeline run at the SOC may only go to level 1.5 and human generated level 2 products may be delivered to the archive from the IOSDC. Automatically generated level 2 products remain a goal.

13 INSTRUMENT PERFORMANCE MODELLING

The Instrument performance is studied using EChOSim, an end-to-end simulator of the EChO observatory,EChOSim implements a realistic, time-domain simulation modelling the current baseline instrument, or the alternative options. This allows a quick and cost-effective evaluation of the proposed design in delivering the EChO science as well as a tool to optimize the instrument, or conduct tradeoff studies when required. EChOSim is in this different from other radiometric models of the EChO mission, as it allows a thorough time-domain assessment of several systematics which would not be possible, or very difficult to study in static simulations. EChOSim allows both the consortium and ESA to ensure that the instrument and spacecraft designs are optimised to enable the science of the mission without unnecessary cost and risk. This simulation tool has been used throughout the preparation of this report to define the expected instrument performance and demonstrate the mission science capabilities.

13.1 ECHOSIM OVERVIEW

EChoSim uses set of input parameters to define the physical properties of the science target, the optics, the spectrographs, and detectors. A thorough description of the scientific and instrument model implemented by EChOSim can be found in the User Requirement Document (URD, [RD18]). A Software Requirements Document (SRD, [RD17]) provides a technical description of the simulator.

Here the overall architecture is briefly summarized. Please, refer to the URD and SRD documents for a thorough description of EChOSim.

EChOSim provides a tool that can be used to estimate the instrument performance in the time domain by simulating the observed scenario and instrumental detection.

EChOSim implements a detailed simulation of the major observational and instrumental effects, and associated systematics. It also allows the influence of each parameter to be studied and thus it represents a key tool in the optimization of the instrument design. Observation and calibration strategies, data reduction pipelines and analysis tools can all be designed effectively using the realistic outputs produced by EChOSim.

Each simulation (see Figure 13-1) begins with a realization of the observed astrophysical scene which is propagated through the instrument simulator mimicking the detection. The outputs of each simulation are the detector timelines stored in binary FITS files allowing time-domain analysis. The output mimics standard astronomical data formats, which allow the objective data reduction/analysis using standard astronomical analysis packages.

Additionally, an advanced data reduction pipeline is also provide with EChOSim to analyse the time-domain simulations, estimating the SNRs as a function of the wavelength, given a user defined integration time. This allows estimations of the required integration times needed to achieve a desired SNR.

EChOSim is implemented in python for cross-platform compatibility, and it is an easy to use, user friendly tool which also targets the larger scientific community. Scientists can use the raw output of EChOSim, which are the individual detector timelines, to develop advanced analysis tools or can use the tool to aid in defining target observations.

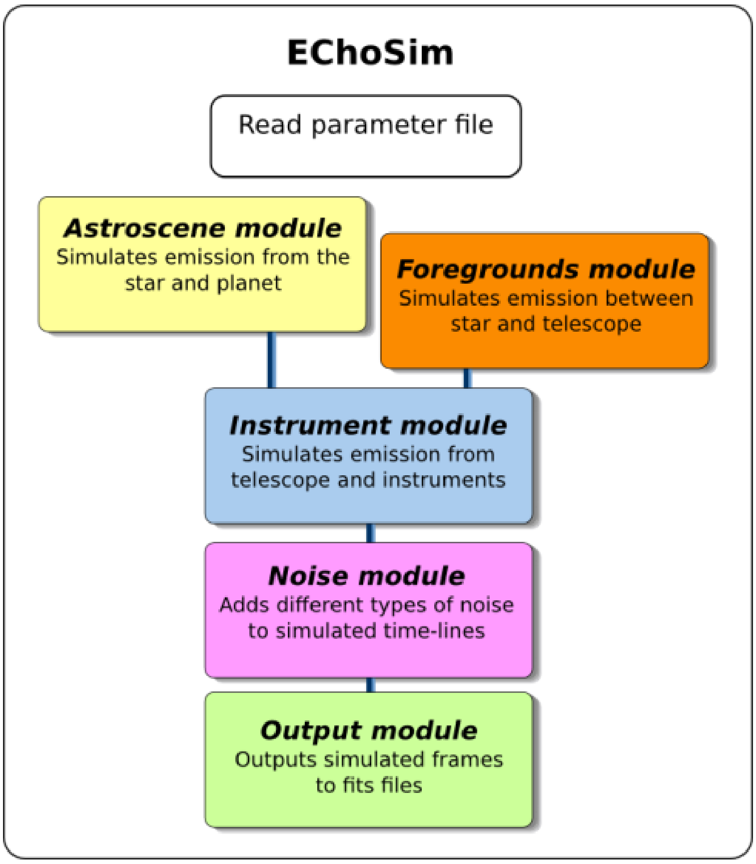

Figure 13-1: EChOSim is a end-to-end simulator of the EChO observatory. A set of input parameter define the physical properties of the science target, the optics, the spectrographs, and detectors. The simulated astronomical scene and foregrounds are collected by the telescope. The radiation is then propagated through the several instruments for detection by the focal plane detector arrays populating the five focal planes. The detector timelines can be analyzed with the data reduction pipeline provided with EChOSim, allowing to estimate the SNR of the detection. Operated in this way, EChOSim is used to assess the scientific feasibility of the EChO mission, given the proposed instrument design. The timelines can also be used to develop advanced analysis techniques for the EChO observed targets.

EChOSim simulations are highly efficient thanks to a careful implementation of sophisticated numerical algorithm. A typical time-domain simulation involving a large number of consecutive transits can be run in only minutes. This also allows EChOSim to be run in Monte Carlosimulations to characterize the likelihood of the detection or to explore the parameter space defining the scientific instruments for tradeoff analyses.

13.1.1 EChOSim Structure

The general philosophy behind the simulator is a central engine running several modules. Each module is specialized to address some aspect of the simulation. The outputs of the simulator can be computed thanks to dynamical parameters estimated within these modules or defined from data considered as inputs and computed by other means (the thermo-mechanical model for instance).

With reference to Figure 13-1 the first module in the EChOSim logical flow simulates the *Astroscene*, providing a description of the astrophysical scene (star + planet).

The *Foregrounds* module implements a description of the observation environment local zodiacal emission.

The *Instrument* module provides a description of the EChO instrument. Comprehends: i) a description of the common parts of the payload (telescope and common optics); ii) a description of the instrument transmission function for each channel as a function of wavelength (including transmission, optical throughput, and spatial modulation transfer function); iii) a description of the focal plane detector system. The module also implements a description of the self emission of the optical elements and of the detector environment.

The *Noise* module provides a description of noise components. This includes: intrinsic detector noise (e.g. dark current, readout noise), photon blip noise, telescope pointing effects.

The Output module is a service module to output the result of the simulations, consisting in individual detector-timeline, into fits files for further analysis.

An advanced observational or data-reduction pipeline is distributed with the EChOSim software package, but it is not part of the EChOSim simulation software. The pipeline reads the EChOSim output and provides a reconstruction of calibrated spectra and an estimate of the associated uncertainties.

An in-depth description of each module is found in the URD and SRD documents.

13.2 ECHOSIM REFERENCE CASES& BENCHMARKING

During each phase of the development of EChOSim, extensive validations have been performed to verify the performance and accuracy of this software tool.

We have compared EChOSim with several and independent software models of the EChO science instrument developed by ESA and consortium members. The history of these validations is documented. The first validation was presented as part of the Mid Term Review data-pack. The second validation between version 2 of EChOSim with the ESA radiometric model can be found in [RD32]. Also discussed there is a validation study on test case showing the accuracy of the software tool, given the assumed input parameters.

The final validation of version 3 of EChOSim, the latest version, with the latest ESA radiometric model is presented in [RD32] showing good agreement between the two models given the assumptions used.

13.3 RESULTS

The performance of technical and instrumental solutions proposed for the EChO space mission have been investigated using simulations performed with EChOSim. Alternative approaches have also been used when required. The result of these studies is discussed in the many documents of this EChO study and technical notes, where appropriate.

14 FGS DESIGN

The FGS is a spacecraft subsystem, but will be provided by the instrument consortium. Its main task is to ensure the centring, focusing and guiding of the satellite, but it will also provide high precision astronometry and photometry of the target for complementary science. In particular, the data from the FGS will be used for de-trending and data analysis on ground. From the scientist's point of view, it can be seen as an independent instrument channel.

During the measurement phase of the instrument a very stable pointing is required which cannot be achieved using conventional attitude sensors. Therefore a dedicated sensor is placed in the EChO optical chain, close to the VNIR as it is shown in Figure 14-1.

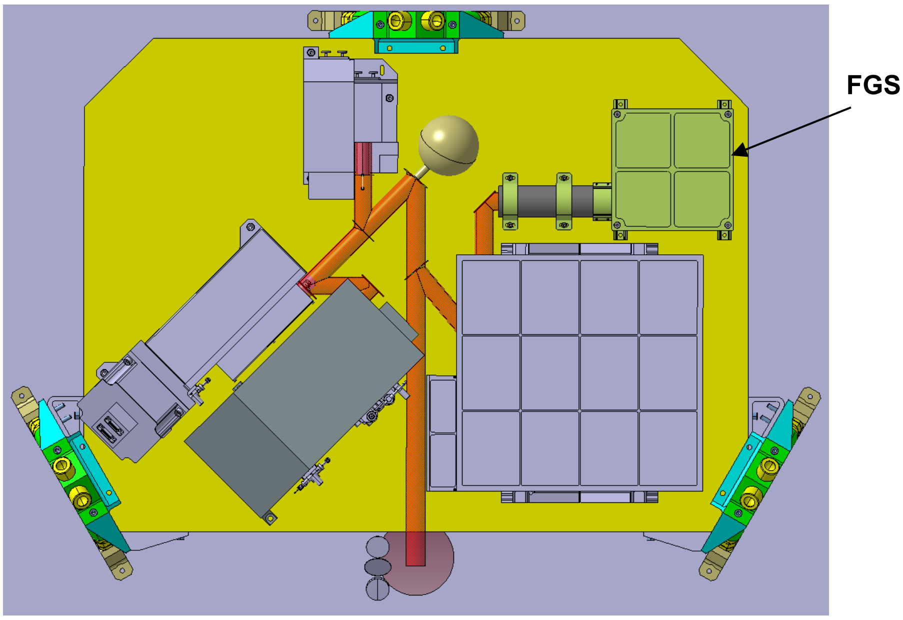

Figure 14-1: Location of the FGS within the FPU

The sensor uses star light coming through the optical path of the telescope to determine the changes in the line of sight of the EChO instrument. The attitude measurement is then fused with the rate information form Star Tracker, a high performance gyro and used as input for the control loop stabilising the spacecraft. The Fine Guidance Sensor is a critical equipment as it is an important contributor for the AOCS RPE performance in terms of the achievable single-star centroiding accuracy .

The system is composed of an optics box at the instrument optical bench (see Figure 14-2) containing cryogenic optics and redundant detector modules at 45K. At an intermediate stage temperature stage of 55K , the main and the redundant cold front-end electronics (CFEE) are located. In the service module the FGS WFEE and FGS control electronics (FCE) are accommodated. These are also redundant and they control and read the detectors and carry out the data processing. FGS systems are independent from the spectrometer instrument, thus have their own power and data interfaces with spacecraft. Figure 14-1 depicts the overall system layout

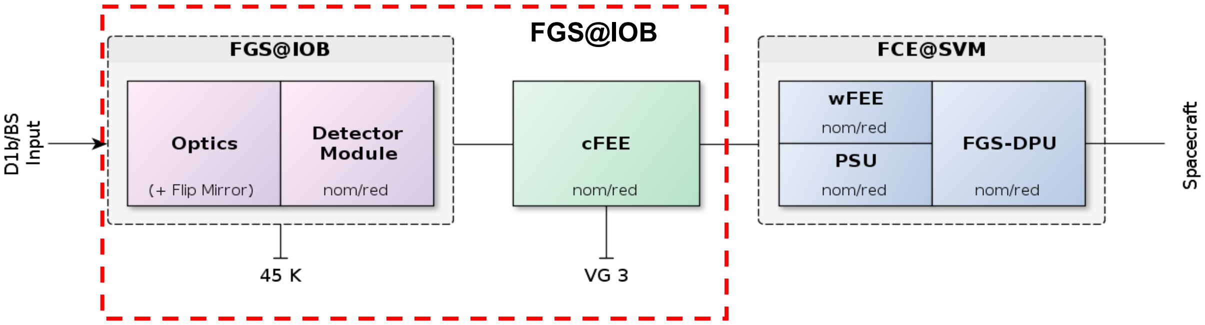

Figure 14-2: FGS Top-Level Architecture

There are considered two options of architecture. Firstly that the CFEE is placed in independent box and second one the CFEE is placed in or on the optical box with the detector.

14.1 FGS KEY REQUIREMENTS

The pointing stability between the instrument LoS and the science target with the FGS in the control loop shall be controlled to ensure compliance with the photometric stability requirements. The light shall be split between the first science instrument channel and the FGS, while ensuring the figures of merit defined in R-PERF-240 are not compromised.

The star centroiding performance of the FGS shall allow compliance with the fine APE and pointing stability requirements defined in R-AOCS-060 and R-AOCS-070 for all possible science targets. The faintest signal to be considered by the FGS is the same as defined in R-PERF-090 (see [AD1]).

The FGS consists of two units: the opto-mechnical part with detectors and Cold Front End Electronics (CFEE) situated on the IOB and the FGS control electronics (FCE) with WFEE and PSU situated on the SVM.

14.1.1 Functional and Performance Requirements

- The FGS shall output the attitude relative to an initial attitude.
- The minimum accuracy of the relative attitude measurement shall be 3 / 8 / 350 mas 1- σ independent of the line of sight of the telescope.
- The FGS shall deliver new relative attitude measurements with 2 Hz update rate.
- The specified attitude measurement accuracy shall be achieved for a spacecraft RPE up to 10 mili arcsec (goal: 5 mili arcsec) 1- σ over 1 sec .
- The time delay between the time of validity of the relative attitude measurement and the delivery of the data at the FGS data interface shall be less than 0.375 s.
- The position stability of the FGS detectors with respect to the cold structure interface shall be better than 120 nm over 585 sec.
- On-sky FoV: likely >20”x20” ~0.33degx0.33deg internal field
- Spectral bandwidth: up to 1um (present cutoff with VNIR shortwave), typically from ~20% to 50% bandwidth (e.g. from 600nm to 1000nm) or more as needed for SNR,
- Low distortion (< 1% level over FoV TBC) + eventual chromatic correction,
- Refractive (~3 lenses typically; ~5-6 lenses max) design & telephoto, for compactness,
- Detector: MCT FPA with array and pixel size linked with pixel scale/sale => typically minimum pixel size (15um for MCT) and ~512x2512 typically,
- Acquisition rate >1Hz & centroiding performance < 0.01” (5E-3” TBC),
- SNR: requirement from the centroiding performance and the targets (?)
- Redundancy: at detector level but not for optics

14.1.2 Assumptions on operation

- Minimum bin/star image spread FWHM: 2x2 or 3x3 pixels
- Able to achieve centroiding to 1/10th of a pixel level

14.1.3 Interface Requirements

The specified performance shall be met for the following telescope optical characteristics:

- Effective focal length (for a 300mm focal length focusing lens) 10568.3055 mm (?)
- Optical interface: collimated/at infinity & 250nm rms WFE, input pupil 25mmx17mm
- Image quality/WFE: diffraction-limited for any λ>3μm (assumed all aberrations, only tip-tilt excluded as part of pointing budget; focus planned to be separated

14.1.4 Output data packet

For each relative attitude measurement the FGS shall provide:

- The position of measured star
- The time of validity for the attitude measurement
- Status information on the operational mode, the sensor health and the attitude quality

14.1.5 Environmental Requirements

14.1.5.1 Operational temperature range

The FGS components shall operate with specified performances in the following temperature range:

- MCT Detector 45K
- CFEE in opto-mechanical box: 55 K
- FCE module: 270 K - 300 K

14.1.5.2 Non operational temperature range

- All FGS components of the PLM shall show no degradation of functionality or performance after an exposure to temperatures of 40 K - 353 K in non-operational mode.
- The FGS detectors shall perform as specified for a radiation dose up to 10 krad (TBC).

14.1.6 Operational Requirements

- The FGS shall start and stop the relative attitude measurement on command from ICU. The attitude at the time of the command shall be used as the initial attitude for the relative attitude measurement.
- The FGS shall dump the complete detector images on command.
- It shall be possible to switch between redundant units on command.
- The FGS shall permit in-orbit reprogramming of its software.

14.1.7 Physical Requirements

The total mass of the FGS components in the IOB shall be less than 2 kg including margin.
The total mass of the FGS components in the SVM shall be less than 6 kg including margin.

The FGS electronics placed in the SVM shall fit into the following allocated volumes:

- Proximity electronic modules: 276x210x160 mm

The thermal dissipation of the FGS components including margins shall be less than

- 0.1W (TBC) for all detector+ CFEE together
- 30 W (TBC)for FCE

14.1.8 Configuration Requirements

All FGS functions shall be maintained with full performance after any single failure.

The FGS system shall consist of

- An optical head consisting one telescope with beam splitter or removable mirror, and main and redundant detectors, one of each has own CFEE
- Main and redundant WFEE

- One data handling unit inside ICU (ESA is responsible for this unit)
- The harness needed to connect the FGS components
- The software needed for measurement processing

FGS mechanical envelope
- 350x180x100 mm (LxWxH) changed compared to ESA document EChO MDR 3.0 (350x100x250)

14.2 FGS OPTICAL MODULE DESIGN

The FGS optical module has been designed for the following basic assumptions:

- On-sky FoV: likely >20”x20” ~0.33degx0.33deg internal field
- Spectral bandwidth: up to 1µm (present cutoff with VNIR shortwave), typically from ~20% to 50% bandwidth (e.g. from 600nm to 1000nm) or more as needed for SNR,
- Low distortion (< 1% level over FoV) + eventual chromatic correction,
- Minimum bin/star image spread FWHM: 2x2 or 3x3 pixels (?)
- Able to achieve centroiding to 1/10th of a pixel level (?)
- Detector: MCT FPA with array and pixel size linked with pixel scale/sale => typically minimum pixel size (15µm for MCT) and ~256 x256 or 512x512 typically,
- WFE: 250nm rms = telescope diff-limit @ 3µm + allocation for dichroics
- Optical axis height above bench: for confirmation with all modules and structures (Figure 14-3)

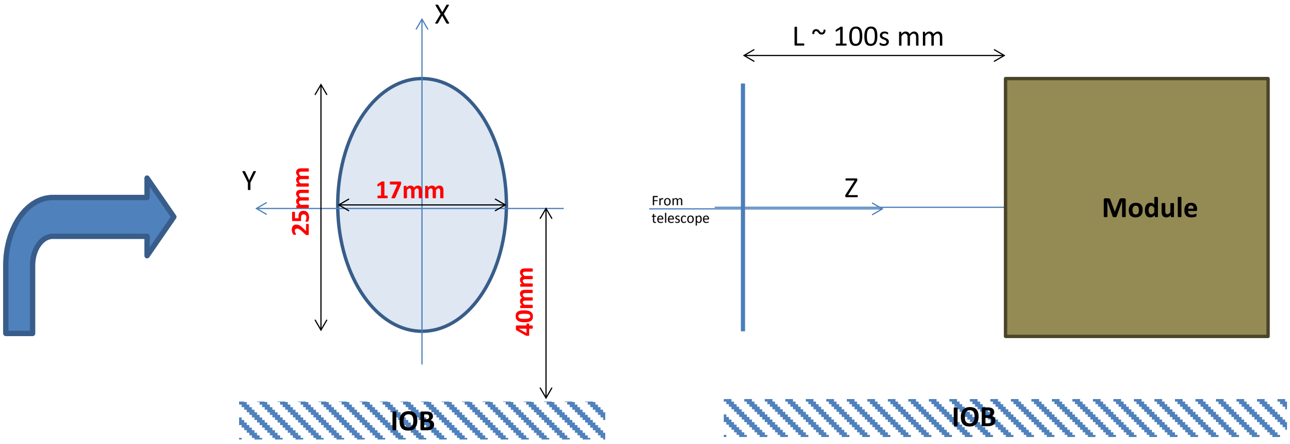

Figure 14-3: FGS Optical Module Interfaces

With the above assumptions, analysis for the two type of MCT detectors 256 x256 and 512x512 has been conducted.

As a first step a variant to the MCT 256x256 pixels was analysed. A refractive telescope design and three options of different types of reflective telescope have been considered and a trade off was studied. For details of these options please see [RD31]. The trade off selected the Gregorian telescope design option, which is detailed below.

14.2.1.1 Gregorian telescope

System properties:

- Focal length: 1300mm,
- Optical system length: 210mm,
- Field of View: 0.33° (full)
- F-number: 52,
- PSF size FWHM: 50µm x 34µm, diffraction limited,
- First mirror parabolic,
- Second mirror spherical,

- Flat folding mirror,
- Central obscuration: ~8%,
- Detector dimension: 7,68 mm (pixel pitch 15x15 µm – 512x512)

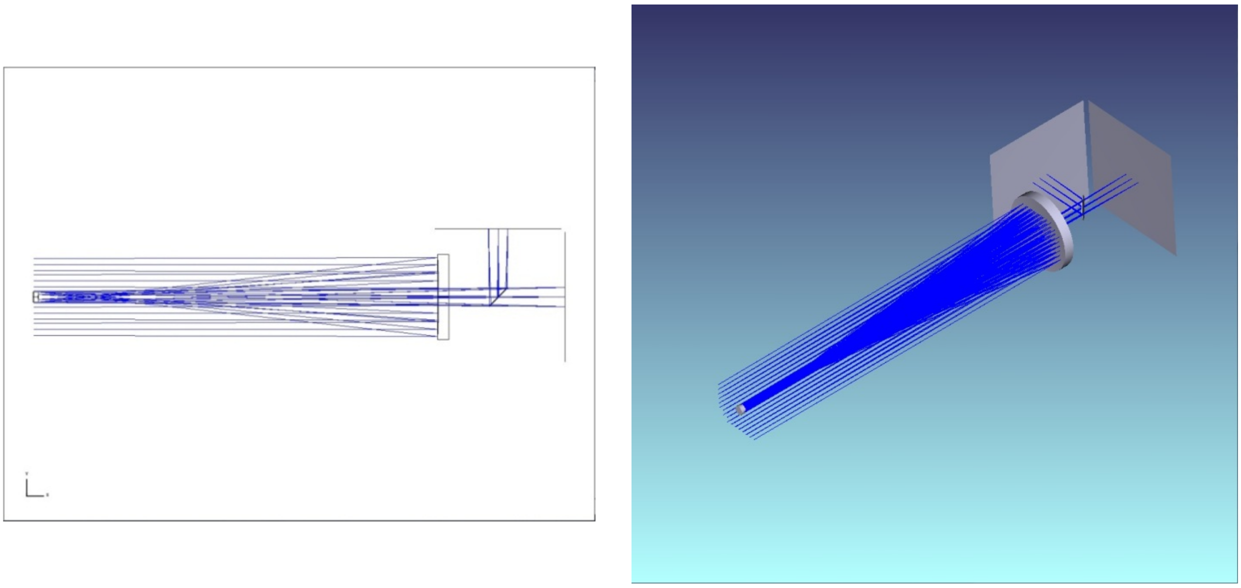

***Figure 14-4**: Optical layout*

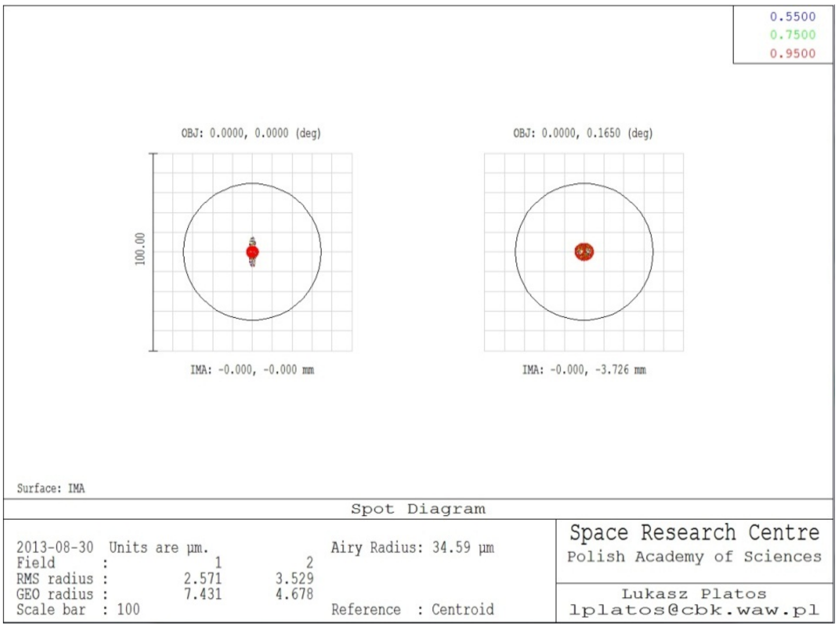

```
2013-08-30  Units are µm.                    Airy Radius: 34.59 µm
Field      :          1          2
RMS radius :      2.571      3.529
GEO radius :      7.431      4.678
Scale bar  : 100                             Reference  : Centroid
```

Figure 14-5: Spot diagram for the FoV (0,0) deg and (0,0.165) deg, wavelengths 0.55, 0.75, 0.95 µm.

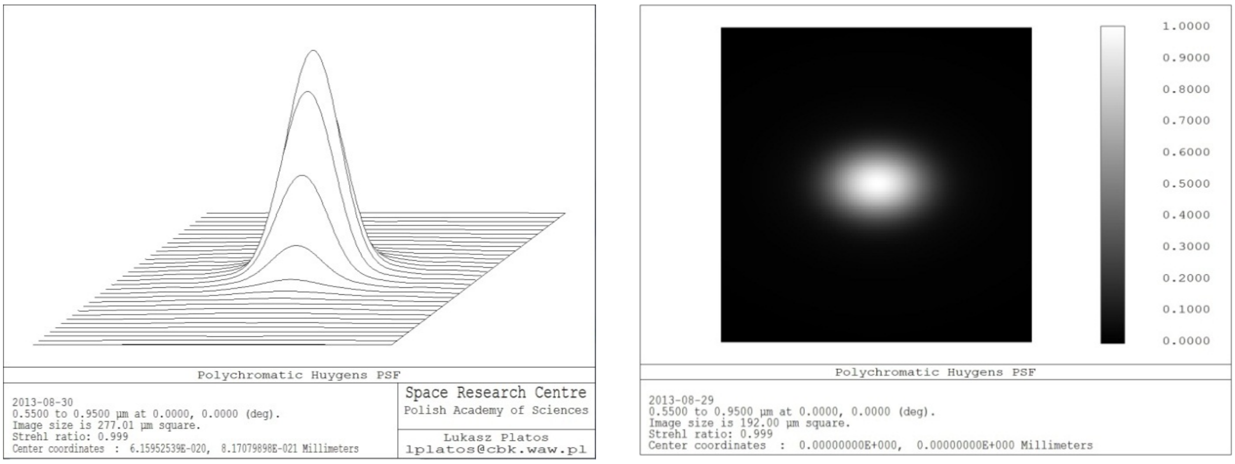

Figure 14-6: Point Spread Function 3D view

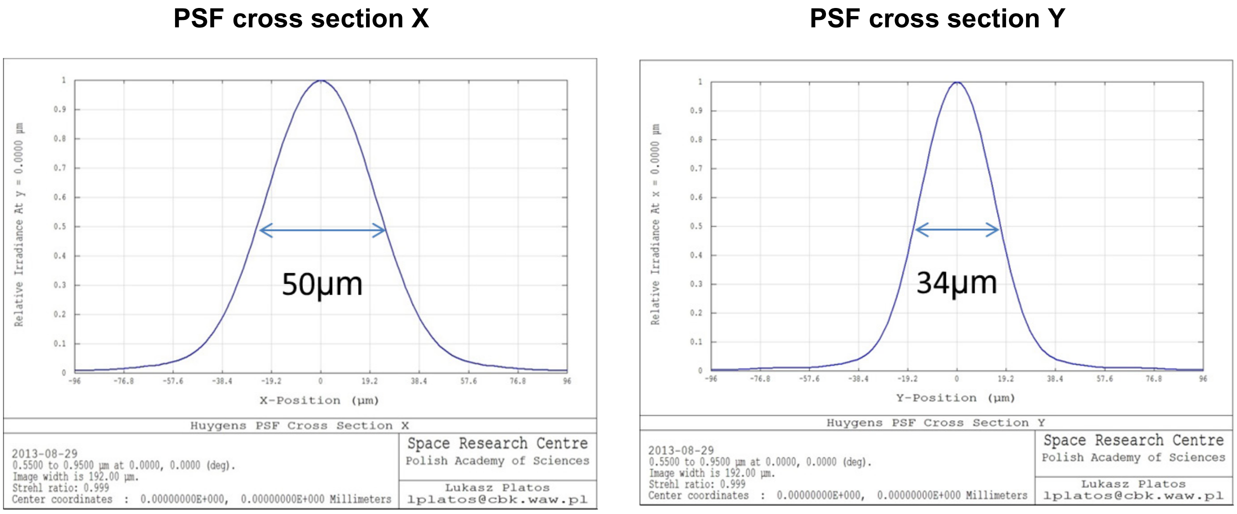

Figure 14-7: Point Spread Function cross sections

Advantages	Disadvantages
Simple optical layout with spherical and parabolic mirror	Second mirror very small: 4mm diameter
Semi athermalization- all elements made from aluminum	Manufacturing technology more complicated compared to refractive systems
Diffraction limited	
Short: 210 mm	
Entrance pupil located several 100s of mm in front of the system with aperture stop at second mirror	

Table 14-1: Advantages and Disadvantages of design solution

Analysis of these solutions lead us to select the Gregorian telescope as a baseline for FGS design. Similar technological level of difficulties, smaller central obstacle, shorter length, better fit to work with telescope are the main advantages of the Gregorian telescope.

14.2.2 Design of the Optical Module

Based on the optical data, mechanical dimensions of the beam splitter or the removable mirror and the MCT detector with accompanying electronics, the design of the unit is presented in Figure 14-8.

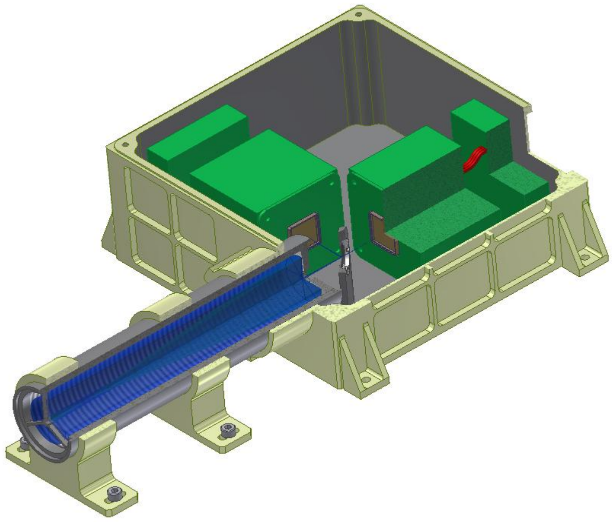

Figure 14-8: FGS Optical Module Design

14.3 FGS DETECTOR SYSTEM

Section 5 describes the process of deriving specifications for the main science channels. The detector for the Fine Guidance Sensor focal planes is chosen to reuse the device specified for the VNIR channel even though it operates as an imager with finer image quality as described above. The specification shown is largely based on the VNIR specification even though some relaxation might be possible given the operating mode.

Parameters	VNIR Specification	Performance
Manufacturer		Teledyne
Materiel		HgCdTe
Wavelength coverage (µm)	0.5-1.0 Goal 0.4 – 1.0	λc=2.53
Pixel size (µm)	15 - 30	18
Format minimum size	256 * 256	2048 * 2048
RQE	>70%	~ 80% (1)
Dark current (e^-/s/pixel)	< 0.01	<< 0.01 (2)
well depth (ke)	≥ 50	120000 (3)
Readout noise(e)	< 15 for CDS	~ 10 e-
Operating temperature	40K - 30K	40K - 30K
ROIC type	/	SFD
Readout mode	Window, NDR, binning	Compliant
Program		Multiple programs including

		JWST
TRL	TR5 in Q3 2015	>> TRL 5

Table 14-2: Baseline FGS Detector Parameters

The Teledyne device is compliant with the RFI specification and when analysed against the science requirements is predicted to perform extremely well.

The one drawback of the Teledyne device is that it is packaged in a 2K * 2K format, which even with the relatively small pixel size is an oversized array. Since this is a well-developed and tested product it is unlikely that developing a smaller array would be financial advisable. The detector would consequently demand extra space at the focal plane area. Clearly it would be possible to window the device to use only the required portion of the detector.

14.3.1 Alternative Options

The most promising of the European options is the SELEX-ES device, which is detailed in the table below. Although there are some areas of non-compliance with the RFI specification, when analysed against the science requirements the SELEX device was found to perform very well. However, it is at a lower TRL and as is discussed elsewhere, the development cost would be high. Since SELEX would be developing the devices specifically for EChO, there would be more opportunity to obtain a device with an MCT area that exactly matches the requirements.

Parameters	FGS Specification	Performance
Manufacturer		Selex-ES
Materiel		HgCdTe
Wavelength coverage (µm)	0.5-1.0 Goal 0.4 – 1.0	λc=2.6
Pixel size (µm)	15 - 30	15
Format minimum size	256 * 256	512 * 512
RQE	>70%	70% (1)
Dark current (e^-/s/pixel)	< 0.01	<< 0.03 (2)
well depth (ke)	≥ 50	>50 (3)
Readout noise(e)	< 15 for CDS	~ 23e
Operating temperature	40K - 30K	40K - 30K
ROIC type	/	SFD
Readout mode	Window, NDR, binning	Compliant
Program		Developed from ESA funded technology programs
TRL	TR5 in Q3 2015	TRL 3-4 presently, with funding will achieve TRL 5 in timescale

Table 14-3: Alternative FGS Detector Parameters

(1) dependent on AR coating
(2) measured 0.03 at 80K for 24 µm pixel so expect much better for smaller pixel and lower temperature
(3) set by a capacitance value, 75Ke is possible

14.3.2 Cold Detector Electronics

The Teledyne device comes with a fully proven SIDECAR ASIC Module to drive the detectors. This ASIC is common to all Teledyne devices under consideration for EChO, which would mean more overlap between the required drive electronics for the FGS, VNIR, SWIR and MWIR channels.

If the SELEX-ES device were used it would also have the advantage that the ROIC would be common to the FGS, VNIR and SWIR channels. However, the drive electronics are also not as developed as the Teledyne ASIC.

14.3.3 Warm Detector Electronics

The FGS control electronics (described below in Figure 14-9) located in the SVM, will contain cold redundant interface boards which are connected with the FGS internal subunits. While the ADC and bias regulation are carried out by the cFEE, digital clocking and pixel addressing are not included in the cFEE ASIC, because they are specific to the detector chip vendor. Also, the detector power regulators are in the FCE, because power dissipation in the cold has to be kept low. So these functions must be provided by the FCE.

Additionally, there may be a flip-mirror in the optics of the FGS, which needs to be controlled, as well as a number of HK sensors, which will report FGS@IOB temperatures, status of flip-mirror, cFEE status.

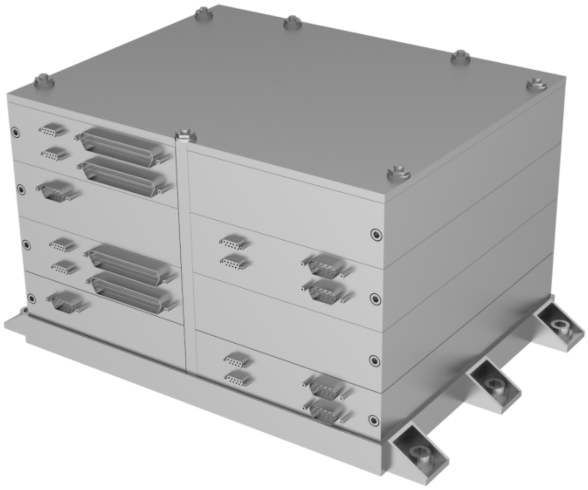

Figure 14-9: Design model of FGS Control Electronics box consisting of 2 processing board units and 2 interface/PSU elements.

14.4 FGS DATA PROCESSING UNIT HARDWARE

The FGS has its own electronics box in the service module, the FCE (FGS Control Electronics). All communication, control and data processing tasks will be carried out by this unit. As a spacecraft subsystem, it has to be fully ECSS compliant. It will drive and read the FGS detector electronics, establish a control loop with the spacecraft and deliver scientific data products. The FCE box in the service module will have its own power supply and be independent from the spectrometer channels and the spectrometer ICU. It will consist of the following sub-units:

- Mechanical Chassis: Typical Warm Electronics box, its envelope is 276x210x160 mm, and its mass estimation is 5.5 kg incl. electronics.
- Processing and control boards: Two processor boards (cold redundant) will be available for data processing and control. Most data processing operations will be in floating point arithmetic.

- Interface boards (cold redundant): Interfaces to spacecraft: power, data, commanding. SpaceWire 1355 / 1553 where applicable. Interfaces to cFEE: Digital (LVDS), power and HK lines.
- FGS power supply unit (cold redundant): S/C 28V input, secondary voltages to FCE, cFEE, FGS detector, FGS Flip Mirror and HK sensors.

14.4.1 Data Processing Boards

The processor boards will have to carry out the centroiding in real-time. For this task, the data frames need to be calibrated first. The most demanding operation is the flatfield correction of the full frame, which requires 655360 floating-point multiplications per second. Once the ROI has been set to a smaller window, the number of pixels and thus the number of operations is greatly reduced. But also the centroiding takes great advantage of available floating-point arithmetic.

All these criteria are met by the “Panther” board, which comes with a rad-hardened LEON2 ASIC at 64-80 MHz, FPU, MMU, 8 MB EDAC-protected RAM, numerous interfaces and EEPROM. With 22 MFLOPS and 54 MIPS, all calibration, centroiding and compression tasks can be carried out.

The power budget of one board is 6W.

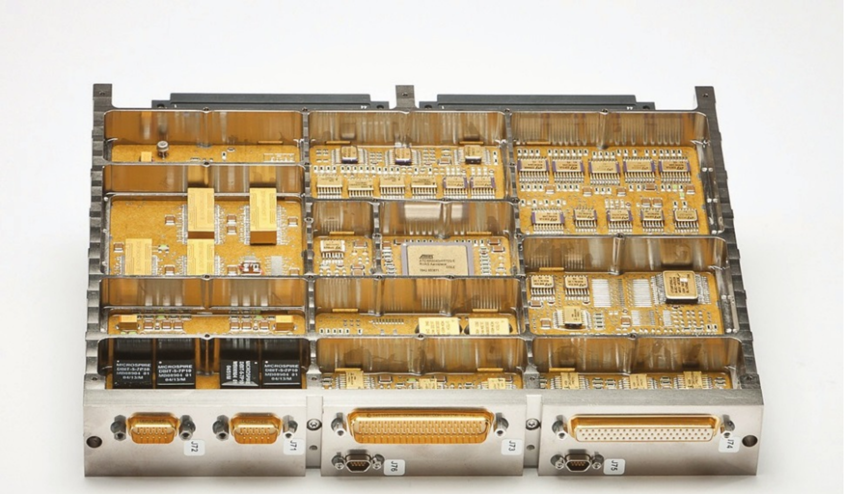

Figure 14-10: RUAG processing board unit. The “Panther” board provides a LEON core with FPU, cache and additional amenities.

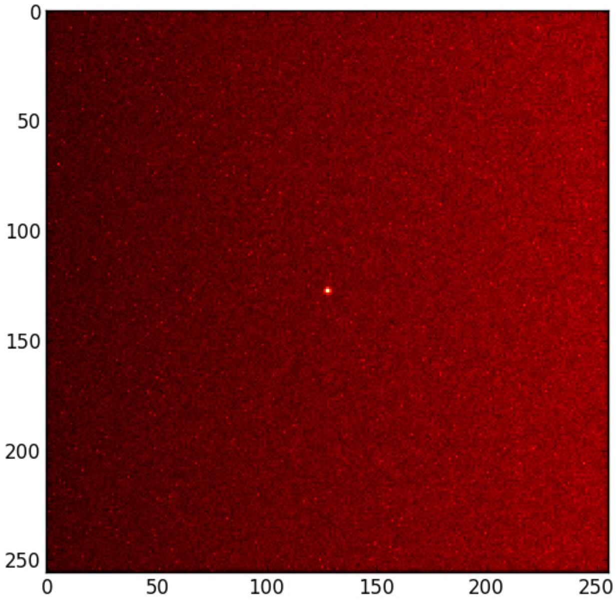

Figure 14-11: ***Data frame from first version FGS simulator.***

14.5 FGS ALGORITHMS AND SOFTWARE DESIGN

The FCE unit will have to carry out and support a number of different tasks. There will be functions to control the FGS subsystems, process the detector data, communicate with the spacecraft, all according to the current mode of operation.

The absolute pointing error of the star trackers is 10" RMS, pointing is then handed over to the FGS. The FGS will find and measure precisely any point sources in its 20” field of view. During peak-up a frame rate of 1 Hz is required, during guiding 10 Hz of a 7x7" region of interest, corresponding to a 70x70 window.

The FGS will also be used for focusing the main telescope. This is limiting the amount of intentional defocus or diffusion. The PSF will be spread over 50-60 pixels, with a FWHM of 3x3 pixel. The main requirement is a 10 milliarcsecond centroiding performance at 10 Hz for the faint targets. The operating wavelength range is 400-800 nm.

In the warm FGS control electronics the data will be processed in real-time. Output data products are calibrated, cropped and reformatted images, centroid coordinates, dimensions and errors in both axes, photometry, glitch count and housekeeping. On-board compression will be used to reduce the telemetry. Additional data processing capabilities include frame stacking for PSF measurements. Figure 14-11 shows the output from a first simulator software used to assess the required processing capabilities of the FCE.

14.5.1 Centroiding

For the best support of the operating modes, several centroiding and data extraction algorithms will be implemented, fully configurable by parameter and command.

A number of calibration steps need to be carried out before the centroiding can be applied, most importantly bias and flatfield correction. The detector is foreseen to be operated in read-reset mode, so no ramp fitting will be required. For the purpose of glitch detection and correction, several frames will be buffered.

Configurable windowing methods to extract the region of interest (ROI) will be available.

Center of Gravity (CoG) based algorithms with different weighting and thresholding strategies will be used to extract the astrometric and photometric parameters. Alternatively, correlation methods will be implemented, as well as general fitting strategies.

14.5.2 Data Products and Telemetry

The FGS will deliver centroid data products and images to the spacecraft. In addition, these data products will be sent as science data products to ground. On top of that, HK are generated and sent. All rates and window sizes are configurable.

A typical centroid dataset will consist of astrometric and photometric measures, plus several bits of status information.

	CONTENTS	SIZE (BYTES)
Astrometry	X/Y position, X/Y FWHM (if applicable), variances	24
Photometry	Integrated flux, FWHM flux, background flux, variances	24
Status	Operating mode, time tag, glitch count, star count, validity flags	6

Table 14-4: Centroid data product. Floats are used where applicable.

During guiding, a 70x70 pixel window will be analyzed at 10 Hz. Assuming 16 bit words, the raw ROI data rate will be 784 kbit/s. In case 256x256 pixels should be transmitted at 10 Hz, a data rate of 1 Mibit would be achieved. Thus, a SpaceWire link would be preferred over MIL-STD-1553. The centroid data will be 54 bytes per frame, or 4.32 kbit/s.

Science data products that will be downlinked will be compressed in a lossless manner. Images will be compressed using an integer wavelet transform with an arithmetic compression backend. This will yield a factor 3, depending on the noise. For the centroids, compression will be much less efficient, as most parameters will be floats. Given the estimated numbers from above, a downlink rate of ~300 kbit/s would be needed for a 10 Hz resolution. For 20x20 pixel window, this would become ~30 kbit/s. If only the centroids and no images are transmitted, 4 kbit/s. All of these rates are configurable to the needs on ground.

The FGS has few sensors and HK values, yielding a data rate in the order of 1 kbit/s. The precise overall telemetry contribution of the FGS depends on the parameter configuration, which is at this point TBD, but our current estimation is 10 kbit/s.

14.5.3 FDIR and SW Infrastructure

In order to guarantee the high reliability of the FGS, the software has built-in functionality for internal monitoring of hardware and software states, self-testing and error management. As a stand-alone unit, the FCE software also has to provide functionality for telecommand verification and execution, on-board time management, HK monitoring and provision, subsystems set-up, etc. Upon a defined set of anomalies the FCE puts its subsystems in a safe state and signals that state to the spacecraft.

The hardware specs are primarily defined by the amount of data to process, combined with the complexity of the centroiding and data compression tasks.

14.6 FGS PREDICTED PERFORMANCE

There are several points that set the FGS apart from guiding systems that have been flown. First, the field of view is only ~20”, it is on axis and it will mostly contain just one single point source during guiding. The FGS will provide centroiding information and imagettes to the spacecraft, but also to ground as a science data product.

Our assessment of the FGS accuracy for the faintest target goal given by G-PERF-120 considering the effective collecting area of the telescope, efficiency parameters of optical elements, beam splitter and QE of the detector lead to a photoelectron count of more than 10^4 per second. Combined with a pixel scale of 0.1” and an FWHM of 2-3 pixels, the centroiding accuracy will be less than 0.1 pixel (following the relations in [RD28]. This is well in line with the required precision. For further details see calculations in [RD29].

For the brightest star, the difference in visual magnitude is 8.72, or a factor ~1500, leading to 10^7 photoelectrons. Since more photons lead to better accuracy, we only have to make sure that we avoid saturation. At 10 Hz, with a FWHM of 3 pixel, the central pixel will have a photoelectron count of ~10^5.

15 VNIR CHANNEL MODULE DESIGN

15.1 INTERFACES

VNIR total coverage is from 0.4 to 2.47 microns, the region from 2.4 to 2.5 μm will be overlapped with SWIR module. The accepted collimated beam is D<25mm and the input WFE is assumed to be <500 nm rms. The spectrometer will be fed by means of two optical fibres working in the wavelength ranges of 0.4-1.0 μm and 1.0-2.5 μm respectively. The one for the 0.4-1.0 μm range shares the input light with the FGS. Two separate focusing elements have to be placed after the dichroic D1b and the FGS beam splitter as input to VNIR, these focus the light onto the two fibres. This is shown schematically in Figure 15-1 below.

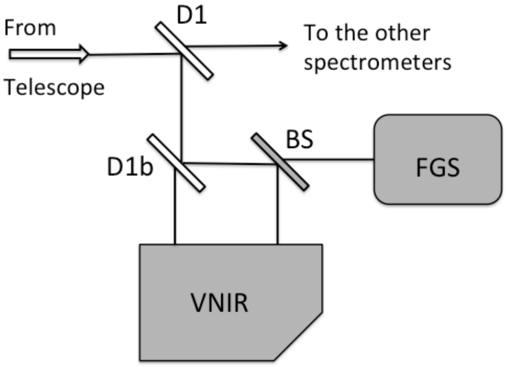

Figure 15-1: VNIR Optical Interfaces

The average transmission from the VNIR entrance to the detector will be about 0.48. This includes estimates for the transmission of the fibres (based on existing technologies and measured data) and realistic estimates for the reflectivity and transmission of all optical elements internal to the module design.

The instrument's box is shown in the picture and it is attached to the payload optical bench by means of four feet that act as mechanical and thermal interface to the bench itself. The Figure 15-2 shows the instrument box with its feet and the two apertures through which the input light will enter the instrument after the dichroic and the beam splitter (see Figure 15-1).

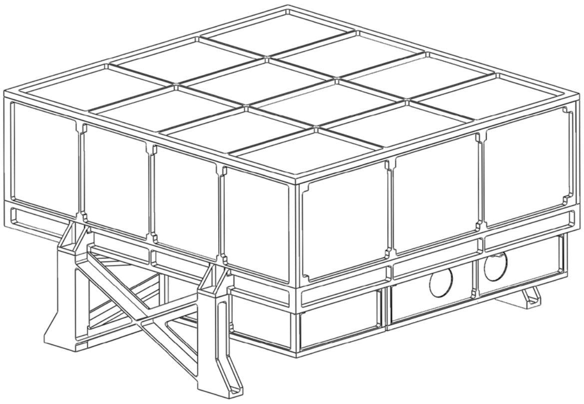

Figure 15-2: VNIR box

15.2 OPTICAL MODULE DESIGN

15.2.1 Optical Design

The optical layout of the instrument is shown in the following figure:

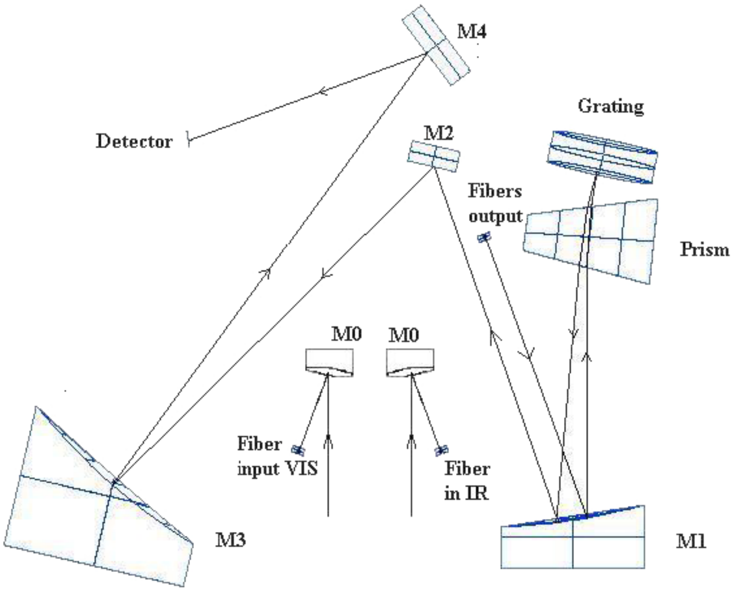

Figure 15-3*: *VNIR optical layout.

The system will actually cover the spectral range of 2.1 μm between 0.4 and 2.5 μm without gaps with the requested spectral resolution. The resulting resolving power is nearly constant and it is R≈330 on the binning that will be operated on the detectors pixels. In the current design presented here in figure 15-4 the spectrum is spread on a 256 by 256 pixels detector with a pixel pitch of 30 μm. However the optical layout would not change for a detector with smaller pixel pitch. At this time the actual baseline solution is a detector of 512 x 512 pixels with a 18-μm pixel pitch. This solution requires a 5x5 binning to obtain the given resolving power.

The wide spectral range is achieved through the combined use of a grating with a ruling of 14.3 grooves/mm and blaze angle of 3.3° for wavelength dispersion in horizontal direction and an order sorting calcium fluoride prism (angle 22°), which separates the orders along the vertical direction. The collimator (M1) and the prism are used in double pass (see Figure 15-3). The prism is the only optical element used in transmission. All remaining optical elements are used in reflection: 2 off-axis conic mirrors, 1 spherical mirror, 1 flat mirror and 1 grating. All reflecting elements will be made of the same aluminium alloy as the optical bench. This simplifies the mechanical mount and alignment of the system.

The light is fed to the spectrometer via two fibres with the output face positioned on the side of the M1 mirror. The fibres are commercial fused-silica with ultra-low OH content and core diameter of 50 μm. The fibres are separately fed by two identical off-axis parabolic mirrors (M0) which intercept the collimated light transmitted from the first dichroic (D1b), (IR), and reflected by the combination of D1b and the beam-splitter, (VIS). The use of an optical fibre coupling gives a larger flexibility in the location of the VNIR spectrometer within the EChO payload module.

The input pupil from the telescope is elliptical, 25mm x 17mm. The f/# of M0 is F/3.5 in the direction of the major axis of the ellipse and F/5.1 in the direction of the minor axis. The average aperture is F/4.3. The scale on the focal plane of the parabola M0 is 0.25mm per arcsec, i.e. the sky projected size of a fibre with D=0.05mm is 2 arcsec.

A Mercury Cadmium Telluride (MCT, HgCdTe) detector has been considered for VNIR. The following figure shows the observable spectral orders, m, projected on the MCT array, starting from *m* = 3 at the bottom (near infrared spectral range) to *m* = 20 on the top (visual spectral range).

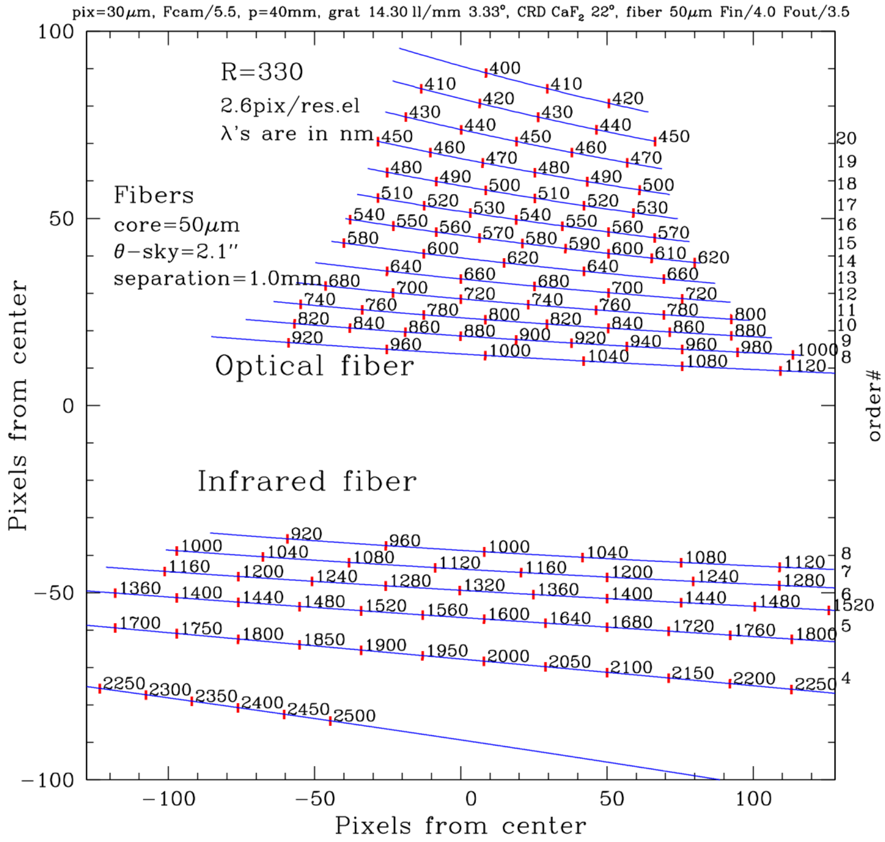

Figure 15-4: Projection of Spectrum onto VNIR Detector

Namely, the figure shows the distribution of the light on the array between 2500 nm (m = 3) and 400 nm (m = 20). The central wavelength in each order m, positioned at the blaze angle of the grating, is given by the relationship $\lambda = 8.1/m$ µm. The VIS and IR spectral ranges are separated on the detector because the fibres at the spectrometer entrance are separated by 1 mm. In general, most wavelengths are sampled twice on different orders, i.e. in different areas of the detector, as Figure 15-4 shows. The spectrum in each order is spread across several pixels in the vertical direction. Thus, a sum over 6x6, 5x5 or 3x3 (according to the chosen detector array) pixels will be done to increase the sensitivity of the system in order to provide a so-called spectral channel.

As previously said, the coupling of the VNIR module to the telescope will be done through the use of a dichroic element that will select and direct the visible and near infrared light towards the combined system VNIR and FGS. A beam-splitter is foreseen to further divide the light beam between FGS and VNIR (see figure above). The balance of this beam-splitter will need to be studied in conjunction with the FGS team during the assessment phase to maximize the science return while maintaining sufficient signal for the guider system. As the performance of the module optics should be very good to assure the observations of transient planets in transit or in occultation of a star, the detector is going to be a key element in the system. In order to meet the EChO visible channel performance requirements, it is possible to pursue different ways, based on different detectors and readout electronics as well as on the optical spectrometer design characteristics.

15.2.2 Internal Calibration Unit

The instrument calibration is going to be performed looking at a known reference star before and after any target observation. The star calibration is meant to verify the position of the spectral lines and the radiometric calibration of the instrument within 5%. However, it is important to monitor the stability of the instrument and, in particular that of the detector gain during each observation session. The observation session is supposed to vary, according the SciRD, from minutes to about 10 hours depending on the characteristic of the target itself. In order to assure the quality of the measurements the calibration unit has to guarantee the possibility of monitoring possible “instrumental” variations of the order and better of 10^{-4} (see the Technote on calibration and processing).

The calibration unit will be equipped with two Halogen-Tungsten lamps for redundancy. Halogen-tungsten lamps are used, and can be traced to Primary Standards (NPL/NIST). The calibration lamps will be equipped with a close loop control system to assure the requested stability over the observation time. The lamps will have colour temperature ~3000K and it will be operate for very short times during the observation sessions.

The lamps inject their light into an integration sphere, which will have two output fibres that will feed the two input fibres to the spectrometer (ranges 0.4-1.0 µm and 1.0-2.5 µm respectively). Figure 15-5 gives the spectrum in input to the fibres. The feeding of the main fibres will be done using 2in-1out fibre connectors. The two fibres will be illuminated at the same time.

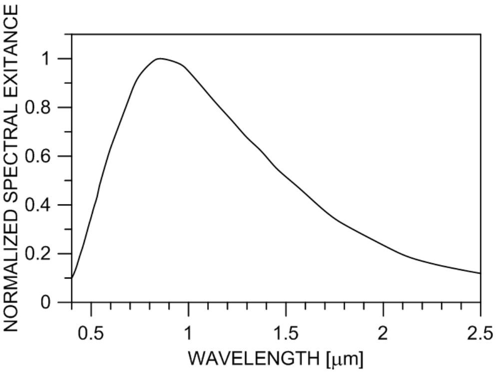

Figure 15-5: Halogen.Tungsten lamp typical emission.

The calibration unit will be located in a separate box on a side of the service box where the mirrors collect the light from the VNIR feeding optics and focus it on the optical fibres inputs. Figure 15-6 shows the calibration unit and its arrangement on the service side of the VNIR optical bench.

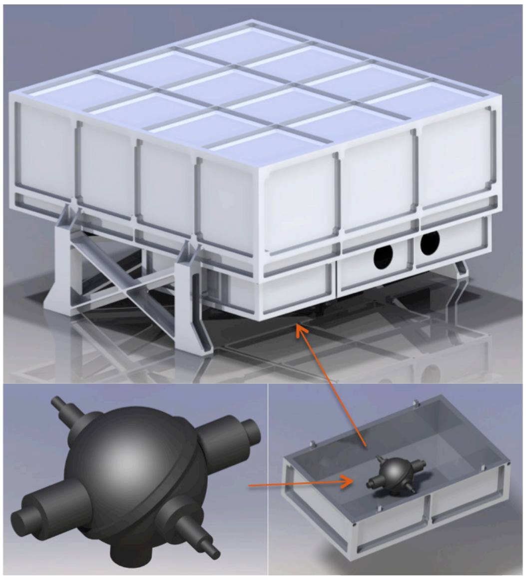

Figure 15-6: the calibration unit and its arrangement in the instrument.

15.2.3 Mechanical Design

The accommodation of the optics inside box is depicted hereafter:

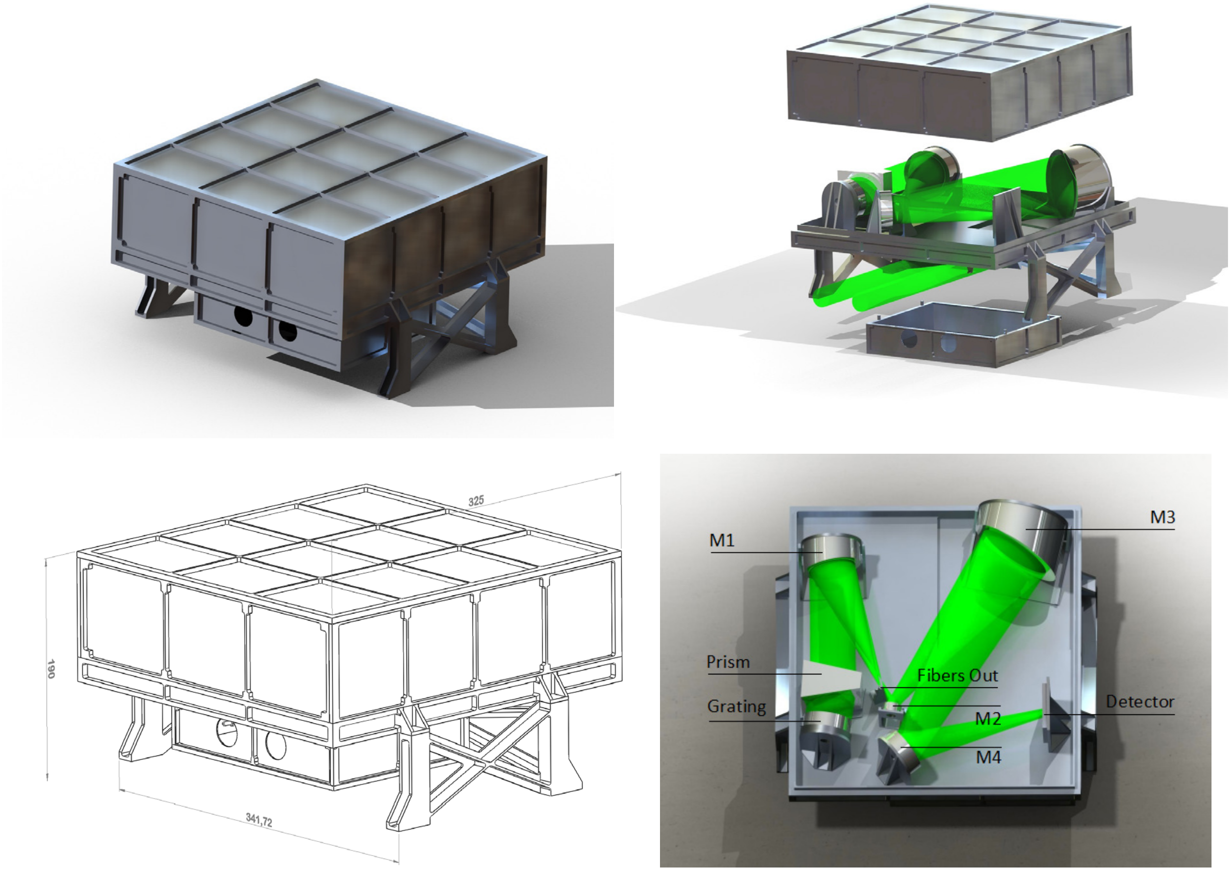

Figure 15-7: VNIR box close (left panels), open (upper right panel) without the internal calibration unit and top view of the spectrometer elements (lower right panel). The path of the light inside the instrument is shown in green.

The optical elements (mirrors and prism) are shown in the right panel of Figure 15-7. The box will be built minimizing the weight and the material will be the same of the payload optical bench. Figure 15-7 shows the box without the calibration unit mounted below the spectrometer optical bench. The overall size is Size: 341.72 x 325 x 190 mm and the dimensions are depicted in the lower left panel. A view inside the box is given in the left side of the figure and the location of the optical elements of the spectrometer is reported (see section 15.2.1 for name references). The lower part of the VNIR optical bench will be dedicated to the services to the spectrometer: the input box where the mirrors M0 concentrate the light on the optical fibres and the calibration unit in two separated box in order to minimize light and thermal contamination of the rest of the instrument (see Figure 15-2 and Figure 15-7).

Item	mass (g)
Main optics	1395,30
Fibers feeder optics	58,46
Base plate	985,54
Main optics cover	1338,90
Fibers feeder cover	196,74
Supporting strut	347,78
Brackets and adapters	571,75
Cal unit	175,00
Harness and FEE	450,00
Total	5519,47
Margin 20%	1103,894
Total with margin	6623,364

Table 15-1: VNIR Mass Breakdown

The mass of the instrument is estimated to be about 6.6 kg (20% margin included) and its breakdown is given in Table 15-1. The VNIR First Resonant Frequency is planned to be larger than >150 Hz. More accurate estimation can be done by a structural analysis that will take into account the effective vibration levels of the spacecraft during the launch.

15.2.4 Adaptation to the payload optical bench

Lately a re-arrangement of the elements below the VNIR optical bench (collector optics and internal calibration units) have been required for making possible the dichroics D1 and D1b to work at an angle around 45° in order to optimise their performances and to more efficiently re-organise the arrangements of the modules on the EChO optical bench. The two elements have been moved around as Figure 15-8 shows. This was quite easy due to the use of the optical fibres in the VNIR module.

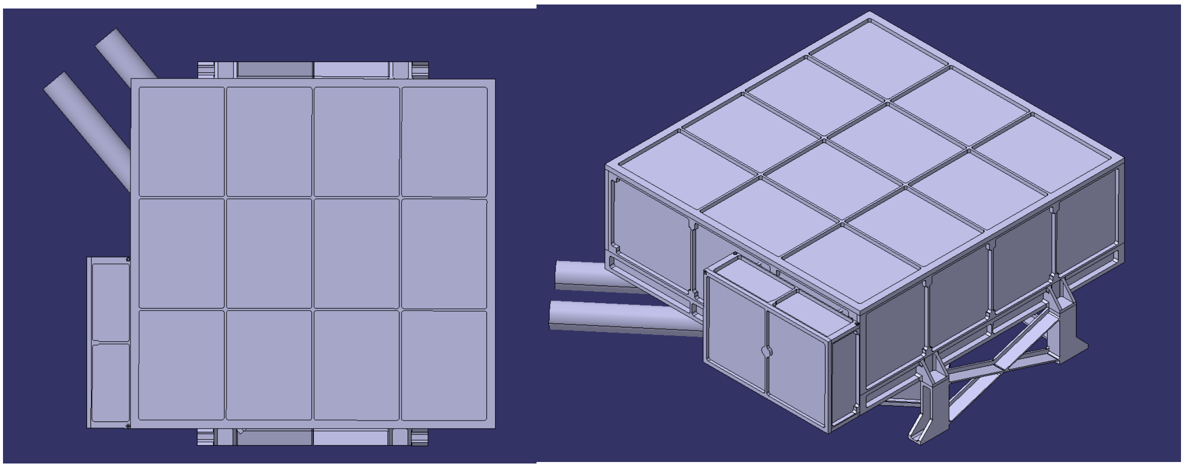

Figure 15-8: Adaptation of VNIR

15.2.5 Thermal Design

The instrument will be built in the same material of the payload optical bench and the box is thermally linked through its feet to it. The optical box and the FEE are supposed to be at temperatures lower that 50K. The FEE would be located on the VNIR module exterior and the thermal load would be sunk to the Instrument Optical Bench (IOB). The detector is planned to work at a temperature in a range of 40-45K dissipating about 30 mW.

15.2.6 Performance vs Requirements

15.2.6.1 Instrument Efficiency

The tracks of the grating's orders of diffraction, as shown in Figure 15-4, on the detector would not be equally illuminated if the input light would have a constant intensity over all the spectrum as the grating's efficiency changes along the order. The maximum efficiency is around the centre of the blue curves in Figure 15-4. In this spectrometer configuration some wavelengths can be observed on two adjacent diffraction order. To completely recover the light at those wavelengths the signal coming from the adjacent order has to be summed. The sum has to be done to maximise the result and keep the highest feasible signal to noise ratio. A reasonable compromise has been found in summing the adjacent orders when the grating efficiency is higher than 80% with respect to the maximum. The result is a component of the Instrument Transfer Function, ITF, of the instrument that will be given as result of the on-ground instrumental calibrations by measuring and combining the optical efficiency of the spectrometer and the detector performances. Figure 15-9 shows the spectrometer efficiency calculated the 80% criterion. The present calculation has been done by considering aluminium mirrors without any coating to improve the performances at wavelengths lower than 1.0 µm. In the picture the expected behaviour obtained by the use of coated aluminium or protected silver mirrors is also shown for comparison.

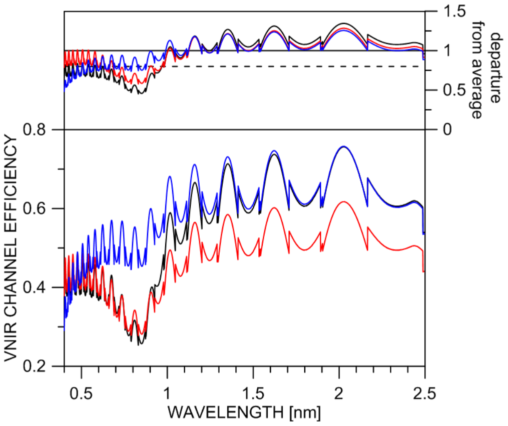

Figure 15-9: VNIR efficiency and its departure from the channel average: black curve, present estimation (this study); red curve: estimation done by using coated aluminium for improving the relative efficiency below 1 µm; blue curve, estimation done by using protected silver for all the mirrors.

15.2.6.2 Point Spread Function

Strehl ratio of PSF obtained on Focal Plane of VNIR channel is calculated at 2.6 micron and 857 nm. The VNIR channel is optically optimized to be diffraction limited (Strehl ratio bigger than 80%) in IR. Figure 15-10 shows obtained results.

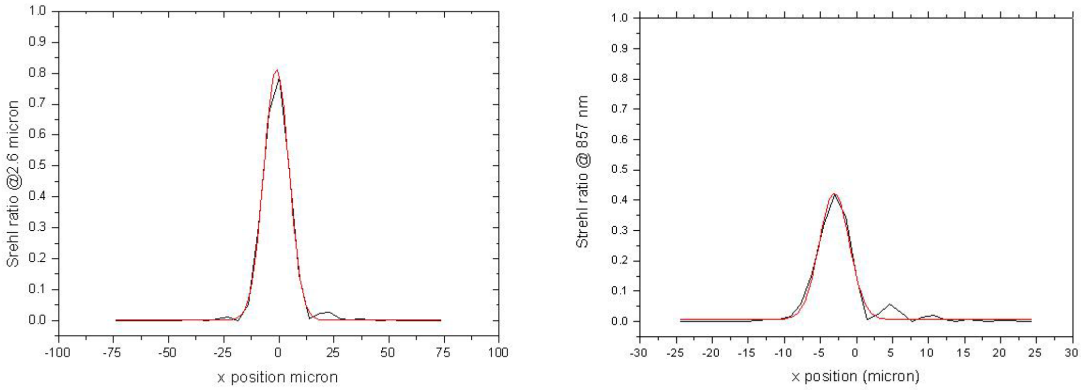

Figure 15-10: Left: PSF on Focal Plane at 2.6 micron. Right: The same at 857 nm. The Strehl ratio results 80%and 45% respectively.

15.2.6.3 Telescope pointing effects

The coupling of the light from the telescope into the input of the optical fibre is affected by the quality of the telescope pointing system. The effect of the mean performance error (MPE) is a loss of efficiency from observation to observation. The effect of the relative performance error (RPE) is a photometric error within an observation. A simulation is performed at two representative wavelengths (800nm and 2.5µm) to estimate the magnitude of both effects. The illumination pattern of the telescope is obtained from optical modelling. The energy collected by the fibre is then studied as a function of MPE, RPE and PRE (performance reproducibility error). The MPE is varied in accordance to EIDA-R-0470. The impact of three different RPEs is studied: i) RPE1 = 30mas-rms from 1 to 10Hz; ii) RPE2 = 50 mas-rms from 1 to 300Hz; iii) RPE3 = 130 mas-rms from 1 to 300Hz. These three cases correspond to three different AOCS solutions. A fixed PRE = 20 mas-rms from 0.020 to 4mHz is used in this simulation.

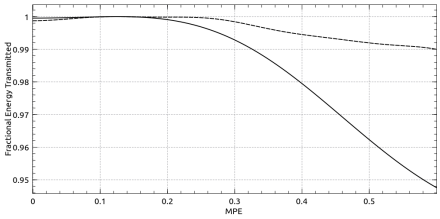

Figure 15-11: Normalized energy loss vs MPE at 800nm (dashed line) and 2.5µm (solid line).

The effect of the MPE on the normalized transmitted energy is shown in Figure 15-11. The combined effect of the RPE and PRE on the photometric error is shown in Figure 15-12. The worst case photometric error is obtained when observing a bright target (R-PERF-110) with the RPE3 option and results in 10% of the total allowed system noise variance in one second of integration for this channel (R-PERF-350).

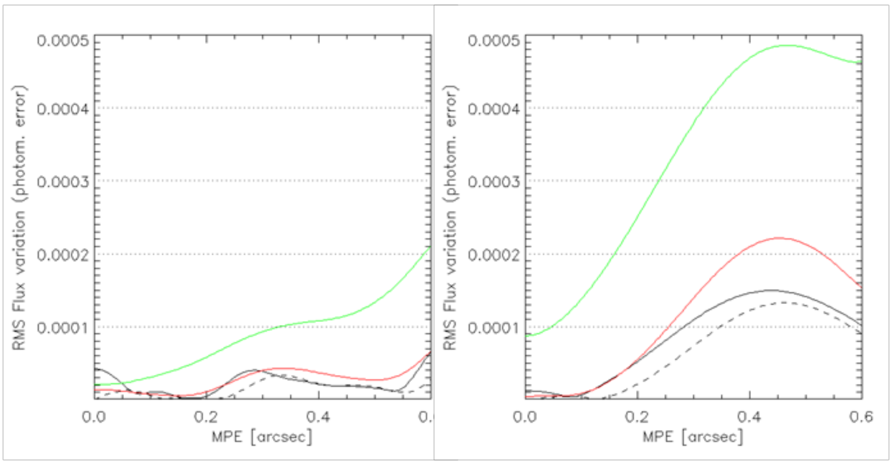

Figure 15-12: Photometric error induced by the combined RPE/PRE at 800nm (left) and 2.5μm (right)in one second of integration. The solid lines correspond to the RPE1 (black), RPE2 (red) and RPE3 (green) cases discussed in the text.

The impact of the pointing errors and the pointing jitter are discussed in more detail in the technical note, ECHO-TN-0003-UCL, [RD30]. The result of the analysis discussed there is that those effect of the pointing do not significantly contribute to the total budget of the photometric error.

15.2.6.4 Fibre efficiency evaluation to assess the coupling into fibre as function of wavelength from aberrated input beam

The analysed optical system is the Echo Telescope and the concentrating system (f#4) in input of fibre. The optimized configuration consists in a primary-secondary mirror telescope distance M_{T1}-M_{T2}=1.500 mm, the defocused configuration determines a WFE 250 rms with shift M1-M2 position of 87 μm. (WFE calculated at 1 micron wavelength). The fibre with 50-μm diameter corresponds to a Field of View (FOV) of 2arcsec.

The spot diagram and the encircled energy are simulated to verify the requirement. Simulation of encircled energy in 250rms WFE generated by defocusing (M_{T1} back with respect to M_{T2}) of 0.087 mm (the simulation considers only defocusing shift on optical axis. It is not a complete evaluation of efficiency because the tilt and lateral shift are not included).

Spot diagram

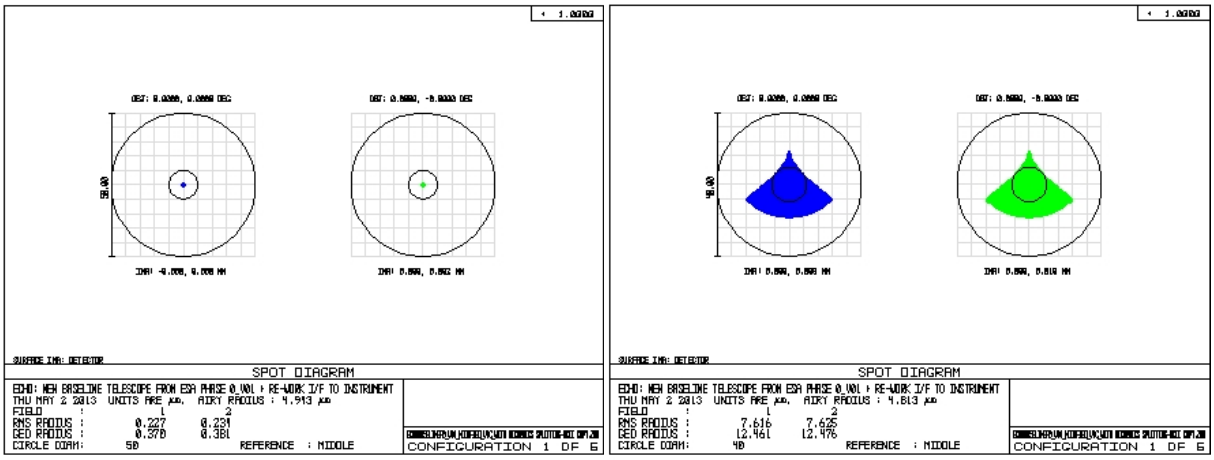

Figure 15-13: Spot diagram of Focused system in 50 micron at central field (0,0)deg in blue and marginal field (0,0.000278)deg in green colour (on left side) and Spot diagram of defocused system in 50 micron at central field (0,0)deg in blue and marginal field (0,0.000278)deg in green colour(right side)

Figure 15-13 shows that the spot diagram of the aberrated beam after defocusing is all collected inside the fibre diameter both for the central and the marginal field.

Encircled Energy

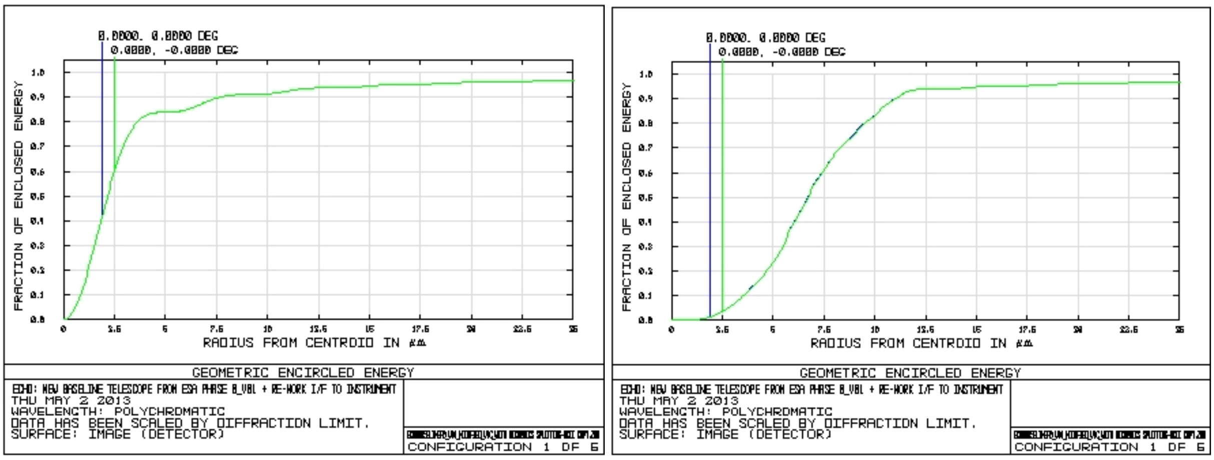

Figure 15-14: Focused system Encircled Energy in 50 µm-fibre diameter at central (blue) and marginal field (green) on left and Defocused system Encircled Energy 50 micron fibre diameter at central (blue) and marginal field (green) on right

Table 15-2 resumes all obtained results, spot diagram and Encircled Energy collected on entrance fibre of VNIR channel.

WFE rms @1 micron	7.3 rms	250 rms
Defocus shift M1-M2 (micron)	0	87
GEO radius spot (micron)	Airy radius 4.9	12.47
Encircled Energy in-fibre diameter (2arcsec)	96.75%	96.75%

Table 15-2: Resuming data of Encircled Energy at focused and defocused system (WFE 250rms)

Spot diagram inside the fibre diameter and collected Encircled Energy (96.75%) demonstrate that the introduction of a defocusing of 250 WFE rms in entrance beam of fibre can be neglected.

15.2.6.5 Fibres efficiency

The efficiency of a fibre is the product of three effects, namely internal transmission (a loss in transmission is at most 5% in our case), reflection losses at the entrance/exit (which amount to 6%) and focal ratio degradation (FRD), which measures the fraction of light exiting the fibre within a given solid angle. The value of FRD depends on the aperture angle (i.e. the focal aperture F/#) by which the fibre is fed, and by the focal aperture accepted by the spectrometer. Typical values of total efficiencies for commercial fibres, similar to that foreseen in VNIR, are plotted in Figure 15-15. The blue dot marks the operative condition of the VNIR fibre, which receives an F/4 input beam and feeds the spectrometer with an F/3.5 output beam. Therefore, the FRD losses are about 5% and total efficiency is about 85%.

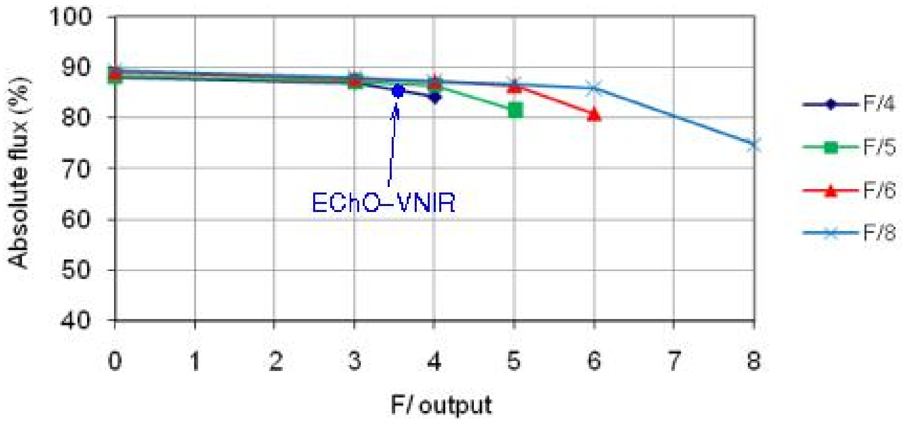

Figure 15-15: Total efficiency and focal ratio degradation of commercial fibres.

15.2.6.6 Fibre scrambling

Fibres are natural light scramblers: movements of the image at the fibre entrance have little effect on the illumination pattern at the fibre exit. The scrambling gain of a fibre is defined and measured by comparing the relative movements of the image at the fibre entrance and on detector of the spectrograph, see Figure 15-16 for details. For commercial fibres similar to those foreseen for VNIR, the measured values of scrambling gain are between 50 and 100 when the fibre is free of bends. Even larger scrambling gains could be obtained by tightly bending the fibre and/or changing the shape of the core from circular to octagonal. This is probably not necessary in the case of VNIR because, just using a bend-free fibre, the requirements can be already relax on image-jittering of the telescope by at least a factor of 50.

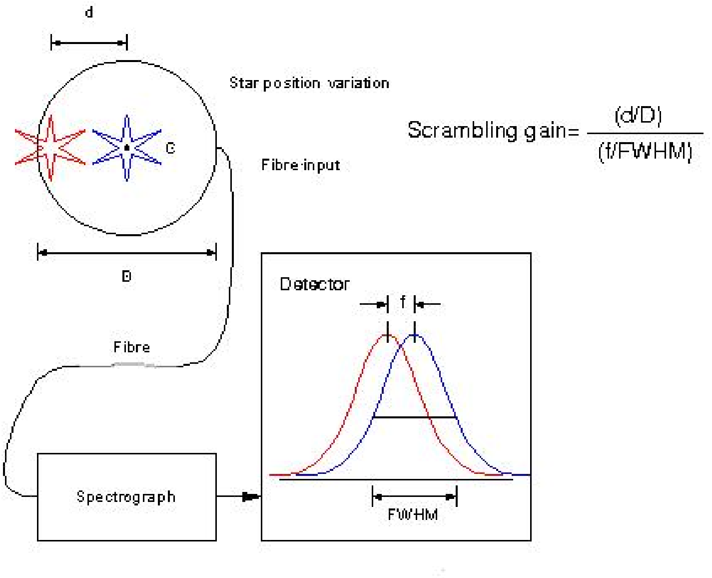

Figure 15-16: schematic description of the scrambling gain

15.2.6.7 Fibres coupling

The light from the telescope can be fed to the fibre on the image plane or on the pupil plane. The former solution is used in HARPS, the ultra-high precision astronomical spectrometer which has reached the highest accuracy in the detection of extra-solar planets. On the other hand, pupil-feeding are often used in fibre-fed astronomical instruments. In the case of VNIR we can use both solutions, as described in Figure 15-17. The only difference is the curvature of the input surface of the fibre which is flat in case of image-feeding. For pupil-feeding, instead, the curvature is such that the first part of the fibre acts as a micro-lens adapter. We plan to test both solutions and select the one providing the best performances in terms of total efficiency and scrambling gain.

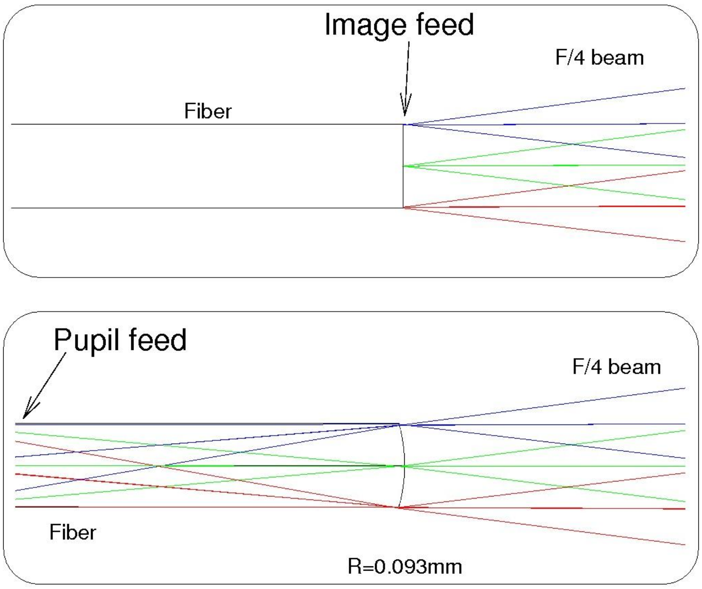

Figure 15-17: Fibre coupling possibilities for VNIR.

15.2.6.8 Fibres testing

A laboratory breadboard is going to be set up to demonstrate that the use of the fibres in the VNIR module is a proper working solution. The breadboard testing is plan to be carried out within the year 2015. However if this activity would demonstrate that the present choice is not the most accurate, it would be possible to go towards a choice of a fibre with a larger core or even if to a classical optical solution with no fibres without any major changes in the basic optical layout of the spectrometer.

15.3 VNIR DETECTOR SELECTION

15.3.1 Baseline Selection and Performance

Section 5 describes the process of deriving specifications for the main science channels. The detector for the VNIR focal plane shares a common design with the FGS device but it drives the specifications as described in section 5.

Parameters	VNIR Specification	Performance
Manufacturer		Teledyne
Materiel		HgCdTe
Wavelength coverage (µm)	0.5-2.52 Goal 0.4 – 2.52	λc=2.53
Pixel size (µm)	15 - 30	18
Format minimum size	256 * 256 for 30 µm	2048 * 2048
RQE	>70%	~ 80% (1)
Dark current (e^-/s/pixel)	< 0.01	<< 0.01 (2)
well depth (ke)	≥ 50	120000 (3)
Readout noise(e)	< 15 for CDS	~ 10 e-
Operating temperature	40K - 30K	40K - 30K
ROIC type	/	SFD
Readout mode	Window, NDR, binning	compliant
Program		Multiple programs including JWST
TRL	TR5 in Q3 2015	>> TRL 5

Table 15-3: Baseline VNIR Detector Parameters

The Teledyne device is compliant with the RFI specification and when analysed against the science requirements is predicted to perform extremely well. It should be noted that a number of other devices are believed to be capable of meeting the science requirements. However, Teledyne gives the best performance of any of the devices considered and is also at the highest TRL, having been previously space qualified.

The one drawback of the Teledyne device is that it is packaged in a 2K * 2K format, which even with the relatively small pixel size is an oversized array. Since this is a well-developed and tested product it is unlikely that developing a smaller array would be financial advisable. The detector would consequently demand extra space at the focal plane area. Clearly it would be possible to window the device to use only the required portion of the detector.

15.3.2 Alternative Options

The most promising of the European options is the SELEX-ES device, which is detailed in the table below. Although there are some areas of non-compliance with the RFI specification, when analysed against the science requirements the SELEX device was found to give almost as good a performance as the Teledyne one. However, it is at a lower TRL and as is discussed elsewhere, the development cost would be high. Since the device is being specifically designed for EChO, it would be possible to produce an array size that exactly matches the requirements.

Parameters	VNIR Specification	Performance
Manufacturer		Selex-ES
Materiel		HgCdTe
Wavelength coverage (µm)	0.5-2.52 Goal 0.4 – 2.52	λc=2.6
Pixel size (µm)	15 - 30	15
Format minimum size	256 * 256 for 30 µm	512 * 512
RQE	>70%	70% (1)
Dark current (e^-/s/pixel)	< 0.01	<< 0.03 (2)
well depth (ke)	≥ 50	>50 (3)
Readout noise(e)	< 15 for CDS	~ 23e
Operating temperature	40K - 30K	40K - 30K
ROIC type	/	SFD
Readout mode	Window, NDR, binning	Compliant
Program		Developed from ESA funded technology programs
TRL	TR5 in Q3 2015	TRL 3-4 presently, with funding will achieve TRL 5 in timescale

Table 15-4:Alternative VNIR Detector Parameters

(4) dependent on AR coating
(5) measured 0.03 at 80K for 24 µm pixel so expect much better for smaller pixel and lower temperature
(6) set by a capacitance value, 75Ke is possible

15.3.3 Cold Detector Electronics

The Teledyne device comes with a fully proven SIDECAR ASIC Module to drive the detectors. This ASIC is common to all Teledyne devices under consideration for EChO, which would mean good overlap between the required drive electronics for the FGS, VNIR, SWIR and MWIR channels.

If the SELEX-ES device were used it would also have a similar advantage that the ROIC would be common to the FGS, VNIR and SWIR channels. However, the drive electronics are not as developed as the Teledyne ASIC.

15.3.4 Warm Detector electronics

The MCT-based detector will be coupled with a ROIC (Read Out Integrated Circuit) bump bonded to the device's sensitive area. The ROIC will act as a proximity electronics in order to extract the low level noise analogue signal from the detector, addressing the very low power dissipation requirements imposed by the environmental thermal aspects (e.g. the power dissipation of the Selex detector+ROIC is < 5 mW). The analogue signal will be amplified by the ROIC output OPAMP(s) (typically 4 or 8 for the two detector halves collecting respectively the VIS and NIR signals of the target spectrum) and fed to the cold front-end electronics (CFEE) where A/D conversion will take place. CFEE is connected to the warm section of the payload electronics by means of suitable low thermal conductive harness. The payload's warm electronics is essentially constituted by the warm front-end electronics (WFEE) generating driving signals for the detector ROIC and the Instrument Control Unit (ICU) acting as the main payload processing electronics and collecting the digitized signals from all scientific channels.

WFEEs will reside in a box specifically designed and located near the ICU which will be kept at a temperature in the range 0 - 40°C.

The detector is expected to be easily integrated and well operated with a range of electronics solutions.

The distance between the Detector Sub Assembly and the CFEE and between the CFEE and the WFEE appears unavoidable in this system presentation and introduces technical challenges associated with a distributed signal chain including driving load capacitance, achieving settling, minimizing cross talk, ensuring stability and reducing noise.

A key challenge will be ensuring that the active differential drive circuit power dissipation can be reduced to an acceptable level for the thermal design constraint and cold electronics operating temperature. The number of video output channels and the operating speed will inform the circuit choice. For a 4 channel circuit operating at e.g. 5MHz pixel rate, it is expected that the CFEE active power dissipation could be reduced to around 50mW whereas for an 8 channel circuit operating at 10MHz pixel rate, the expected power dissipation would increase to 200-300mW. Clearly decreasing the power is desirable and would be a key aim and design trade in the design phase. Anyway, using 4 outputs of our ROIC and a sampling frequency (frame sampling) of the order of 10Hz we will operate our detector at a frequency less than 700 KHz/channel.

The electronics circuit technology and level to which the active power dissipation can be reduced is likely to be a key element to determine whether the electronics can be implemented at the cold (45K) or warm (120K) point in the system. It is considered desirable to implement the differential drive circuits near to the detector where possible to minimize common mode noise.

Current Selex electronics solutions for standard detectors range from laboratory instrumentation to airborne qualified designs are considered TRL3. Whereas the designs have strong design heritage and a high level of maturity it is recognized that additional development and qualification work is required within a stringent product assurance framework to achieve space qualified flight models at TRL5. This would need a phased development activity to achieve the qualified design. The development activity is expected to last 10 months and comprise up to 3 iterations including the provision of qualification test samples.

An alternative approach would be for Selex to be partner of another organization or company to support or to deliver this development. Clearly there are benefits to reducing development overhead and engineering risk. For example, Selex has previously worked with ComDev on other space and airborne electronics development projects, and believes this approach to be viable and mutually beneficial to the Echo program.

The detector is also expected to interface easily with the SIDECAR electronics solution, which is expected to help mitigate a number of the design challenges in implementing a CFEE and WFEE solution. The key benefit is the closer integration of the ADC to the detector which is expected to simplify the interface design, safeguard SNR and mitigate cross talk and some noise sources. The detector interface signals are understood to be compatible with the SIDECAR digital and analogue interfaces and the video may be optimized by using gain and offset adjustments.

Functionally, both WFEE and CFEE configure and operate the detector and provide digitized data to the ICU. WFEE therefore includes power supply fine-regulators and voltage references, while CFEE will hosts ADCs and differential video signal drivers/receivers.

The WFEE will receive a system clock and use this to provide all CFEE and detector ROIC timings as well as digital clocks and a SPI interface by means of an on-board rad-hard FPGA. Selex favors a register-based control system, however, it considers important to maintain good phase stability between the detector and ADC clocks to mitigate the risk of differential clock jitter noise affecting the digitized image data. For this reason Selex in the first instance advocates this approach, as the separation between the WFEE and the ICU is not defined and the influence of other circuits on adjacent channels, for example, is not clear.

The WFEE will provide one or more high speed serial differential data ports corresponding to the number of analogue video channels. The FPGA could also provide a data multiplexing function to simplify the interconnections to the ICU although separate channels are preferred to improve redundancy. Whereas Selex routinely provide serial data in LVDS, ChanneLink and CameraLink formats, other formats can be easily integrated into the WFEE design, like the SpaceWire link. The WFEE will have a serial control port to configure and operate the WFEE and detector and communicate BIT and status information.

The WFEE should provide a local and stabilized power supply for the ADC, CFEE and detector circuits. It will be connected to the CFEE using a suitable cryo harness design. This critical subsystem is designed as part of the signal interface between the detector, CFEE and WFEE in order to ensures that the best system design and trades as well as required signal performance is achieved by design.

16 SWIR CHANNEL MODULE DESIGN

16.1 INTERFACES

The entrance beam is elliptical input beam of 25mmx17mm. It is located at 40mm height from the IOB. The SWIR channel envelope is 240x210x210mm with a total mass of 6kg (including 20% contingency).

16.1.1 SWIR/Optical Bench Interface:

- 3xM5 20mm screws (A286) with 1.5mm Invar washers (Al box plate 5 mm).
- Positioning through 2x5mm ϕ pins: a dowel-pin, and a slotted dowel-pin

16.2 SWIR OPTICAL UNIT DESIGN

16.2.1 Optical Design

The Spanish-provided SWIR module is a grating spectrometer providing the required R>300 coverage from 2.45 to 5.45 μm. The design provides internally a high optical quality performances in a compact opto-mechanical packaging.

The SWIR module baseline has evolved from a two instrument concept, covering the spectral range from 900nm to 5200nm, with an incident beam diameter of 20mm, to a single instrument concept that will cover the spectral range from 2450nm to 5450nm.

After several optical design trades, and taking into account the available detector technology in this spectral range, a detector pixel size of 18 microns was set.

SWIR optical design has been evolved to achieve following features in the current design:

- Elliptical Input beam updates in size : 25 × 17 mm2 at SWiR entrance pupil
- Solved the overlapping of harmonics for this channel by a combination of Prism+Grism
- Defocus included for PSF proper sampling
- Ge selected as main optical elements material, except for the grism where a ZnSe is proposed.

The baseline design of the spectrometer is based on the use of a relay to adapt the incident beam size, in this case, an elliptical input beam of 25mmx17mm to the output beam at relay second mirror, corresponding to a relay M of 1.25m. A slit between relay mirrors is used as a field stop.

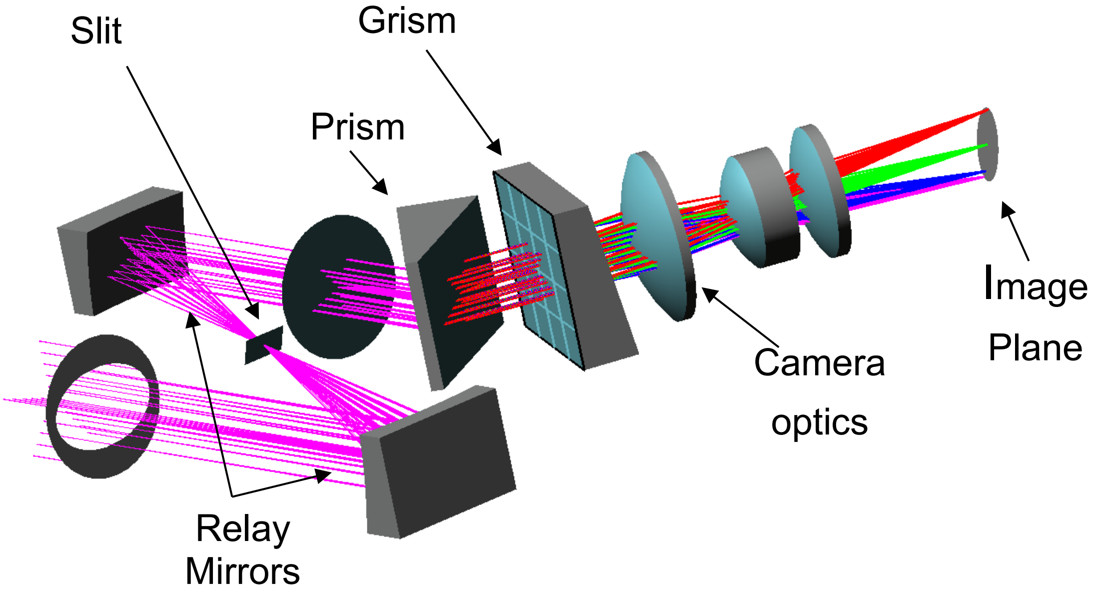

Figure 16-1: Baseline SWIR Optical Design

A grism is used to spectrally disperse the beam. The design of this element is in a such way that the central wavelength of the spectrum (3950 nm) is not deviated through the *grism-Camera optics* , and consequently can be selected as the optical axis for AIV proposes.

In order to avoid the overlapping of the harmonics produced by the dispersive response of the grating (from 2450nm to 2725 nm) a prism is introduced with an apex angle that is defined orthogonally to those used on the grism device. The incorporation of this element allow us to avoid the overlapping of the spectrum.

The alternative of using a filter (Linear Variable Filter) just in front of detector is considered as more critical solution by two reasons; the alignment of this element with respect the dispersive properties of the grism is a complex task during AIV phase and, more relevant, we have not found yet a space-qualified version of this element, so the base line selected is the use of a dispersing prism as mentioned.

SWIR optical layout is the following:

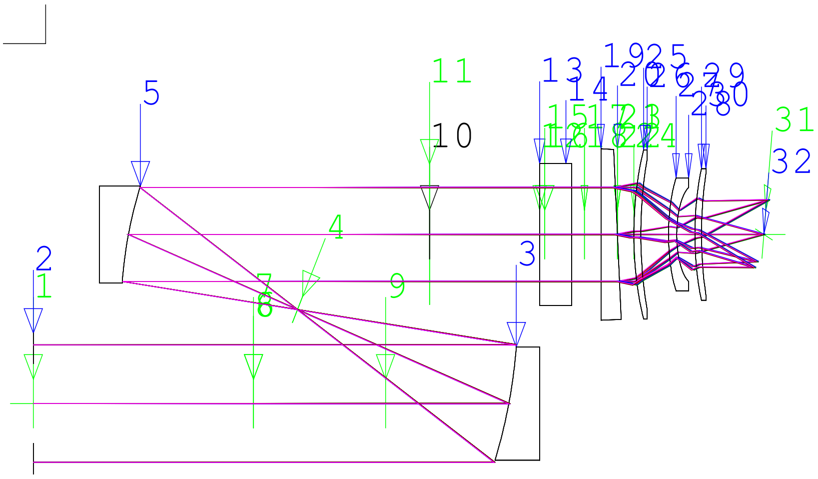

Figure 16-2 SWIR Optical Layout

PSF sizes (spect × spat) at image plane will be different for each wavelength, for this reason a defocus of 88 microns has been introduced in the optical design. The result is PSF size constant in SWIR spectral range and depending on the wavelength, PSF values are:

5450 nm: 40.5 × 59.6 mm2 = 2.3 × 3.3 px2 with 88microns defocus 2.3 × 2.3 px2

3950 nm: 29.2 × 42.9 mm2 = 1.6 × 2.4 px2 with 88microns defocus 2.2 × 1.8 px2

2450 nm: 17.7× 26.1 mm2 = 1.0 × 1.4 px2 with 88microns defocus 2.3 × 2.5 px2

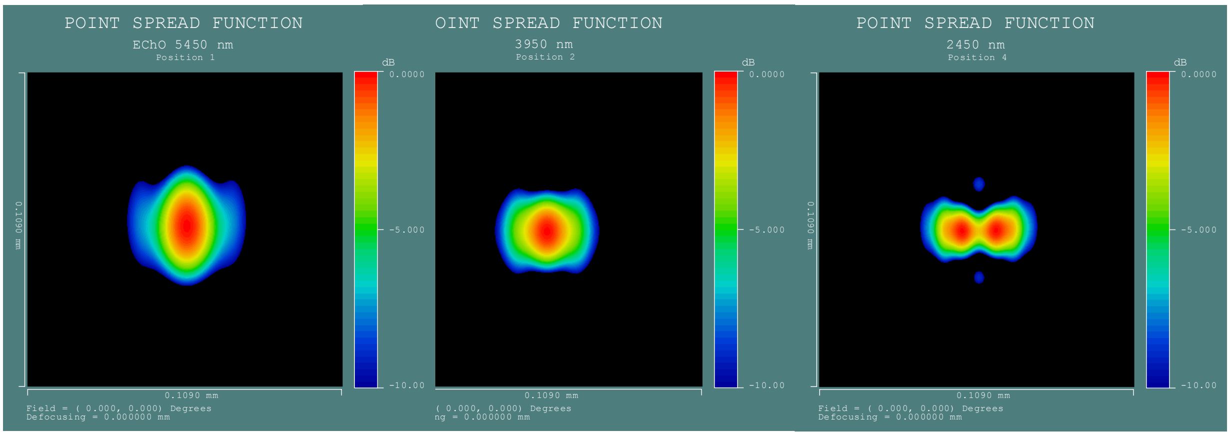

Figure 16-3: SWIR Point Spread Function at Different Wavelengths

Resolving power will be also different meeting the requirement that R>300 for each wavelength (all assuming a 2 pixel spectral resolution element:

≈ 401 @ 2450nm (2 or 3px as resolution element, respectively);

≈ 627 @ 3950nm (2 or 3px as resolution element, respectively);

≈ 852 @ 5450nm (2 or 3px as resolution element, respectively).

-

With this optical design the required detector size is ≈17.3 mm (≈962 pix @ 18mm/px),

The optical element materials used in the design are:

- Lenses material: Ge;
- Prism: Ge, α = 10º;
- Grism: ZnSe; β = 24.2º; 90 l/mm

16.2.2 Mechanical Design

The mechanical design accommodates the SWIR channel within a box with an envelope of 240x210x210mm and with a total mass of 6kg (including 20% contingency). The box plate will be constructed of 3mm thick Al 6061-T6.

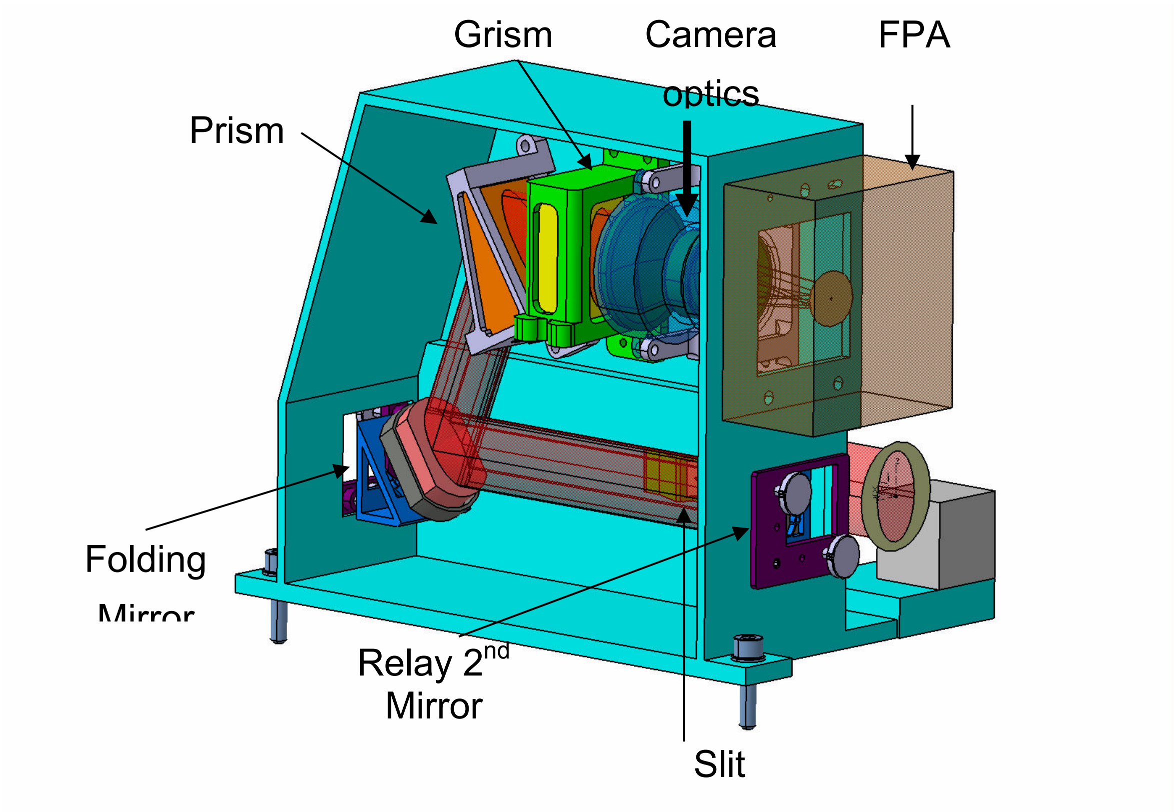

Figure 16-4 SWIR Mechanical design

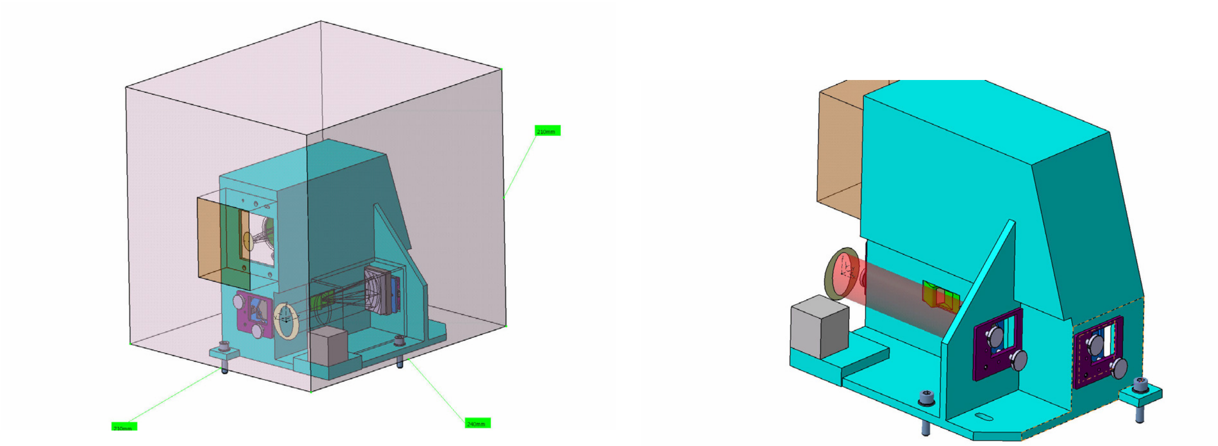

Figure 16-5 SWIR module envelope and SWIR Reference System

The SWIR module uses its own internal reference system with the original at the mounting reference hole (main dowel-pin) with:

- 1 axis parallel to the entrance beam and contained in a rectified plane parallel to the iOB (optical cube location);
- 1 axis perpendicular to such a rectified plane;
- the third forms a Cartesian right-handed coordinate system.

The detector is located into the Focal Plane Assembly, it is attached to the SWIR Optical bench trough the following interfaces:

- 2x2mm φ pins, one fixed and the other situated on a linear slot parallel to Y axis, perpendicular to the entrance beam (X axis), Z axis is perpendicular to the IOB plane.
- Mounting patter consists of a bolt fitting, 3 bolts of M4

16.2.3 Thermal Design

All mechanical elements will be built in the same material of the payload optical bench for CTE-matching purposes. The thermal operating temperature of both the IOB and the detector is assumed to be 45 – 50 K.

16.2.4 Performance vs Requirements

The key performance parameters of the SWIR module are compared to the requirements in the table below.

Spectral Range	2450 – 5450 nm
SWiR Dichroic (common optics)	R > 90% (TBC) for l ∈ (2450 – 5450) nm
	T > 90% (TBC) for l ∈ (5450 – 16000) nm
EFL	4439.944 mm for 5450 nm
	4416.03 mm for 3950 nm
	4349.612 mm for 2450 nm
SWiR Grism Grating	90 l/mm (-1st order)
SWiR Optics	Ge (except for the Grism, ZnSe)
SWiR FPA1	H1RG from Teledyne, although European MCT (TBD) is the back-up solution
	Pixel size: 18 mm (TBC)
Spectrum Length	≈ 17.3 mm, 962 px
R (l/Dl)	401 & 268 @ 2450 nm (2 or 3 px as resolution element, respectively)
	852 & 568 @ 5450 nm (2 or 3 px as resolution element, respectively)
T	45% of averaged in-band T (TBD pending on coatings)

Table 16-1: SWIR Key Performance Parameters

16.3 SWIR DETECTOR SELECTION

16.3.1 Baseline Selection and Performance

Section 5 describes the process of deriving specifications for the main science channels. The specification for the SWIR focal plane is repeated below together with the performance of the base-lined Teledyne device.

Parameters	SWIR Specification	Performance
Manufacturer		Teledyne
Materiel		HgCdTe
Wavelength coverage (µm)	2.42 – 5.45	λc=5.3
Pixel size (µm)	15 - 20	18
Format minimum size	1024 * 10	2048 * 2048
RQE	>70%	~80%
Dark current (e^-/s/pixel)	< 0.1	<< 0.1
well depth (ke)	≥ 75	~ 80 (3)
Readout noise(e)	< 18 for CDS	< 15e
Operating temperature	40K - 30K	40K - 30K
ROIC type	/	SFD
Readout mode	Window, NDR, binning	compliant
Program		Multiple programs including JWST
TRL	TR5 in Q3 2015	>> TRL 5

Table 16-2: Baseline SWIR Detector Parameters

The Teledyne device is compliant with the RFI specification and when analysed against the science requirements is predicted to perform extremely well. It should be noted that a number of other devices are believed to be capable of meeting the science requirements, even if they are not compliant in all RFI areas. However, Teledyne gives the best performance of any of the devices considered and is also at the highest TRL, having been previously space qualified.

The one drawback of the Teledyne device is that it is packaged in a 2K * 2K format, which even with the relatively small pixel size is an oversized array. Since this is a well-developed and tested product it is unlikely that developing a smaller array would be financial advisable. The detector would consequently demand extra space at the focal plane area. Clearly it would be possible to window the device to use only the required portion of the detector.

16.3.2 Alternative Options

The most promising of the European options is the SELEX-ES device, which is detailed in the table below. Although there are some areas of non-compliance with the RFI specification, when analysed against the science requirements the SELEX device was found to perform satisfactorily. However, it is at a lower TRL and as is discussed elsewhere, the development cost would be high. Since the SELEX device would be developed specifically for EChO it would be possible to get an array size that more closely matches the 1024 * 10 requirement.

Table 16-3: Alternative SWIR Detector Parameters

Parameters	SWIR Specification	Performance
Manufacturer		Selex-ES
Materiel		HgCdTe
Wavelength coverage (µm)	2.42 – 5.45	λc=5.8 – 6.0
Pixel size (µm)	15 - 20	15
Format minimum size	1024 * 10	1024 * ~ 32

RQE	>70%	70%
Dark current (e^-/s/pixel)	< 0.1	<< 0.03 (1)
well depth (ke)	≥ 75	>75
Readout noise(e)	< 18 for CDS	~ 23e
Operating temperature	40K - 30K	40K - 30K
ROIC type	/	SFD
Readout mode	Window, NDR, binning	compliant
Program		Developed from ESA funded technology programs
TRL	TR5 in Q3 2015	TRL 3-4 presently, with funding will achieve TRL 5 in timescale

(1) measured 10^5 at 80K but expect to get 0.1 at the lower temperature and low background design

16.3.3 Cold Detector Electronics

The Teledyne device comes with a fully proven SIDECAR ASIC Module to drive the detectors. This ASIC is common to all Teledyne devices under consideration for EChO, which would mean excellent overlap between the required drive electronics for the FGS, VNIR, SWIR and MWIR channels.

If the SELEX-ES device were used it would also have a similar advantage that the ROIC would be common to the FGS, VNIR and SWIR channels. However, the drive electronics are not as developed as the Teledyne ASIC.

17 MWIR CHANNEL MODULE DESIGN

17.1 INTERFACES

The entrance beam is collimated with an elliptical section of 25x17mm^2. It is located at 40mm from the IOB.

The MWIR main structure is mounted on the IOB or inside a mechanical support via 3 mounting points.

The MWIR channel volume is 325 x 195 x 170 mm^3

The total mass including 20% margins is 5.8kg

17.2 MODULE DESIGN

17.2.1 Optical Design

The MWIR module shown in Figure 17-1 is covering the bandpass [5.05-11.5]µm and is split into two channels: MWIR1 from 5.05µm to 8.65µm and MWIR2 from 8.25µm to 11.5µm. The collimated beam coming from the common optics is refocused on the module entrance slit by an off-axis parabola. Two airy rings at the maximum wavelength of the bandpass plus a 1.5arcsec pointing error dimension the entrance slit used as the field stop. Another off-axis parabola collimates the beam to an internal dichroic that splits the bandpass: MWIR1 band is reflected whereas MWIR2 band is transmitted. A set of two flat mirrors (the roof mirrors) folds back the long wavelength channel to the common path in order to focus the two spectra on a unique detector. A prism is used to spectrally disperse the beams that are re-imaged by three-lens objectives on the detector. Classical space qualified optical materials (Cleartran and ZnSe) are chosen to avoid any absorption feature in the bandpass. All materials are well known and already used in previous space missions for spectrometers.

The spectra imaged on the MCT detector cover 55 and 80 pixels for respectively MWIR1 and MWIR2. To allow a windowing with optimized integration time, the two spectra are slightly shifted in line (gap of 45 pixels).

First module tolerance analysis does not show any design weakness as all the modelled sensitivities remain within manufacturing or alignment achievable limits.

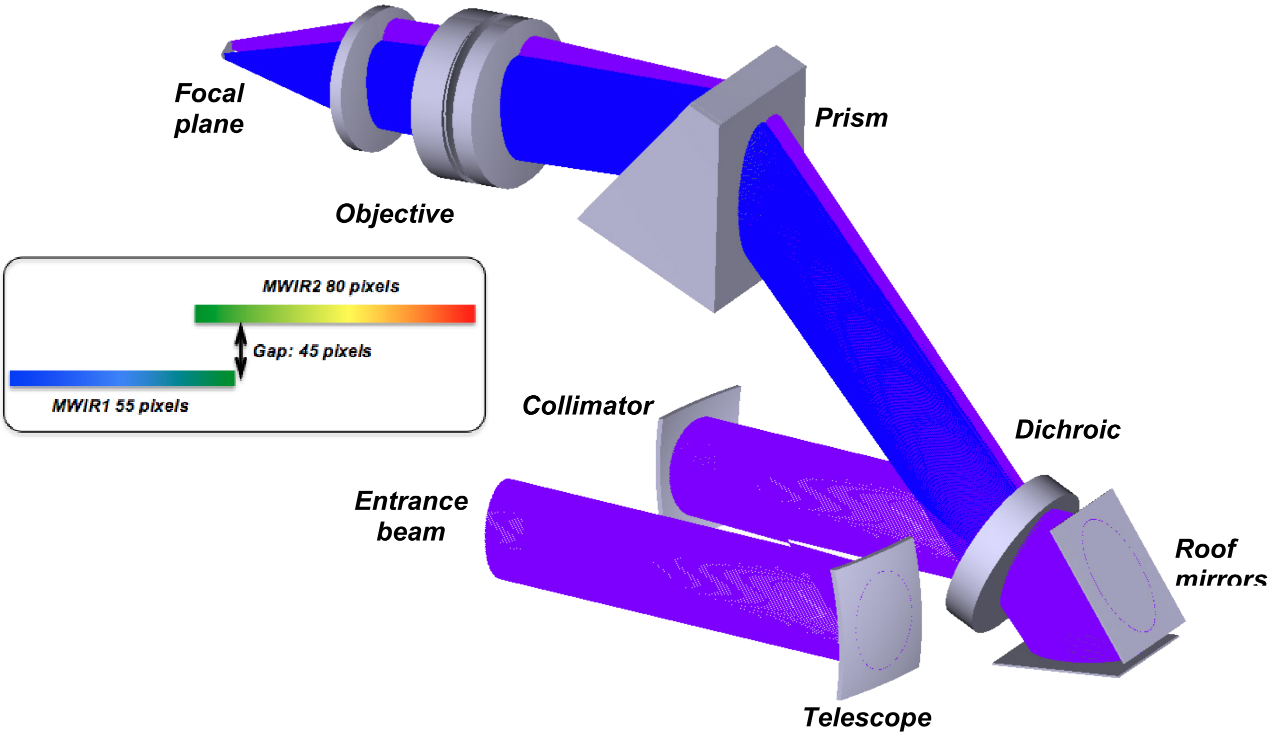

Figure 17-1: MWIR Optical Design.

Table 17-1:summarizes the optical parameters.

		MWIR 1	MWIR 2
Bandpass		**[5.05 - 8.65]µm**	**[8.25 - 11.50]µm**
Slit IFOV		20 arcsec in the spatial direction 8.8 arcsec in the spectral direction Orientation of the slit: parallel to IOB	
Airy disk radius @8.5µm		22.2µm spectral (F/2.1) 32.5µm spatial (F/3.1)	
Entrance objective			
	Type	Off-axis parabola	
	Focal length	50mm	
	F/#	2.84	
Slit height		0.172mm	
Collimator			
	Type	Off-axis parabola	
	Focal length	50mm	
	F/#	2.84	
Prism			
	Material	CLEARTRAN	
	Prism angle	37.52 deg	
	Incidence angle	45.59 deg	
Objective			
	Type	Triplet (pure spheres)	
	Materials	ZnSe/ CLEARTRAN/ ZnSe	
	Focal length	29.13mm	
	F/#	1.65	

Table 17-1: MWIR optical parameters.

17.2.2 Mechanical Design

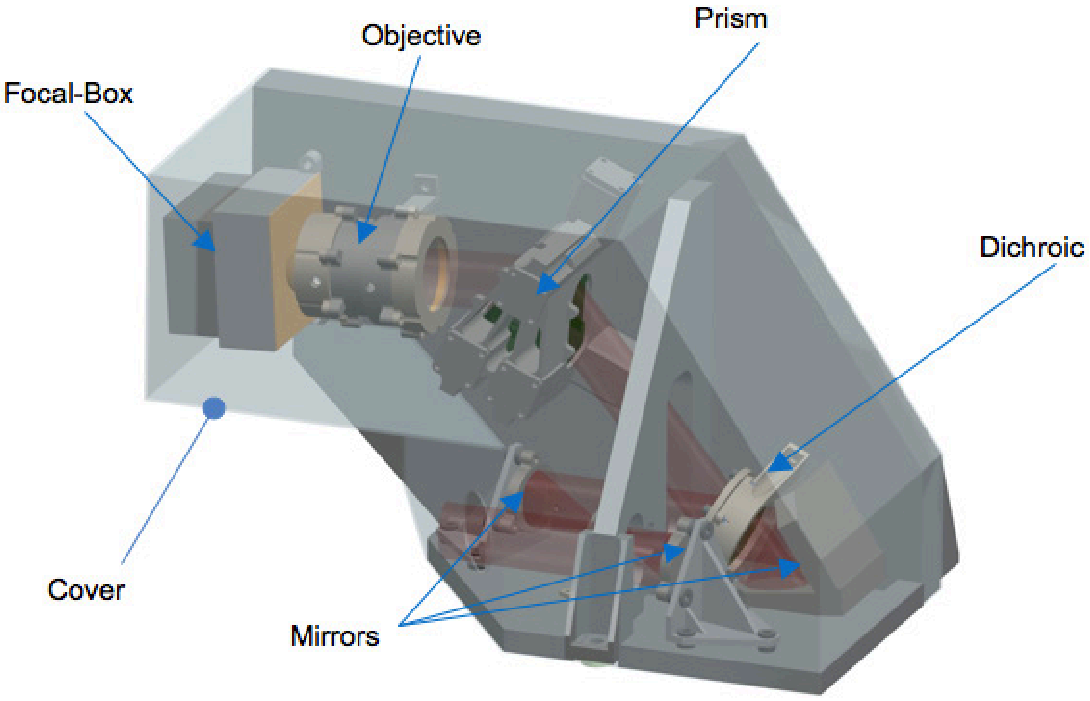

Figure 17-2: Mechanical design overview

Three aluminium plates to provide two perpendicular planes for fixing the optical mounts compose the MWIR structure. The structure is mounted on the IOB plate using three isostatic mounting points insulated by epoxy/fiberglass washers.

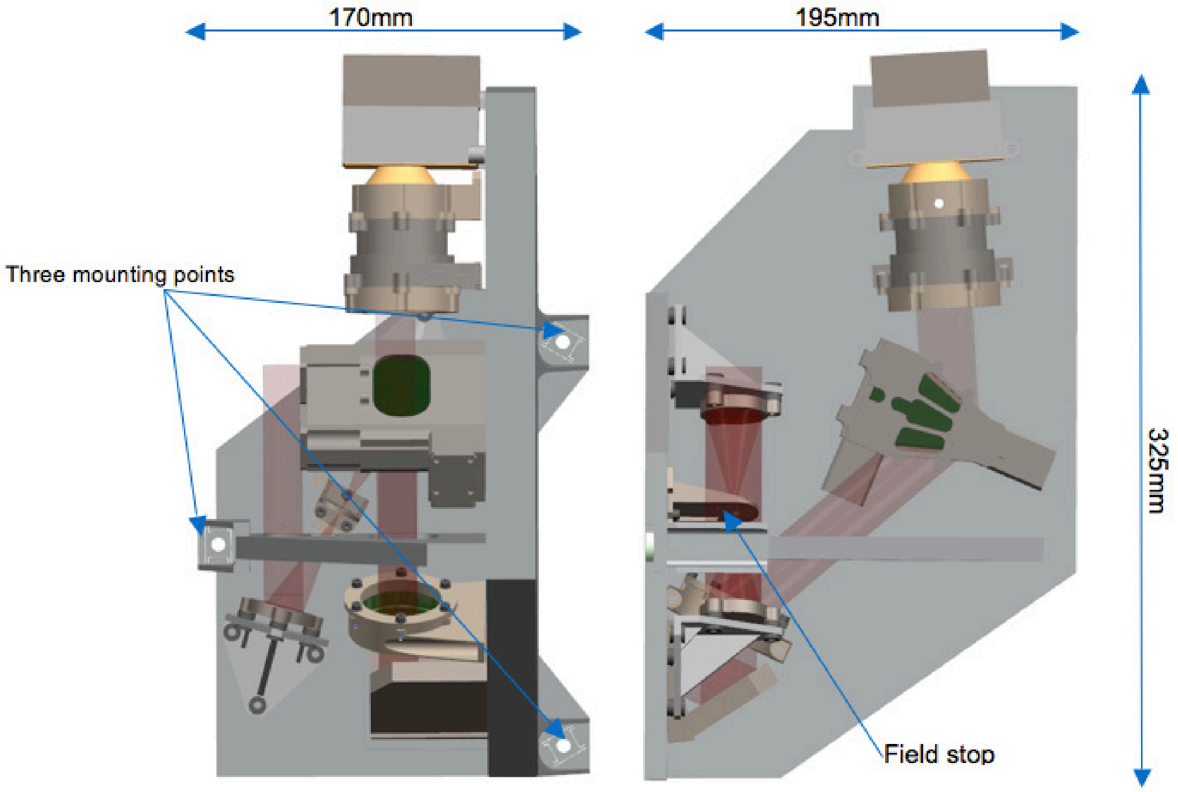

Figure 17-3: MWIR Dimensions

All optical mounts are made in aluminium 6061 to avoid any differential thermal expansion and to allow a good conductivity contact with the MWIR structure.

All the mirrors are made in the same material as their mechanical support.

Lenses, dichroic and prisms are mechanically constrained via springs to avoid any movement with static load of 100g in any direction and allow any differential thermal expansion between the optical materials and their mounts. The constraint increased when cooling down and by design, all constraints are limited to avoid any optical and mechanical effects.

For telescope integration and adjustment purpose, a mechanical system allowing 6 degrees of freedom on the two first mirrors (entrance objective and collimator) is used to perform optical alignment between the telescope line of sight and the MWIR optical axis. The field stop support has one degree of freedom to be properly aligned on the optical path.
The focal-box uses mechanical system with 5 degrees of freedom to position the detector sensitive surface.
All opto-mechanical adjustments are done using adjusted shims (no complex systems are used).

The estimated mass for the MWIR channel is 5.8kg. For detailed mass breakdown see mass budget in Figure 17-4

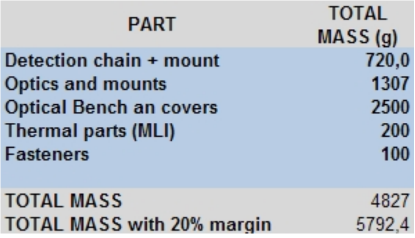

PART	TOTAL MASS (g)
Detection chain + mount	720,0
Optics and mounts	1307
Optical Bench an covers	2500
Thermal parts (MLI)	200
Fasteners	100
TOTAL MASS	4827
TOTAL MASS with 20% margin	5792,4

Figure 17-4 : MWIR Mass Budget Breakdown

17.2.3 Performance vs Requirements

The image quality is evaluated with the ensquared energy profile in a pixel. Figure 17-5 shows for both channels the ensquared energy in 50µm (2 pixels) with the diffraction-limited performance. Within the nominal requirement bandpass the instrument is almost diffraction limited.

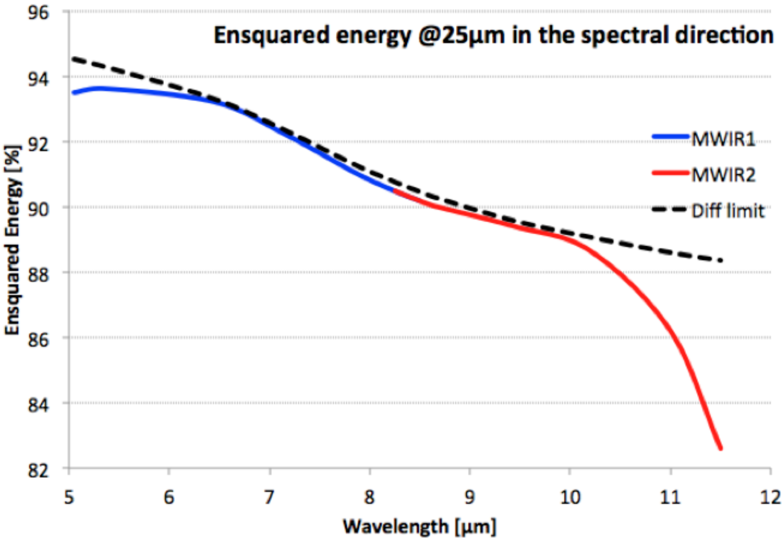

Figure 17-5: Ensquared energy in 25µm.

The spectral resolution is calculated for all the wavelengths by convolving the instrument PSF (including diffraction pattern and geometrical aberrations) and the spectral profile of the field stop image. Two pixels are considered per Δλ so the spectral resolution is the sampled resolving power: R=λ/(2Δλ). Figure 17-6 shows the profile of the spectral resolution in the whole spectral band, and Figure 17-7 shows the consecutive PSFs separated by 2 pixels at the edges and center of the bandpass.

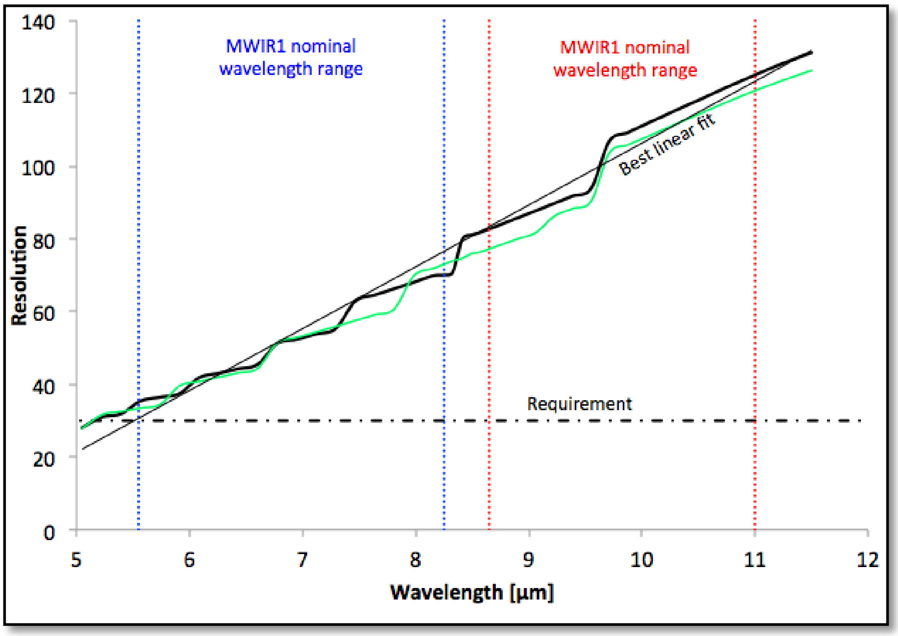

Figure 17-6: MWIR spectral resolution. In black: the resolution taking into account only MWIR optical aberrations. In green: the resolution taking into account MWIR optical aberrations and the WFE of the telescope and common optics as defined in ICD

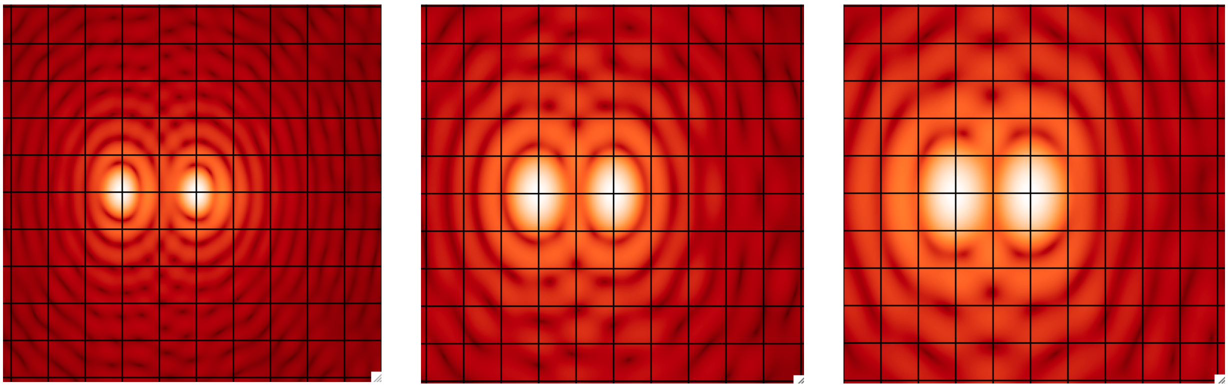

Figure 17-7: PSFs for consecutive wavelengths at the edges and center of the bandpass (left: 5.05µm, center: 8.5µm, right: 11µm).

The transmission profile shown on Figure 17-8 includes:

- Internal absorption of the materials,
- 99% reflectivity per mirror surface,
- 90% transmission / reflection of the internal dichroic,
- AR coating from Reading University Multilayer Lab.

Excludes:

- Internal dichroic absorption,
- Detector response.

Figure 17-8: MWIR transmission.

The optical performances fullfil the requirements in terms of spectral resolution (minimum sampled resolution > 30) and image quality (almost diffraction limited on the overall spectra with PSF sampled on two pixels at 8.5µm).

17.3 MWIR DETECTOR SELECTION

17.3.1 Baseline Selection and Performance

Today, the baseline detector for the MWIR channel is the NEOCam Detector from Teledyne. This detector is constituted of an of a HgCdTe detection layer assembled on top of a silicon CMOS readout circuit by mean of indium bumps illustrated in Figure 17-9. The detector layer features a cut-off wavelength of 10.6 µm. The readout electronics consist of unit cell electronics that provide the detector bias, photocurrent integration (i.e. charge-to-voltage conversion – PMOS transistor SFD; Source Follower per detector) and pixel selection, and peripheral electronics for addressing the unit cell electronics, external interfacing and additional output buffering.

Parameters	MWIR Specification		baseline
Manufacturer			Teledyne
Materiel			HgCdTe
Wavelength coverage (µm)	5.15-8.65	8.25-11.5	λc=10.6
Pixel size (µm)	25-30		18
Format minimum size	90x10	60x10	1024x1024
RQE	>60%		65% (1)
Dark current (e$^-$/s/pixel)	<270	<200	<200
well depth (ke)	65 to 1Me		>55ke
Readout noise(e)	<60 if FWC=65ke <250 if FWC=1Me		22e
Operating temperature	40K - 30K		40K - 30K
ROIC type	/		SFD
Readout mode	Window		/
Program			NASA technology development for NEOCam
TRL	TR5 in Q3 2015		TRL4

Table 17-2: Baseline MWIR detector specifications

(1) non-AR coated

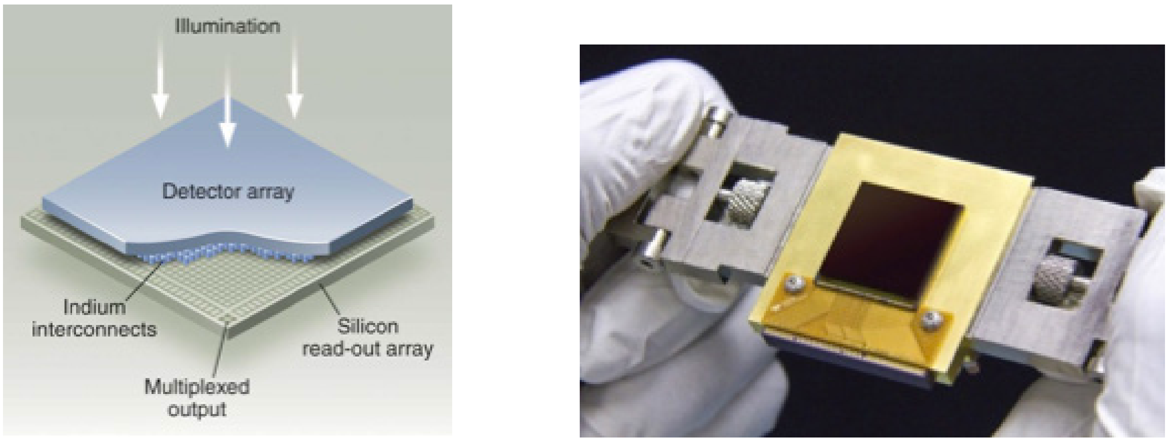

Figure 17-9: Sensor Chip Assembly (left) and NEOCam detector (right)

17.3.2 Alternative Options

Parameters	MWIR Specification		Alternative
Manufacturer			CEA/LETI
Materiel			HgCdTe
Wavelength coverage (µm)	5.15-8.65	8.25-11.5	λc=10.4
Pixel size (µm)	25-30		30
Format minimum size	90x10	60x10	240x320
RQE	>60%		70%
Dark current (e^-/s/pixel)	<270	<200	40(1)
well depth (ke)	65 to 1Me		1120 ke(2)
Readout noise(e)	<60 if FWC=65ke <250 if FWC=1Me		150e(2)
Operating temperature	40K - 30K		40K - 30K
ROIC type	/		CTIA
Readout mode	Window		/
Program			CNES/CEA technology development for ECHO
TRL	TR5 in Q3 2015		TRL3

Table 17-3: Alternative MWIR detector specifications

(1) For the best technology variation
(2) Use of an already existing ROIC one specific to ECHO shall be developed.

First Echo MCT detector R & D supported jointly by CNES and CEA start in 2012. 4 components were characterized from 80 to 30K.The aim of this R&D was to explore the LETI p/n technology. The results are very promising as two technological variation show low dark current at 40K that fit Echo requirement. A new batch of detectors will be realized at LETI by the end of 2013 with a targeted cut off wave length at 12.5µm @40K.

17.3.3 Detector Electronics

The detector baseline electrical system is composed of:

- • the cold electronics (operated at 35 - 40 K):
    - the detection layer
    - the cold readout electronics (HRG1)
- • the SIDECAR electronic stage (TBD K)
- • the cryo-harness
- • the warm electronics (operated at room temperature).

The next figure depicts the corresponding electrical system.

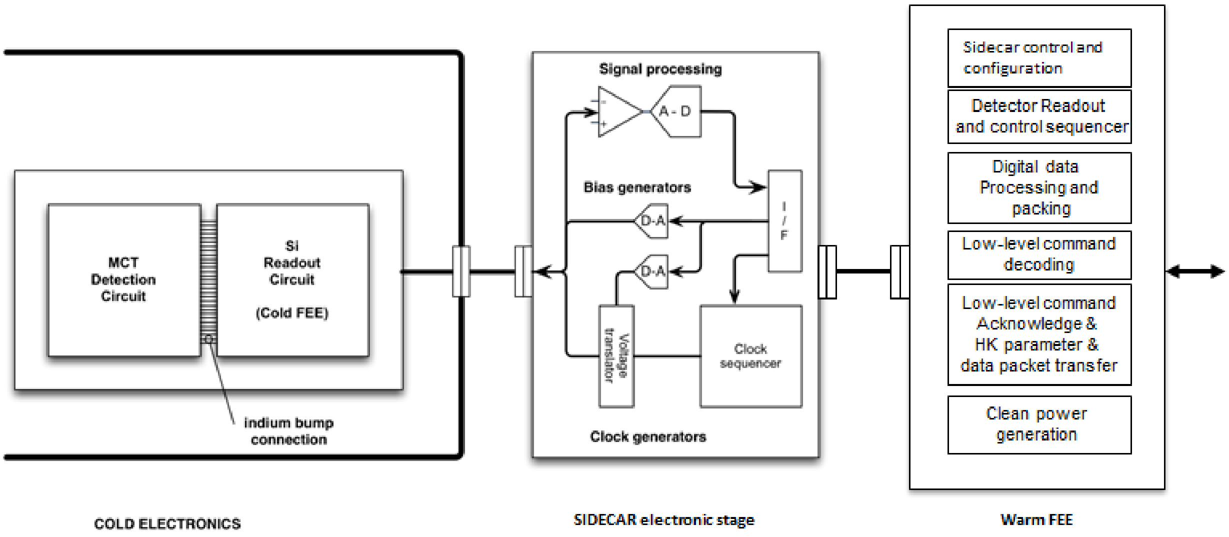

Figure 17-10: MWIR Detector Electrical System Schematic

18 LWIR CHANNEL MODULE DESIGN

18.1 LWIR MINIMUM REQUIREMENTS & DERIVATION OF PERFORMANCE

The LWIR channel provides spectral coverage from 11 - 16 μm, with a spectral resolving power (λ/Δλ) of *R*=30. Several designs were considered during the study phase, including dispersive spectrometers based on prisms and gratings, as well as a static Fourier transform interferometer. In addition to the spectral range and resolving power, further considered requirements were:

- Static designs (no moving parts in the optical system);
- Flat optical throughput with good transmission (> 0.25) across the LWIR spectral band [G-PERF-230];
- Photon noise-limited operation, if permitted by available detector arrays, for the 'Bright' and 'Faint' limits described in the ESA MRD [AD2], R-PERF-350];
- Flexible design allowing for
  - Contributions from the diffuse Zodiacal and payload module backgrounds to be managed;
  - Adjustment of (fixed) resolving power to accommodate near-term future developments in LWIR detectors.

Analysis of the static Fourier transform design showed that whilst it had advantages of excellent optical throughput and programmable resolution, pixel position error noise would reduce its ability to work in the photon noise limit. Analysis of available prism materials showed that a dispersive system based on the thallium bromide/chloride glass KRS-6 allowed a comparatively straightforward design of beam expander, prism and germanium lenses that met all of the requirements for the channel (Section 18.3.4).

18.2 INTERFACES

The LWIR module is attached to the payload module optical bench via four M6 screws to maximise the efficiency of the thermal interface to the 45 K optical bench. Thermal straps from the active cooler stages are required to cool regions of the module close to the optical path to approximately 25 - 29 K to reduce the thermal background from the instrument module.

18.3 MODULE DESIGN

18.3.1 Optical Design

The baseline design (Figure 18-1) is a prism-based spectrograph using a detector array with a 25 μm pitch. The choice of prism material having both sufficient dispersion and low absorption (<0.7) is somewhat limited in the 11 - 16 μm wavelength range; however there are options. The material selected for the baseline design is KRS-6, a thallium bromide/chloride crystal. The final focusing optic is a coated germanium lens. Many different prism materials were considered during the study phase and alternative designs using Cadmium Telluride and Zinc Selenide were also developed.

The LWIR module takes the elliptical 25 x 17 mm diameter collimated input beam from the common optics chain and passes it through a x1.5 beam expander. The beam expander includes a slit compatible with a 20'' x 8.3'' rectangular field stop at the intermediate focus. The beam is then dispersed onto the detector array by a KRS-6 prism with a 30° angle prism and an anamorphic germanium lens. The focal ratio of the final lens was selected so as to minimise the thermal load on the detector from non-astrophysical background sources, such as self-emission from the payload module itself. The working focal ratio of the system is approximately 2. The spectrum is recorded on ~50 pixels, assuming a 25 μm pitch array.

To prevent longwave thermal radiation from reaching the detector, a shortwave bandpass filter window with a cut-off at 16 μm is fitted to the detector array. Contributions from wavelengths <11μm are removed by the dichroic chain.

Using the model of the Zodiacal light described in [AD2], a significant contribution to the signal in the LWIR channel signal can be expected for the faint star target. One approach to reduce the relative spatial contribution of the diffuse zodiacal light is to use an anamorphic system to maintain the same spectral sampling whilst increasing the spatial sampling. This is achieved in the optical design by combining the elliptical pupil, provided by the common optics chain, with an anamorphic germanium lens.

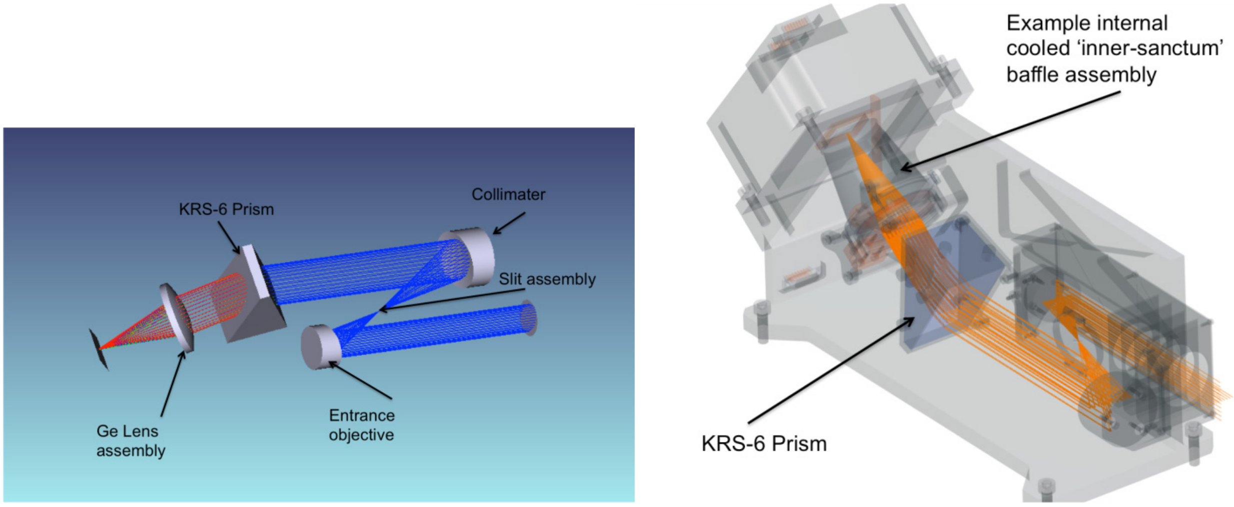

Figure 18-1. Baseline LWIR optical layout.

18.3.1.1.1 LWIR Performance.

Assuming 3 pixels per spectral interval, the resolving power varies between approximately 27 and 56, with an average value of 42 across the LWIR wavelength range of 11 - 16 μm, meeting the requirements in the EChO Mission Requirements Document [AD2]. If compatible with detector performance, the mechanical envelope of the module has sufficient margin to accommodate a larger prism with higher dispersion (e.g. increasing the dispersion to 46 - 96 across the LWIR band).

KRS-6 has good transmission properties across the LWIR bandpass, with an estimated transmission of 75% at an incidence angle of 30° (Figure 18-4). The multilayer broadband anti-reflection coating on the germanium lens is based on the current flight design used by the mid-infrared spectrometer on the Composite Infrared Spectrometer (CIRS) on the Cassini spacecraft, currently in orbit around Saturn. The anti-reflection coating gives transmission across the LWIR spectral range varying between ≈ 0.65 - 0.8. To prevent longwave thermal radiation from reaching the detector, a shortwave bandpass filter window with a cut-off at 16 μm is fitted to the detector array. Contributions from wavelengths <11μm are removed by the dichroic chain.

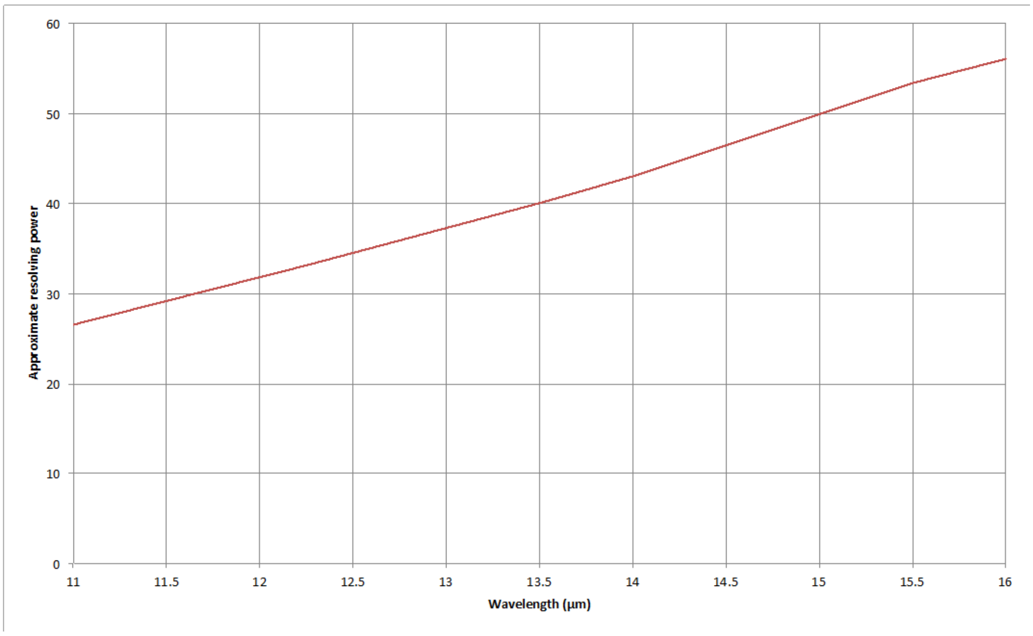

Figure 18-2: Approximate resolving power for the LWIR baseline design.

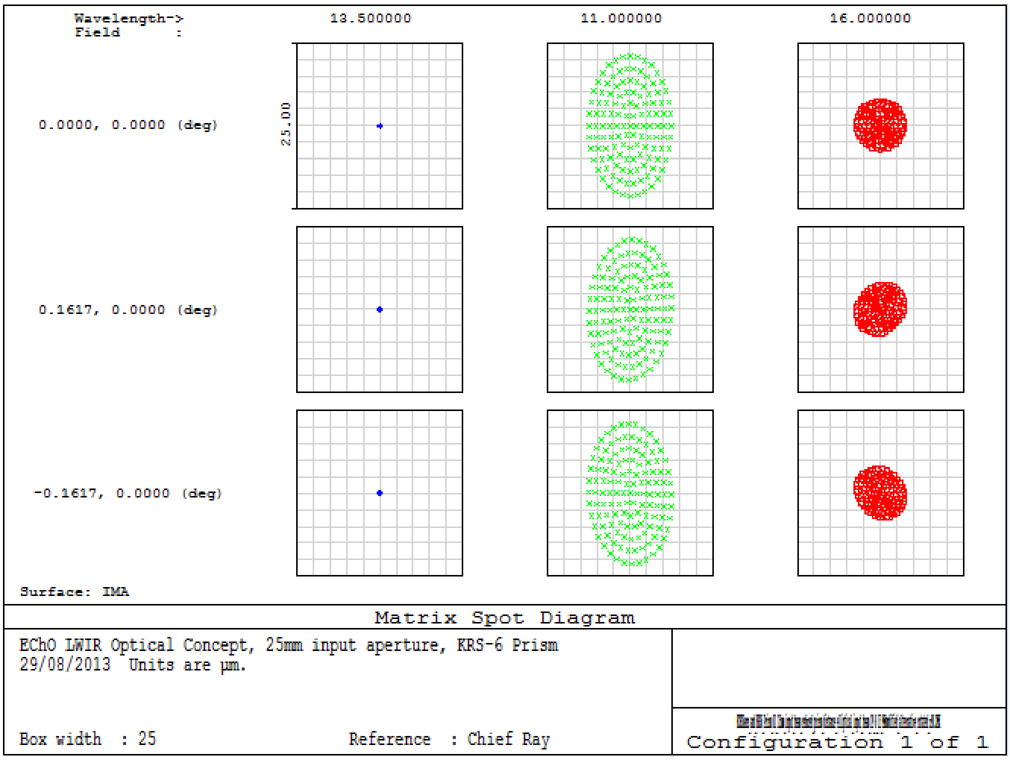

Figure 18-3: Monochromatic spot diagrams for the baseline LWIR channel design.

Figure 18-4: Approximate transmission for the coated Ge lens and KRS-6 prism.

18.3.2 Mechanical Design

The LWIR channel spectrometer (Figure 18-5) uses aluminium optical mounts and diamond-turned mirrors. The mirrors are supported using three axis kinematic mounts. The germanium lens and KRS-6 prism are mounted using arrangements derived from the Cassini/CIRS instrument.

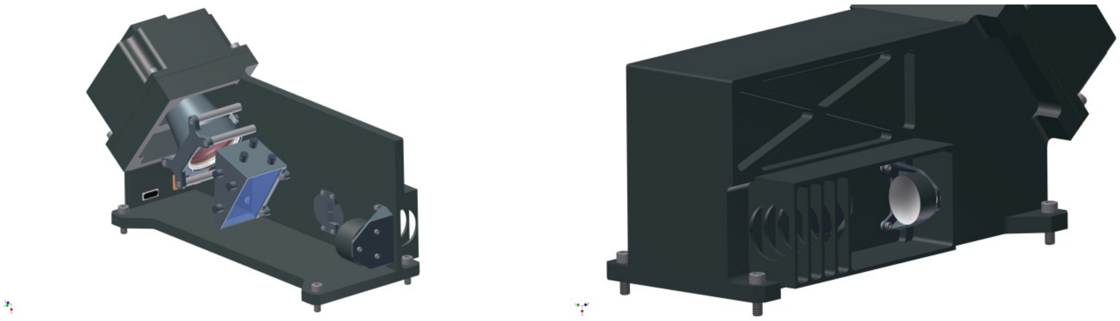

Figure 18-5: Cut-away showing mechanical accommodation for the LWIR channel. Approximate dimensions are 139 x 347 x 182 mm, with a mass of 5.47 kg with 20% margin and MLI blankets (not shown).

18.3.3 Thermal Design

The module enclosure is kept in good thermal contact with Payload Module Optical bench via four M6 bolts, at a nominal 45 K. The exterior of the module is covered in multi-layer insulation blankets to reduce the radiative load from the rest of the payload module.

To reduce the background signal at the detector due to thermal emission from the instrument enclosure, additional baffles are included around the optical path and are cooled to approximately 27 - 29 K using the active cooler. The baffles create a low-temperature ‘inner-sanctum’ within the instrument enclosure (ECHO-TN-0006-RAL, [RD39]), and the transmissive optical component mounts are thermally-isolated from the optical bench. For example, the germanium lens mount is based on the Cassini/CIRS instrument cryogenic design, and a similar mounting system is used for the prism that includes the necessary thermal isolation.

18.3.4 Performance vs Requirements

The LWIR module design has sufficient spectral resolving power (between 27 and 56) across its waveband (G-PERF-160, R-PERF-190 AD2) and optical throughput of 0.65 - 0.8 (G-PERF-220) to meet the requirements for the goal LWIR channel. The LWIR slit is sized (R-PERF-250) so that the given (full) widths are determined by the size of the Airy discs at 16 μm, with the necessary added margin for static random pointing error (fine APE & quasi-static RPE residual) and co-alignment.

The current optical design of the channel has been optimised for a 25 μm pitch detector array and assumes 3 pixels per spectral sampling element (R-PERF-260). The noise performance of the module is dependent on the choice of array, described in more detail in section 18.4.

18.4 LWIR DETECTOR SELECTION

18.4.1 Baseline Selection and Performance

Detector options with both high TRL and the necessary low dark current performance (e.g. < 100 e^-/s) for the faint noise limit defined in AD2 are limited at the wavelengths covered by the LWIR module. The most appropriate detector, with the best demonstrated performance and high TRL, are Si:As BIB arrays such as those used in the MIRI instrument for JWST. These offer the necessary dark current performance for EChO including read noise) and are well characterised. The main difficulty with selecting these detectors is that they require an additional active cooling stage to reach temperatures of 7 K. MCT detectors….

18.4.2 Alternative Options

For the LWIR waveband, detectors based on Mercury-Cadmium-Telluride tend to be of the photoconductive rather than photovoltaic type, and have limited dark current performance - typically of order (10^4-10^6 e^-/s) at temperatures of 28 K.

Other options include Si:Ga BIB detectors at ~20 K. Si:Ga arrays were developed by a US company, DRS infrared (Hogue et al. 2010), for NASA as part of the initial detector technology programmes for the Next Generation Space Telescope and Terrestrial Planet finder. However, these were not developed beyond prototypes once 7 K space-rated coolers became available. Based on the work described in Atkins et al 2010 (Figure 18-6), Si:Ga devices may not have the performance necessary for the R=30 spectrometer but could be suitable for a lower resolving power spectrophotometer.

A spectrophotometer can be constructed using, for example, 5 - 7 lower-performance detectors (dark currents ~40 k e^-/s) along the spectral dimension of the dispersed prism output. This configuration allows the module to capture key diagnostic spectral features of specific gases such as carbon dioxide, water vapour and hydrogen cyanide. This information can then help to break the degeneracies that are present in data analysis techniques used to determine temperature structure and relative abundances of these important constituents (e.g. Barstow et al. 2013 [RD25] and ECHO-TN-0002-OXF [RD26]).

The Si:Ga BIB detectors remain in development by DRS Infrared, with a current TRL of 4. TRL of 5 is expected in first quarter of 2014, rising to 6 by the third quarter 2015.

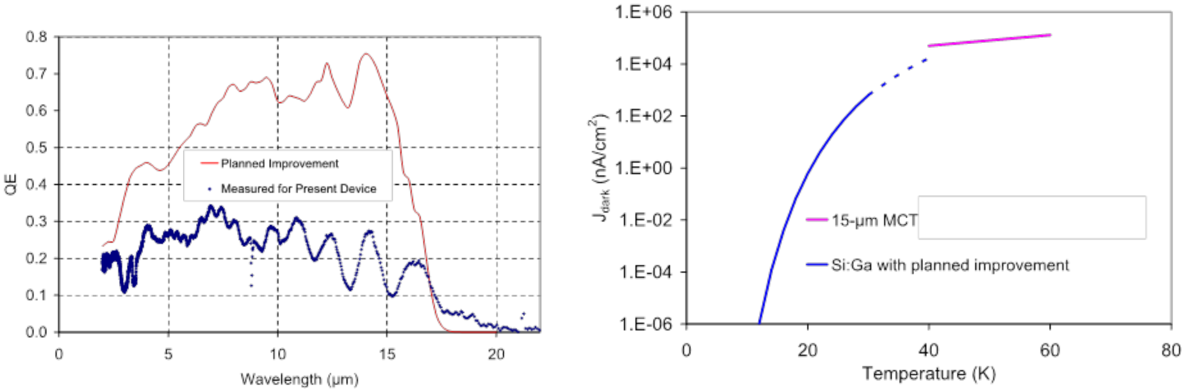

Figure 18-6: Expected performance of the Si:Ga detector arrays described in Hogue et al 2010.

18.4.3 Detector Electronics

For the case of a feasible detector from Si:Ga it is expected that the detector electronics architecture would probably be based on MIRI or similar, based on the Hogue et al. 2010 paper [RD27].

19 AIV AND GROUND CALIBRATION

The EChO instrument will follow a pFM approach to overall qualification. Some major design aspects will be de-risked earlier in the program using the prior models (as discussed in sections below), but it is planned that formal environmental qualification takes place on the pFM instrument.

The basic philosophy for the EChO verification programme is to test the critical interfaces, environmental requirements and functionality as early as possible during phases B/C/D to remove as much risk as possible from the proto flight model programme. This applies to all levels in the instrument and system build. The development and verification of the instrument will be undertaken in accordance with the requirements in the EID-A and the guidance in the applicable ECSS standards.

In order to allow early de-risking we plan to build a Performance Verification Model (PVM) of the instrument Focal Plane Unit (FPU) and electronics (WEU) that will be form, fit and functionally compliant but with no compulsion that the units within it are capable of undergoing environmental testing to qualification level. This is effectively the Engineering Model (EM) of these units. This model will not be environmentally tested to qualification levels and is not proposed to be deliverable to spacecraft level. By following this programme rather than committing to a full qualification model we allow flexibility in the schedule. That is, we are not dependent on completion of all unit qualification programmes to start the interface and performance verification activities at Instrument level.

At subsystem level there are a variety of qualification approaches being followed. Some subsystems (i.e. the cooler) have a dedicated qualification model which will undergo a full suite of environmental testing (including lifetime testing) prior to the FM builds. Full details are contained in the EChO Instrument Design, Development and Verification Plan (RD24).

19.1 MODEL PHILOSOPHY

The EID-A calls for the following instrument models to be delivered to system level: a Structural Thermal Model, an Engineering Model and a Flight Model. We have reinterpreted these models as outlined in the follow sub-sections to better fit with our development plan, the need to de-risk major interfaces with the spacecraft as early as possible and to reduce the overall model development schedule. The EChO Instrument Level AIV program will have three models:

1. Structural Thermal Model (STM)
2. Avionics Model (AVM)
3. Proto Flight Model (pFM)

In addition there will be a Performance Verification Model (PVM) of the Instrument Focal Plane Unit and Instrument Electronics.

The STM will provide verification of the mechanical and thermal behaviour of the structure as well as optical alignment.

The AVM will provide verification of the communications and electrical behaviour and instigate ground test sequences and flight operations.

The experience from the STM and AVM programmes will ensure that the pFM design and AIV program are optimised.

19.1.1 Deliverable Structural Thermal Model (STM)

The STM EChO instrument that will be delivered to S/C level AIV:

- Basic FPU structure with mass and thermal dummies – no functional requirements
- Mechanical and thermal interfaces flight representative but not necessarily form compliant
- Optical alignment jig fitted to allow chief ray/pupil alignment verification
- Development or engineering model (EDM) coolers delivered alongside STM with EM cooler drive electronics

- Capable of undergoing full system level environmental testing to qualification levels and has been tested to qualification levels before delivery (TBC)
- Demonstrate thermal design and provide correlation for TMM
- Used for mechanical fit check, optical alignment interface check, vibration testing and thermal tests at S/C level

19.1.2 Deliverable Avionics Model (AVM)

The AVM EChO instrument that will be delivered to S/C level AIV:

- ICU plus PSU simulator and EGSE to simulate instrument function
- Pull through of instrument AIV process including test facilities and procedures
- Used for Electrical interface compatibility testing at S/C level
- Used at system level to check out electrical and communications interfaces and set up ground test sequences and flight operations.

19.1.3 Deliverable Proto Flight Model (pFM)

The pFM EChO instrument that will be delivered to S/C level AIV will provide for:

- pFM approach to most design aspects except as outlined elsewhere in this document
- Full AIV sequence including appropriate system level performance verification and calibration

19.2 GROUND TESTING REQUIREMENTS

19.2.1 Module Level

- The detectors will be tested before channel/payload integration with suitable stand alone readout electronics. Further testing with the actual instrument readout electronics may be done prior to payload testing. This testing should include determination of:
    - Yield
    - Noise
    - QE
    - Dark current
    - Well depths
    - Effects of temperature on responsivity
- The detector readout electronics, instrument control electronics and processing electronics will require standalone testing before delivery to payload, it is likely an instrument simulator will be required for these tests. The detector electronics (both cold FEE and warm electronics) will need to undergo EMC testing and characterisation at unit level prior to delivery to the next level of integration – this will require flight-like harnessing and detectors to be used.
- Optical testing of each channel will be done by the channel module providers. The scope of this is TBD but as a minimum it will check focus and internal alignment of the channel with respect to an external alignment reference. The maintenance of this alignment throughout the temperature regime foreseen in ground test and in flight should also be checked at module level.
- The internal calibrator will also require stand alone testing under operating conditions, for this a high stability sensor will be required to verify the stability of the internal calibrator.
- It is assumed that all modules will undergo qualification and acceptance vibration and thermal testing at module level prior to delivery to the overall instrument AIV.

19.2.2 Payload Instrument Level

19.2.2.1 Structural

At integrated payload level the instrument would undergo a structural testing campaign to prove both the overall structural design (including qualification / acceptance of the common structural elements) and the workmanship associated with the instrument integration process, The structural testing at instrument level on the prototype model (STM) would be suitably instrumented (accelerometers etc) and used to derive the input requirements for the lower level structural qualification and acceptance. On the flight model the instrumentation would be used to ensure that the levels to which subsystems have been qualified are not exceeded.

It would be expected that force limited vibration testing would be implemented on the instrument level vibration tests in order to protect the hardware from damage, and to ensure that the specified interface forces are generated in test. The consortium has extensive experience of conducting this type of testing on large test items, including the monitoring of alignment stability of items during the test.

19.2.2.2 Alignment

The alignment of the modules will be conducted at ambient temperature during the assembly of the instrument. External reference features on each module will be related to one another such as to ensure that the co-alignment of the common fields of view is achieved. At ambient temperature the focus position and pupil shear of each module can be checked with respect to a common reference.

The knowledge of the alignment location of the instrument with respect to an externally accessible reference (for example alignment cubes & fiducials) will be measured at instrument level in order to allow easy checking of the correct alignment between instrument and telescope at the next level of integration.

19.2.2.3 EMC Testing

At instrument level the cross-compatibility of the individual detector systems will be checked and proven. Additionally there can be a cross-check of the susceptibility and emissions testing that would have been first conducted at lower level (for example at ICU or detector system levels).

19.2.2.4 Thermal Testing

The overall thermal balance verification of the temperature distributions, heat loads to the cryogenic stages etc will be verified at instrument level. The representation of the cryo-cooler performance in the instrument thermal balance test would be TBD, but a goal would be to provide an environment that simulates the end-to-end environment for the coolers and the instrument. The complexity of such a test would be high, and early debugging of the bespoke test facility that would be needed would be vital (and part of the planned STM test program).

An alternative option would be to separately verify the performance of the cryo-coolers and the instrument, with the results from one test feeding into the boundary conditions of the other. This approach has been adopted on previous missions (for example Planck, JWST) and would be valid, although somewhat higher heat load margins may be desirable in this case due to the late verification of the overall cooling chain.

19.2.2.5 PVM / FM Performance Testing

- Prior to testing we will require EGSE integration testing, these tests should include the instrument electronics and an instrument simulator.
    - These tests also allow finalisation of scripts and procedures
    - The also allow a test of the data system through to QLA/data processing system
    - A full test will be required prior to the first full campaign, a reduced scope, more functionally orientated test will be required for subsequent campaigns.
- Functional Tests
    - Functional tests will be run with the instrument both warm (at ambient) and cold.

  - In the current design there are no moving parts to test but if these were introduced for future designs they would need to be part of functional testing.
  - Any instrument monitoring systems e.g. thermometry will be checked out.
  - It is expected that the detectors can be operated in a warm state, hence the functional testing will include detector operation.
  - It is assumed that the internal calibration source can be operated warm.
  - In addition to the instrument the test facility should also be functionally checked, this is especially critical if a cold test facility is required but it is good practice anyway.
- Performance Tests
  - The following list includes the type of tests that are likely to be needed. A full list along with a verification matrix can be drawn up once a full set of instrument requirements are in place. These tests would all be run with the instrument in a flight-like environment and running at operational, cryogenic, temperatures.
  - Detector
    - Determination of dead and bad pixels
    - Detector (plus readout electronics) characteristics e.g. latency, persistence, droops, other non-linearity
    - Dark current and it's stability
    - Initial look at characterisation and removal of glitches (full characterisation completed in-flight)
    - Ability to stack ramps in a 90 second (TBC) interval
    - Noise
    - Effects of temperature on responsivity
    - Periodically check responsivity to check for other affecting factors such as drifts in electronic gains.
    - Flatfield
  - Optical
    - Check focus at operating temperature and check the co-focality of all modules
    - Throughput
    - Internal alignment (confirmation)
    - PSF
    - Opto-mechanical stability
    - Wavelength registration
    - Determine if there is any crosstalk
    - Simulated pointing offsets and jitter via test facility source
  - Calibration
    - Check level and stability of internal calibration source
  - Operations
    - Run tests of on-board data processing by taking data using standard observational modes and then processing ramps both on-board and on the ground.

19.2.3 Spacecraft Level

- Commissioning
    - Essentially running through a functional checkout in flight
    - Does not require any optical input i.e. no lid is envisaged in current design but if one was, these tests could be done with the lid closed
    - Real time operation (during flight to L2), may require instrument team to be located at the MOC
- Performance verification
    - This is essentially a repeat of the performance tests but in flight and using astronomical sources instead of a test facility. The reasons for doing this include
        - Establish that the instrument parameters have not changed during launch
        - Checking the affects of the space environment, in particular the effects of glitches and any straylight
        - Checking that the spacecraft itself has no adverse affects on the instrument, in particular the thermal environment provided by the spacecraft
        - Setting up the spacecraft/instrument pointing (possibly a major undertaking for EChO)
        - Optical characterisation of the instrument + telescope system
        - Calibration, in particular flux calibration/ RSRF requiring astronomical sources
- Science verification
    - This phase is commonly used by observatories to confirm the validity of observing modes offered to observers.
    - For EChO the observing approach will need to be validated before the full programme begins although this may not require a formal phase.
    - Depending on the knowledge of the host stars we may also wish to visit as many as possible during the early mission to check for short term stellar variability, knowledge of which may feed back into long term mission planning.

19.3 CLEANLINESS AND CONTAMINATION CONTROL

The cleanliness and contamination control requirements for EChO are TBD. The need for a mirror cover shall be assessed in future study phases depending on the mirror contamination constraints.

The requirements are expected to be comparable with similar visible and IR space instrumentation of which the Consortium have experience.

The JWST MIRI contamination requirements at delivery of the instrument are for a surface cleanliness (on optical surfaces) of 300 (particulate) and A (molecular). The requirements for EChO will be similar and will be defined in detail during the next phase. The allowable degradation of cleanliness through flight is governed by the loss of throughput, and the appearance of spectral features caused by contamination deposition on the optical surfaces. Using an allocation of a 10% relative loss of throughput throughout the mission leads to an EOL allocated cleanliness level of 350D on optical surfaces. This degradation has been calculated, to first order, to be acceptable for the science requirements of capability to stack observations if assumed that the degradation is at an approximately constant rate, it can then be removed from the data by the planned in flight calibration.

Although working to these levels of cleanliness presents challenges and care is necessary in all aspects of the design and AIV, they are achievable through existing means; the verified molecular cleanliness levels of JWST MIRI are <A/10 ($<1 \times 10^{-8}$ g/cm^2) at delivery with a particulate contamination of better than level 300 on all optical surfaces.

19.3.1 On-Ground AIV Budget

In order to be able to meet the 300A specification, a contamination budget was derived taking into account the spreading into sub-systems under the responsibility of different organisations within the EChO Consortium as well as detailing the budget for the main AIV phases. Further splitting into type of components is made in order to reflect the criticality of the composing elements (optics, structure).

The recommended IOB contamination budget breakdown is as follows:

IOB		**Modules**		**Cooler**		**FGS**	
Optics	Structure	Optics	Structure	Optics	Structure	Optics	Structure
250A/5	**300A**	**250A/5**	**300A**	**250A/5**	**300A**	**250A/5**	**300A**

IOB integration	Internal optics	**250A/3**
	Internal structure	**300A**
	External structure	**350B**
IOB handling & test	Internal optics	**250A/2**
	Internal structure	**300A**
	External structure (before cleaning & TV bake-out)	**400C**
IOB delivery to ESA	External structure (incl. MLI)	**300A**
	Internal optics & structure	**300A**

Table 19-1: On-ground contamination budget for AIV phase

19.3.2 Contamination analysis

This is detailed in the Instrument Contamination Control Plan, [RD23]. The effects of deposited layers of various contaminants on the instrument were assessed. The preliminary conclusion is that the maximum level of acceptable surface contamination for optical surfaces (more critical than external thermal control surfaces in terms of instrument performance degradation) is an ice layer of thickness 0.01μm max (total for all chemical species, including water and others) with total max flux through the instrument apertures (towards the cold optics) <10-14g/cm^2/s average during the instrument lifetime.

19.3.3 Contamination Control & Monitoring

The contamination of the sensitive elements (optics and FPAs) of emissions from surrounding units or structure can be minimised by ensuring the material visible to the elements generates negligible outgassing products. In order to limit this instrument internal contamination, efforts will be made to select low-outgassing materials with the following characteristics:

TML<0.2% and CVCM<0.1%

Units or parts likely to produce significant outgassing contaminants in orbit or require a high degree of cleanliness before assembly will be subjected to a pre-outgassing operation (i.e. bake-out). The temperature, vacuum and time required for this operation will be assessed for each unit or part but the following baseline will be used:

- either a bake-out at temperature T>80°C over a period of 48hours minimum, under pressure environment <10^{-5} Torr,
- or, in case this temperature is higher than the recommended one before component damage or material degradation, a bake-out at a minimal temperature of T=(max T during on-ground and on-orbit life)+15°C over 4 days (TBR).

If paints, adhesives, MLI and harness materials have TML and CVCM characteristics too close or beyond the above specifications (after measurement), higher temperatures will be applied during bake-out (typical range 100-130°C), except where damage of the material or component is expected. In this case, the supplier of these components should check the use of ESA approved materials database and comply with related curing and bake-out procedures.

Internal contamination monitoring shall be undertaken using QCM devices located on the IOB. These shall be read out during the AIV phase and ground testing only, and not during flight. The exact number of QCM devices is TBD, but shall be greater than or equal to 1 and shall not exceed 3.

Fabrication of spacecraft parts will generally take place in controlled environments, specific to each module provider. The AIV phase for the PLM will take place at RAL and the detailed specifications for the environmental and test facilities are given RD23, chapter 5.

The cleanrooms at RAL contain particle counters for standard cleanroom air quality monitoring. Witness plates (horizontal and vertical) will be used on and around the IOB and on any GSE to monitor localised particulate fall-out and surface cleanliness. Molecular fall-out is measured by FTIR spectroscopy[3]. Visual inspection will take place under ambient and UV light. Tape-lift methods will be used to determine the localised surface particulate cleanliness on the IOB.

Due to the inaccessibility of internal components after their integration into sub-units, the general approach is more based on active prevention via preliminary bake-outs and limitation of exposure. In case of external surface contamination detection and/or long unprotected test periods in cleanrooms, the following methodology will be applied:

- Molecular contamination:
    - solvent wiping: precise procedure dependent on component criticality e.g. optics or structure.
- Particulate contamination:
    - contact method: solvent wiping;
    - non-contact method: gas jet spray (clean dry air or nitrogen), only if large particles are detected on surfaces;

Typical solvents are: water-free acetone, ethanol, methanol, isopropanol. Clean gloves shall be worn during all cleaning activities.

Post-testing cleanliness inspections of external surfaces will be performed to assure that surface cleanliness levels have not been exceeded.

In the thermal vacuum chamber TQCMs are used to determine mass loss, outgassing and deposition rates. An RGA is used as a complement to the QCMs (as they can provide info on molecular weight of outgassed material and therefore chemical composition, unlike QCMs) before/after thermal vacuum testing and at steady state. Witness plates are once again used for monitoring particulate contamination but are post-processed by inspection under UV light and IR reflectance spectroscopy.

---

[3] The procedure used at the RAL Molecular Spectroscopy Facility is based on the document: *Witness mirror measurement*, ISO9:SPAP MSF 001 issue 1 (26/07/2004)

20 TECHNOLOGY READINESS ASSESSMENT & PLANS

20.1 ASSESSMENT OF CURRENT TRLS

The initial assessment of the Technology Readiness Levels (TRLs) of the key technologies of the baseline design presented above is detailed in Table 20-1 and Table 20-2 below. In this assessment both the current level of technology is assessed, plus the level at which this would be at the end of the assessment phase study (assumed to be at the end of 2012) given the existing plans and programs for technology development in which consortium members are participating. Some of the key technologies which are to be considered as options to our baseline design in the trade studies planned are also assessed for comparison. The TRL levels used here are based on the ESA definitions as well known throughout European industry.

This table clearly shows that the baselined design largely has a high level of technology readiness, with few key technologies selected requiring significant development in order to be at a feasible level for selection (for example TRL ≥5). In cases where relatively low TRL technologies are baselined, alternative options with a higher TRL have already been identified as options.

Baseline Design				
Technology	**Use in EChO Design**	**Current TRL**	**Expected TRL at SRR**	**Comments**
Teledyne MCT Detectors 0.5 – 2.5 microns	VNIR / FGS Channels	5-6	6+	JWST NIRCam / NIRSpec heritage among others
Teledyne MCT Detectors 2.5 – 5 microns	SWIR Channels	6-9	6-9	JWST NIRCam / NIRSpec heritage among others
Teledyne MCT Detectors 5 – 11 microns	MWIR Channels	4-5	5+	Developments for NASA NEOCam Mission. Contract in place to reach TRL5 in 2014. EChO will follow on from this existing NASA contract.
Cross-dispersed Spectrometer	VNIR Channel	6-9	6-9	All selected optical materials are space qualified or have space qualified equivalents available. Cross-dispersed spectrometers in flight on Rosetta and Venus Express.
Dispersive Optical Module Designs	SWIR, MWIR & LWIR Modules	9	9	Similar optical designs have flown on multiple missions.
Various transmissive optical materials	Lenses and dispersive elements in SWIR and MWIR modules	>5	>5	All selected optical materials are space qualified or have space qualified equivalents available
SW Dichroics	D1, D1b for VNIR module and FGS BS	>5	>5	Similar specification required to that in use on JWST NIRCam BS. Minor modification to substrate required to allow transmission to 11 microns and beyond
MW & LW IR Dichroics	D2, D3 and D3b for SWIR and MWIR pick-off	>5	>5	Similar specification and technology to EarthCare BBR and many other UoR dichroics
JT Cooler	26 K Stage Cooling	>4	>5	Builds on Planck heritage with evolutionary design changes
All Aluminium Construction	Structures and reflective optical elements	9	9	Builds on design heritage from Herschel and JWST MIRI.

Table 20-1: Assessment of TRL of Key Technologies in Baseline Design

Options				
Technology	**Use in EChO Design**	**Current TRL**	**Expected TRL at SRR**	**Comments**
CEA / Air Liquide PT Cooler	18 K Stage Cooling Option	≤4	5	Breadboard tested in frame of GSTP contract
2-stage Stirling Cooler	18 K Stage Cooling	~4	>5	Builds on previous heritage with evolutionary design changes.
Static FTS Module Concept	LWIR Module design alternative	4/5	5	Proven at 77K in ground test
Raytheon SiAs Detectors	MWIR and LWIR Channels	6-9	6-9	Spitzer and JWST MIRI heritage
Sofradir MCT detectors	VNIR & SWIR channels	≤4	~5	On-going development work in frame of ESA TRP contract for testing and European Euclid detector development. Would require further ESA development funding to get to flight ready arrays
Selex MCT detectors	VNIR & SWIR channels	≤4	~5	On-going development work in frame of ESA TRP contract for testing and European Euclid detector development.. Would require further ESA development funding to get to flight ready arrays

Table 20-2: Assessment of TRL of Key Technologies held as Options

20.2 SUMMARY OF PLANS IN PLACE FOR TRL RAISING ACTIVITIES

The following activities are either on-going, or planned (with secure funding known to be in place) for the near future. These are aimed at increase the technology development level of technologies for EChO to the point that they can be part of a coherent baseline design at the point of mission selection (expected in mid- to end- of 2013).

- Detector development and testing activities:
    - ESA Funded:
        - There are two ESA funded activities shortly to begin to conduct testing of existing IR detector devices in the 1 – 11 microns wavelength band. This testing is to demonstrate the performance of the current generation of devices, and to enable targeted development work to take place in those areas that show the most promise.
        - Developments of IR detectors (especially NIR detectors) are also taking place within the frame of the Euclid program. Although the detector requirements for EChO are different from these, there is likely to be some significant synergies between the necessary developments which could be leveraged to raise the TRL level of the European candidate detectors for EChO.
    - Nationally funded:
        - For the MWIR channel (5 – 11 microns range) there is a CNES funded development program ongoing as reported in section 17.3.2 above. This has included the manufacture of a number of new devices which are currently undergoing testing and showing promising results. Further testing and development work are planned for the next 6 months.
        - There is a (non-EChO specific) detector development activity taking place funded by UKSA in which Selex and UK ATC are considering detectors for the 2 – 5 and 11 – 16 microns bands.
- There are existing TRP contracts in place with the major suppliers of cryogenic coolers (in the frame of Darwin and other missions) which are helpful in increasing the development status of

some of the key components that will be needed for an EChO cryogenic system. Although none of these are directly targeted at EChO, the background knowledge can be applied for the EChO system.

- A small nationally funded development study for the IR dichroics is taking place within the UK as part of this study to assess the feasibility and likely performance of the baseline D2, D3 and D3b dichroics in the baseline payload design as outlined in this document.

20.3 DESIRABLE ADDITIONAL TECHNOLOGY DEVELOPMENTS

There are some additional technology development activities that (we believe) are not currently being actively pursued, and at this time the conduct of these activities would be outside the scope of the possible consortium funded activities.

- Further detector development to transition the European detector options from research to a flight-ready product. As noted in the Cost Report, [RD37] the European detector option is preferred by the consortium due to the political and control aspects. However the large (c.€7M) cost delta incurred by selecting European rather than the higher TRL US detectors is not feasible for the consortium. The development to take the European products to a flight-ready standard would have to be a strategic decision taken by the Agencies (ESA & National) and financially supported as such. This could include:
    - A development and demonstration program for the use of European MCT detectors operating at ~40K to read down to 550nm.
    - Development and optimisation of LWIR detectors operating at 28 – 40K to read out to 16 microns wavelength with sufficiently low dark current and noise for the EChO application.
- There is not currently known to be a suitable European supplier of NIR dichroics that could meet the requirements of the D1 and D1b dichroics in the baseline design. It is thought that Barr associates in the US likely have the necessary technologies (as demonstrated in JWST NIRCam), but a European development activity in this area may be worthwhile.

21 ANNEX A: CONSORTIUM CONTRIBUTORS

Listed here are the participating scientists and engineers that are working phases within the consortium on the phase A study and would continue to work through the definition, implementation and operations phases.

21.1 PRINCIPAL INVESTIGATOR

Giovanna Tinetti, University College London, UK

21.2 Co-PI's

Jean-Philippe Beaulieu, Institut d'Astrophysique de Paris, France
Denis Grodent, Université de Liège, Belgium
Manuel Guedel, University of Vienna, Austria
Paul Hartogh, Max Planck Sonnnensystem, Germany
David Luz, Universidade de Lisboa, Portugal
Giusi Micela, INAF – Osservatorio Astronomico di Palermo, Italy
Hans Ulrik Nørgaard-Nielsen, DSRI, Denmark
Tom Ray, Dublin Institute for Advanced Studies, Ireland
Ignasi Ribas, CSIC – ICE, Spain
Hans Rickman, Space Research Centre, Polish Academy of Science, Poland / Department of Physics and Astronomy at Uppsala University
Avri Selig, SRON Netherlands Institute for Space Research, Netherlands
Mark Swain, NASA Jet Propulsion Laboratory, USA
Bruce Swinyard, RAL Space / University College London, UK

21.3 Co-I's

Marek Banaszkiewicz, Space Research Centre, Polish Academy of Science, Poland
Mike Barlow, UCL, UK
Neil Bowles, University of Oxford, UK
Graziella Branduardi-Raymont, MSSL, UK
Vincent Coudé du Foresto, LESIA-Astro, France
Pierre Drossart, LESIA-Planeto, France
Pieter Deroo, JPL, USA
Jean-Claude Gerard, Université de Liège, Belgium
Laurent Gizon, MPS-Heliosism. Germany
Allan Hornstrup, DTU Space, Denmark
Christopher Jarchow, MPS-Planeto, Germany
Franz Kerschbaum, University of Vienna, Austria
Géza Kovacs, Konkoly Observatory, Hungary
Pierre-Olivier Lagage, CEA – Saclay, France
Tanya Lim, RAL Space, UK
Mercedes Lopez-Morales, CSIC – ICE, Spain
Giuseppe Malaguti, INAF – IASF – Bologna, Italy
Marc Ollivier, IAS Paris, France
Emanuele Pace, Università di Firenze, Italy
Enric Pallé, IAC, Spain
Enzo Pascale, Cardiff University, UK
Giuseppe Piccioni, INAF - IASF – Roma, Italy
Alessandro Sozzetti, INAF – Osservatorio Astrofisico di Torino, Italy
Bart Vandenbussche, Leuven University, Belgium
Gillian Wright, UK ATC, UK
Gonzalo Ramos Zapata, INTA, Spain
Maria Rosa Zapatero Osorio, CAB, Spain

21.4 TECHNICAL TEAM COORDINATORS

21.4.1 Consortium Project Manager

Paul Eccleston, RAL Space, UK

21.4.2 Instrument Scientist

Marc Ollivier, IAS Paris, France

21.4.3 Payload Scientists

Giorgio Savini, UCL, UK

TBC, Italy

21.4.4 Payload Engineering Manager

William Grainger (TBC), RAL Space, UK

21.4.5 Consortium PA Manager

Richard Stamper, RAL Space, UK

21.4.6 Consortium SGS Lead

Tanya Lim, RAL Space, UK

21.4.7 Systems Engineering Working Group Coordinators

Ana Balado, INTA, Spain
Ian Bryson, UK ATC, UK
Raymond Burston, MPS, Germany
Vincent Coudé du Foresto, LESIA-Astro, France

Martin Crook, RAL, UK
Anna Di Giorgio, Italy
Kevin Middleton, RAL Space, UK
Frederic Pinsard, CEA – Saclay, France
Gianluca Morgante, INAF – IASF Bologna, Italy
Emanuele Pace, Università di Firenze, Italy
Pep Colomé, ICE – CSIC, Spain
Ranah Irshad, RAL, UK
Bruce Swinyard, RAL Space / UCL UK
Berend Winter, MSSL, UCL, UK

21.4.8 Consortium Management Advisor

Matt Griffin, Cardiff University, UK

21.4.9 Module Design Leads

Alberto Adriani, IAPS – IAPS, Italy
Neil Bowles, University of Oxford, UK
Kevin Middleton, RAL Space, UK
Roland Ottensamer, University of Vienna, Austria
Gonzalo Ramos Zapata, INTA – LINES, Spain
Jean-Michel Reess, LESIA-Planeto, France

21.4.10 National Project Managers

Ruymán Azzollini, DIAS, Ireland
Raymond Burston, MPS, Germany
Josep Columé, CSIC – ICE, Spain
Ruud Hoogeveen, SRON Netherlands Institute for Space Science, Netherlands
Roland Ottensamer, University of Vienna, Austria
Emanuele Pace, Università di Firenze, Italy
Mirek Rataj, Space Research Centre, Polish Academy of Science, Poland
Jean-Michel Reess, LESIA-Astro, France
Jan-Rutger Schrader, SRON Netherlands Institute for Space Science, Netherlands

21.5 SCIENCE TEAM COORDINATORS

21.5.1 Study Science Team Co-coordinators

Giovanna Tinetti, UCL, UK and Pierre Drossart, LESIA-Planeto, France

21.5.2 Science Team Working Group Leads

F., Allard, ENS, France
J., Barstow, Oxford University, UK
J., Cho, QMUL, UK
C., Cockell, ROE, UK
A., Correia, IN, Portugal
L. Decin, University of Leuven, Belgium
P., Deroo, JPL, USA
T., Encrenaz, LESIA, France
F., Forget, LMD, France
A., Glasse, UK ATC
C., Griffith, UoA, US
T., Guillot, Nice Obs., France
P., Hartogh, MPS Germany
T., Koskinen, UoA, US
H. Lammer, IWF, Austria
J. Leconte, LMD, France
P. Maxted, Keele University, UK
G., Micela, INAF – Palermo, Italy
I., Mueller-Wodarg, Imperial College, UK
R., Nelson, QMUL, UK
C., North, Cardiff, UK
E., Pallé, IAC, Spain
I., Pagano, OAT, Italy
G., Piccioni, INAF – IASF, Italy
D., Pinfield, UH, UK
R., de Kok, SRON, Netherlands
I., Ribas, CSIC – ICE, Spain
F., Selsis, Un. Bordeaux, France
A., Sozzetti, INAF Torino, Italy
L., Stixrude, UCL, UK
J., Tennyson, UCL, UK
D. Turrini, INAF-IASF, Italy
M.R., Zapatero-Osorio, CAB, Spain

21.6 PARTICIPATING SCIENTISTS

21.6.1 Austria

W., Magnes, IWF Graz
E., Dorfi, University of Vienna
M., Güdel, University of Vienna
F., Kerschbaum, University of Vienna
A., Luntzer, University of Vienna
E., Pilat-Lohinger, University of Vienna
T., Rank-Lüftinger, University of Vienna

21.6.2 Belgium

B., Bonfond, Université de Liège
J.-C., Gerard, Université de Liège
M., Gillon, Université de Liège
J., Gustin, Université de Liège
B., Hubert, Université de Liège
A., Radioti, Université de Liège
L., Soret, Université de Liège
A., Stiepen, Université de Liège

21.6.3 Czech Republic

D., Heyrovsky, Charles University

21.6.4 Denmark

A., Andersen, DARK Cosmology Center

L., Buchhave, DARK Cosmology Center
D., Watson, DARK Cosmology Center
N., Christian Jessen, DTU Space
I., Lundgaard Rasmussen, DTU Space

21.6.5 France

C., Cavarroc, CEA
S., Charnoz, CEA
E., Pantin, CEA
C., Alard, IAP
V., Batista, IAP
A., Cassan, IAP
J.-P., Maillard, IAP
J.-B., Marquette, IAP
P., Bordé, IAS
O., Demangeon, IAS
P., Gaulme, IAS
P., Lognonné, IPGP
C., Michaut, IPGP
S., Jacquemoud, IPGP
P., Fouqué, LATT
B., Bézard, LESIA
P., Kervella, LESIA
E., Lellouch, LESIA
B., Sicardy, LESIA
S., Vinatier, LESIA
T., Widemann, LESIA
D., Cordier, Obs. Besancon
M., Agundez, Obs. Bordeaux
M., Dobrijévic, Obs. Bordeaux
V., Eymet, Obs. Bordeaux
I., Gomez-Leal, Obs. Bordeaux
E., Hébrard, Obs. Bordeaux
F., Hersant, Obs. Bordeaux
A.-S., Maurin, Obs. Bordeaux
O., Venot, Obs. Bordeaux
P., Tanga, Obs. Cote d’Azur
F., Vakili, Obs. Cote d’Azur
L., Abe, Obs. Nice
V., Parmentier, Obs. Nice
R., Petrov, Obs. Nice
F.-X., Schmider, Obs. Nice

21.6.6 Germany

M., de Val-Borro, MPS
N., Krupp, MPS
U., Mall, MPS
W., Markiewicz, MPS
A., Medvedev, MPS
M., Rengel, MPS
N. Iro, Hamburg University

21.6.7 Ireland

A., Scholz, DIAS

21.6.8 Italy

L., Testi, ESO
A., Bulgarelli, IASF-Bologna
F., Gianotti, IASF-Bologna
G. Malaguti, IASF-Bologna
M., Trifoglio, IASF-Bologna
F., Capaccioni, IAPS-Roma
M.T., Capria, IAPS-Roma
F., Altieri, IAPS-Roma
G., Bellucci, IAPS-Roma
D., Biondi, IAPS-Roma
R., Cerulli, IAPS-Roma
A.M., Di Giorgio, IAPS-Roma
N., Fabrizio, IAPS-Roma
G., Filacchione, IAPS-Roma
M., Giuranna, IAPS-Roma
D., Grassi, IAPS-Roma
S.J., Liu, IAPS-Roma
S., Pezzuto, IAPS-Roma
D., Turrini, IAPS-Roma
C., Baffa, OA-Arcetri
C., Del Vecchio, OA-Arcetri
E., Giani, OA-Arcetri
L., Gambicorti, OA-Arcetri
F., Massi, OA-Arcetri
E., Oliva, OA-Arcetri
F., Palla, OA-Arcetri
K., Readorn, OA-Arcetri
A., Tozzi, OA-Arcetri
E., Poretti, OA-Brera
J., Alcala, OA-Capodimonte
E., Covino, OA-Capodimonte
P., Ballerini, OA-Catania
N., Lanza, OA-Catania
G., Leto, OA-Catania
G. Scandariato, OA-Catania
S. Scuderi, OA-Catania
G., Strazzulla, OA-Catania
R., Claudi, OA-Padova
E., Giro, OA-Padova
L., Affer, OA-Palermo
C., Cecchi Pestellini, OA-Palermo
A., Ciaravella, OA-Palermo
A., Collura, OA-Palermo
U., Lo Cicero, OA-Palermo
A., Maggio, OA-Palermo
L., Prisinzano, OA-Palermo
A., De Sio, UniFirenze

M., Focardi, UniFirenze
M., Pancrazzi, UniFirenze
S., Shore, UniPi

21.6.9 The Netherlands

C., Dominic, University of Amsterdam
I., Snellen, Leiden University
R., Waters, SRON

21.6.10 Poland

H., Rickman, SRC-PAS
M., Banaszkiewicz, SRC-PAS
M., Błęcka, SRC-PAS
A., Wawrzaszk, SRC-PAS
T., Wiśniowski, SRC-PAS
M., Rataj, SRC-PAS
P., Sitek , SRC-PAS
R., Graczyk, SRC-PAS
M., Stolarski, SRC-PAS
P., Wawer, SRC-PAS
R., Pietrzak, SRC-PAS
W., Winek, SRC-PAS

21.6.11 Portugal

M., Montalto, CAUP
V., Adybekian, CAUP
I., Boisse, CAUP
E., Delgado-Mena, CAUP
P., Figueira, CAUP
M., Monteiro, CAUP
N., Santos, CAUP
S., Sousa, CAUP
T., Kehoe, I3N
H., Morais, I3N
M., Abreu, CAAUL
D., Berry, CAAUL
A., Cabral, CAAUL
S., Chamberlain, CAAUL
R., Herdero, CAAUL
P., Machado, CAAUL
J., Peralta, CAAUL
J., Rebordão, CAAUL

21.6.12 Slovakia

J., Budaj, Slovak Academy of Sciences

21.6.13 Spain

D., Barrado, CAB-INTA
H., Bouy, CAB-INTA
N., Huelamo, CAB-INTA
J., Martín Torres, CAB-INTA
M., Morales-Calderón, CAB-INTA
A., Moro Martín, CAB-INTA
A., Moya Bedon, CAB-INTA
J., Sanz Forcada, CAB-INTA
E., García Melendo, FOED/ICE
P., Amado, IAA
A., Claret, IAA
M., Fernández, IAA
M., Lopez-Puertas, IAA
M.A., Lopez-Valverde, IAA
C., Allende Prieto, IAC
C.A., Alvarez Iglesias, IAC
J.A., Belmonte Avilés, IAC
H.J., Deeg, IAC
M., Espinoza Contreras, IAC
M., Esposito, IAC
B., Femenía Castella, IAC
R.J., García López, IAC
J., Gonzalez Hernandez, IAC
B., González Merino, IAC
G., Israelian, IAC
B., Laken, IAC
J., Licandro Goldaracena, IAC
N., Lodieu, IAC
P., Miles-Paez, IAC
P., Montañés Rodríguez, IAC
F., Murgas Alcaino, IAC
H., Parviainen, IAC
K.Y., Peña Ramírez, IAC
R., Rebolo López, IAC
V.J., Sánchez Béjar, IAC
E., Sanromá Ramos, IAC
B.W., Tingley, IAC
M.L., Valdivieso, IAC
J., C. Morales, ICE
J., Colomé, ICE
E., Garcia-Melendo, ICE
L., Gesa, ICE
J., Guardia, ICE
E., Herrero, ICE
F., Rodler, ICE
C., Eiroa, UAM
J., Maldonado, UAM
E., Villaver, UAM
F.J., Alonso Floriano, UCM
D., Montes, UCM
H.M, Tabernero, UCM
R., Hueso, UPV
S., Perez-Hoyos, UPV
A., Sanchez Lavega, UPV

21.6.14 Sweden

N., Piskunov, Uppsala University
U., Heiter, Uppsala University

21.6.15 UK

C., MacTavish, Cambridge
P., Ade, Cardiff
S., Eales, Cardiff
W., Gear, Cardiff
H., Gomez, Cardiff
M., Griffin, Cardiff
P. Hargrave, Cardiff
M., Galand, IC
J., Haigh, IC
J., Harries, IC
A., Coates, MSSL
R., Cole, MSSL
G., Jones, MSSL
A., Smith, MSSL
C. A., Haswell, OU
G., White, OU
L., Fletcher, Oxford
P., Irwin, Oxford
M., Tecsa, Oxford
J., Temple, Oxford
P., Read, Oxford
C., Agnor, QMUL
I., Polichtchouk, QMUL
C., Watkins, QMUL
T., Lim, RAL
D., Waltham, RHUL
N., Achilleos, UCL
A., Aylward, UCL
R. J., Barber, UCL
C., Danielski, UCL
P., Doel, UCL
S., Fossey, UCL
P., Guio, UCL
M. Hollis, UCL
O., Lahav, UCL
C., Lithgow-Bertelloni, UCL
G., Morello, UCL
H., Osborne, UCL
R., Prinja, UCL
M., Rocchetto, UCL
G., Savini, UCL
M., Tessenyi, UCL
S., Thompson, UCL
S., Viti, UCL
R., Varley, UCL
I., Waldmann, UCL
S.N., Yurchenko, UCL
J., Frith, UH
H., Jones, UH
I., Bryson, UK ATC
A., Glasse, UK ATC
G., Wright, UK ATC
N., Iro, Un. Keele
P., Maxted, Un. Keele
M., Burleigh, Un. Leicester
E., Kerins, Un. Manchester
D., Ward-Thompson, Un Lancaster

21.6.16 USA

H., Thrastarson, Caltech
Y., Yung, Caltech
D., Kipping, CfA
L., Brown, JPL
G., Orton, JPL
G., Bakos, Princeton
J. Moses, SSI
A. Showman, UoA
C., Griffith, UoA
T., Koskinen, UoA
R., Yelle, UoA

P., Mauskopf, UoA

22 CURRICULA VITAE OF KEY INDIVIDUALS

Giovanna Tinetti – Consortium Principal Investigator / Science Team Co-Lead

Professor of Astrophysics at University College London and Royal Society University Research Fellow.

PhD in Theoretical Physics from University of Turin, she has coordinated at UCL a team on exoplanets since 2007. ESA external fellow 2005-2007, NASA Astrobiology Institute/NRC fellow at Caltech/JPL 2001-2005.

Awards: Institute of Physics Moseley medal 2011 for pioneering use of IR transmission spectroscopy for molecular detection in exoplanet atmospheres. 2010 NASA Group Achievement award with Swain and Vasisht for first detection of methane in an exoplanet.

Editor of American Astronomical Society DPS journal, ICARUS. Counts over 100 peer reviewed publications and over 120 invited talks/seminars on exoplanets. Recent appointments in advisory boards: ESA EChO Study Science Team, Cycle 20 and Cycle 21 Hubble panel chair/TAC member, Hubble and Spitzer panel member 2010, ESO Espresso Instrument Science Team, ESA Exoplanet Roadmap Advisory Team (2009-2010).

Paul Eccleston – Consortium Project Manager & UK National Project Manager

Senior Spacecraft Systems Engineer, RAL Space, Rutherford Appleton Laboratory

Currently Consortium Engineering Manager for the SPICE (Spectral Imaging of the Coronal Environment) instrument on Solar Orbiter. Coordination and management of all engineering and technical activities for the consortium and subcontractors on this challenging, fast delivery instrument project.

Previously the Assembly, Integration and Verification (AIV) Manager for JWST MIRI. Control of all instrument level AIV activities, including co-ordination of activities across 11 country international consortium. Design authority for thermal, mechanical and electrical design of complex cryogenic test facility to simulate all interfaces for the instrument. Test director for all instrument environmental, qualification and calibration tests. Also RAL deputy project manager for JWST MIRI. Management of project schedule, cost at completion estimates, and leading project team through day to day activities. Formally thermal lead for JWST MIRI project responsible for all aspects of thermal design of instrument and integral member of instrument systems engineering team. Extensive expertise in active and passive thermal control systems for cryogenic infra-red space instrumentation.

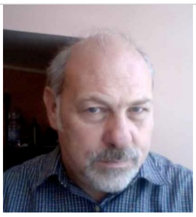

Alberto Adriani – Visible Module Design Lead

Senior Scientist, Institute of Interplanetary Space Physics (IAPS), INAF, Rome, Italy

More than 30-years experience in studying Earth and Planetary atmospheres and designing, developing and using atmospheric active and passive remote sensing and in situ instrumentation from ground-based, balloon-borne, airborne and space-borne platforms.

Presently Principal Investigator for the JIRAM (Jovian InfraRed Auroral Mapper) experiment, funded by the Italian Space Agency (ASI), on board Juno, a NASA mission to planet Jupiter; Co-Investigator of Juno; Participating Scientist to the NASA Cassini mission to the Saturn planetary system.

Ruymán Azzollini – Ireland National Project Manager

PhD. in Physics by the University of La Laguna in 2009, his graduate studies were financed by a grant/contract as "Resident Astronomer" by the Instituto de Astrofísica de Canarias (Spain), which runs the European Northern Observatory ("El Roque de los Muchachos" and "Izaña" Observatories, in the Canary Islands).

He's been member of the Test and Science Teams of the Mid Infrared Instrument

(MIRI) of the James Webb Space Telescope (JWST) since 2009, actively participating in the testing and data analysis that lead to the formal delivery of the instrument to NASA. He is also participating in the "crio-vac" testing campaigns at Goddard Space Flight Center (MD, USA) of MIRI. Between 2009 and

2012 he worked in Centro de Astrobiología (Madrid Spain), and since 2012 he works at Dublin Institute for Advanced Studies (Dublin, Ireland), as software developer for MIRI, while pursuing his research interests, which concern Star Formation and Galaxy Evolution.

Jean-Philippe Beaulieu – France Co-PI

Directeur de Recherche CNRS, Institut d'Astrophysique de Paris, France and honorary reader at University College of London, UK

Authored 125 refereed papers with a total of 5291 citations and has a H factor of 39. He has been leading the PLANET collaboration (35 people, 10 countries) since 2002. It led to the discovery of 13 exoplanets, including the first frozen super-Earth and the first statistics of the abundance of exoplanets at the snow line. He is a member of the EUCLID Science Group in charge of the legacy science microlensing program to perform a full census on exoplanets down to the mass of Mars. He co-authored the first discovery of water in an exoplanet atmosphere in 2007 and Methane in a hot Neptune. He also co-authored the first description of the EChO instrument simulator, and has been a long term collaborator of a number of people from the EChO consortium. His expertise covers data processing, photometry and spectroscopy, both in the optical and Infrared, statistics and managing large international consortiums.

Neil Bowles – LWIR Module Design Lead

Lecturer in the sub-department of Atmospheric, Oceanic and Planetary Physics (AOPP), department of Physics, University of Oxford, UK

Previous experience with space missions and infrared instruments covers the full range of activities from instrument design and proposal to delivery of flight hardware, operations and data analysis. Specific roles include: Principal investigator for UK research council instrument development grants, e.g. Compact Modular Radiometer now being prepared for flight as part of the UK TechDemoSat programme and the Asteroid Thermal Mapping Spectrometer, an imaging Fourier transform spectrometer breadboard for future flight opportunities. Also a co-investigator on the JPL/NASA ExoMars Climate Sounder and Diviner Lunar Radiometer instruments, as well as a science team member for instruments on Cassini and Mars Reconnaissance Orbiter.

Josep Colomé – Spain National Project Manager

Technician R+D+i CSIC, Institut de Ciències de l'Espai, Spain

Main areas of expertise are control software for the operation of telescopes, systems engineering and project management processes applied to astronomical instrumentation. Main technical experience covers activities for the development of the control layer of ground-based astronomical observatories, from the control infrastructure design to the implementation of software applications. Specific projects and roles: systems engineer and project manager for the TJO robotic telescope (OAdM observatory, Spain); task leader for the TCS at the SuperWASP Qatar robotic Telescope (ORM observatory, Spain), the operations scheduler and the ICS at the CARMENES instrument, and the operations scheduler for the Cherenkov Telescope Array observatory (CTA); local project manager for the mentioned projects and national documentation manager for the LISA Path-Finder mission (ESA).

Vincent Coudé du Foresto – Instrument Science and Performance Modelling Working Group Coordinator

Staff Astronomer at Paris Observatory – LESIA

Specialist in instrumentation techniques dedicated to high dynamic range observations in high angular resolution astronomy. With the instrument FLUOR, pioneered in the early 90's the practice of spatial filtering that has been adopted since by most stellar interferometers. Led the development at LESIA (and under contract by ESO) of VINCI, the instrument that was used for first fringes and commissioning of the VLT interferometer. Also involved in the study of ground and space-based precursors (GENIE, PEGASE, ALADDIN) for the DARWIN mission. Current science interests include characterization of fundamental stellar parameters and observation of exozodiacal dust in planetary environments of nearby stars.

Martin Crook – Cooler Systems Lead

Deputy Head of the Cryogenics and Magnetics group, Technology, Rutherford Appleton Laboratory

Responsible for the management and delivery of a range of frontline R&D programs in cryogenics for space and ground based use. Current work includes a 2K cooler for astronomy, a small scale cooler for scientific microsatellites and planetary probes, and a Stirling cycle generator for power generation in space using radioisotopic heat sources.

Previous experience with all aspects of the 4K cooler for the ESA Planck mission, from conception through manufacture and test, and finally to integration on the spacecraft.

Pierre Drossart – Consortium Science Team Co-Lead / LESIA Co-I

Director, LESIA, Observatoire de Paris, Meudon, France

Author of more than 250 refereed publications. Team Member in Galileo/Near Infrared Mapping Spectrometer : study of Jupiter atmosphere structure and composition. Team Member in Cassini/Visual and Infared Mapping Spectrometer: study of Saturn and Titan atmospheres from nadir and occultation experiments. Ground-based observations of Jupiter and Giant Planets from many large telescopes on Earth : IRTF, CFHT (Hawaii), ESO-3.60m and VLT since 1983. Specialist of radiative transfer in planetary atmosphere with more than 45 refereed publications related to Jupiter's atmosphere, including first observations of H_2O and H_3^+.

Team Leader (co-PI) on VIRTIS/Rosetta experiment. PI on VIRTIS/Venus Express experiment with G. Piccioni. Member of ESA Juice Science Study Team during the definition phase. Member of ESA Echo Study team. Management experience: Chairman of Solar System Working Group at CNES (2001-2005), Director of LESIA (2010- …)

William Grainger – Engineering Manager

Systems Engineer, RAL Space, Rutherford Appleton Laboratory, UK

Currently central member of the instrument system engineering team & AIV manager for SPICE instrument on Solar Orbiter, and part of the ground calibration team for BBR instrument on EarthCARE.

Previous projects and responsibilities include AIV planning and work for the Clover (ground based CMB polarization experiment) cryogenics system, AIV planning, co-ordination and work for EBEX (balloon based CMB polarization experiment) attitude control system and experimental platform. Lead in developing lab-based spectral/spatial interferometry testbed (demonstrator for FIRI (Far Infrared Inteferometer)). Design and commissioning of control and monitoring system for AMI (ground based interferometer)

Matt Griffin – Consortium Management Advisor, Project Team

Over thirty year's experience infrared astronomy from the ground and from space. PI of the international Herschel-SPIRE consortium from the proposal stage to the present day, including all aspects of instrument and ground segment design and development, consortium funding, organisation, and management, instrument operations, scientific preparation and exploitation, and public outreach. Also worked as Co-I on ISO-LWS and Planck-HFI, with responsibility for detector system on LWS. Familiar with UK, European and ESA funding and programmatic systems.

Manuel Guedel – Austria Co-PI

Professor, Deputy Chair of the Department of Astrophysics, University of Vienna, Austria, and Associate of Physics Department, ETH Zurich, Switzerland.

Previously staff member and lecturer, Institute of Astronomy, ETH Zurich (2008-2010), lecturer at ETH Zurich (1997-2010), staff astrophysicist and deputy chair of laboratory, Paul Scherrer Institut, Switzerland (1994-2007), postdoctoral research associate, JILA, University of Colorado (1991-1994), graduate student, Institute of Astronomy, ETH Zurich (1987-1991).

Member of ESA mission consortia (XMM-Newton: Science Co-I; JWST/MIRI:

Co-PI; EChO: Co-PI; PLATO: Co-PI; CHEOPS: Science Team; SPICA/Safari:

Science associate; BRITE-Constellation: Board); Co-PI of E-ELT/METIS instrument project; member of telescope allocation committees (XMM-Newton, Chandra). PI of national key project on planetary habitability, participant in EU FP7 program. Author of about 200 refereed papers and ~210 conference contributions with ~6600 citations. Scientific interests in star formation, stellar X-ray and radio astronomy, high-energy and plasma astrophysics, protoplanetary disks, exoplanetary atmospheres and star-planet interactions.

Paul Hartogh – Germany Co-PI

Scientist at the Max Planck Institute for Solar System Research, Germany.

PI of the Herschel Guaranteed Time - Key Programme Water and Related Chemistry in the Solar System. Herschel/HIFI Co-Investigator, Co-Investigator of MAS/ATLAS, Rosetta/MIRO and SOFIA/GREAT. General circulation modeling of Earth, Mars and Jupiter, chemistry transport modeling. Research interests include dynamics and chemistry of planetary atmospheres, radiative transfer/retrieval of planetary/cometary atmospheres, FIR/IR observations of planetary atmospheres, development of FIR/IR instrumentation.

Ranah Irshad – Lead Systems Engineer

Systems Engineer, RAL Space, Rutherford Appleton Laboratory, UK

Has undertaken Systems Engineering, QA, Planetary Protection and Design roles for ExoMars, TechDemoSat and InSight missions and has been responsible for mechanical design and modelling, thermal design and modelling, radiation modelling and testing, optical design and modelling, calibration and AIV activities for instruments such as EMCS (ExoMars Climate Sounder), CMS (Compact Modular Sounder), ATMS (Asteroid Thermal Mapping Spectrometer), ORTIS (ORbiter Terahertz Infrared Spectrometer), JSTIM (Jupiter System Thermal Infrared Mapper) and SEIS. As a PDRA at the University of Oxford she was involved in the planning and writing of proposals for a number of missions and developed expertise in spectroscopy, seismometry, particulate modelling and satellite data retrieval and analysis.

Tanya Lim – Consortium Science Ground Segment Lead

Astronomy Group Manager, RAL Space, Rutherford Appleton Laboratory, UK

Currently the Herschel SPIRE consortium project manager and Instrument Control Centre Manager leading the multinational operations team. During development led the SPIRE test activities and calibration development. The calibration lead role has continued in-flight, now with leadership of the routine calibration programme. In parallel to SPIRE development also worked on MIRI during the early development in a dual role as the test team lead and EGSE system engineer. Test lead activities included recruiting the test team, formulating test facility requirements, writing functional and performance test plans. Previous experience also includes deputy leader of the ISO LWS instrument dedicated team for operations, ISO calibration science and ISO science preparation. Research interests include stellar atmospheres, dusty environments of evolved stars and rocky bodies in the solar system.

David Luz – Portugal Co-PI

Planetary scientist at the University of Lisbon's Centre for Astronomy and Astrophysics.

Member of the Venus Express mission's VIRTIS team and of the worldwide network of ground-based support observers. His research focuses on the following topics:

•Measuring winds in the atmosphere of Venus

•Developing data-analysis procedures for the Doppler velocimetry and cloud tracking techniques.

•Modeling the global atmospheric circulation to characterize composition and dynamics.

Giuseppina Micela – Italy Co-PI

Director, INAF-Osservatorio Astronomico di Palermo, Italy

Previously Senior CNR/NATO fellow at Dept. of Astronomy & Astrophysics, Univ. of Chicago (1996); Ricercatore Astronomo at Osservatorio Astronomico di Palermo (1990-2003); Graduate student at Palermo University (1987-1990); CNR fellow at IAIF/Palermo (1986-1987); CNR fellow at Harvard Smithsonian Center for Astrophysics (Cambridge – MA, 1985).

Member of telescope time allocation committees (TNG, ESO, Chandra), of ESA mission science teams (Eddington, Simbol-X, PLATO, EChO), of consulting bodies (AWG, ASI astronomy group, EPRAT) and responsible for national fund allocation (ASI). Responsible of several national grants (MIUR, INAF, ASI) and European Marie Curie Programs (FP5, FP6, FP7). Author of ~200 refereed papers with more than 5000 citations. Main scientific interests are physics of the high stellar atmosphere, young stellar coronae, X-ray stellar emission and its evolution, star formation and stellar clusters, stellar populations in the solar neighborhood, effects of stellar high energy radiation on the circumstellar environment, disks and planets.

Kevin Middleton – Optics Lead

He joined the Rutherford Appleton Laboratory, as an Optical Systems Engineer in the Space Science and Technology Dept. His work is in the design and development of optical systems for space applications. Projects have included the design, manufacture, alignment and test of high stability interferometers for gravitational wave detection, and the development of high-resolution camera systems for earth observation. He is responsible for development of the flight-model star tracker lens referred to in the lightning camera proposal.

Gianluca Morgante – Thermal Lead

Staff Researcher, INAF – IASF Bologna, Italy

Over 15 years experience in experimental cosmology from ground, balloon and space platforms. Research activities are mainly focussed on instrument design and implementation, with particular interest in all issues related to the cryogenic and thermal design of the experiment. From 1998 to 2004 worked at the labs of JPL Low Temperature Physics Group collaborating to the design, implementation and test of the Sorption Cooler System (SCS) of the Planck ESA mission. In the last years has led all Planck SCS System Engineering activities in Europe, including AIT and flight operations. Coordinator of the Planck LFI Thermal WG, of the SCS Operations Team and a member of the Planck Cryo Operations Engineering Group. Presently part of the System Team of the NISP Instrument on board the Euclid ESA mission as responsible of the thermal design.

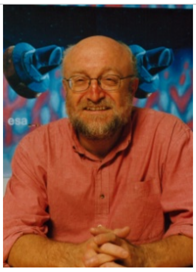

Hans Ulrik Nørgaard-Nielsen - Denmark Co-PI

Senior scientist, DTU Space, Copenhagen, Denmark

In charge of the development and testing of the Planck CFRP reflectors, the CFRP Primary Structure Hexapod and Thermal Shield Support Structures for the MIRI instrument onboard the James Webb Space Telescope. Also responsible for the preliminary mechanical design of the CFRP support structure of the telescopes on the ESA LISA mission

Marc Ollivier – Instrument Scientist / IAS Co-I

Astronome Adjoint, IAS, University of Paris-Sud, France

Member of the CoRoT science team and works as deputy instrument scientist for this mission. Developer of several instrument models for CoRoT (lightcurves simulator) and EChO (existing ETC). Developed the first nulling interferometry test bench in Europe (1999). PI of the PEGASE proposal in 2007 (ESA CV1/CV2 call for proposals).

Roland Ottensamer – Austria National Project Manager

Senior Research Engineer at Department of Astrophysics, University of Vienna

Previously PostDoc at Inst. for Computer Graphics at TU Graz, MSc and PhD in Astronomy at University of Vienna; Reviewer for Applied Optics, 30+ publications; Expert in on-board data processing with 12 years of experience in space instrumentation, most notably Herschel

Emanuele Pace – Italy National Project Manager / Electrical & Electronics Lead

Permanent staff Researcher at the Department of Physics & Astronomy, University of Florence, Italy

Activity is mainly focused on optical systems and radiation detectors for ground- and space-based applications, being involved also in astrobiology and exoplanet research programs. PI of the DIASPACE program on the Russian FOTON-M3 mission and PI of the 3DISS experiment on board the International Space Station. Also Co-I of the HERSCHEL rocket mission, WSO/UV UV telescope, EUSO telescope and PLATO space telescope.

Mirek Rataj – Poland National Project Manager & SWIR Detector System Lead

Over 25 years of experience with the project management, design, tests, calibration and science of spectrometers and radiometers, working in optical and microwave range for remote sensing purposes.

Participation in satellite missions: MARS-EXPRESS and VENUS EXPRESS – experiment Planetary Fourier Spectrometer design and project management - module S, mission Herschel experiment HIFI design and project management of HLCU unit, mission Bepi

Colombo- experiment MERTIS- Pointing Unit design and management. Participation in FP6th and 7th projects. Other projects include: design of the hyperspectral imaging–spectrometer for UAV or a small planes, design of Fourier Spectrometers for atmospheric measurements.

Tom Ray – Ireland Co-PI & Dichroics Lead

Professor of Astrophysics in the Dublin Institute for Advanced Studies (DIAS)

Research centered on understanding mass loss from young stars during the earliest phase of their evolution both from an observational and theoretical perspective.

Member of ISOPHOT (photometer) team, one of the major instruments on board the European Space Agency's Infrared Satellite Observatory (ISO). Currently a Co-PI of the Mid-Infrared Instrument (MIRI) on JWST with responsibility for the filters and dichroics. Has been awarded time on a number of occasions on the Hubble Space Telescope both as a principal investigator and as a co-investigator.

Current or previous membership of many national and international committees including the Irish National Committee for Astronomy and Space Research, the National Committee for Physical Sciences, the Hubble Space Telescope Time Allocation Committee, the United Kingdom Panel for Allocation of Telescope Time.

Jean-Michel Reess – France National Project Manager & MWIR Module Design Lead

Optical Engineer and Project Manager, Paris Observatory - LESIA, France

Project manager and optical designer of several Cosmic Vision AO (MarcoPolo, JUICE, SPICES,..). Project manager of the coronagraph subsystem of MIRIM/JWST. Responsible of optical subsystem of the infrared high resolution spectrometer VIRTIS-H/ROSETTA and VenusExpress and deeply involved in the optical calibration and tests of the infrared mapping spectrometer OMEGA/MarsExpress.

Etienne Renotte – Belgium National Project Manager

Space Systems Program Manager, University of Liege – Centre Spatial de Liege (CSL)

Following an MSc in Aerospace engineering, Liege, 1990, Etienne has more than 22 years of experience in space instruments design, integration and test gained in ESA and NASA programmes, for example ISO, XMM-OM, IMAGE FUV/SI, INTEGRAL OMC, Herschel PACS, JWST MIRI, ExoMars LaRa, etc. He is leading the "*Space Systems Programme*" of the *Centre Spatial de Liège* (CSL), which is active in the development of space instruments, optical design and calibration, metrology, remote sensing, signal processing and environmental testing. He was the system engineer of the IMAGE FUV Spectro-Imager developed in collaboration with UC Berkeley, local project manager for INTEGRAL OMC, local project manager for the Herschel PACS grating mechanism and control electronics and National project manager for JWST MIRI subassemblies. He is the project manager of Solar Orbiter EUI and Co-I for ExoMars TGO NOMAD.

Ignasi Ribas – Spain Co-PI

Científic Titular CSIC, Institut de Ciències de l'Espai, Spain

Main areas of expertise are stellar physics and exoplanets, on which he has authored around 100 refereed publications.

Some of his main scientific accomplishments are: (i) Discovery of the important effects of magnetic activity on stellar radii and temperatures; (ii) characterization of the time-evolution of high-energy emissions of low-mass stars with direct application to planetary atmospheres; (iii) use of dynamical perturbations to a transiting exoplanet as the signpost of further planets; (iv) detection of various molecules in the atmospheres of hot Jupiter planets; (v) use of eclipsing binaries to probe stellar interiors and as distance indicators. He is co-PI of the EChO space mission proposal, Project Scientist of the CARMENES instrument – a visible and near-IR spectrograph for precise radial velocities of M stars, and co-I of the CoRoT space mission. Dr. Ribas is also President of IAU Division G on "Stars and Stellar Physics", Director of Montsec Astronomical Observatory, and advisor to the

Spanish Ministry of Economy and Competitiveness.

Hans Rickman – Poland / Sweden Co-PI

Professor at Uppsala University (Sweden) and PAS Space Research Center, Warsaw (Poland)

Former General Secretary of the IAU and President of IAU Comm. 20, Member of the Swedish Royal Academy of Sciences and the International Academy of Astronautics. More than 250 publications whereof more 100 refereed. Founder of the Asteroids, Comets, Meteors conference series (Uppsala, 1983), editor of several books and co-organiser of many international meetings dealing with the small bodies of the Solar System, e.g., Nobel Symposium 135 "Physics of Planetary Systems". Member of the ESA Space Science Advisory Committee 2007-2010. Honorary Presidential Professorship awarded in Poland in 2011; David Bates Medalist of the European Geosciences Union in 2012.

Avri Selig – Netherlands Co-PI

Head of division Earth and Planetary Science (EPS), SRON Netherlands Institute for Space Research

1993 – Present: Senior Staff member at SRON-NL (Utrecht). 2000 – present: Head of division Earth & Planetary Science at SRON-NL. Member of MT SRON. Instrument Development and Remote Sensing of the Earth atmosphere. Tropospheric composition, NIR-SWIR carbon and water cycle trace gases and VNIR aerosol: ESA Envisat-Sciamachy, ESA-NL Sentinel-5/TROPOMI, future SPEX2Earth. Stratosphere composition (submm Cl and Br compounds): TELIS balloon-borne. 2001 – present: ESA DOSTAG (Data Operation Science & Technology Advisory Group) Earth Observation, National Delegate. 2000 – 2012: NIVR-PEP (preparatory ESA programs) evaluation committee (ARTO); personal nomination by ministry of economic affairs. 1996 - 2000: NL Project manager ESA GOCE (pre-phase A to pre-phase B). 1994 – 1996: Project manager SRON of NL-D-Be SCIAMACHY Instrument. 1993 - 1994: Assistant project manager for the Detector Modules of SCIAMACHY (at SRON)

Richard Stamper - Consortium Product Assurance Manager

Head of the Product Assurance Group, RAL Space, STFC Rutherford Appleton Laboratory

Joined RAL in 1993 after starting his career in software and database development for British Airways, followed by software research at Oxford University. At RAL he has continued to make technical contributions to space data projects and carry out published research while also taking on roles in project management and quality assurance. He now leads the RAL Space Product Assurance Group, responsible for the department's ISO9001 system and for providing product assurance support to all projects needing to comply with space product assurance requirements, and is the groups expert on software product assurance.

Mark Swain – US Co-PI

Research Scientist, Jet Propulsion Laboratory, USA

PI of the FINESSE Explorer 2011 mission concept for exoplanet characterization. Led discovery team for detection of CH4 and CO2 in an exoplanet atmospheres. Member of the NASA Balloon Program Working Group representing exoplanets community. Lead for the ExoSpec team working on exoplanet characterization. PI for numerous exoplanet spectroscopy programs with HST, Spitzer & IRTF. Originator of the THESIS exoplanet spectroscopy mission concept. Expertise in Exoplanet spectroscopic characterization, high dynamic range spectroscopy & interferometry techniques and infrared instrumentation, integration and test, and system engineering.

Recipent of the NASA Exceptional Scientific Achievement Medal (2010), JPL Ed Stone Award (2009) & NASA group achievement award (2009).

Bruce Swinyard – UK Co-PI

Professor of Astronomical Instrumentation, Department of Physics and Astronomy, UCL / Head of Astronomy Group, RAL Space, STFC Rutherford Appleton Laboratory

Significant technical leadership roles in two of the largest worldwide infrared missions launched in the last 20 years – the Infrared Space Observatory (ISO 1995-1998) and the Herschel Space Observatory. In the past decade has also had a significant role in the development of JWST - MIRI and led the successful proposal for ESA involvement in the next generation FIR mission, SPICA. Served on the PPARC Astronomy Advisory Panel, is a current member of the ESA SPICA Science Advisory team. Provided technical consultancy and expertise for the successful proposal for the EChO, acting as technical advisor to Dr Giovanna Tinetti. Published over 100 refereed papers and 100's of technical papers.

Berend Winter – Mechanical Lead

Head of Mechanical and Thermal Engineering, MSSL, UCL, UK

Wealth of experience regarding mechanical design and analysis. In particular in design/analysis/test of systems and subsystems with respect to stiffness, strength and minimised thermal parasitic heatloads.

Recent experience includes: Project leader and principle engineer for Herschel / SPIRE structure design; Mechanical design and development of ESA ADR – cryogenic cooler based on adiabatic remagnitisation refrigeration; In flight and ground calibration sources for NIRSpec, mechanical, thermal design manufacture and test; Mechanical engineer for initial design studies for SPICA / SAFARI – cryogenic instrument.

Gonzalo Ramos Zapata – SWIR Module Design Lead & INTA Co-I

AIV and Optical Engineer, Space Instrumentation Laboratory (LINES) of the National Institute of Aerospace Tehcnique (INTA), Spain

Eleven years experience in optical metrology, optical instrumentation alignment, test and analysis of optical instrumentation in vacuum and thermal controled conditions, and structural resistance control of materials through holographic techniques.

Participation in space and aeronautic projects is: OMC-INTEGRAL, OSIRIS Filter Wheel-ROSSETA, Raman-EXOMARS, IMaX-SUNRISE, a stellar, telescope and atmospheric turbulence simulator for IAC (IACATS), GAIA secondary mirror positioning mechanism cryogenic test, SENTINEL-3 scanning system thermal and vacuum test, and JWST / MIRI MTS positioning system characterization in cryogenic conditions.